2001-05-01

In-situ Spectroscopic Studies of Electronic Processes in Buckminsterfullerene Thin Films

Gordon Chambers
Technological University Dublin, Gordon.chambers@tudublin.ie

Recommended Citation

Chambers, G. (2001). *In-situ spectroscopic studies of elecronic processes in Buckminsterfullerene thin films*. Doctoral thesis. Technological University Dublin. doi:10.21427/D79W33

In-Situ Spectroscopic Studies of Electronic Processes in Buckminsterfullerene Thin Films

By

Gordon Chambers

A thesis submitted to the Dublin Institute of Technology,
for the award of Doctor of Philosophy
(PhD)

Focas/ School of Physics,
Dublin Institute of Technology,
Kevin Street,
Dublin 8

April 2001

Declaration

I certify that this thesis which I now submit for examination for the award of the degree of Doctor of Philosophy (PhD) is entirely my own work and has not been taken from the work of others unless cited and acknowledged within the text of my work.

This thesis was prepared according to the regulations for postgraduate studies by research of the Dublin Institute of technology and has not been submitted in whole or in part for an award in any other Institute or University.

The institute has permission to keep, to lend and copy this thesis in whole or part on condition that any such material be duly acknowledged and referenced

Signature: Gordon Chambers. **Date** April 2001.

Gordon Chambers

Acknowledgements

"Accept these humble words of praise and my gratitude for those glorious days"- Muhammad Ali

I would like to thank Dr Hugh Byrne for all his help and supervision and for giving me the opportunity to undertake this research with the Physics of Molecular Materials group (POMM). I would also like to thank Dr. Vincent Toal for allowing me to work within the school of Physics. I must also extend my warmest thanks to all members of POMM particular Dr. Alan Dalton for his support and advice during the project. I am also very grateful for the help I received from the physics, chemistry and FOCAS technicians in particular Jane Torris, Joe Keogh, Garret Farrell and Laura Evans. Many thanks also to Dr. Mary M^{c} Namara and Dr. John Cassidy, from the school of Chemistry and Dr. James Walsh from the school of Physics. I would also like to thank my fellow postgraduates both in Physics and Chemistry.

I would also like to thank Prof. Werner Blau (TCD) and his research group for allowing me to participate in their group and the use of their facilities, I would especially like to thank Dr Jonny Coleman Dr. Andy Davey, and Dr. Diarmuid O'Brein.

Finally a special thanks to my Family and Emer for all their help and support for the last few years and for the years to come. Without their support, kindness and understanding this thesis would have been a lot harder and much lonelier. I hope I can repay you with the same kindness in the future. Thanks for a million for everything.

If I have forgotten anyone my apologies but thanks to everyone who helped me during this project.

Thank you

Abstract

This study attempts to develop an understanding of the electronic processes active within the solid state of C_{60}. The emphasis throughout the work has been upon the generation and spectroscopic identification of any species, which could potentially contribute to electronic conduction in thin films of C_{60}. The relative importance of these inter- and intramolecular processes in terms of their contribution to the electronic transport is discussed through the comparison of the properties of the molecule with the properties of the bulk solid.

Initially the low intensity optical properties of the C_{60} molecule in solution and in solid were assessed. Vibrational spectroscopy of C_{60} in the solid state indicated that C_{60} was predominantly molecular in character, however electronic spectroscopy revealed features, which were specific to the solid. These features have been attributed to an intermolecular charge transfer state, which can potentially contribute to the generation of photocarriers. Further optical analysis at higher intensities revealed that the excited state properties of molecular C_{60} were dominated by an extremely fast intersystem crossing rate (~1.2ns) to the first triplet state manifold. This was indicated by the rapid evolution of a triplet – triplet absorption at ~750nm in the transient absorption measurements. This molecular triplet was assigned the Raman signature 1466cm^{-1} and was seen to play an integral part in the 2+2-cycloaddition mechanism proposed for the photopolymerisation of C_{60} from solution. In the solid the excited state photodynamics were seen to differ considerable to those in solution. The molecular triplet was identified for the first time in the solid state using Raman spectroscopy and was seen to be positioned at 1466cm^{-1} as in solution. In addition to the molecular triplet a second excited state species positioned at 1463cm^{-1} was observed in the solid state. It was proposed that the species positioned at 1463cm^{-1} was an excited co-operative involving two or more molecules in the solid. A temperature dependence study of the excited state species in the solid indicated that the co-operative species was extremely non-linear and intrinsic to the material below the orientational

phase transition, which occurs at 249K in C_{60}. Both the molecular triplet state and the excited states specific to the solid were seen to have active roles in the photopolymerisation and depolymerisation of C_{60}. The Raman signature of the photopolymer of C_{60}, seen at ~1458cm^{-1}, completed the optical characterisation of all the photophysical states of C_{60}. This characterisation raised a number of questions regarding the triplet excited state and the role of excited state species in the conduction process.

The electrical generation of ionic species that can contribute to the electronic transport processes in solid state C_{60}, were also examined using electron injection techniques. In solution it was seen that the C_{60}^{-1} and C_{60}^{-3} ionic species, which are analogues to the highly conducting and superconducting salts KC_{60} and K_3C_{60} respectively, could be readily produced by the application of moderate voltages. Raman spectroscopy indicated that the C_{60}^{-1} species was analogous to the aforementioned excited state co-operative observed in the solid. In the solid state structural rearrangements and subsequent electronic interactions resulted in the formation of polymeric species. The formation of these polymeric species complicated the generation of anionic species and inhibited the conductivity of the solid state. The effect of this was evident from reported conductivity measurements on C_{60} drop cast films, and the current-voltage characteristics of vacuum evaporated C_{60} films incorporated into sandwich type structures. The effect of the structural rearrangements and electronic interactions was overcome for the sandwich type structure by cooling the arrangement down to 20K. At this low temperature a relatively stable, highly conducting film was produced. However the nature of the conducting species remains to be determined. It is speculated to be a reduced form of C_{60}, which may resemble the excited states co-operative species, which is intrinsic to the material at these low temperatures.

It was proposed that the key to preserving the conducting species was the stabilisation of the C_{60} lattice against a polymeric breakdown, thereby shifting the phase transition at 249K to higher temperatures. This was done through the incorporation of neutral solvent molecules into the lattice, which then behave as 'molecular spacers', inhibiting the

formation of polymeric bonds. The incorporation of the solvent molecules was seen to result in a change in the crystal packing with the emergence of a new phase as evident from X-ray diffraction data. This type of solvent inclusion compound is referred to as a clathrate. Alternatively structural enhancement was also achieved by thermal annealing. The annealing process also resulted in an apparent change in phase. This new phase in both techniques appears to be resistant to photodegradation indicating an enhanced lattice stability at room temperature. In the future this enhanced stability should allow a more detailed exploration of the highly conducting species for application in optical and electronic devices. A number novel thin film devices have been discussed as well as the potential of this excited material for non-linear optical applications.

Table of Contents

Chapter 1

Introduction

1.1: Introduction

The discovery of the closed cage carbon molecule C_{60} or Buckminsterfullerene ranks among some of the greatest moments in modern science. The story of the discovery of this unique molecule and its subsequent exploration, highlights the importance of collaboration from within the different scientific disciplines. In the early stages of 'Fullerene science', chemists, physicist, astronomers and mathematicians worked together fruitfully and often the work was carried out on the back of other funded projects, creating a true interdisciplinary branch of science.

1.2: Historical Background

The notion of a hollow carbon sphere is nothing new to science and has appeared on at least two occasions [1,2] in the decades prior to the actual discovery of the Buckminsterfullerene by Kroto and Smalley [3] in 1985. One of the earliest papers on the concept appeared in the popular science journal New Scientist in 1966, when David Jones, under the pseudonym Deadalus, speculated on the possibility of creating large graphitic "balloons" [1]. However the earliest record of C_{60} in literature is contained in an article written by Eiji Osawa in 1970 in which he conjectured that if such a molecule could be synthesised it would be stable [2]. As a result of Osawa's paper, a number of other theoretical papers appeared on the subject. [4,5]

The discovery of the Buckminsterfullerene by Kroto and Smalley [3] in 1985 was however, purely accidental. During experiments aimed at understanding the mechanism by which long-chain carbon molecules might be formed in red giant carbon stars, Kroto and Smalley stumbled upon a strange material which had a peak at 720amu in its mass spectrum. They proposed that by vaporising a graphite target under a high density helium flow using an excimer pulsed laser, a remarkably stable carbon cluster consisting of sixty atoms resulted. They suggested that the carbon atoms were arranged at the vertexes of a truncated icosahedron shown in figure 1.1. The striking resemblance of this structure to the geodesic domes designed by Richard

Buckminster-Fuller led the researchers to christen this new molecule Buckminsterfullerene. When a carbon atom is placed at each vertex of this football type structure its valences can be satisfied by two single bonds and one double bond, i.e. each carbon has a sp^2 hybridised bonding arrangement, which gives rise to sixty delocalised electrons around the carbon cage.

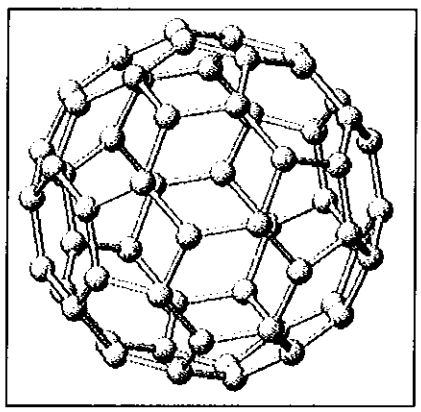

Figure 1.1: The proposed truncated icosahedral structure of the Buckminsterfullerene (C_{60}). Note the resemblance to a football

The physical and chemical properties of Buckminsterfullerene (C_{60}), and in particular the sixty delocalised electrons generated a huge interest throughout the scientific community. However the lack of availability of the material, initially limited scientific research into the molecule to theoretical studies based upon the proposed structure [4,5]

In 1990, five years after the initial discovery of the Buckminsterfullerene, IR and NMR [6,7] spectroscopy confirmed the structure originally proposed by Kroto and Smalley. Simultaneously, in 1990, the first macroscopic synthesis (100mg/day) and isolation of fullerenes was performed by Hoffman and Krätschmer [8]. This opened up the entire area to the research community. Since the development of a synthetic method for fullerene production, the area of fullerene science has grown enormously, leading to the discovery that the Buckminsterfullerene (C_{60}) is merely one molecule belonging to a family of molecules [3] referred to as the fullerenes, including the

much researched carbon nanotubes, carbon onions, C_{70} and numerous other large carbon cluster molecules (figure 1.2), of which C_{60} is the archetype.

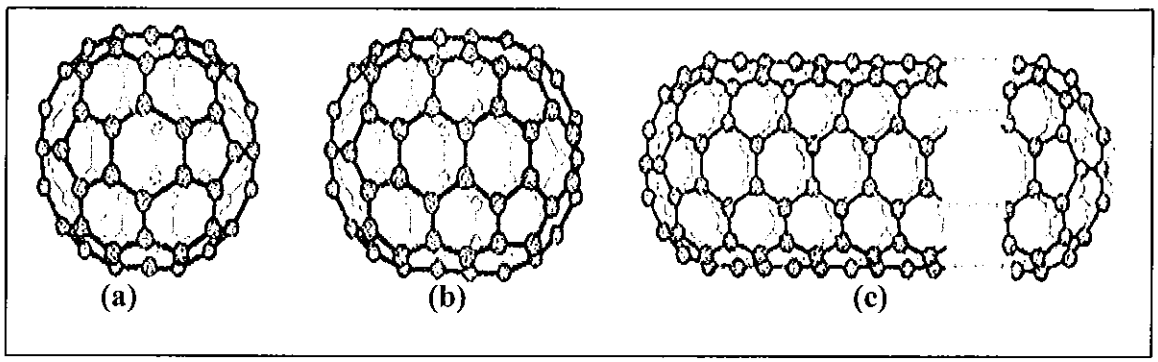

Figure1.2: A selection of the many carbon clusters in the Fullerene family (a) C_{70} (b) C_{80} and (c) a single wall nanotube.

It is said that C_{60} has received more attention than any other molecule in history, being the subject of the ten most cited papers of 1991 [9]. It has stimulated countless publications, which in the first few years was estimated at one every thirteen hours on the subject. In spite of this intense scientific investigation being conducted by the scientific community, no commercial application for C_{60} or any other fullerene has emerged as of yet, although several intriguing applications have been proposed. Nevertheless in 1996 the Nobel Prize in chemistry was awarded to Rick Smalley, Harry Kroto and Bob Curl for the discovery of the Buckminsterfullerene.

1.3: Proposed Applications of C_{60}

The award of the Nobel Prize to the discovery of C_{60} is testimony to the importance of the fullerenes in terms of their contribution as a model molecular system as well as to the promise they hold for technological development. Since their discovery, numerous potential and optimistic applications have been proposed for the fullerene family, from every discipline in science. Over the past decade they have intrigued and inspired scientists and industrialists alike. Backed by such giants as NEC, AT&T, Du Pont, Exxon and IBM [9,10], a highly competitive search for practical applications

began and continues today with possibilities ranging from the creation of a revolutionary rocket fuel to nanotechnology. One of the most exciting findings and potentially one of the most important applications, was the discovery that fullerenes and their derivatives can potentially show bioactivity against living cells and enzymes, [11]. In particular they have shown an inhibition against the HIV protease and can also be used to selectively fragment DNA effectively and efficiently [12]. Other novel applications, which are being considered for commercial development, which are more relevant to this thesis, are:

1. Sensor Applications [13]
2. Battery and Fuel Cell Electrodes[13,14]
3. Optical Limiting [15]
4. Conductivity and Superconductivity [16,17,18]

These applications all derive from the optical and electronic properties of C_{60} as determined by the 60 delocalised electrons. The effect of these electrons upon the above applications will be looked at throughout the thesis, with reference to the effect of moving from the isolated molecule to the solid state.

1.3.1: Fullerene-Based Sensors

Fullerene-based inter-digitated capacitors (IDCs) have recently been developed to explore sensor applications [13]. This novel solid state sensor design is based on the electron accepting properties of fullerene films and the changes that occur when planar molecules interact with the film surface. Fullerene chemistry provides a high degree of selectivity and the IDC design provides high sensitivity. The solid state chemical sensor's small size, simplicity, reproducibility and low cost makes them attractive candidates for fullerene applications development.

Studies of IDC configurations with fullerene films have established that a fullerene based sensor is capable of detecting less than 1ppm H_2S in N_2, and is able to sense

water in isopropanol with a resolution of 40 ppm [13]. These results demonstrate the feasibility of using fullerenes as selective dielectric films for IDC chemical sensors. The selectivity of the dielectric fullerene film can be further improved by modifying the fullerene chemically or physically. These modifications are easy to perform because of the ease with which fullerenes can be made to undergo addition reactions. Clearly, fullerenes have an exciting potential role in sensor technology.

1.3.2: Batteries and Fuel Cell Electrodes

The field of rechargeable batteries for consumer electronics has been dominated by Nickel-Cadmium technology. However, the development of Nickel-Metal hydrides and lithium-ion batteries is aggressively substituting for NiCd batteries, and is also opening up new markets. Fullerenes, it has been suggested, have the potential to impact on both the nickel-metal hydride and lithium-ion battery technology since they possess an extremely rich electrochemistry.

The electrochemical reduction of these materials was found to be highly reversible, [14] hence promoting the idea that fullerenes might be employed as a novel material for rechargeable batteries. Since reduced fullerenes are sensitive to ambient conditions, it is reasonable to suppose that organic electrolytes would be used particularly in conjunction with lithium to maximise its energy density. Initial research into the use of C_{60} in such applications has resulted in relatively poor results in comparison to existing technologies. However hope can be taken from the fact that the Materials and Electrochemical Research Corporations (MER) have produced a prototype Ni/ C_{60} rechargeable battery whose performance is estimated to be superior to that of Ni/Cd batteries [14].

1.3.3: Optical Limiting

The optical properties of C_{60} are well characterised and have shown that fullerenes display distinct properties with a variety of potential applications. One of the most interesting optical properties is optical limiting [15]. This refers to a decrease in transmittance of a material with increased incident light intensity. The phenomenon of optical limiting has significant potential for applications in eye and sensor protection from intense sources of light. Over the past decade studies on the optical limiting of fullerenes and their derivatives have shown that C_{60} is a good optical limiter at a wavelength of 532nm, [15] and solvated multi-walled nanotubes were seen to perform better than C_{60} at this wavelength [19]. Nevertheless a C_{60} charge -transfer complex (C_{60} / tetraphenyl porphyrin) exhibited a strong saturable absorption at long wavelengths (around 750nm) [13] (which is similar to the triplet absorption discussed in chapter 5) demonstrating that C_{60} complexes are broadband optical limiters. Hence, based on the optical limiting properties of fullerenes and in particular C_{60} and its excited states, one can make an optical limiter which allows all light below an activation threshold to pass and maintains the transmitted light at a constant level below the damage threshold for the eye or a sensor.

1.3.4: Conductivity and Superconductivity

One surprising result of research into fullerenes is that when solid state C_{60} (fullerite) is doped with alkali metals, such as Potassium or Rubidium with a stoichiometry of 1:1, a metallic -like conducting state can be achieved i.e. A_1C_{60} [16]. Similarly if the stoichiometry is changed to three alkali metals to one C_{60} (i.e. A_3C_{60}) then a superconducting state is obtainable. Using potassium as the dopant i.e. K_3C_{60}, originally obtained a temperature transition (T_c) of 18K [17]. It is interesting to note that the doping of graphite with potassium also results in a superconducting state but at a significantly lower temperature [19].

Evidence for this superconducting nature of fullerene based crystals has been recently provided by Harald Weber [20]. By direct magnetic measurements on single K_3C_{60}

crystal samples they have confirmed that the superconductive behaviour of C_{60} can be explained in terms of conventional bulk superconductivity. That is, although K_3C_{60} shows all the characteristic signs of a superconductor, such as the expulsion of magnetic flux at low temperatures and zero resistance to electrical current, the reported current densities are much lower than in other superconductors. Weber's results suggest that fullerenes are molecular superconductors, in which supercurrents flow due to Josephson coupling between the C_{60} molecules. Therefore the superconducting properties should not be affected by the sample size, but instead by cracks in the crystals inhibiting the Josephson coupling, hence reducing the current densities. Nevertheless, although these results are very encouraging, for useful applications, the transition temperature will have to rise, at least to 77K (liquid nitrogen), before any superconducting application can be realised. Doping with rubidium (Rb_3C_{60}) has already allowed transition temperatures of up to 43K to be obtained [18], however much more work is required in order to obtain higher transition temperatures.

Much of the interesting physics of the conducting and superconducting molecules arises from the population of the lowest unoccupied molecular orbital (LUMO), by electron transfer from the dopant metals [21]. Such a population is also obtainable without doping via optical excitation or by electron injection [4]. In the solid state, a stoichiometric 100% population of this upper state results in the formation of a metallic -like state [16]. When the population of the state is obtained by optical excitation from the ground state, the metastable metallic state is highly luminescent and non-linear [22]. Similarly when produced by electron injection a broad intense luminescence is produced with the additional interest that the current characteristics of the material became highly non-linear [23].

The commercial implications of a material which theoretically has the ability to go from an insulator to conductor, to a superconductor and back under controlled conditions would be phenomenal. With numerous applications such as MRI magnets, high speed computer chips based on Josephson junctions and other electronic devices based on SQUIDS (Superconducting Quantum Interference Devices) [13].

1.4: Thesis Outline

The aim of this study was to characterise the optical and electronic properties of C_{60} thus pointing the way towards future applications. These properties have received a considerable amount of attention in recent years due to their potential in the development of novel applications. The emphasis in this study will be upon the generation of the optically and electronically induced states, which can potentially contribute to the realisation of one or more of the proposed applications, particularly those associated with optical and electronics based industries. The subsequent characterisation of these generated states via spectroscopic techniques will then be used to aid future research.

Initially, in chapter two the structure of C_{60} is discussed and the first comparison between the properties of the isolated molecule and the solid state is drawn, a theme which is maintained throughout the thesis. This chapter also introduces some of the main concepts in molecular physics such as molecular symmetry and its significance to C_{60} is discussed. Similarly, the electronic structure is examined through the use of the Hückel molecular orbital theory and the computer package Hyper-Chem is introduced and used to calculate a variety of constants associated with the C_{60} molecule. In general the chapter raises a number of questions concerning the electronic configuration of the solid state, specifically whether the sixty delocalised electrons of the C_{60} molecule become delocalised across the solid or remain located on the individual molecules. As a result this chapter essentially sets up the arguments for doing the research.

Chapter 3 explains the methodology used throughout the study. It explains how the C_{60} was original produced and fabricated into film form. The spectroscopic techniques and instruments used in this study are also discussed. IR, Raman, and UV/Vis spectrometers were all used as well as potentiostats and other electronic injection techniques.

Chapter 4 begins the experimental exploration of C_{60}. By using low intensity spectroscopy the various ground state spectra for both solution and solid state C_{60} were obtained and interrupted in conjunction with the structural and electronic information outlined in chapter 2. Chapter 5 on the other hand explores the high intensity or excited state spectroscopy of C_{60}. Transient Absorption measurements showed that the triplet-triplet absorption of the C_{60} molecule and the Raman signature of the molecular triplet is revealed for the first time both in solution and in the solid state. The excited state photodynamics of the solid are also explored with respect to temperature. The polymerisation of C_{60} is then explored and characterised in chapter 6 in the solid state and for the first time the photopolymerisation from solution is performed and examined.

Chapter 7 sees a shift away from the optical generation of species, which can contribute to the realisation of the aforementioned applications and instead turns to the electrical generation of these species. This involves the use of cyclic voltammetric and electronic injection techniques to generate the species of interest. The spectroscopic signature of each of the electrically generated species has also been presented and compared to the spectroscopic signatures of the optically generated species. In this chapter the generation of a highly conducting reduced form of C_{60} is observed in an electrically driven Mott-like transition and is seen to be stable at low temperatures. This phenomena thus leads into the final experimental chapter, chapter 8, which is concerned with the stabilisation of the lattice against optical and electrical degradation at temperatures approaching room temperature. The methods explored in this chapter are thermal annealing and the formation of clathrate compounds via the inclusion of neutral solvent molecules into the C_{60} lattice.

The final chapter of the thesis is a general discussion of the work presented. It highlights the continuing need for fundamental research into the properties of C_{60}, and the possible implications of this thesis on future C_{60} research. It discusses also the potential of C_{60} as a model molecular system upon which other systems can be modelled. Finally the closing remarks of the thesis indicate some future directions of fullerene research involving nanotubes. Within the context of this thesis it will be

shown that C_{60} still holds great potential for future applications and that the there is a wealth of knowledge left to be discovered, in particular concerning polymeric phases of C_{60}, excited state species and the electrical properties of C_{60}.

Chapter 2

Structure and Symmetry of C_{60}

2.1: Introduction: Defining a Fullerene

The structural properties of fullerenes, in particular C_{60}, have been studied extensively over the past decade [8,24,25] and a considerable understanding of the molecule's structure both in the solid and its isolated form has evolved. In this chapter the internal structure of the C_{60} molecule as well as the intermolecular structure of the solid (i.e. fullerite) is discussed with particular reference to the physical, electronic, and geometric (symmetry) structure of the molecule. The molecular modelling package Hyper-Chem. 5.1 [26] was used to construct and analyse an ideal C_{60} molecule (Appendix 1). Throughout this chapter and subsequent chapters this Hyper-Chem model will be referred to continuously as a standard reference.

2.1.1: Defining a Fullerene

In general a fullerene molecule can be defined as a closed cage molecule in which the atoms are arranged at the vertices of hexagonal and pentagonal rings. In order for such a structure to exist there must be exactly 12 pentagonal faces and an arbitrary number of hexagonal faces [19]. This definition can be deduced mathematically from Euler's theorem [27], which relates the number of vertices v, faces f, and edges e, for any polyhedron as follows,

$$v + f = e + 2 \qquad \text{Eq. 2.1.1}$$

If we consider a structure that only contains pentagons (p) and hexagons (h), then we can say that the number of faces should equal the sum of all the pentagons (p) and hexagons (h) i.e.

$$f = p + h \qquad \text{Eq. 2.1.2}$$

The number of bonds in such a molecule will be equal to the number of edges and is equal to 3v/2 since each edge joins two faces it can be written.

$$e = \frac{(5p + 6h)}{2} = \frac{3v}{2} \qquad \text{Eq. 2.1.3}$$

Combining the above equations yields Eq 2.1.4.

$$6(f + v - e) = p = 12 \qquad \text{Eq. 2.1.4.}$$

Hence 12 is the minimum number of pentagons required to close the cage, whereas an arbitrary number of hexagonal faces is allowed. Also, only molecules with an even number of atoms are possible. The smallest possible carbon based fullerene, which fits this definition is C_{20}, which forms a dodecahedron consisting of 12 pentagonal faces and no hexagonal faces.

However, such a molecule is energetically unfavourable since the presence of only pentagonal faces increases the curvature of the molecule and in turn increases the strain within the molecule [19]. The addition of hexagonal faces isolates the pentagonal faces and hence reduces the intramolecular strain. This tendency for pentagons not to be adjacent is called the isolated pentagon rule. The smallest carbon based fullerene to satisfy this isolated pentagon rule is C_{60}. Hence C_{60} is the smallest stable fullerene and is regarded as the archetype fullerene.

2.2: Structure of C_{60}

2.2.1: The Isolated Molecule

Buckminsterfullerene is a supramacromolecule, which consists of sixty carbon atoms arranged in twelve pentagonal rings and twenty hexagonal rings, as shown in figure 1.1. In the structure originally proposed by Kroto and Smalley [3], each vertex of the truncated icosahedral is occupied by a carbon atom. The carbons are in chemically equivalent environments, which is consistent with the observation of a single peak in the NMR spectrum of C_{60} [7]. Each carbon atom is connected to three other carbon atoms in an sp^2 hybridised bonding arrangement. Carbon atoms with this kind of connectivity are usually referred to as "sp^2 carbons" because the orbitals used to sigma-bond the three adjacent carbons are hybrids of the 2s orbital and the two 2p orbitals ($2p_x$ and $2p_y$). The remaining 2p orbital ($2p_z$) is responsible for the pi-bond on the hexagonal faces making the hexagons electron rich, whereas the pentagons are electron deficient. The bond length of each C-C bond has been measured by Hedberg et al [28] using electron diffraction and it was seen that the carbon pentagons have a bond length of a = 1.44Å and the carbon hexagons have a bond length of b = 1.40Å

(Figure 2.1). Using Hyper-Chem the bond lengths of an idealised C_{60} molecule were found to be a =1.44 Å, and b = 1.38Å respectively. The bond angles on the hexagonal and pentagonal faces are 120.01°and 108.00° respectively. Table 2.1 shows some physical constants for the C_{60} molecule, calculated using Hyper-Chem and compared to literature values.

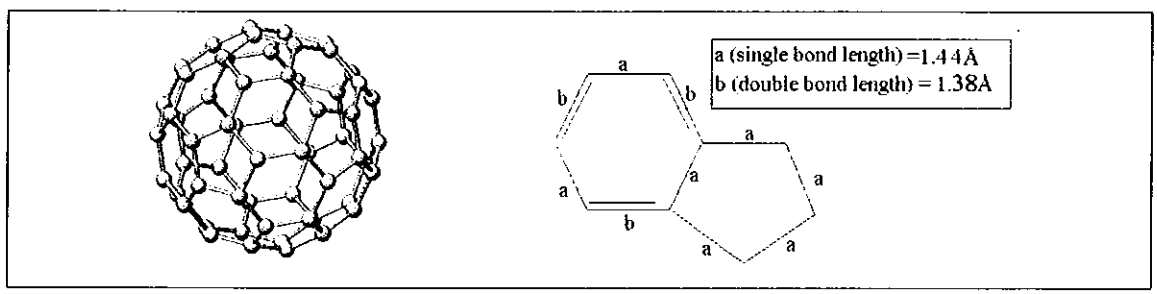

Figure 2.1: C_{60} molecule and bond lengths

Quantity	Hyper-Chem	Reference value
Average C-C distance	1.41 Å	1.44 Å [28]
C-C Bond length on a Pentagon	1.44Å	1.46Å [28]
C-C Bond length on a Hexagon	1.38Å	1.40 Å [28]
C_{60} mean ball diameter	7.14Å	7.10 Å [19]
C_{60} diameter with electron cloud	10.48Å	10.34 Å [19]
Bond angles of hexagons	120.01°	120.00 [19]
Bond angles of pentagons	108.00°	108.00 [19]

Table 2.1: Physical Constant for C_{60}

The sp^2 bonding arrangement of C_{60} gives rise to 60 delocalised electrons located around the fullerene sphere. Figure 2.2 shows a 2-D cross-section of their distribution [9]. These electrons are of particular interest when considering the electronic and optical properties of C_{60}. Their manipulation using alkali metals has led to many proposed applications of C_{60} as discussed in chapter 1. However many questions remain concerning the exact nature of the electronic configuration, particularly in the solid.

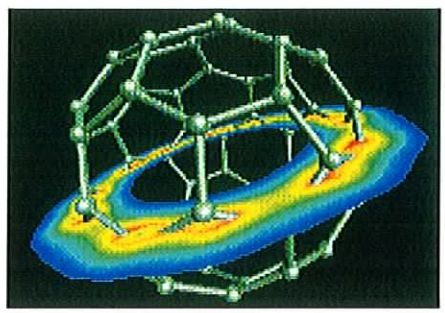

Figure: 2.2. A 2-D slice through the electronic distribution of C_{60} [9]

2.2.2: The Solid State structure of C_{60}

In the solid state, C_{60} molecules can crystallise into a number of solid state phases dependent upon temperature and pressure. At room temperature the C_{60} molecules are bound together by weak Van der Waals interactions and are packed in a face centred cubic (fcc) lattice arrangement (figure 2.3). The molecules spin freely around the lattice positions and are crystallographically equivalent due to this rapid rotation rate. This cubic structure has a lattice constant of 14.17Å, a centre to centre C_{60}-C_{60} distance of 10.02Å and a density of 1.72 g/cm^3 (corresponding to 1.44 x 10^{21} C_{60} molecules /cm^3).

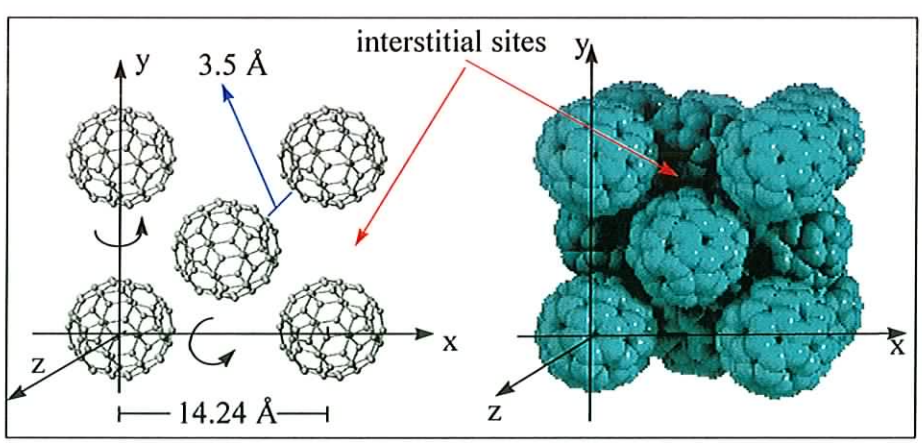

Figure 2.3: Solid state structure of C_{60}

The fcc phase is referred to as the rotary phase due to the rotation of the molecules. This rotation leads to a dynamic disorder, which decreases or 'freezes out' at low temperatures [29]. Fischer et al [30] using x-ray studies demonstrated that an ordered phase transition occurred at 249K, whereupon the x-ray form factor changed from that characteristic of fcc to that of simple cubic (sc). Above 249K, the C_{60} molecules can spin randomly around the lattice position however below this temperature the molecules can no longer spin. The 'freezing out' of the balls rotation leads to the alignment of a non-reactive (electron deficient) pentagonal face opposite a reactive (electron rich) hexagonal double bond. As a result of this alignment the C_{60} molecules at the lattice positions are no longer equivalent and the lattice constant decreases by 0.013nm [19]. This new low temperature phase of C_{60} has the characteristics of a simple cubic lattice [29] and is commonly referred to as the Rachet phase. Figure 2.4 demonstrates this phase change schematically.

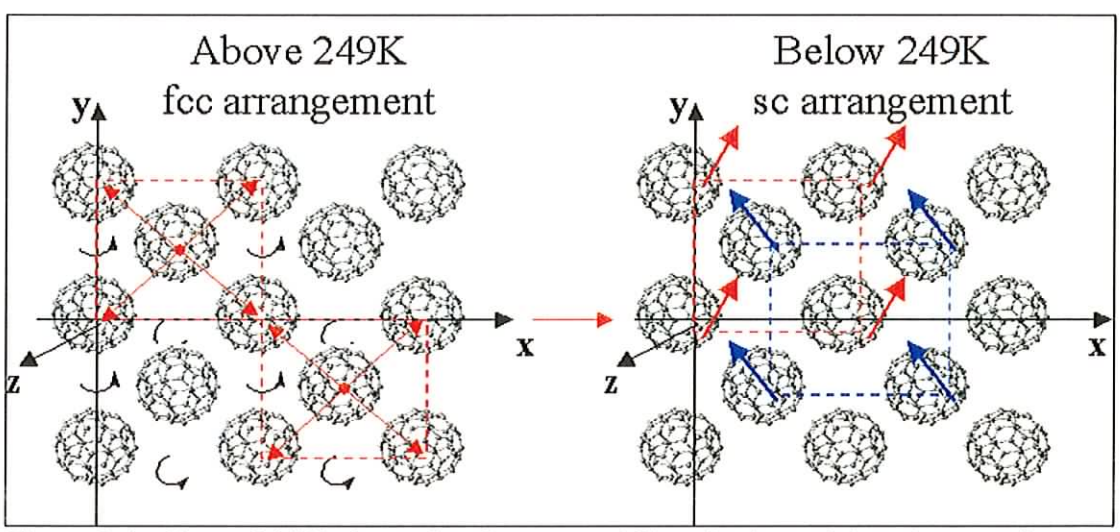

Figure 2.4: Above 249K, the molecules are rapidly spinning, giving rise to a fcc type lattice arrangement. However below 249K the spinning motion is frozen out and a simple cubic type lattice results

While the structural properties of C_{60} have been ascertained, there still remain a number of unanswered questions regarding the molecular interaction in the solid specifically with respect to the 60 delocalised electrons. It is known that in the absence of oxygen, a photoinduced polymerisation of C_{60} can occur both in solid and in solution [31,32] (discussed in Chapter 6), which demonstrates some degree of

interaction and between the C_{60} π-electrons in the solid state. However in pristine solid C_{60} it is unclear as to the nature and extent of the electronic interaction, specifically whether the molecular electrons remain located on the C_{60} molecules or whether they are delocalised across the solid. This has serious implications for any proposed electronic or optical applications for C_{60} e.g. in optical switches or luminescent displays. These questions among others will be addressed in the context of this thesis.

2.3: Symmetry

2.3.1: What is Symmetry and its significance?

The symmetry or shape of the C_{60} molecule has been directly related to many of the special properties of this remarkable molecule. Hence no discussion about the structural aspects of C_{60} would be complete without reference to symmetry. Molecular symmetry makes it possible to classify molecules according to their geometrical shape (i.e. point group). Through the use of group theory, the significance of molecular symmetry becomes much more apparent. For instance, through symmetry it is possible to derive the selection rules that govern the intensities of spectroscopic transitions, such as electronic transitions, rotational transitions and vibrational transitions. As a result, the combined use of symmetry and spectroscopy has played a vital role in the elucidation of the structure of C_{60} [6,7].

2.3.2: C_{60} Symmetry and point group

The C_{60} molecule has an icosahedral symmetry, which was originally thought to be rare in nature. However since the discovery of C_{60} and other fullerenes this symmetry group has become increasingly evident. The relevant point group for the icosahedral symmetry is I_h (table 2.2), it has 120 distinct symmetry elements and is the largest of the 32 point groups. The high degree of symmetry of the C_{60} molecule means that symmetry considerations play a very important role in the understanding of the

THE MULTIPLICATION TABLE OF THE GROUPS I AND I_h

I/I_h	E	$12C_5$	$12C_5^2$	$20C_3$	$15C_2$	i	$12S_1$	$12S_{10}^3$	$20S_6$	15σ	III	IV	
							0						
A_g	1	1	1	1	1	1	1	1	1	1			
T_{1g}	3	$\frac{1}{2}(1+\sqrt{5})$	$\frac{1}{2}(1-\sqrt{5})$	0	-1	3	$\frac{1}{2}(1-\sqrt{5})$	$\frac{1}{2}(1+\sqrt{5})$	0	-1	(R_x, R_y, R_z)		
T_{2g}	3	$\frac{1}{2}(1-\sqrt{5})$	$\frac{1}{2}(1+\sqrt{5})$	0	-1	3	$\frac{1}{2}(1+\sqrt{5})$	$\frac{1}{2}(1-\sqrt{5})$	0	-1			
G_g	4	-1	-1	1	0	4	-1	-1	1	0			
H_g	5	0	0	-1	1	5	0	0	-1	1		$(2z^2-x^2-y^2)$ x^2-y^2 xy,yz,zx	
A_u	1	1	1	1	1	-1	-1	-1	-1	-1			
T_{1u}	3	$\frac{1}{2}(1+\sqrt{5})$	$\frac{1}{2}(1-\sqrt{5})$	0	-1	-3	$-\frac{1}{2}(1-\sqrt{5})$	$-\frac{1}{2}(1+\sqrt{5})$	0	1	(x,y,z)		
T_{2u}	3	$\frac{1}{2}(1-\sqrt{5})$	$\frac{1}{2}(1+\sqrt{5})$	0	-1	-3	$-\frac{1}{2}(1+\sqrt{5})$	$-\frac{1}{2}(1-\sqrt{5})$	0	1			(x^3,y^3,z^3)
G_u	4	-1	-1	1	0	-4	1	1	-1	0			$[x(z^2-y^2),y(z^2-x^2),$ $z(x^2-y^2),xyz]$
H_u	5	0	0	-1	1	-5	0	0	1	-1			

Table 2.2: The I_h character table for C_{60}

electronic and vibrational properties of the C_{60} molecule. In reviewing the symmetry properties of C_{60} in the solid and in its isolated form, it is natural to begin with the symmetry operations for icosahedral symmetry. This group of operations has sixty elements: fifty-nine rotations, in which all vertices of the C_{60} cage move, and an identity element, in which every vertex remains fixed. The rotational symmetries of C_{60} are defined in terms of three sets of axes (a) fifteen axes of twofold symmetry, (b) ten axes of threefold symmetry, and (c) six axes of fivefold symmetry (figure 2.5).

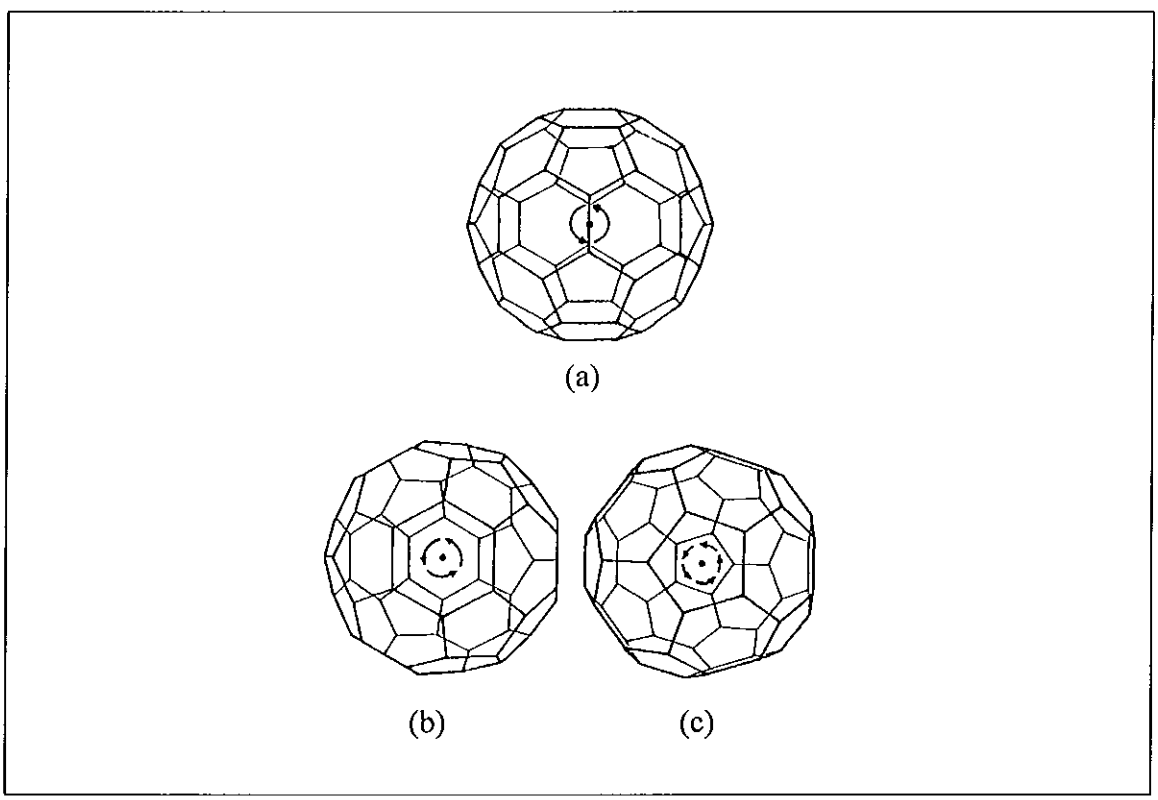

Figure 2.5: Rotational symmetries of the C_{60} molecule. (a) Twofold axes pass through opposing pairs of hexagon-hexagon edges: (b) threefold axes connect midpoints of hexagonal faces related by inversion: (c) fivefold axes connect midpoints of pentagonal faces related by inversion [33].

The two fold axes are most easily defined in terms of the carbon double bonds. Every double bond on C_{60} is matched by another double bond on the opposite side of the molecule. That is, each double bond is mapped to another double bond by inversion through the molecule's centre (figure 2.5(a)). Each such pair of bonds is associated with a twofold axis of rotation, which passes through the midpoints of both bonds.

There are thirty double bonds resulting in the fifteen twofold axes of rotation. The threefold symmetry axes lie along lines that connect the midpoints of hexagonal faces paired by inversion (figure 2.5(b)). C_{60} possesses twenty hexagonal faces and thus there are ten pairs of such faces and ten threefold axes. These axes are threefold symmetric rather than sixfold, due to the alternation of single and double carbon bonds along the edges of each hexagonal face. Finally the six fivefold axes lie along lines that connect the midpoints of opposing pentagonal faces on the molecule (figure 2.5(c)). Each pentagonal face in a pair is related to its partner by inversion and any rotation by a multiple of 72° about one of the fivefold axes maps the C_{60} molecule into itself. There are thus twenty-four unique fivefold rotational symmetry operations. The fifty-nine rotational symmetry operations (15+20+24) and the identity operation define the sixty elements of the icosahedral group, I. However we must include one more symmetry operation, before defining the full symmetry group for C_{60}.

The C_{60} molecule possesses inversion through its centre as a further class of symmetry operations. Interchanging any of the sixty carbon atoms with its opposite by inversion leaves C_{60} unchanged. Thus we can include P, the parity operator, as an additional symmetry operator for C_{60}. Combining P with the sixty elements in the aforementioned icosahedral group, I, creates a new 120-element group I_h, the full icosahedral point group. The character table for the I_h group is shown in table 2.2 and displays the 120 symmetry elements for molecular C_{60}. Using this table and group theory it is possible to obtain an expression, known as an irreducible representation, which for molecular C_{60} is,

$$\Gamma = 2A_g + 3F_{1g} + 4F_{2g} + 6G_g + 8H_g + 1A_u + 4F_{1u} + 5F_{2u} + 6G_u + 7H_u. \qquad \text{Eq.2.2.1}$$

This representation essentially describes the 46 fundamental non-degenerate modes of vibration for the C_{60} molecule [34]. When a C_{60} molecule vibrates it perturbs these elements and therefore the resulting vibrational spectrum can be discussed in terms of these symmetry elements. The frequency of vibration of any molecule is governed by the relative bond strengths and hence the σ and π electrons. As a result vibrational spectroscopy is a useful probe of the electronic properties of C_{60} and any perturbation

to its symmetry. The significance of vibrational spectroscopy and the effects of symmetry on it will be discussed in greater detail in chapter 4. However our discussion now will look at the symmetry changes in C_{60} when one moves into the solid state.

In the solid state the simplest case to consider is one where the crystal has four identical C_{60} molecules per fcc unit cell. This arrangement leads to a space group T^3_h which has a maximum point group symmetry of T_h [19]. This point group represents a lowering of the symmetry in the icosahedral molecules now placed in a fcc lattice. This occurs due to the introduction of crystal fields effects on the molecule. In fact crystal field effects are evident only very weakly in experimental measurements [29] (e.g. Raman spectroscopy) suggesting that the molecule largely retains its I_h character in the solid confirming the importance of the Icosahedral symmetry and structure to the C_{60} molecule and its derivatives

2.4: Electronic Structure of C_{60}

The structural and symmetrical properties of C_{60} can be attributed to the arrangement of the σ electrons of the single bonds, which form the icosahedral cage. However it is the π electrons which dictate the electronic properties of C_{60} and make it potentially attractive for electronic and optically based applications. In this section the electronic structure of these π electrons will be discussed, completing the picture of both the electronic and structural properties of molecular C_{60}.

The electronic structure of C_{60} is a complex 'many body' problem as there are 60x 6=360 electrons involved [4]. However, approximations can be made to simplify the problem. If weak σ-π orbital interactions are neglected, then it can be suggested that the σ and π orbitals of C_{60} are approximately pure, thus only the π-orbitals need to be considered in models of the electronic structure. Also the C_{60} molecule may be

considered as a 'big atom', with a "pseudo-nucleus" because it has a closed almost spherical electronic shell with the unique icosahedral symmetry. These two approximations allow simple theoretical descriptions of the C_{60} molecule's electronic structure.

The simplest model is the atomic orbital model. In this model the C_{60} is treated as a 'pseudo-atom' in which the carbon skeleton acts as a pseudo-nucleus and the π electrons orbit this nucleus in Bohr-like orbitals, with corresponding discrete orbital levels. The orbitals are characterised by quantised values of the orbital angular momentum L, i.e. $L = l(l+1)$ where l is the angular quantum number and is equal to l=0,1,2,3,4,5,6. These orbital levels correspond directly with the atomic orbitals of a full rotation group R_3 i.e. s,p,d,f,g,h,i. respectively. The degeneracy of these orbitals is given by $2(2l+1)$. A schematic of this model is shown in figure 2.6. It should be noted that the first five orbitals, s to g are completely filled whereas the sixth orbital h (l=5) is only partially filled. The lowest energy excitation which satisfies the La Porte selection rule ($\Delta L = \pm 1$) is from the highest occupied atomic orbital to the lowest unoccupied atomic orbital and is the l=5 to l=6 transition which is dipole allowed. The energy of this transition is $\geq$ 6eV, which would suggest that C_{60} is a transparent material. However this is clearly not the case and for this reason a more complex model known as the Hückel Molecular Orbital model (HMO) [35] must be applied to the C_{60} molecule.

The HMO model was originally designed to deal with unsaturated hydrocarbons. However over the years variations on it have allowed it to be easily and simply applied to many types of molecules. The model uses the same assumptions as the atomic orbital model but considers the effect of the carbon skeleton on the orbital energy levels. Figure 2.6 shows the resulting HMO diagram for C_{60}. In the diagram the energy in electron volts for each molecular orbital level is displayed between the vertical arrows. To the right of the arrows are the Hückel molecular orbitals of C_{60} in the ground state. The noticeable differences from the atomic orbitals is that the l= 3, 5 and 6 levels have split into a number of non-degenerate energy levels. The result of this is to allow for a much more accurate electronic structure with a symmetry

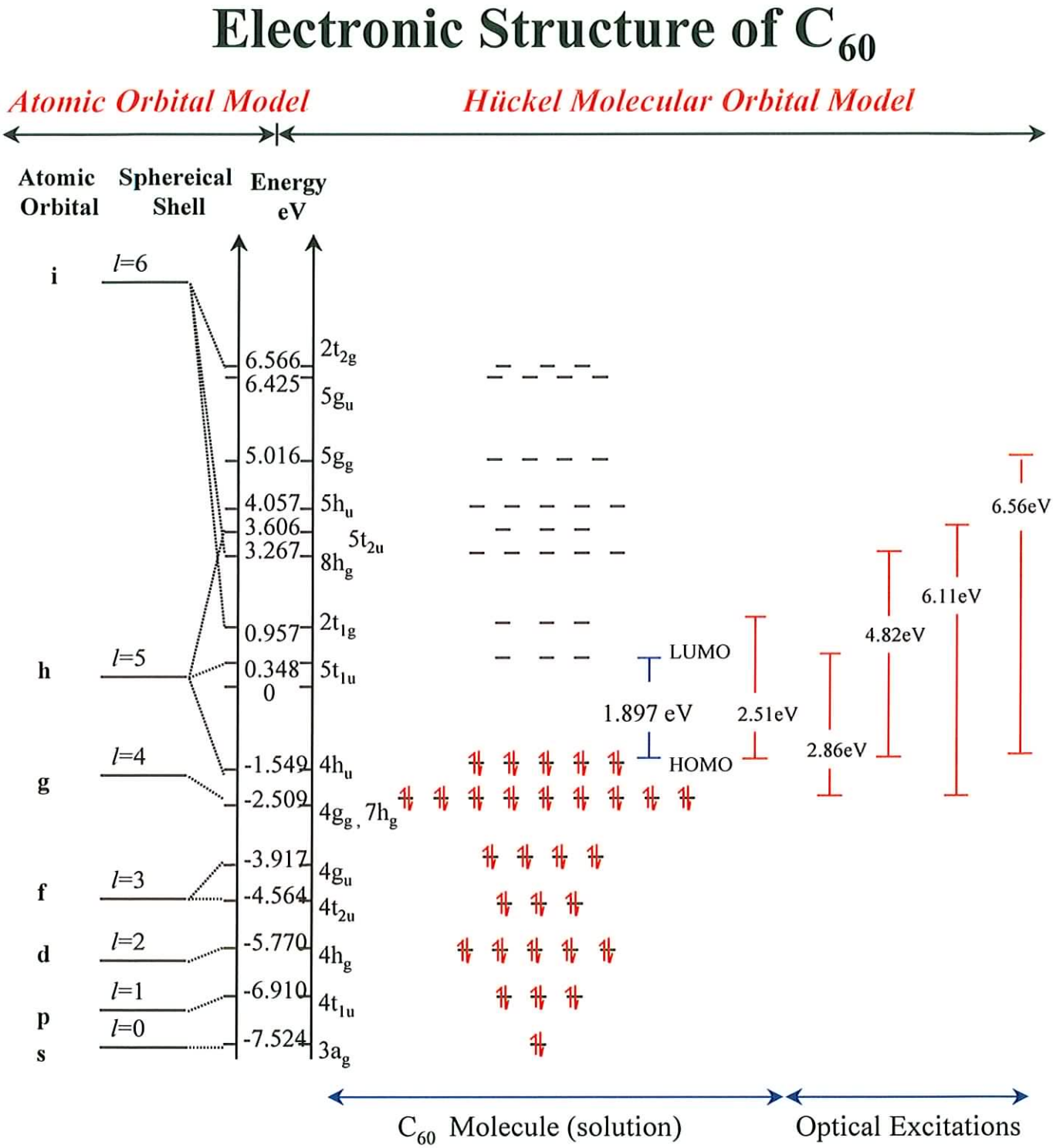

Figure 2.6: Electronic structure of C_{60}. On the left of the diagram is the Atomic Orbital model with the energy levels of a sphereical shell. The black dotted lines connect these orbitals to the pi type molecular orbitals of the HMO model on the right. The HMO model also displays the energy of some optical transitions associated with the molecule

representation. The black dotted lines connecting the C_{60} molecular orbitals to the spherical shell were drawn in accordance with Braga et.al. [36] and indicate the correlation between the molecular orbitals of I_h (C_{60}) and the atomic orbitals of R_3. It can be deduced from the diagram that the full degeneracies of the atomic orbitals are conserved in the correlation i.e.

$$l=3, \Rightarrow 4g_u 4t_{2u}$$

$$l=6, \Rightarrow 2t_{1g} + 5t_{2u} + 2t_{2g}$$

Leach [37] stated that the symmetric ground state 1^1A_g of C_{60} due to the π orbitals was

$$...3a_g^{(2)}\, 4t_{1u}^{(6)}\, 4h_g^{(10)}\, 4t_{2u}^{(6)}\, 4g_u^{(8)}\, 4g_g^{(8)}\, 7h_g^{(10)}\, 4h_u^{(10)} \longrightarrow 1^1A_g.$$

It is thus relatively easy to predict the first three excited states of C_{60}. These states have been shown below with their corresponding symmetries.

$$... 7h_g^{(10)}\, 4h_u^{(9)}\, 5t_{1u}^{(1)} \longrightarrow {}^{1,3}T_{1g},\ {}^{1,3}T_{2g},\ {}^{1,3}G_g,\ {}^{1,3}H_g \quad \text{HOMO to LUMO}$$

$$... 7h_g^{(9)}\, 4h_u^{(10)}\, 5t_{1u}^{(1)} \longrightarrow {}^{1,3}T_{1u},\ {}^{1,3}T_{2u},\ {}^{1,3}G_u,\ {}^{1,3}H_u \quad \text{(HOMO-1) to LUMO}$$

$$... 7h_g^{(10)}\, 4h_u^{(9)}\, 2t_{1g}^{(1)} \longrightarrow {}^{1,3}T_{1u},\ {}^{1,3}T_{2u},\ {}^{1,3}G_u,\ {}^{1,3}H_u \quad \text{HOMO to (LUMO+1)}$$

The lowest excitation from the Highest Occupied Molecular Orbital (HOMO) to the Lowest Unoccupied Molecular Orbital (LUMO) i.e. h_u to t_{1u} gives a value of 1.897eV as the energy gap (E_g) of C_{60} in solution. The electronic interactions of these two orbitals is shown in figure 2.7 based on Hyper-Chem calculations. It should be noted that in the simple model the corresponding transition was between l=5 and l=6 whereas here it is within the l=5 atomic orbital which is dipole forbidden (this will be discussed further in chapter 4). The next highest unoccupied molecular orbital, t_{1g}, is interesting as the first optical transition which occurs from, h_u to t_{1g}, with an energy value of 2.5eV. There are five more possible optical excitations: h_g to t_{1u}, h_u to h_g, g_g to t_{2u}, h_g to t_{2u}, and h_u to g_g all of which have been indicated on the HMO diagram with their respective E_g [4].

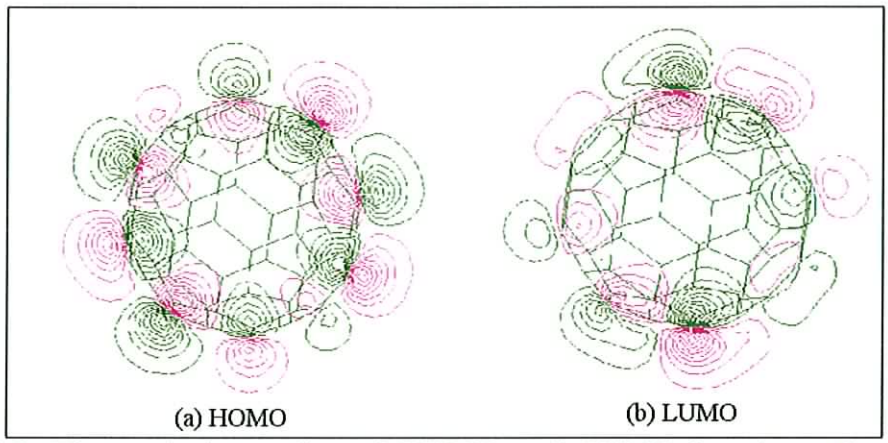

Figure 2.7: Electronic interaction of HOMO and LUMO based on Hyper-Chem calculations (a) HOMO (b) LUMO.

The charge distribution of the C_{60} molecule based on the Hyper-Chem calculations shows that the position of the carbon atoms is within the electron cloud (figure 2.8). The diameter of C_{60} is about 1nm with the electron cloud, while the diameter of the position of the carbon cage is about 0.71nm. A picture of hybridised molecular orbitals of the C_{60} molecule is also presented. Hexagons and pentagons are easily recognisable in this picture and an electron density hole is also clearly visible.

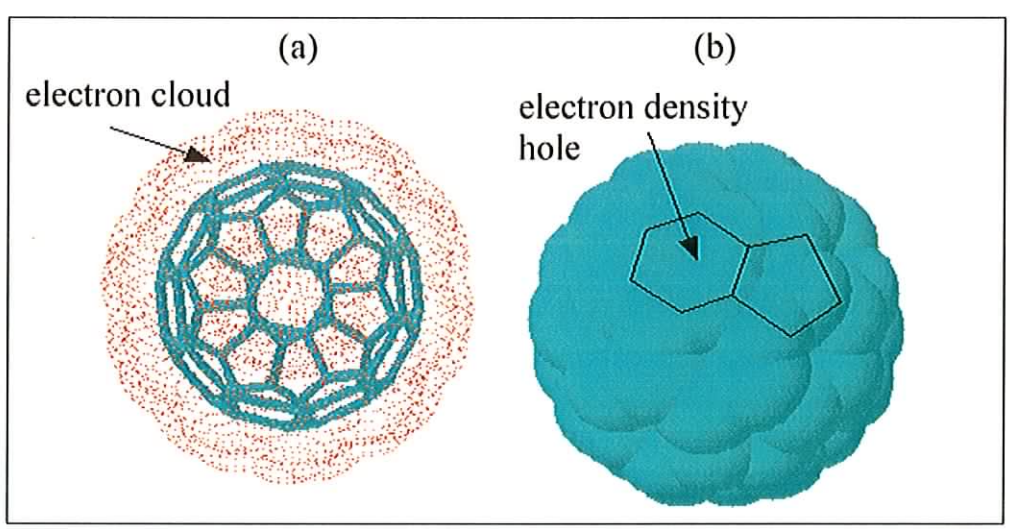

Figure 2.8: (a) electronic structure of C_{60} showing the electron cloud (b) Molecular orbitals of C_{60} pentagons and hexagons are clearly visible.

Finally, in the solid the electronic structure is still largely unknown. Band gap energies have been calculated for C_{60} in the solid state and are reported to be in the range 1.54eV to 1.35eV [19]. Such a deviation from the molecules band gap (1.89eV) implies a significant interaction between electronic states in the solid. However the question regarding the exact nature of the electronic interactions has never been answered, particularly whether the electrons remain localised on the individual molecule or if they become delocalised across the solid.

2.5. Summary:

C_{60} is a large carbon molecule which contains sixty carbon atoms arranged in 12 five membered rings (pentagons) and 20 six membered rings (hexagons) with an icosahedral symmetry I_h. In the proposed structure for C_{60}, each vertex of the truncated icosahedral (football) is occupied by a carbon atom each carbon is connected to three other carbon atoms in an sp^2 hybridised bonding arrangement which gives rise to sixty delocalised electrons distributed around the carbon cage. In the solid state, the C_{60} molecules are bound by weak van der Waals interactions and at room temperature are packed together in an fcc lattice arrangement, which causes a reduction in symmetry. Many questions still remain concerning the electronic configuration of the solid state, and it is hoped that within the context of this thesis that some of these questions may be answered.

Chapter 3

General Experimental

3.1: Introduction

In this chapter a general description of the various instruments and procedures used throughout the research is given. A broad range of instruments and techniques has been used and adapted through the course of this study and where necessary further details about specific experimental set ups will be given in the relevant chapters.

3.2: Fullerene Synthesis and Purification

Fullerenes can be synthesised by virtually any high temperature process that produces carbon atoms in the gas phase and provides annealing for clustering of the carbon atoms into linear carbon chains and monocyclic rings of C_2 to C_{18}. Which can then assemble themselves into fullerene molecules C_n where n= 60, 70, 84 etc. [38]. Thus the production of fullerenes revolves around the ability to produce gaseous carbon atoms.

To date, all commercially available fullerenes are synthesised via the Arc vaporisation of graphite in methods similar to the original method of Krätschmer [8]. Arcing graphite is an efficient process for the production of gaseous carbon. Fullerene production has typically employed the arcing of two graphite rods, as shown schematically in figure 3.1.

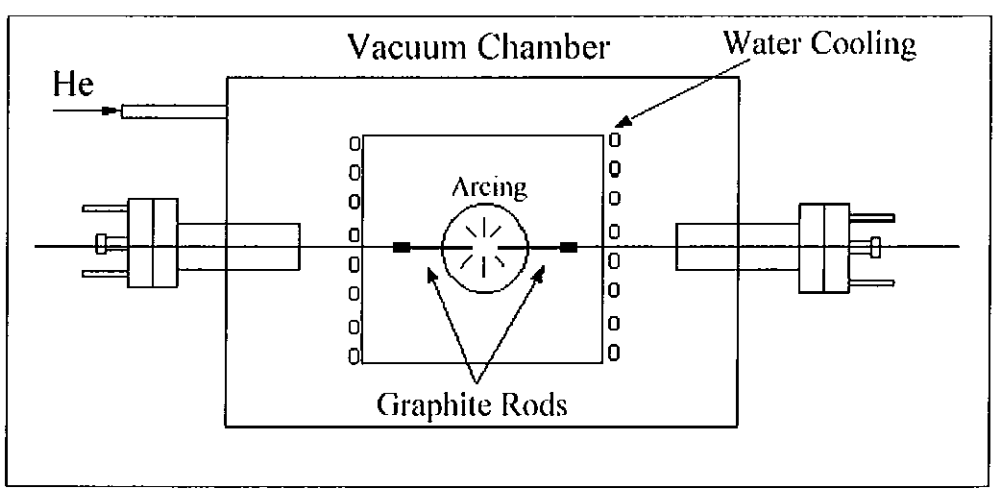

Figure 3.1: Schematic of a Fullerene Generator for the production of gram quantities of Fullerenes. [27]

The graphite rods (electrodes) are brought into close contact with each other and an arc is struck in an atmosphere of 100-200 Torr of helium or argon. To sustain the arc, a voltage of ~20V (AC or DC) is necessary [13]. For a graphite rod of 6mm diameter, about 50-200A may be consumed. Generally, spectroscopically pure graphite of high porosity is used so that the evaporation rate is high. The resultant soot is collected on a water-cooled surface such as the inner walls of the vacuum chamber. After sustaining the arc for several minutes, the vacuum is broken and the soot collected. At this point the carbon soot consists of a mixture of fullerenes i.e. C_{60}, C_{70}, higher fullerenes, nanotubes, carbon onions and some amorphous carbon. The ratio of the components is dependent upon the concentration and type of gas in which the arc is struck. A typical yield of C_{60} is in the order of 100mg per day [8].

The laser vaporisation of graphite in a helium atmosphere which was originally used by Kroto and Smalley to identify C_{60} results in a relatively higher yield of fullerenes compared to the arc process. However the capital cost is high and the energy efficiency of the lasers are relatively low resulting in a much higher cost of the fullerenes produced [11]. Thus the laser vaporisation of graphite is not a likely candidate for the commercial production of fullerenes.

No matter which process is utilised to generate fullerenes, the fullerenes must be separated from the soot for useful research and applications. Since fullerenes can be sublimed, it is possible to separate the fullerenes from the soot by vacuum sublimation [39]. However the separation process that is most often used takes advantage of the fullerene's solubility by extraction with an organic solvent such as benzene or a substituted benzene [40]. Toluene is typically used, but higher fullerenes (above C_{84}) have limited solubility in toluene. Due to this relatively low solubility of fullerenes in most solvents, large volumes of solvent are required to produce meaningful quantities of fullerenes. Once extracted, the fullerenes are typically recovered by evaporation of the solvent, which is somewhat energy intensive. If a purified compound such as C_{60} is desired, which was the case in this study, then the various molecular weight compounds must be fractionated by differential solubility in solvents or by chromatography. Solid phases that are known to provide fractionation are alumina,

silica gels, activated carbon and some organic phases [27]. These solvent extraction and fractionation steps contribute significantly to the cost of fullerenes.

The C_{60} sample used throughout this study was purchased from Hoechst AG. and was gold grade C_{60} power. The sample had residues of,

Toluene.....0.0089%
Acetone.....0.051%
Diemethylether.....0.46%

3.3: Preparation of Solutions of C_{60} for Spectroscopy

Prior to solution and film preparation the C_{60} was out gassed in a vacuum oven for 24 hours at 100°C [27].

Two solvents were used to make the C_{60} solutions used for the spectroscopic measurements. The first was chlorobenzene (5.2g/l) and the second was toluene (3.4g/l). The solutions were filtered through a 0.5μm filter to remove any particles which could potentially contribute to non-linear scattering [48]. The solutions were then placed into quartz cuvettes (1cm for spectroscopic measurements or 1mm for transmission measurements). For excited state measurements and transmission measurements the samples were degassed by bubbling nitrogen gas through them for ~40 minutes. It should be noted that for triplet state measurements some gas remained in the cuvettes, providing the option of illuminating at a solution/ cuvette interface or through the cuvette/ gas interface into the solution.

The solutions used for the electrochemistry were made up in dichloromethane (DCM) with a 0.5mM concentration of C_{60}. The support electrolyte used was tetrabutyl ammonium tetrafluoroborate ($TBABF_4$) (0.1mM) and as with the spectroscopic solutions, the samples were degassed for ~40 minutes before use. All the solutions were stored in the dark and kept at room temperature.

3.4: C_{60} Film Depositions

There were two types of C_{60} films fabricated throughout this study, vapour deposited films (or evaporated films) and drop cast films. The evaporated films were fabricated on glass and indium tin oxide (ITO)/glass coated substrates, whereas the drop cast films were formed on platinum (Pt) foil and a glassy carbon disc. The drop cast films were used exclusively for electrochemistry. All the substrates were cleaned by boiling in propanol for ~40 minutes prior to deposition.

3.4.1: Experimental Set-up for Evaporated films

The sublimed C_{60} films were vapour-deposited onto the substrate by resistively heating a tungsten boat containing C_{60} powder. The evaporation unit was an Edwards coating system E305A. The experimental set-up (figure 3.2) consisted of two heating electrodes across which the tungsten boat containing the C_{60} soot was placed. The substrates were placed above the boat with a shutter in between, which was preferentially opened or closed to expose or protect the sample (film) from exposure to the evaporated material

The evaporation chamber was evacuated to 10^{-5} to 10^{-6} mbar with the shutter closed. The tungsten boat was then heated by gently passing a current, which was controlled from an in built power supply. Once the current reached ~60A the shutter was opened and the current was then gradually increased to ~100A. The deposition continued until an acceptable amount of material had been deposited. The shutter was then closed and the system allowed cool for an hour. The films were then stored in the dark at room temperature. In some cases an aluminium layer was deposited on top of the C_{60} layer utilising the same procedure.

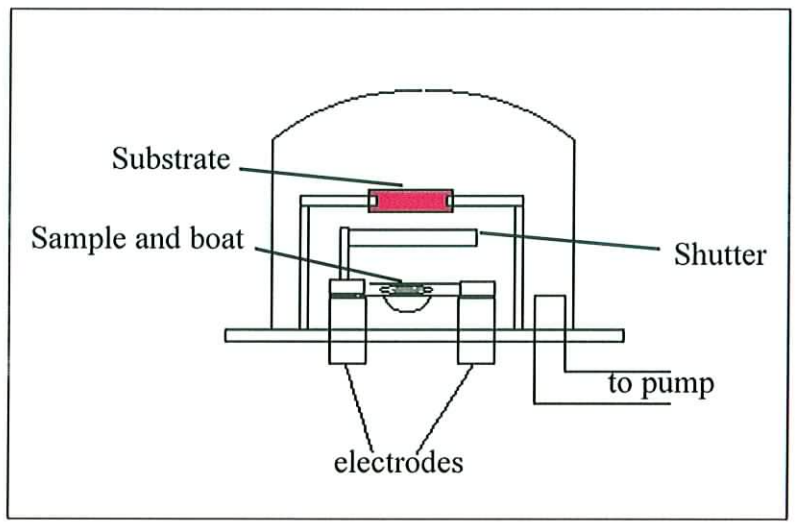

Figure 3.2: Schematic of film preparation apparatus.

3.4.2: General Experimental Set-up for Drop Cast films

The drop cast films were formed on a platinum foil (5x5mm) substrate and a glassy carbon disc of diameter 3mm. The substrates were cleaned in boiling propanol, then washed in toluene and finally allowed to dry at 45°C. The C_{60} films were then deposited on the substrates by the successive fast drying of thin layers of a concentrated solution of C_{60}. This technique involved the dissolution of C_{60} in toluene to give a 3.4g/l solution. Using a 0.5ml pipette, a drop of this solution was placed on to the substrates, which were maintained at 60°C by a heating stage. As the solvent evaporated the solution rapidly became saturated until only a thin layer of C_{60} remained on the substrate. This procedure was repeated several times until a visible C_{60} coating appeared. In the case of the Pt foil the reverse side was painted with an insulating laquer. The films were carefully stored in the dark at room temperature.

3.4.3: Determination of Film Thickness

Film thickness for the evaporated films, was determined from the absorption of thin films and a set of published calibration curves of absorbance against film thickness at

610nm and 436nm [42][43]. Absorption spectra were recorded using a Shimadzu UV-2101PC Absorption Spectrophotometer (section 3.5.3).

According to the Beer-lambert law, [44] absorbance can be defined as

$$A = \varepsilon . c . d \qquad \text{(Eq. 3.1)}$$

where A is the absorbance at a specific wavelength, ε the corresponding extinction coefficient for that wavelength, c the concentration and d the path length. If there are two absorbances, A_1 and A_2, for a solid material at the same wavelength then it can be said that,

$$\frac{A_1}{d_1} = \varepsilon . c \qquad \frac{A_2}{d_2} = \varepsilon . c$$

and hence $$\frac{A_1}{d_1} = \frac{A_2}{d_2} = \varepsilon . c$$

Therefore if d_1, A_1 and A_2 are known then d_2 can be easily found from equation 3.2,

$$d_2 = \frac{A_2}{A_1} d_1, \qquad \text{(Eq 3.2)}$$

In this study a number of film thicknesses were produced in the range 0.3μm to 0.85μm.

3.5: Spectroscopic Methods

A number of spectroscopic methods where employed during this study to examine C_{60} both in solution and solid form. The spectroscopic methods used allowed the exploration of these phases of C_{60} in their ground states (Raman and IR), in their excited states (flash-photolysis and high intensity Raman spectroscopy) and their transitions to and from excited states (UV/Vis, Fluorescence).

3.5.1: Raman Spectroscopy

Raman measurements for both the ground state and excited state studies were taken using an Instruments S.A. Labram 1B Raman Spectrometer. The Labram system is a confocal Raman imaging microscope system. An in built Helium-Neon laser (632.8nm, 11mW) and an external Lexel 100-Argon ion (514.5nm, 50mW) were available as sources. The external Lexel 100-Argon ion was used for transmission and excited state studies. For conventional operation, the light is imaged to a diffraction limited spot (typically 1 μm) via the objective of an Olympus BX40 microscope. The scattered light is collected by the objective in a confocal geometry, and is dispersed onto a Peltier cooled CCD array by one of two interchangeable gratings, 600 lines/mm or 1800 lines/mm, allowing the range from $150cm^{-1}$ to $4000cm^{-1}$ to be covered in a single image, or with greater resolution in a combination of images respectively. With the latter, a spectral resolution of $1cm^{-1}$ per pixel is achievable. The confocal, microscopic system allows measurements of powdered samples with no further sample preparation, direct measurement of liquids and solutions, as well as thin films. Low temperature Raman measurements were obtained using the same system in conjunction with a Linknam cooling stage, (77K-600K)

In this study the Raman spectrometer was also used as an extremely sensitive luminescence spectrometer. The confocal geometry the Labram system can detect low level luminescence where the laser is resonant with the material. A Perkin-Elmer LS50B Luminescence Spectrometer was also available which is capable of measuring

fluorescence or phosphorescence using a gated photomultiplier with a signal to noise ratio of 500:1rms. However the Labram system is equipped with a rugged, compact, Peltier-cooled CCD which exhibits an exceptionally low dark current (250 electrons/pixel/hour) and high dynamic range (65535 counts max). The high sensitivity of the Labram is due to an improved signal to noise ratio (S/N) obtained by combining the charges of adjacent illuminated pixels and ignoring the dark signal produced from the non-illuminated pixels. As a result, according to Felgett's S/N rule [45] the signal increases directly with the number of pixels combined but the noise only increases with the square root of the number of pixels hence the s/n is greatly improved. Allowing low level luminescence at resonant wavelengths to be detected.

3.5.2: Infra-Red Spectroscopy

Infra-Red (IR) measurements were taken using two instruments, a Mattson Infinity FTIR Spectrometer and a Nicolet Continuum FTIR microscope. The Mattson Infinity spectrometer is a single-beam, Michelson interferometer based, Fourier transform infra-red spectrometer. It has an operating range in the mid and far infrared, covering $200cm^{-1}$ to $5000cm^{-1}$ with a resolution of $0.5cm^{-1}$. Measurements taken in solution were performed using a standard IR solution cell and solid measurements were done by making KBr discs with an approximate ratio of 50:1 KBr:C_{60}.

The Nicolet Continuum FTIR microscope was use primarily for photopolymer measurements. This instrument uses infinity corrected optics which transmits light in the form of a collimated beam rather than the focused beams used by other infrared microscopes. Using a collimated beam greatly minimises spherical aberrations and provides a flat field of view at the sample giving a good signal-to-noise ratio.

It should be noted that although Raman and IR spectroscopes are employed to measure the ground state spectroscopic properties of C_{60} it is only IR spectroscopy, which truly is a ground state measurement. Since the wavelengths used in the Raman spectroscopy are weakly resonant.

3.5.3: Absorption (UV/ Visible) Spectroscopy

UV/ Visible (UV/ Vis) measurements were taken using a Shimadzu UV-2101PC. The Shimadzu UV-2101PC is a double beam, direct ratio photometric measuring system using a dynode feedback method. It has a photometric range of -4 to ~5 in Absorbance, 0 to ~999.9% in Transmittance. It employs a 50W halogen lamp and a deuterium lamp. Spectra are dispersed by a Czerny-Turner monochrometer with a high performance blazed holographic grating, and detected by an R-928 photomultiplier. The instrument has a range of 190nm to 900nm. Solution spectra were taken in a 1cm quartz cell with the solvent system as reference whereas solid samples were mounted in the cell compartment and run against a blank substrate as reference.

3.6: Excited State Spectroscopy

The excited state spectroscopy of C_{60} was performed using a flash-photolysis system arranged in a right angle configuration as shown in figure 3.3. The C_{60} in chlorobenzene (2g/l) was excited using a 20ns 355nm frequency tripled, Q-switched Nd^{+3}:YAG laser pulse and the broad band light source was a Xe Arc lamp (190-800nm). The detector used was an intraspec-CCD. The solution sample was placed into a 1cm cuvette and degassed for 40 minutes prior to measurement. In the solid a thin film was placed into a cuvette containing deionised water for cooling purposes.

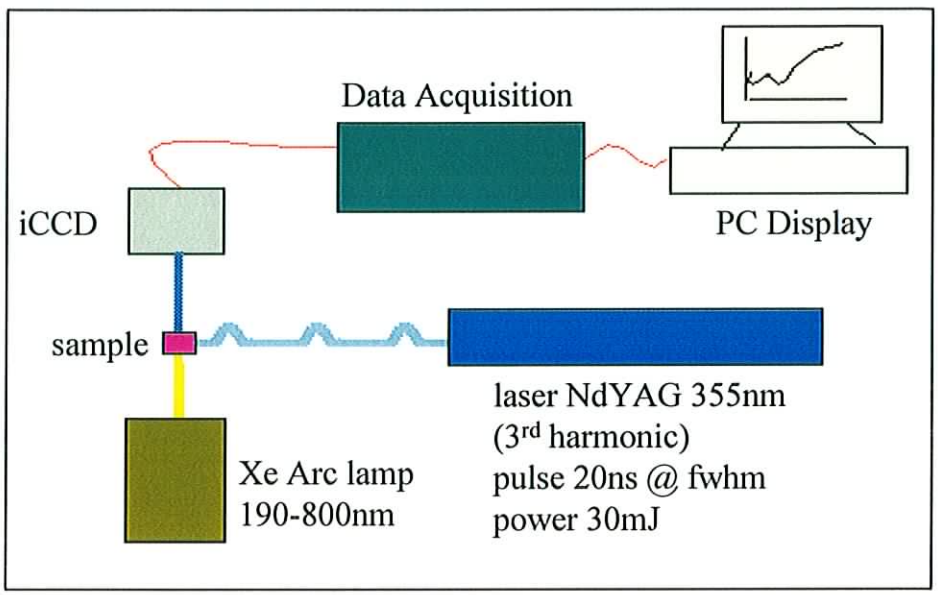

Figure 3.3: Schematic of Flashphotolysis system used for trasnisent absorption of C_{60}

3.7: Cyclic Voltammetric Measurments

The cyclic voltammetry measurements in solution were performed using a Sycopel Scientific DD10M potentiostat. The solvent system was C_{60} (0.5mM) in dichloromethane (DCM) with tetrabutyl ammonium tetraflouroborate ($TBABF_4$) (0.1M) as support electrolyte. The analysis was carried out at room temperature using a two electrode cell. The cell consisted of a platinum rotating disc electrode, as the working electrode (i.e. the electrode at which the species of interest are produced) and a carbon rod was used as the auxiliary electrode (i.e. current sink usually to protect the reference electrode).

The Pt rotating disc electrode was vertically mounted in the shaft of a synchronous controllable-speed motor and rotated with a sweep rate of 100mV/s about an axis perpendicular to the plane of the Pt disc. As a result of this the motion the fluid in an adjacent layer is continuously forced away from the electrode surface and replenished by a fresh layer from the bulk solution in a pump like action. The rotating disc electrode provides an efficient and reproducible mass transport and hence analytical

measurements can be made with high sensitivity and precision. The electrode surface was treated prior to analysis by polishing with an alumna slurry on felt.

The electrochemistry of the solid films was performed using an EG&G model 363 potentiostat. The solvent system was Acetonitrile (MeCN) with $TBABF_4$ (0.1M) as support electrolyte. The C_{60} was drop cast from a toluene solution onto either Pt-foil electrodes (5x5mm) or onto a glassy carbon electrode (3mm diameter) to form the working electrode. The auxiliary electrode was a Pt-wire and a Saturated Calomel Electrode (SCE) was used as the reference. All the cyclic voltammetric measurements where performed under nitrogen.

The Raman spectro-electrochemical measurements were performed exclusively in a reflection geometry using the Instruments S.A. Labram 1B Raman Spectroscopic microscope as shown in figure 3.4. The electrochemistry was performed as described above for the drop cast films. However Raman measurements were recorded in situ by holding the film potential at a required voltage to produce a specific ionic species. The Raman spectrum was then recorded for that species, for 1 second before the cyclic sweep of potential was resumed.

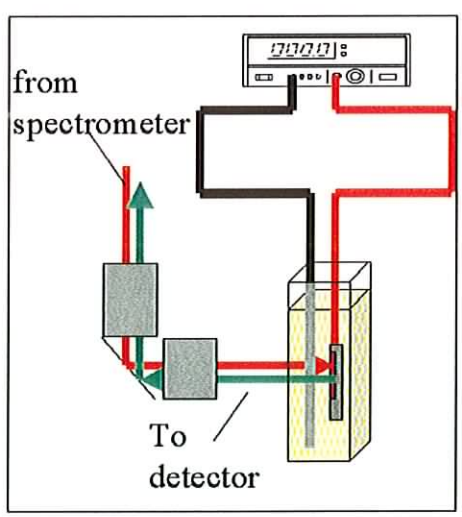

Figure 3.4: Spectroelectrochemistry arrangement in reflection geometry.

The Tetrabutyl Ammonium Tetraflouroborate used throughout this study as the support electrolyte was synthesised as follows: Tetrabutyl ammonium hydrogen

sulphate (100g) was weighed out and dissolved in the minimum amount of water required. Sodium tetrafluoroborate (32.27g) was weighed out and similarly dissolved in the minimum amount of water required. Both solutions were then added together in a large extraction funnel. A white precipitate was observed as dichloromethane (60ml) was added to the funnel to extract the product. The mixture was then shaken and some ice added to lower the solubility of the product in water. The dichloromethane was removed and diethyl ether (300ml) was added to the resulting solution while the solution was stirred rapidly. The product was then filtered off and dried in a vacuum oven for several hours.

3.8: Solid State Electronic Measurements

Vacuum evaporated C_{60} thin films of varying thickness were prepared on an ITO electrode. Aluminium was employed as a top electrode thus forming a sandwich type structure as shown in figure 3.5. The samples were then mounted in a cold finger of a closed cycle helium refrigerator and electrically contacted. The set-up was then mounted in a cryostat, which could be evacuated to 10^{-6} mbar. The electrical properties of the structure were monitored using a Keithley electrometer and power source.

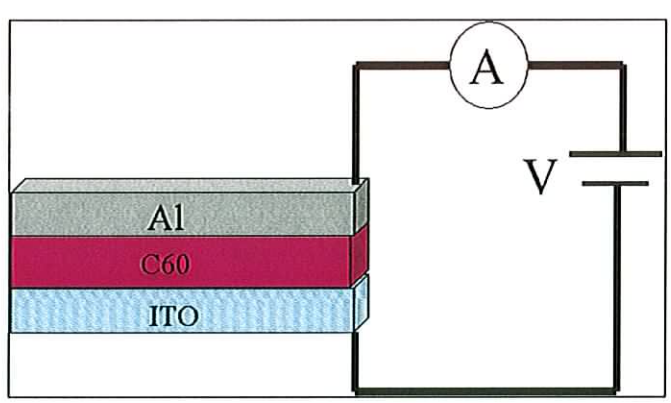

Figure 3.5: Schematic of sandwich structure experiment

3.9: Methods Used To Stabilise Lattice

Two methods were examined to help stabilise the C_{60} lattice against electronic and photo-induced degradation processes. The first method was thermal annealing and the second method was clathrate formation or solvent inclusion.

3.9.1: Thermal Annealing of C_{60} films

The evaporated thin films where annealed by postdeposition heating in a Varian vacuum oven at 200°C at a pressure of ~10^{-5} mbar for 100 hours. The temperature was somewhat arbitrarily chosen to be sufficiently below the sublimation temperature. The absorption spectrum of the films was recorded occasionally to monitor the changes during the heating process. After the annealing process the films were examined using optical and electron microscopy, powder x-ray analysis and Differential Scanning Calorimetry (DSC). Powder x-ray diffraction measurements were taken using the CuK αline (0.154nm) and DSC measurements were performed using a Rheonmetric Scientific DSC.

3.9.2: Solvent Inclusion into C_{60} films

Chlorobenzene, N,N diethtlaniline (DEA), hexane and pentane solvent molecules were individually included into the C_{60} lattice of the evaporated films by a slow evaporation method. This involved placing ~10mls of the solvent into a Petri dish, a C_{60} film (on a glass substrate) was then attached onto the inside of the dish's lid as shown in figure 3.6. The absorption spectrum of the film was monitored hourly and only after consecutively consistent spectra of the film were obtained did further analysis proceed. The time of exposure of the individual solvents ranged from 4-8 hours. The films were then analysed using optical and electron microscopy, powder x-ray diffractions and DSC as with the annealed films.

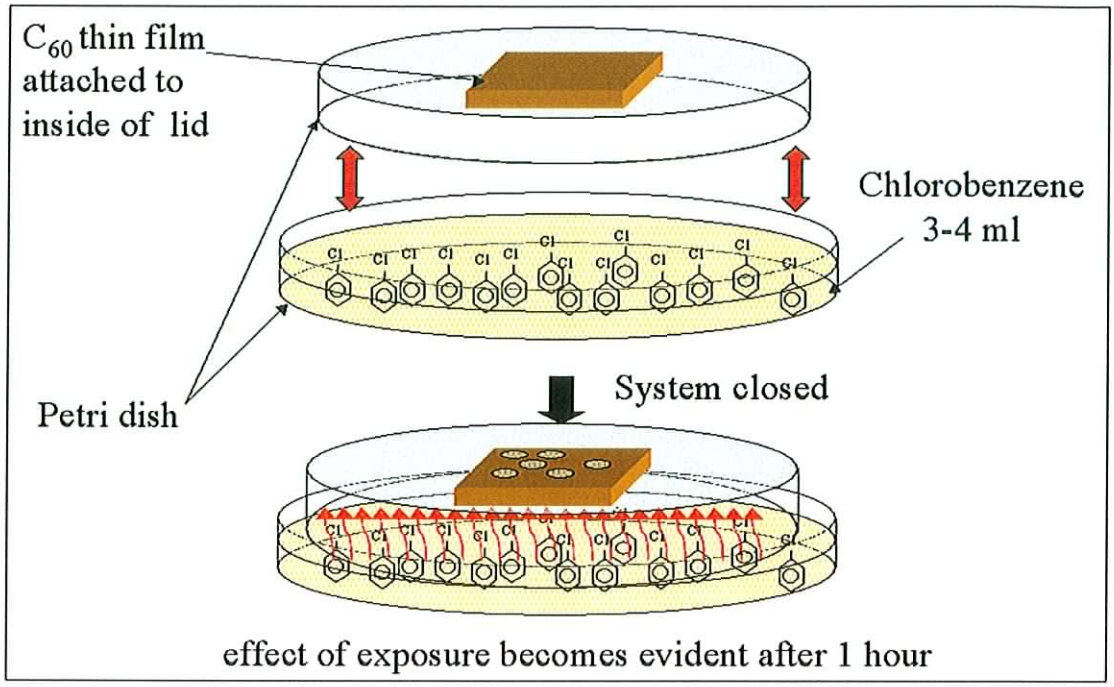

Figure 3.6: Set-up used to exposed solvent vapours to C_{60} evapourated films

3.10: Summary

A broad range of experimental techniques has been utilised throughout this project to study the optical and electronic properties of C_{60}. Nevertheless the techniques discussed in this chapter can be divided up into specific types of analysis. For example IR and Raman spectroscopy give information on the symmetry and structural properties of a molecule whereas electronic spectroscopy (i.e. UV/Vis and luminescence) gives details of the optical properties of the sample, the electronic configuration and charge transfers states. Further information can be derived from these spectroscopic techniques by varying the intensity of the light used or the wavelength, for example resonant Raman spectroscopy or transient spectroscopy. These techniques yield the same information as above but for excited state species and may also be used to induce and monitor the evolution of photochemical reactions.

Alternatively, information regarding the electronic structure of a system may be obtained through the use of electrical methods such as cyclic voltammetry. In this

technique ionic species are produced by electron injection (reduction) or electron removal (oxidation) due to the application of specific voltages. The information, which can be derived from this type of experiment, can allow the estimation of electron affinities, ionisation potentials and diffusion coefficients for a particular molecule [46]. However in this study cyclic voltammetry is used exclusively for the generation of ionic species which contribute to the conduction processes in solid state C_{60}. Once these species are generated and their influence on the conduction process assessed then a direct comparison to similar C_{60} species produced optical can be made hence a good understanding of the optical properties of C_{60} is essential.

Chapter 4

Low Intensity Optical Spectroscopy

4.1: Introduction

Throughout the development of the field of fullerene research, optical spectroscopy has played an important role. The research activities of Krätschmer and Huffman, which ultimately led to the recognition that fullerenes could be produced in substantial quantities in a carbon arc [8], were driven by their interest in the strong 5.7eV maximum in the absorption spectrum of interstellar dust [47]. Although the proposition that fullerenes were responsible for this feature appears to be incorrect, their work made fullerenes available in large quantities, having a huge impact on the intensity of research activities.

The range of optical spectroscopes available constitutes a valuable tool for the analysis of the electronic properties of new materials such as the fullerenes. In particular vibrational and electronic spectroscopy have proven to be valuable probes of these materials [34]. The field of study of the optical properties of fullerenes is broad and impossible to fully encompass within the scope of this thesis. The optical responses of the isolated C_{60} molecule have been studied extensively and match well with theory (chapter 2, Hyper-Chem) however there remain many open questions concerning those of the solid state [34]. In this chapter the ground state vibrational and electronic spectroscopic properties of both will be analysed and experimental results will be discussed in terms of molecular versus solid state behaviour. Although some gas phase measurements have been reported in literature [48] for the isolated molecule, solution measurements are more accessible, and the absence of any reported solvato-chromic behaviour indicates that solvated fullerenes are a good approximation to isolated molecules.

4.2: Vibrational Spectroscopy

4.2.1: Introduction

Since their discovery, fullerenes have been exposed to numerous methods of analysis, which have helped to elucidate their structure and properties. One of the most common techniques used in the initial research was Raman spectroscopy [39,44,]. In

recent years Raman spectroscopy has become an extremely useful tool, due to advances in detector technology with the advent of charge coupled detectors (CCDs). Raman spectroscopy is based on an optical scattering process. When light passes through a medium there are scattering processes and absorption processes in operation. The scattering processes can be either elastic (Rayleigh scattering) or inelastic (Raman scattering). It is this inelastic interaction of the photon with the medium that essentially gives rise to the field of Raman spectroscopy [49]. Another useful tool in the elucidation of fullerene properties is infrared spectroscopy [7,44]. It is however, one which seems to be somewhat under used in the area of fullerene research. IR spectroscopy is closely related to Raman spectroscopy, since they are both molecular spectroscopy techniques, which involve vibrational transitions, accompanied by rotational transitions. One difference between these two types of spectroscopy, which is of interest to this study is that IR spectroscopy is not resonant with the electronic transitions and hence it is a true representation of the ground state properties of a molecule. Raman spectroscopy on the other hand is resonant at the particular wavelengths and can thus form excited states.

4.2.2: Vibrational Spectroscopy of C_{60}

Vibrational interactions have a considerable influence on the optical and electronic properties of fullerenes both in the solid state and in their isolated forms. The C_{60} molecule has 3(60)-6 normal modes of vibration and thus 174 vibrational degrees of freedom. Due to its icosahedral symmetry, the modes are highly degenerate and the number of fundamental non-degenerate vibrational modes is reduced to 46 [34]. They are described by the irreducible representation:

$$\Gamma=2Ag+3F1g+4F2g+6Gg+8Hg+1Au+4F1u+5F2u+6Gu+7Hu \qquad \text{Eq.2.2.1}$$

This expression has been discussed in chapter 2 in terms of symmetry. In this chapter we will see the relevance of this expression to the prediction of bands in the Raman and IR spectra of the molecule as well as to the electronic structure of the molecule.

The 46 non-degenerate modes of vibration predicted by this expression can be reduced further by a set of selection rules [44] for both IR and Raman spectroscopy. These rules can be summarised as follows,

1) For a vibration to be IR active there must be a change in the dipole moment of the molecule i.e. $d\mu/dr$ at the mean of the vibration is non-zero where r is the bond length and μ is the dipole moment.

2) For a vibration to be Raman active there must be a change in the polarisablity tensor, α i.e. $d\alpha/dr$ is non-zero

Due to these selection rules, only the $2A_g$ and $8H_g$ modes are Raman active, thus the Raman spectrum for C_{60} should be dominated by ten strong lines. The remaining 36 modes are silent in the isolated C_{60} Raman spectra. Similarly in the IR spectra the selection rules only permit four active modes i.e. $4F_{1u}$, the remainder being silent. In literature, vibrational spectroscopic measurements of fullerenes have predominantly been performed in the solid state [8,29,39] and indeed, the spectra are dominated by 10 strong lines in the case of Raman and four in the case of infrared, table 4.1(a) and (b) [50] shows the positions of these modes respectively.

Table 4.1 (a): Raman modes

ref.[7] Crystal/ cm^{-1} (40K)	ref.[8] Film /cm^{-1} (20K)	Calculated /cm^{-1} [9,10]	Assignment /cm^{-1} [42,51]
497.5	497.5	497.5	$A_g(1)$
1468	1470	1470	$A_g(2)$
272	273	273	$H_g(1)$
428	432.5	432.5	$H_g(2)$
709	711	711	$H_g(3)$
772	775	775	$H_g(4)$
1099	1101	1101	$H_g(5)$
1252	1251	1251	$H_g(6)$
1426	1426.5	1426.5	$H_g(7)$
1577.5	1577.5	1577.5	$H_g(8)$

Table 4.1(b): IR modes

ref.[7] Crystal /cm^{-1} (40K)	ref.[8] Film /cm^{-1} (20K)	Calculated /cm^{-1} (Hyper-Chem)	Assignment /cm^{-1} [42,51]
527	533.5	526.5	$F_{1u}(1)$
579	580.5	575.8	$F_{1u}(2)$
	1187	1182.9	$F_{1u}(3)$
1425	1426.5	1429.2	$F_{1u}(4)$

It should be noted however that the calculated modes for both the Raman and IR spectra are based on the isolated molecule. Since the peaks match with those observed for the solid state it can be concluded that the effect of the solid state of C_{60} on the vibrational spectrum as measured by Raman and IR, is extremely weak. Also important is the effect of resonance. IR spectroscopy is the only true ground state vibrational analysis of C_{60}, since C_{60} is slightly resonant at most laser wavelengths used in Raman spectroscopy i.e. 633nm and 514.5nm. However the effect of this weak resonance is small at low intensities and the Raman spectrum of C_{60} can be taken as been representative of the ground state vibrational character.

Figure 4.1 shows the Raman spectrum of C_{60} soot measured by the Labram at a wavelength of 633nm. The spectrum contains six clearly visible C_{60} peaks. The four peaks which are not clearly identifiable are the H_g modes of vibration at ~429cm^{-1}, 709 cm^{-1}, 1100 cm^{-1} and 1576 cm^{-1}. In the solution spectrum only four peaks are clearly distinguishable at 265.8cm^{-1}, 490.1cm^{-1}, 1468.2cm^{-1} and 1564.5cm^{-1} (figure 4.2). The reason for this is due to the solvent peaks in the solution phase and the spectrometer sensitivity [31,50]. In thin film form at room temperature eight modes of vibrations were detected with only, the $H_g(2)$ and $H_g(5)$ modes not distinguishable (figure 4.3). However at low temperatures (77K) the ten allowed modes of vibration are clearly visible (figure 4.3). The detectable peaks in all the Raman spectra have been outlined in table 4.2. It can be seen from all the spectra that the two A_g modes are present at approximately 490cm^{-1} ($A_g(1)$) and 1469cm^{-1} ($A_g(2)$). These modes are the strongest peaks present in the ground state C_{60} Raman spectrum. The $A_g(1)$ represents the contraction of the pentagons (i.e. the pentagonal pinch mode) whereas

the $A_g(2)$ mode is representative of the expansion of the hexagonal rings (i.e. hexagonal breathing mode).

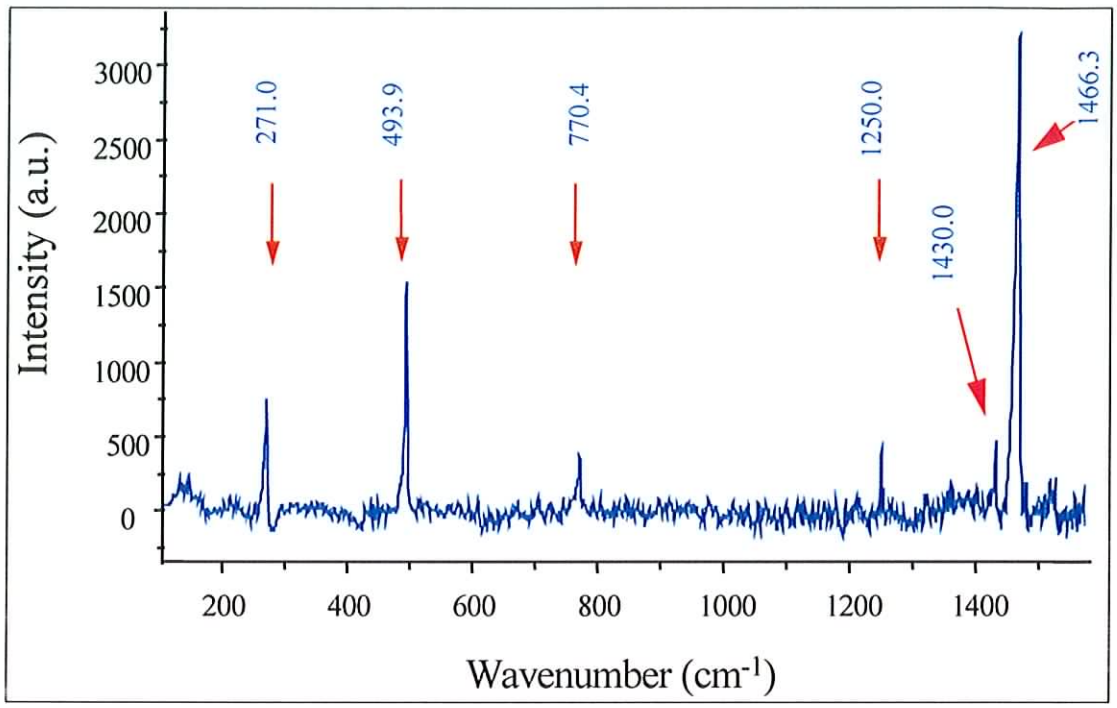

Figure 4.1: Raman spectra of powder C_{60} at room temperature

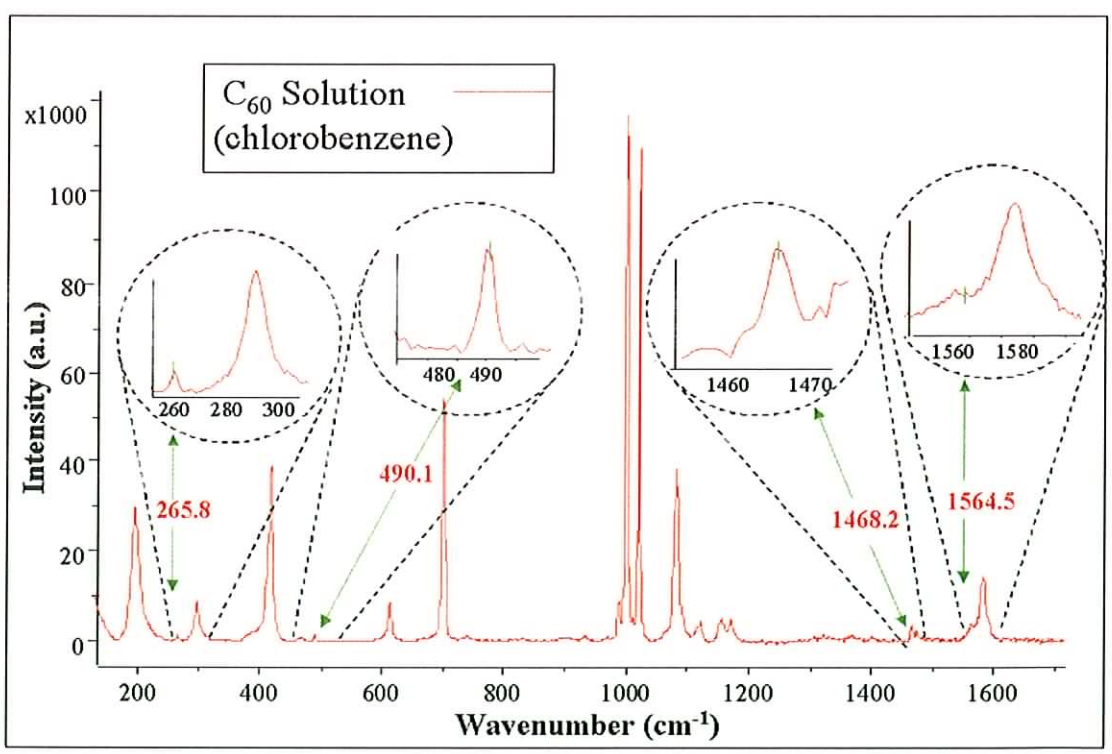

Figure 4.2: Raman spectra of C_{60} in solution

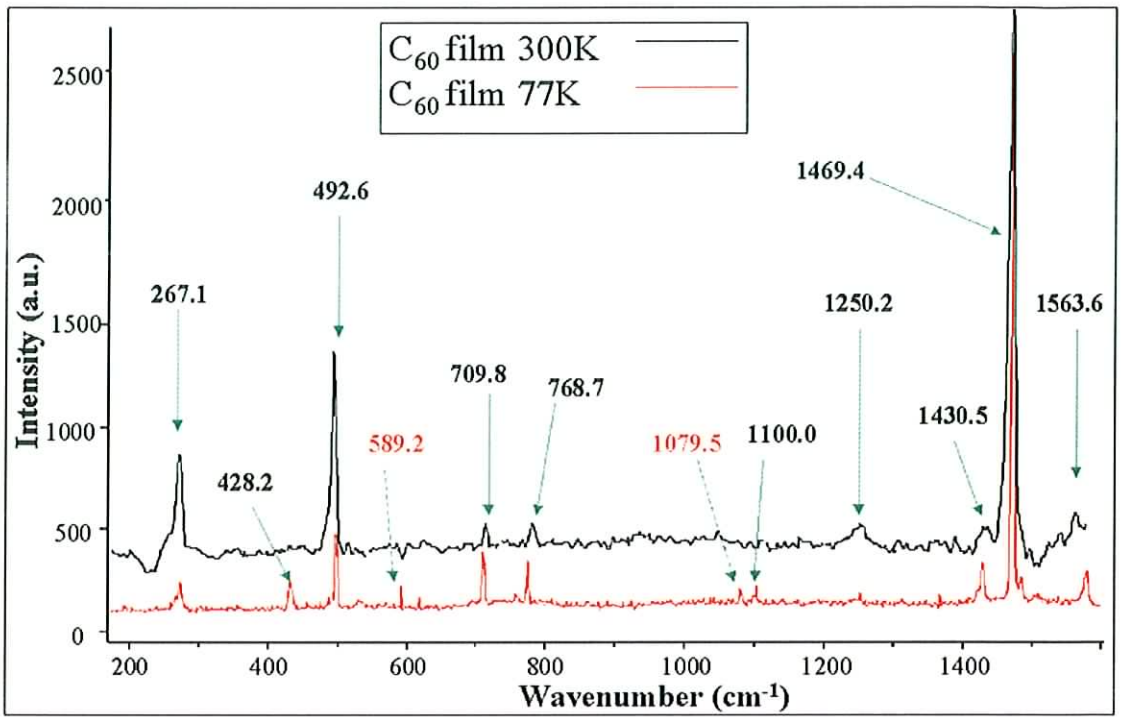

Figure 4.3: Raman Spectra of C_{60} thin film at 300K and 77K

Table 4.2: Detectable Raman modes. Blanks indicate undetectable modes.

Powder/ cm^{-1} (300K)	Film/ cm^{-1} (300K)	Film/ cm^{-1} (77K)	Solution/ cm^{-1}	Assignment/cm^{-1} [42,51]
493.9	492.6	492.6	490.1	$A_g(1)$
1466.3	1469.4	1469.4	1468.2	$A_g(2)$
271	269.1	269.1	265.8	$H_g(1)$
-	-	428.2	-	$H_g(2)$
-	709.8	709.8	-	$H_g(3)$
770.4	768.7	768.7	-	$H_g(4)$
-	-	1100.0	-	$H_g(5)$
1250.0	1250.17	1250.17	-	$H_g(6)$
1430	1430.58	1430.58	-	$H_g(7)$
-	1563.5	1563.5	1564.5	$H_g(8)$

In the solid-state at room temperature, the vibrational spectrum as measured by Raman (figure 4.3) predominantly retains its molecular character, which may be interpreted as a strong indication that the molecular levels are at most weakly perturbed by the solid

state environment. The symmetry of the molecule, as discussed in chapter 2, is however affected by its interaction within the fcc lattice [52]. The symmetry of the molecule is reduced to T_h, resulting in a lifting of the degeneracy. This is evident by the splitting of the H_g modes into two lines E_g and F_g at room temperature and eight lines at temperatures below the phase transition of 249K [53], where the rotation of the balls is hindered and finally frozen out below 90K. Significant symmetry reduction due to crystal-field effects is predicted at these low temperatures and a clearly enriched Raman spectrum is obtained as can be seen from figure 4.3. Figure 4.4 shows the $H_g(1)$ mode (~270cm^{-1}) taken from the aforementioned spectra (i.e. figure 4.1, 4.2 and 4.3). It can be seen from the spectra that as one moves from solution to solid at room temperature the emergence of a shoulder at ~265cm^{-1} is clearly visible. This shoulder maybe attributed to the onset of the $H_g(1)$ mode splitting into the E_g and F_g modes, since in solution there is no evidence of its presence. Further to this as the temperature is decreased from 300K to 77K evidence of the $H_g(1)$ mode splitting into multiple modes is seen, as mentioned previously the $H_g(1)$ mode at temperatures sufficiently below the phase transition of 249K can split into eight lines [53]. Hence this feature highlights the importance of symmetry to the C_{60} molecule as well as demonstrating the influence of the solid state environment to enhance forbidden lines.

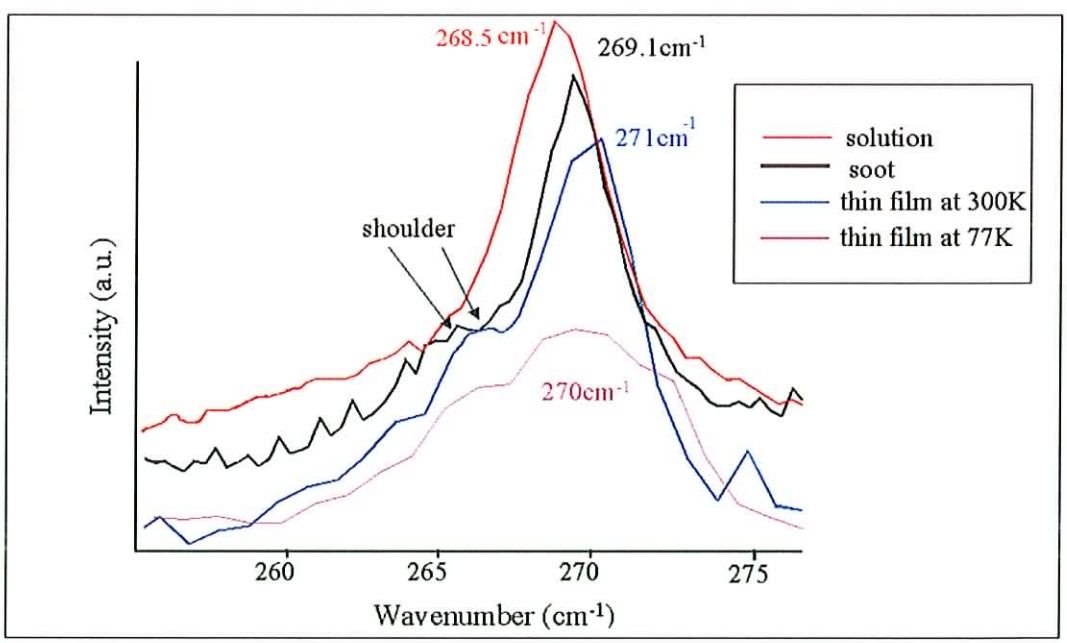

Figure 4.4: The $H_g(1)$ mode (~270cm^{-1}), The diagram shows the onset of the mode splitting in the C_{60} due to a reduction in symmetry.

A further contribution to the relaxation of symmetry selection rules can, however, result from isotope effects. With a natural abundance of 1.1% ^{13}C, there is a 34.4% probability of inclusion of one such higher isotope in a C_{60} molecule. The incorporation of ^{13}C reduces the symmetry to C_V and this should create a softening of the allowed fundamental modes. Several studies have attempted, therefore, to determine the relative strength of molecular and solid state contributions in C_{60} vibrational spectra.

Van Loosdrecht et al. [54] have reported the appearance of a significant number of new Raman lines in the low temperature spectrum of a C_{60} crystal and have assigned them all only to the activation of the silent *gerade* fundamentals. Two such modes can be seen in figure 4.3 positioned at 589.2cm^{-1} and 1079cm^{-1}and can be assigned to the silent *gerade* fundamentals $F_{2g}(1)$ and $G_g(4)$ respectively (highlighted in red). The reduction in symmetry of the C_{60} molecule implicit in the activation of these silent modes, as well as the splitting of some of these modes, has been ascribed solely to the effects of the crystal-field [54]. The assignment of the new spectral features to only gerade modes implies that the centrosymmetric character of the molecule is retained. This treatment neglects symmetry reduction processes due, for example, to isotopic variance.

In contrast, Dong et al. [51] have observed rich high and low temperature Raman spectra measured in films and have assigned the vibrations as active and silent fundamentals, overtone and combination modes. Indeed the mode $H_g(8)$ at 1575cm^{-1} in figure 4.3 which is an allowed mode of vibration, may have a contribution from a combination or overtone mode and as such the strengths of the frequency position may not necessarily be representative of the strength of the assigned mode. The activation of the silent modes by Dong et al. [51] was attributed to the presence of isotopes on the basis of a lack of spectral temperature dependence. No additional features which may be attributed to peak-splitting due to crystal-field effects are discussed. A somewhat similar model was developed by Love et al. [55], who assigned the lifting of degeneracy of the H_g modes strictly to the influence of ^{13}C. The activation of many of

the silent modes was proposed to lie in the mixing of silent modes with closely lying active-modes. The activation of these modes was again assigned solely to the presence of ^{13}C. The activation of silent modes well-removed from Raman-active modes was assigned to sample disorder effects. The crystal-field effects were proposed to be insignificant. This interpretation was strongly contradicted by Burger et al. [56], who examined the splitting of the $H_g(1)$ mode as a function of polarisation of the scattered light. The strong polarisation dependence of the splitting observed confirms the significant influence of the crystal-field.

The relaxation of the selection rules in the IR spectrum of C_{60} is not as evident as can be seen from figure 4.5, which shows the IR spectra for C_{60} in solution and figure 4.6 in the solid. One plausible reason for this is that in IR spectroscopy the molecule is not resonant whereas in Raman spectroscopy it is slightly resonant. The selection rules for IR spectroscopy permit only the four F_{1u} modes to be active. In figure 4.5 the range is limited by the solvent peaks and the concentration of C_{60} however figure 4.6 the solid state spectrum shows the four strong F_{1u} modes with an additional peak at ~1538cm^{-1}. This weak feature has been attributed to the higher order effects as discussed by Eklund [19]. Table 4.3 shows the detected peaks and their assignments. Comparative analysis of room temperature infrared spectra led Wang et al. [57] to assign the appearance of all silent fundamental modes to isotopic effects. In a more recent publication, Akselrod et al. [50] have analysed a low temperature Raman spectrum and assign the activation of silent modes to isotopic effects, as well as identifying the splitting of the allowed fundamentals due to the crystal field.

In both infrared and Raman spectroscopy, there is little evidence of strong intermolecular modes. At low temperatures however, a number of weak intermolecular modes have been observed. [52]. Appearing between 15 and 60cm^{-1}, their low force constant and oscillator strength is strongly suggestive of a minimal coupling between the molecules in pristine fullerenes.

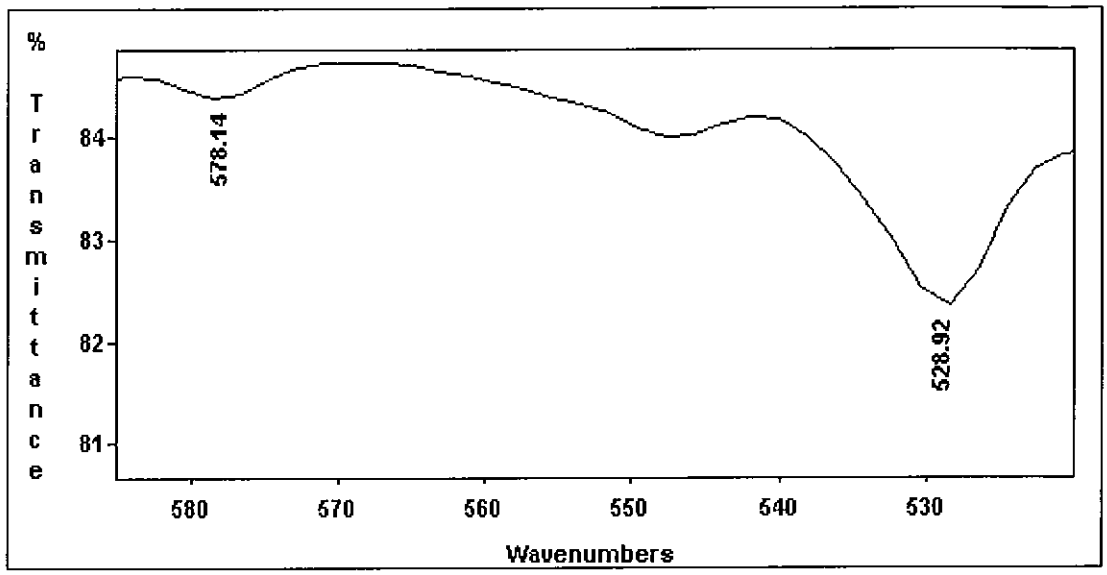

Figure 4.5. IR spectra for C_{60} in solution.

Table 4.3: Detectable IR modes.

Solution (cm^{-1})	Solid (cm^{-1})	Calculated (cm^{-1}) (Hyper-Chem)	Assignment (cm^{-1}) [9,10]
527	526	526.5	F_{1u} (1)
579	576	575.8	F_{1u} (2)
-	1182	1182.9	F_{1u} (3)
-	1428	1429.2	F_{1u} (4)

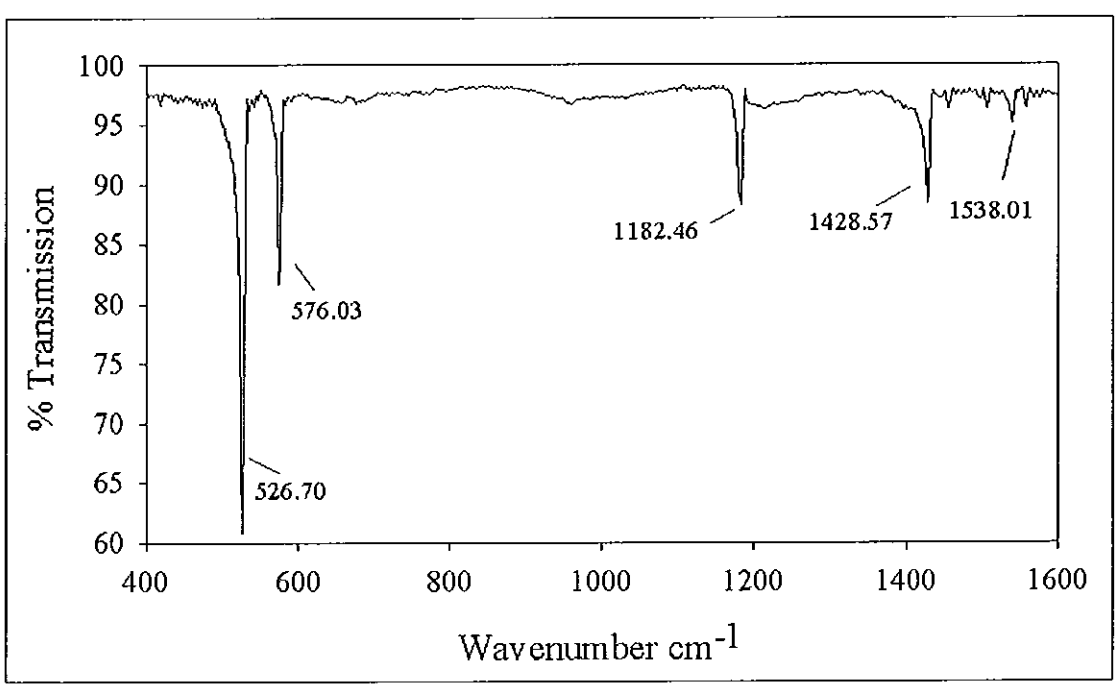

Figure 4.6: IR spectra for C_{60} in solid state (KBr disc)

4.2.3: Conclusions

In summary, the vibrational spectrum of C_{60} has been extensively studied and many of the observed modes may be unambiguously assigned. There does remain some degree of discussion regarding the activation of the silent fundamentals and the contributions of crystal field. In particular the influence of structural aspects on the spectrum have not been satisfactorily elucidated. Nevertheless the solid state's vibrational spectrum retains its molecular character, which may be interpreted as a strong indication that the molecular levels in the ground state are at most weakly perturbed by the solid state environment and hence C_{60} behaves as a molecular solid.

4.3: Electronic Spectroscopy

4.3.1: Introduction

Electronic spectroscopy deals with the absorption and emission of electromagnetic radiation by a substance, resulting in an electronic transition from one electronic state to another [44]. Electronic transitions generally involve energy changes of 1eV or more and are characterised by absorption in the near infrared, visible or ultra violet region [58]. These transitions can be evaluated by ultra violet/ visible and or near IR absorption spectroscopy, which monitors the absorption of monochromatic incident light of frequency ν as a result of the energy change ($h\nu$) between quantised energy levels of the molecule. This gives information about the electronic structure of the molecule and to some degree about whether the transition is allowed or disallowed.

Radiative transitions from higher to lower electronic energy states may also be detected and analysed by the frequency of the emitted light through fluorescence spectroscopy. This involves the irradiation of a sample with a monochromatic energy beam of light of frequency within the absorption band of the system, which promotes an electron to the first singly excited state. When the electron relaxes back to the ground state the subsequent emitted light is recorded. Such transitions correspond to emission in the visible, the ultraviolet or near infrared and are termed fluorescence. Alternatively phosphorescence can occur which, involves the emission of light from a

triplet excited state. General radiative emission is termed luminescence. In this section we shall look mainly at absorption spectroscopy, although the luminescence of C_{60} will also be discussed [44].

4.3.2: Electronic Spectroscopy of C_{60}

Figure 4.7 shows a typical absorption spectrum for C_{60} in solution, recorded between 400 -800nm, using a Shimadzu UV-2101PC Absorption Spectrophotometer. As is the case in the vibrational spectroscopy, the high degree of symmetry of the fullerenes plays an important role in the electronic spectroscopy of the molecules. In C_{60} the closed shell icosahedral symmetry renders the HOMO-LUMO transition dipole forbidden [59]. Figure 2.6 (chapter 2) highlighted this transition as the lowest energy excitation and was seen to give a value of ~1.897eV as the energy gap of isolated C_{60}.

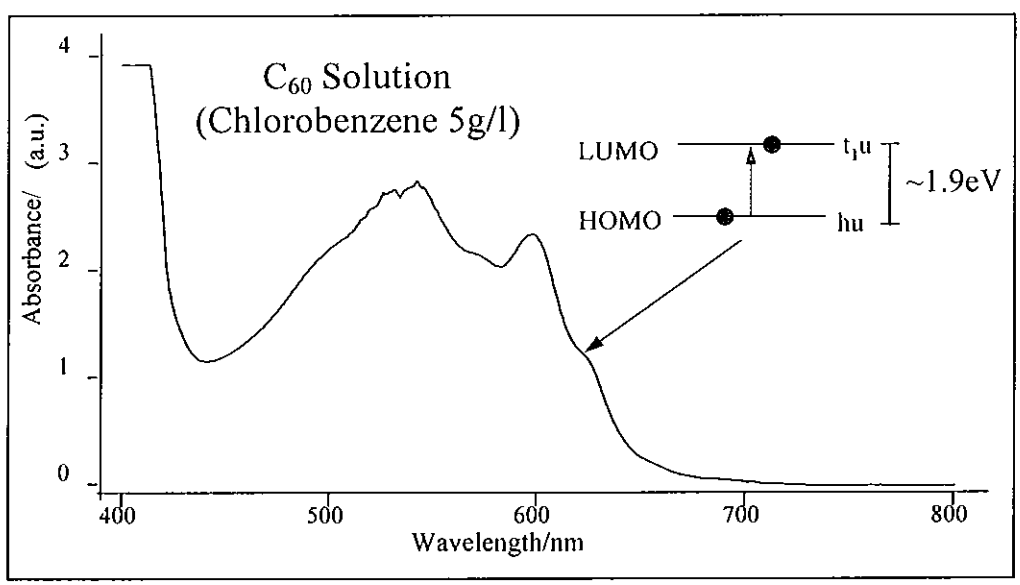

Figure 4.7: Absorption spectrum of C_{60} in Solution

As discussed in chapter 2 this transition is forbidden, since it has a zero transition dipole moment. Nevertheless this HOMO -LUMO transition is visible in the absorption spectrum of C_{60}, as indicated in figure 4.7, around 640nm. This transition gives C_{60} solutions their distinctive burgundy colour. Two photon luminescence excitation spectroscopy of a C_{60} single crystal at 4.2K [48] revealed the onset of the

absorption to be 1.846eV, which is in good agreement with the HMO model (chapter 2). The appearance of this band is due to the relaxation of the selection rules which allow forbidden transitions to occur weakly via Hertzberg-Teller vibrational coupling or Jahn-Teller distortions [60]. As a result the broad absorption between 450nm and 640nm has been ascribed entirely to the HOMO-LUMO transition. This relatively weak absorption processes has a rich vibrational structure and hence a detailed understanding of the vibrational spectroscopy is essential in order to analyse the absorption spectrum of C_{60}. There have been many reports describing the UV/ visible absorption spectrum of C_{60}, but the most detailed analysis has been presented by Leach et al [60]. In his work, he divided the absorption spectrum into four regions. Between 190 and 350nm, there exists three strong bands, and these, in addition to weaker, vibronically structured bands in the region of 350 - 430nm, are assigned to nine orbitally allowed singlet-singlet transitions. The vibrational structure has been assigned to the effects of Hertzberg-Teller distortions. These bands are not visible in the range scanned in the absorption spectrum shown in figure 4.7, although in the region shown, there are several superimposed peaks and weak shoulders on the HOMO-LUMO background. These bands have been attributed to vibronic transitions in which the excitation of a vibration of suitable symmetry enables the forbidden transition to "steal" intensity from allowed transitions. Leach [60] also identified four extremely weak bands between 627 and 690nm and assigned them to vibronic features of the spin forbidden singlet to triplet transition.

It can be seen that the absorption spectrum of C_{60} in solution is independent of the solvent system used. Figure 4.8 shows a set of absorption spectra of C_{60} in toluene at five different concentrations. The features as discussed for the C_{60} in chlorobenzene (figure 4.7) are also clearly visible in this solvent system. Using these spectra and the Beer-Lambert law [44] i.e. Eq 4.1 it is possible to calculate the extinction coefficient for C_{60}.

$$A = c\varepsilon d \qquad \text{Eq.4.1}$$

A= absorbance (a.u.) ε = extinction coefficient ($mol^{-1}\ l\ cm^{-1}$)

c= concentration (mol/l) d = path length (1cm)

A plot of absorbance at 532nm against the concentration (figure 4.9) gives a linear graph of slope $1.2861 g^{-1}l$, hence the extinction coefficient of C_{60} can be obtained and was found to be 926 mol^{-1} l cm^{-1}. This result is in good agreement with literature values for the extinction coefficient [41].

The absorption spectrum of C_{60} is largely temperature independent and comparison of the solution spectrum to gas phase EELS spectra show negligible differences, the former being slightly red shifted [61] supporting the assumption that solvated fullerenes are a good approximation to isolated molecules. The linear dependence shown in figure 4.9 also supports this notion since the Beer-Lambert law assumes no aggregation of the molecules in solution.

Vibrational spectroscopy of C_{60} showed strong evidence that the solid state environment exerts only a minimal perturbation on the electronic structure of the fullerene molecule due to the similarity of the spectra. A comparison between the absorption spectra in film and in solution figure 4.10 shows that the onset of the absorption in the solid is slightly red shifted from that of solution [43]. A close examination of the spectrum shows that the lowest energy transition in the solid state, which has maximum at ~630nm, possesses a vibrational structure similar to that of the isolated molecule. Furthermore, all of the higher order, allowed molecular transitions (190-350nm not shown) [48] also appear in the solid state spectrum, also slightly red shifted. On this basis, the solid state of C_{60}, appears to behave like a classical molecular solid in which the molecular wavefunctions are minimally perturbed, the principal influence of the crystalline environment being in symmetry breaking

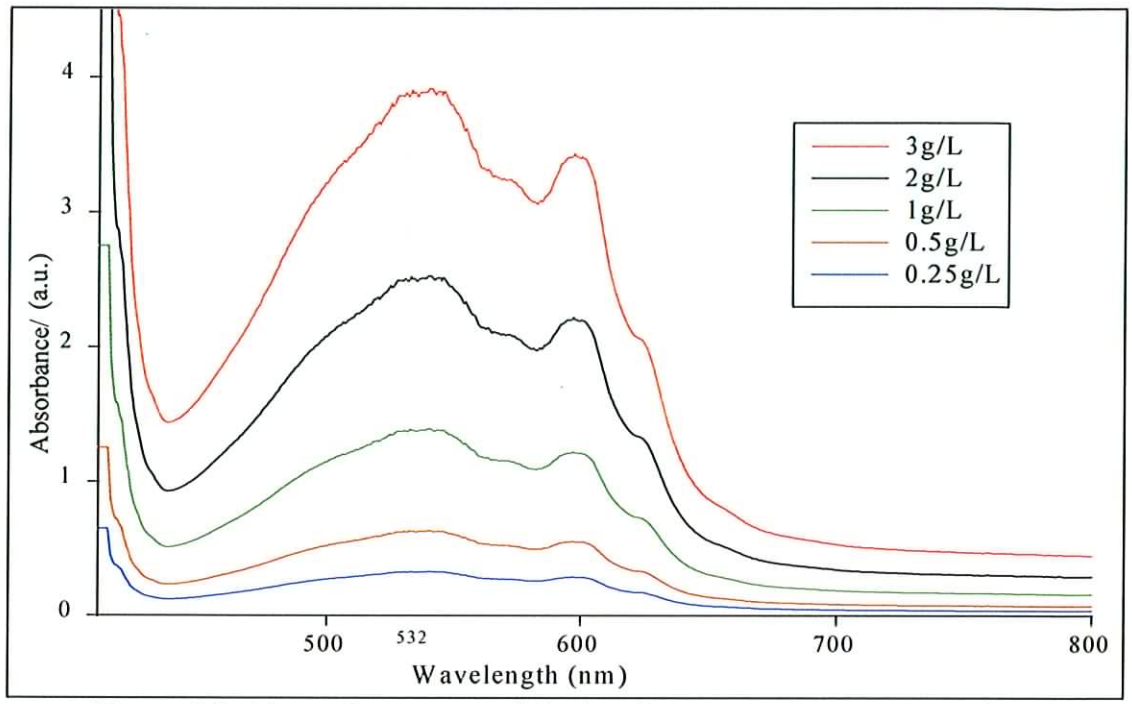

Figure 4.8: Absorption spectra of C_{60} in toluene at various concentrations

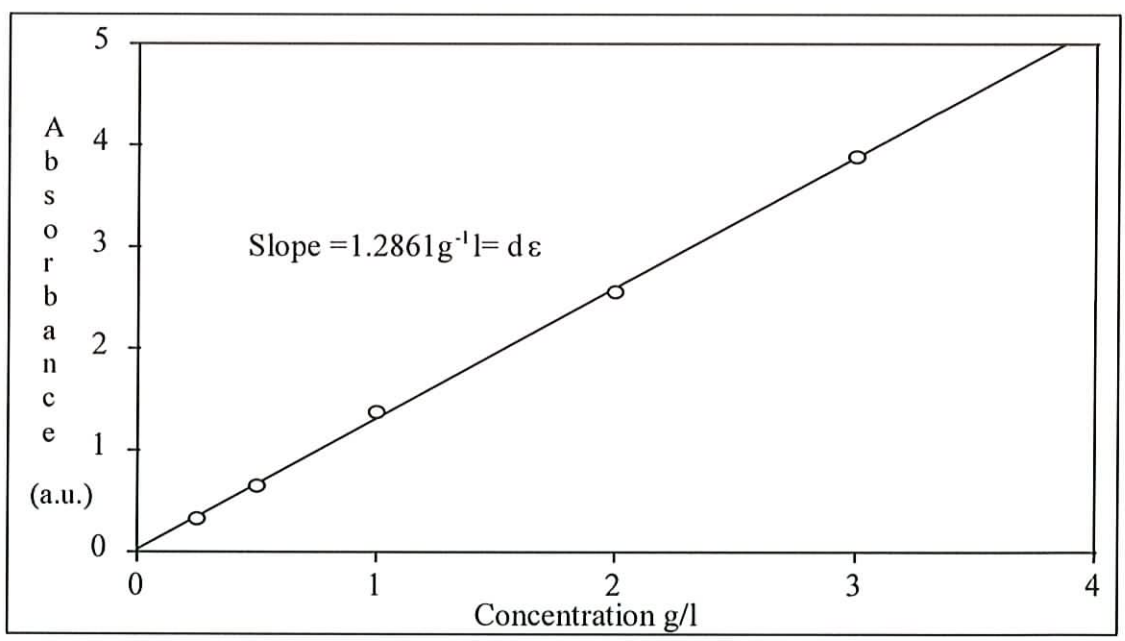

Figure 4.9: A plot of absorbance at 532nm against the concentration

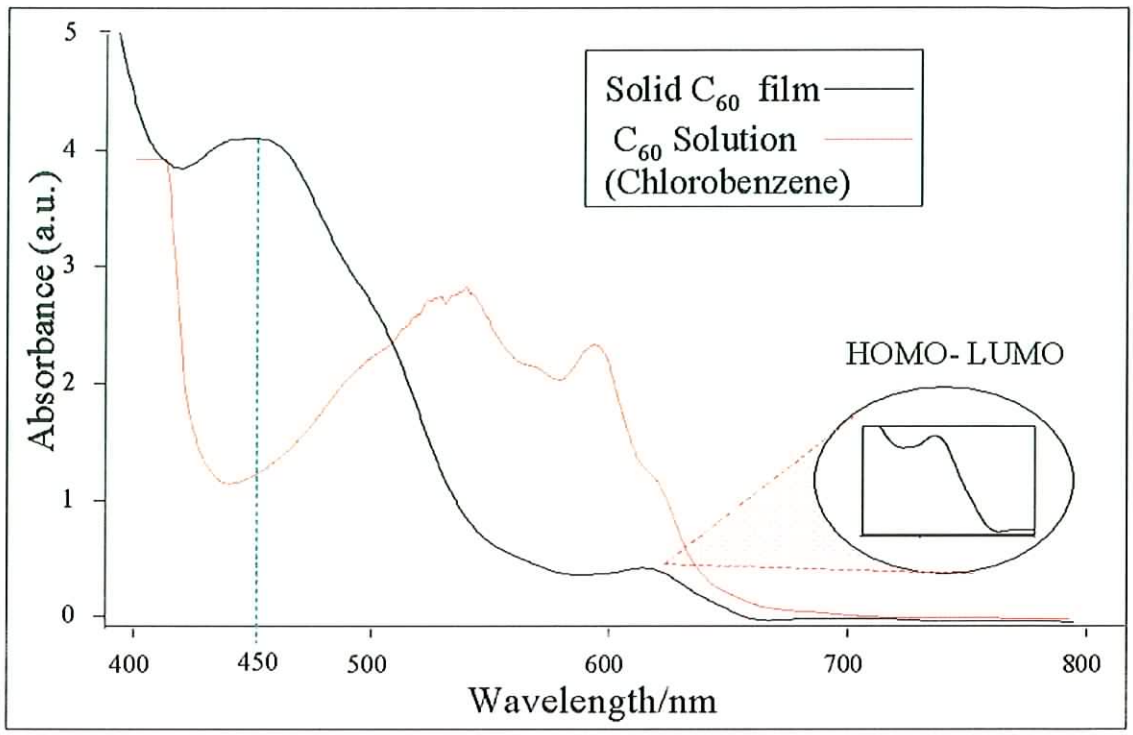

Figure 4.10: A comparison between the absorption spectra in film and in solution

However, there is one feature which, appears strongly in the solid state spectrum but not in that of the isolated molecule. Although this difference between the two spectra has received little attention, it is the first strong indication of an influence of the solid state on the electronic properties and thus merits consideration. In figure 4.10 the thin film absorption spectrum of C_{60} shows a broad, relatively strong absorption in the range ~420nm-500nm with maximum at ~450nm. This feature is absent in solution absorption measurements and in literature gas phase EELS spectra [48,61] hence suggesting that it is not molecular in origin. Further to this photoconductivity and electro-absorption similarly indicate a photoexcited species which is not molecular in origin [62,63]. Kazaoui et al [62], have demonstrated, via electro-absorption that the feature at ~450nm derives from a series of charge transfer states. Where by the transition occurs between the HOMO of one molecule to a higher unoccupied state whose wavefunction derives from a mixture of the molecular state with those of its next nearest neighbours. It is thus now widely accepted [34] that this feature is in fact due to the solid states influence on the electronic properties of the molecule, hence it is not molecular in character but instead is the result of an intermolecular charge

transfer excited state. This state can be explored further by the use of excited state spectroscopy as will be demonstrated in chapter 5.

The principles which render the HOMO-LUMO transition forbidden in the absorption spectra also inhibit the radiative recombination of the singlet excited state species in the fullerene molecule. This is highlighted by the fact that for many years no fluorescence spectrum of C_{60} in solution was observed. Intersystem crossing is the favoured mechanism by which the singlet excited state is depopulated yielding ~100% triplet population. The fluorescence yield is estimated to be $\sim 10^{-5}$ [64] and the fluorescence life time is ~1.2nsec [65] in solution which is the same rate for the intersystem crossing, supporting the notion of ~100% population of the triplet state. In this study the Raman spectrometer was used as an extremely sensitive luminescence spectrometer. Figure 4.11 shows the luminescence spectrum of C_{60} in chlorobenzene. The spectrum has a maximum at ~720nm. Similar to the absorption spectrum Hertzberg /Jahn –Teller distortions result in the spectrum having a rich vibrational structure. It should be noted that the sharp feature at ~633nm is the result of the laser and the feature at 840 is an artefact of the spectrometer

In the solid, a weak luminescence is also observable, shown in figure 4.11. The maximum of this emission is ~750nm and is red shifted with respect to the solution measurements which was similarly observed in the absorption spectrum. Although the spectrum appears less structured than in solution, high resolution measurement [66] on single crystals show that the spectrum is highly structured. This structure is assignable to molecular vibrations due the Hertzberg-Teller interactions. The similarity of the solution and solid state spectra supports the assignment of the lowest excited state as molecular in character. Such an assignment is further supported by the observation that the time decay of the fluorescent emission is 1.2nsec at low temperature [65], remarkably similar to that in solution [64]. The fluorescent yield is similarly low in the solid state, implying, by analogy, that photoexcitation to the molecular singlet results in a high efficiency intersystem crossing to a molecular triplet state. Indeed, early reports of Photoluminescence Detected Magnetic Resonance indicated the presence of identical triplet states to those present in solution

as well as a species which was postulated to be localised on a single pentagon due to intermolecular interactions [67]. The triplet species are extremely long lived and that they decay primarily nonradiatively is evidenced by the difficulty in observing phosphorescent emission from C_{60} solid. The nature of this species and the differences to the molecular levels have yet to be fully elucidated.

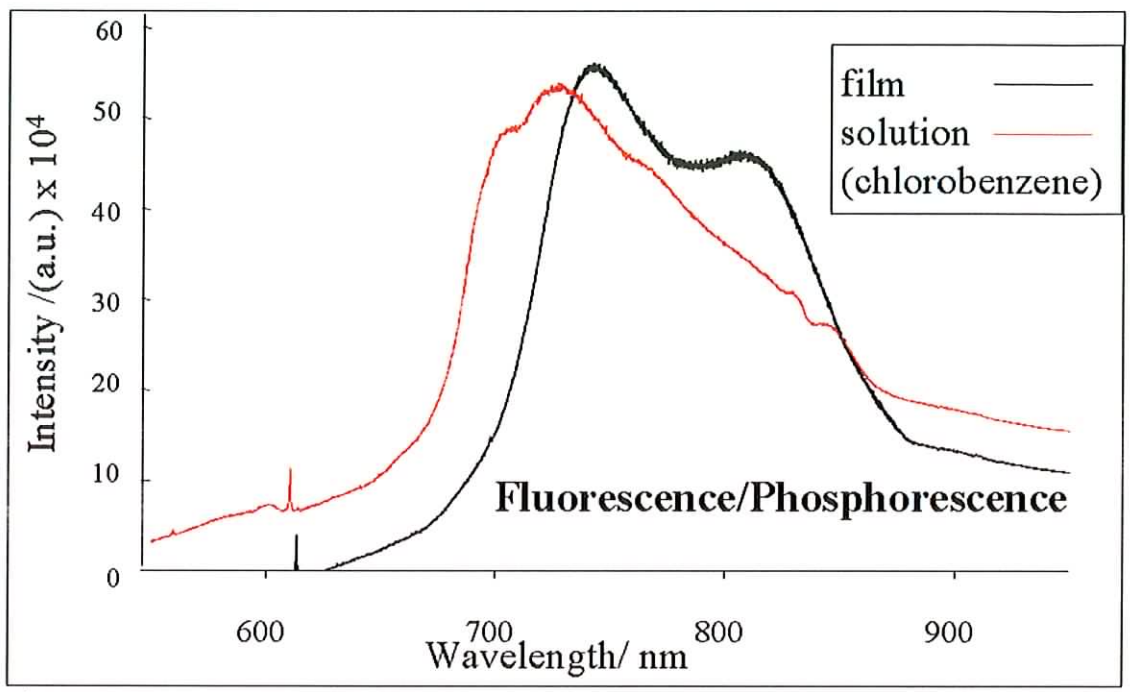

Figure 4.11: The luminescence spectra for C_{60} as taken using the Raman spectrometer

4.3.3: Summary of Electronic Spectroscopy

In summary, although the vibrational, UV/Vis and luminescence spectroscopy of C_{60} indicates that solid C_{60} is molecular in character, the emergence of the new feature at 450nm in the solid state UV/Vis, as well as the HOMO –LUMO transition being present suggests an interaction in the excited state. This additional feature in the solid spectrum has been attributed to a charge transfer type exciton at high energy, which contributes to the generation of photocarriers in the solid state. This feature can be explored further by the use of excited state spectroscopy as shall be seen in chapter 5.

4.4: Conclusions

The field of study of the optical/ spectroscopic properties of fullerenes is broad and impossible to fully encompass within the scope of this text. In this molecule, the restrictions imposed by the symmetry are most severe, and thus the response is most sensitive to perturbations. In the isolated molecule, the optical properties are strongly influenced by vibrational interactions, which are themselves rendered highly degenerate by the molecular symmetry. The vibrational spectroscopy of C_{60} indicates that the solid state is predominantly molecular in character, with the solid state packing having only a weak influence on the spectra. Electronic spectroscopy however reveals features that are specific only to the solid. This is the first indication of an interaction in the solid state. The prospect that such a communication of molecularly localised π electrons between molecules can contribute to the conduction process has huge implications regarding possible applications of the molecule. Thus further investigations of the excited states of C_{60} are required to completely assess the significance of this feature.

Chapter 5

C_{60} Excited states and their Spectroscopy

5.1: Introduction

Chapter 4 showed that the ground state optical properties of C_{60} behave well with respect to theory and a good understanding of the low intensity optical properties of both the solution and solid has evolved [34]. The most notable difference between the solid state and solution was evident in the absorption spectra where a feature at ~450nm appeared in the solid state spectrum with no corresponding feature in solution. This solid state feature was attributed to an intermolecular charge transfer excited state. Electro-absorption measurements indicated that this feature was the result of transitions between the HOMO of one molecule to a higher unoccupied state whose wavefunction is a mixture of the molecular state with those of its next nearest neighbours [62]. This intermolecular interaction is the first indication of a deviation of solid state C_{60} from the properties of the isolated molecule. To further examine this deviation it is necessary to use higher intensities thereby probing the excited state species directly.

In recent years extensive experimental and computational investigations of the photophysical and photochemical properties of fullerenes have been undertaken to attempt to clarify the variation between the solution and solid state photodynamics [15,19,68,69]. It is now well established that the high molecular symmetry and spherical π-electronic system of C_{60} has a profound effect on the excited state processes, particularly in the solid state. Furthermore in the solid state a number of competing processes such as excitonic interactions [19] and carrier trapping processes, characteristic of disordered semiconductors [69] have been proposed to complicate the photodynamics. The emerging picture then is of a new unique class of material with conjugated electronic structures, which is testing the limits of existing photophysical and photochemical principles. The question is, can traditional photophysics provide the proper tools and concepts for describing the behaviour of excited state C_{60}.

In this chapter transient absorption measurements have been used to examine the fundamental differences in the excited states of C_{60}. In addition Raman spectroscopy

is shown to be an extremely useful tool in the elucidation of the photoexcited states of C_{60}, including for the first time the Raman spectroscopic signature of the molecular triplet of C_{60} in solution and in the solid state positioned at ~1466cm^{-1}. Further to this, in the solid state, a second species is identified at ~1463cm^{-1} and is proposed to be an excited state co-operative involving two or more excited states. The temperature dependence of the excited state species in solid C_{60} are also discussed and by doing so many questions regarding the nature of the excited state species in the solid will be answered and indeed posed.

5.2: Introduction to Excited States and their Spectroscopy

In chapter 4, the ground state optical properties of C_{60} were discussed. In such a discussion the focus is essentially on the primary absorption of light by a molecule promoting an electron from the ground state (S_0) to the first excited state (S_1) which is commonly referred to as the singlet excited state (figure 5.1). This singlet state has an overall spin angular momentum of zero.

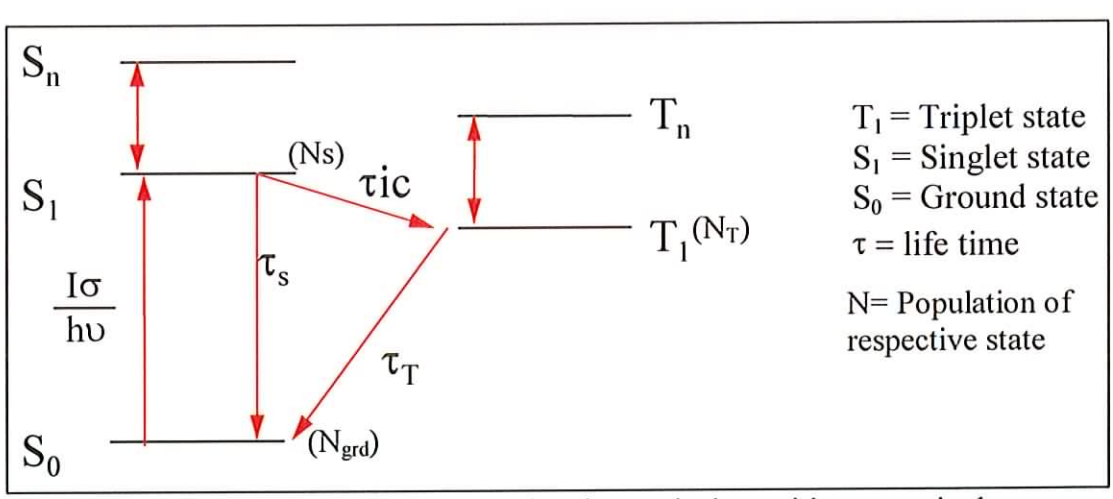

Figure 5.1: Jablonski level diagram showing optical transition to excited states.

Such an excitation can then be followed by a number of physical processes such as relaxation to the ground state S_0, via radiative (fluorescence) or non-radiative decay, further excitation to a higher singlet state (S_n) or intersystem crossing into the triplet manifold. The latter gives rise to a triplet excited state (T_1) which has a non-zero spin

angular momentum and hence lies lower in energy than the singlet state in accordance with Hund's rule [44].

The optical analysis of a molecule in these excited states (singlet/ triplet) is referred to as excited state spectroscopy. As in electronic spectroscopy, excited state spectroscopy optically examines the transitions from one energy level to another. For example ground state spectroscopy essentially looks at transitions from S_0 -S_1 (figure 5.1). However in excited state spectroscopy we can have transitions from S_1 - S_n or T_1 - T_n depending upon the spin angular momentum of our excited state. The singlet - singlet absorption (S_1 - S_n transition) of a molecule will yield a differential absorption which has a life-time, typically of the order of nano-seconds, governed by the decay of S_1. The triplet -triplet absorption in general is relatively long lived, typically around milli-seconds governed by the decay of T_1. The photodynamics of the system shown in figure 5.1 can be described by the following rate equations:

$$\frac{dN_{grd}}{dt} = -I\frac{\sigma N_{grd}}{h\nu} + \frac{N_T}{\tau_T} + \frac{N_S}{\tau_S} \qquad \text{(Eq.5.1)}$$

$$\frac{dN_T}{dt} = \frac{N_S}{\tau_{IC}} - \frac{N_T}{\tau_1} - I\frac{\sigma_T N_T}{h\nu} + \frac{N_{Tn}}{\tau_n} \qquad \text{(Eq.5.2)}$$

$$\frac{dN_S}{dt} = I\frac{\sigma N_{grd}}{h\nu} - \frac{N_S}{\tau_{IC}} - \frac{N_S}{\tau_S} - I\frac{\sigma_S N_S}{h\nu} + \frac{N_{Sn}}{\tau_n} \qquad \text{(Eq.5.3)}$$

Where N_{grd}, N_S and N_T are populations of the ground state, singlet state and triplet state respectively. I is the intensity of the applied light, n denotes a higher excited state, ν the frequency of the light, τ the life times of each state from figure 5.1, h is Planck's constant and finally σ is the ground state absorption cross-section while σ_S and σ_T are the absorption cross-sections of the singlet and triplet respectively. The contributions of the higher excited states in equations 5.2 and 5.3 can be neglected in accordance with Kasha's rule [70]. Kasha's rule states that luminescence can only occur from the lowest excited singlet or triplet state irrespective of higher excited

states into which the molecule has been excited [70] implying that a decay from these states is ultrafast. Hence equations 5.2 and 5.3 can be reduced to:

$$\frac{dN_T}{dt} = \frac{N_S}{\tau_{IC}} - \frac{N_T}{\tau_I} \qquad \text{(Eq.5.4)}$$

$$\frac{dN_S}{dt} = I\frac{\sigma N_{grd}}{h\nu} - \frac{N_S}{\tau_{IC}} - \frac{N_S}{\tau_S} \qquad \text{(Eq.5.5)}$$

The generation and analysis of excited species can be done in a number of ways. The simplest method is a single beam intensity dependent transmission experiment. If figure 5.1 is reduced to a two level system where the singlet and triplet populations are considered as one (N_{ex}) with a life time τ, then under steady state conditions for this two level system equation 5.1 is equal to zero and reduces to:

$$I\frac{N_{grd}}{N_{ex}} = \frac{h\nu}{\sigma\tau} \qquad \text{(Eq.5.6)}$$

If $N_{grd} = N_{ex}$ then the system is saturated and the saturation intensity can be defined as,

$$I_{SAT} = \frac{h\nu}{\sigma\tau} \qquad \text{(Eq.5.7)}$$

In the absence of an excited state absorption, increasing the intensity beyond I_{SAT} results in bleaching, whereupon only a small fraction of the applied intensity is used to populate the excited state, and the remainder is transmitted. This process is generally called saturable absorption. In the case where the highly populated excited state can itself absorb, just as the ground state the system will bleach to a level whose transmission is not 100% but which is characterised by an excited state absorption cross section, σ_{ex}. If $\sigma_{ex} > \sigma$ then the excited state absorption is greater than the ground state absorption and an inverse saturable absorption results. By monitoring the transmitted intensity with respect to the input intensity an intensity-dependant

transmission curve can be obtained which can then be modelled by the aforementioned equations thus yielding photophysical parameters for the system.

The information derived for a single wavelength is however extremely limited. Further information about an excited state can be obtained by using pump and probe techniques. These techniques involve two beams, one a strong pump beam to generate the excited state and the second a weak probe beam. Essentially this technique monitors the transmission of the probe beam as a function of the pump beam. Using pulsed lasers with pulses less then or equal to the lifetime of the excited species allows the dynamics of the system to be explicitly monitored.

The most common technique for analysing the absorption spectra of excited states is flash-photolysis or transient absorption spectroscopy [72]. Originally developed for the analysis of radicals in fast photochemical reactions in the gaseous or liquid phase, it was soon seen that the same technique could be applied to monitoring the evolution of excited states. Early flash-photolysis systems excited (pumped) the sample by using a photolytic flash of light with a typical energy output of 10^5J and a pulse duration of $\sim 10^{-5}$s. However since the advent of the laser and particularly short pulse generation it has been possible to obtain pulses of nanosecond duration in most standard flash photolysis systems (with pico- and femto- second still begin too expensive for most standard systems). Once the sample is excited, the changes in the absorption spectrum can be monitored spectrophotometrically using a range of detectors, the best being charged coupled detectors.

5.3: Excited State Spectroscopy of C_{60}

5.3.1: Triplet -Triplet absorption of C_{60} using flash Photolysis

The properties of the triplet state of C_{60} are of potential importance in several fields, in particular energy transfer to oxygen with its consequences on photodegradation, photopolymerisation and biological effects including cancer photochemotherapy [14]. Furthermore, as discussed in chapter one, non-linear optical effects based on the photophysics of C_{60} and its triplet state have potential applications in optical limiter devices.

In this study the excited state spectroscopy of C_{60} was performed using a flash-photoylsis system arranged in a right angle configuration (figure 3.3 chapter 3). The C_{60} in chlorobenzene solution was excited using a 20ns, frequency tripled (355nm) Q-switched Nd^{+3}:YAG laser pulse and the broad band light source was a Xe Arc lamp (190-800nm). It was found that the degassed sample was unstable at high laser powers and hence in accordance with previous studies [68] the laser power was always kept below 1.3mJ/pulse focused on $0.2cm^2$. Immediately after excitation the singlet state S_1 is populated. Ebbesen [68] showed that this initial period results in a differential absorption characteristic of the singlet excited state transition S_1 - S_n with a maximum at ~900nm. This absorption however quickly evolves (~1.2ns) [65] into the triplet excited state spectrum, due to ~100% efficiency of the inter-system crossing to the triplet manifold. This rapid evolution is remarkably similar to the fluorescence life-time of C_{60} discussed in the previous chapter. As a result of this intersystem crossing rate the experimental set up used in this study was insufficient to detect this singlet to singlet absorption. However the triplet -triplet absorption (T_1 - T_n) has a longer lifetime (~40ms) [68] and was easily detected by the arrangement. Figure 5.2 shows the triplet absorption spectrum for C_{60} which has a maximum absorption at ~760nm. The most probable assignment of this maximum is to the electronic transition 1^3T_{2g} - 2^3G_u [48]. This relatively high rate for the spin forbidden intersystem crossing is attributable to the strong spin-orbit coupling in these spherical molecules and the relatively low S_1-T_1 energy splitting, estimated by triplet - triplet quenching processes

to be ~9 kcal/mol [73,74]. This can be accounted for by the small electron-electron repulsive interactions which occur on such a large delocalised molecular system.

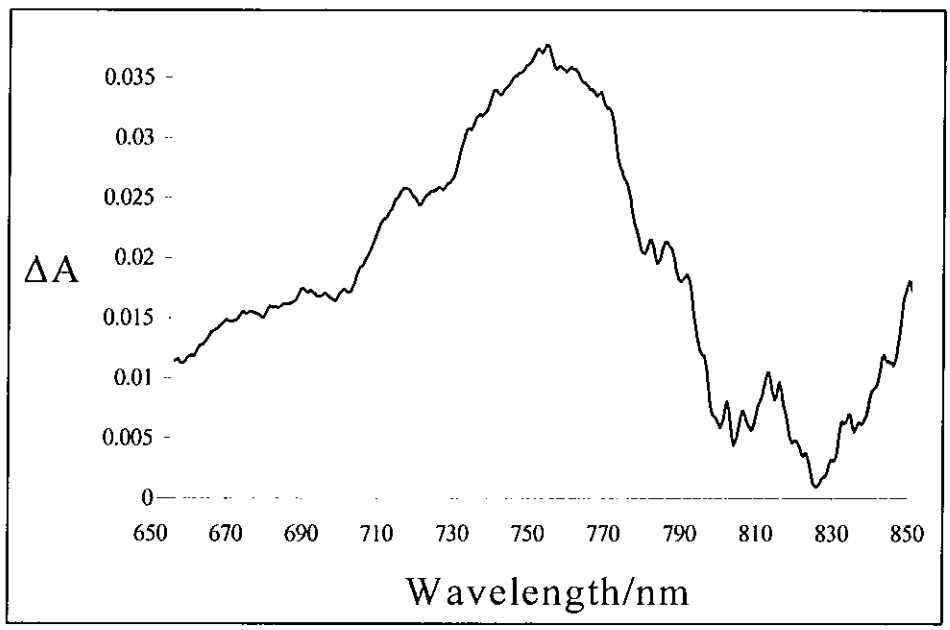

Figure 5.2: The Transient absorption spectrum for C_{60} with a maximum at ~760nm.

In the solid, the excited state photodynamics differ considerably to those in solution, as shown in figure 5.3 [69]. The initially generated species has a dramatically different spectrum than that of solution, and most significantly there is no evidence of a spectral evolution, on a time scale of ~1nsec, to a second species which can be ascribed to the triplet state. In the solution, such an evolution, due to strong intersystem crossing, accounts for the decay of the fluorescence and the low fluorescence quantum yield. The absence of an equivalent behaviour in the solid state strongly indicates that the photodynamics of solid state C_{60} differs considerably from that of the isolated molecule. Despite the fluorescent lifetime of C_{60} both in the solid and in solution being 1.2ns [65].

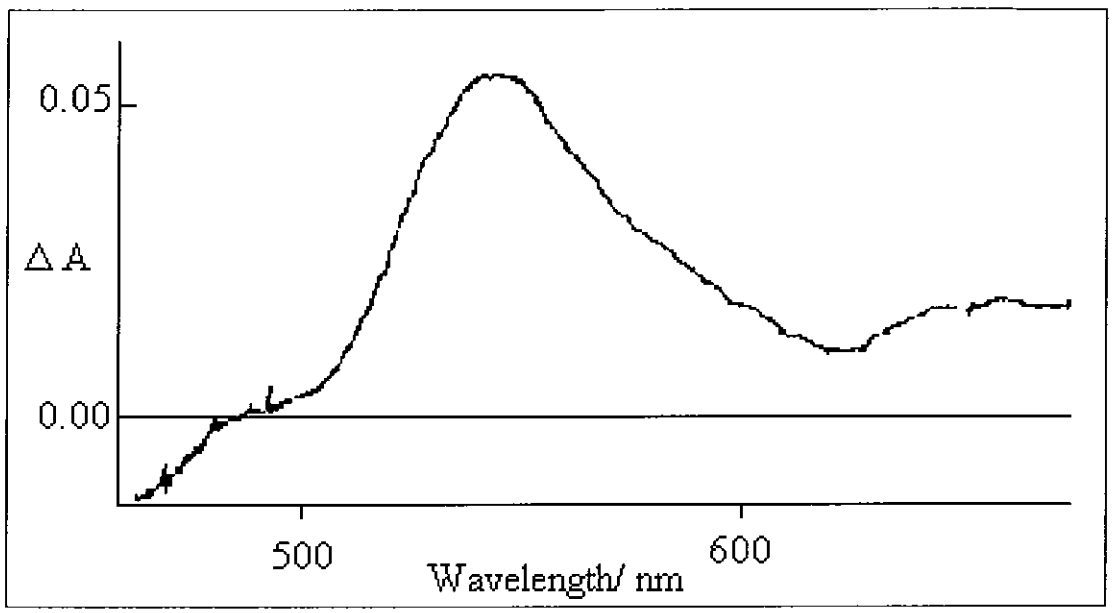

Figure 5.3: Transient absorption spectrum immediately after excitation of a C_{60} thin film adopted from Ebbesen [69].

The crucial question then is, what is the nature of the excited state species in the solid. The evidence from the photoinduced absorption measurements is further proof of a substantial departure of the properties of the molecules in the solid state from those in solution. Ebbesen et al. [69] have discussed this departure in terms of the generation of a free-singlet-exciton which is generated immediately upon excitation and becomes self trapped on the order of a few picoseconds at room temperature, with little mobility. The nature and/or spatial extent of the exciton is not however, discussed. EPR measurements on the other hand have indicated a spatially delocalised triplet in C_{60} single crystals [75]. Such an excited state delocalisation lends support to the suggestion that the solid state feature observed at 450nm in the absorption spectrum of solid state C_{60} is the result of overlapping wavefunctions of neighbouring molecules. Electro-absorption measurements [62] as discussed in chapter 4 also seem to point towards such a mixing of the wavefunction.

Although it does not account for the absence of the strong triplet-triplet absorption, the proposal by Thomas et al [76] that the photoinduced absorption spectrum originates from an enhanced ground state absorption in molecules neighbouring

excited species merits consideration. Indeed the maxima in the observed spectra do correspond approximately to those in the ground state as can be seen from figure 5.3.

The apparent absence of the triplet state in photoindiuced absorption measurements of the solid raises serious questions about the optical properties of fullerenes. The similarity of the luminescence spectra of the solution and solid as discussed in chapter 4, coupled with similar fluorescent life times, ~1.2ns [65], indicated that the lowest excited state was molecular in character thus contradicting the photoinduced absorption measurements. Furthermore Photoluminescence Detected Magnetic Resonance (PLDMR) indicated the presence of identical triplet states to those present in solution plus a second species which was postulated to be localised on a single pentagon due to intermolecular interactions [67]. The similarities of the excited state properties of solid state fullerenes to those in solution as measured by photoluminescence and PLDMR spectroscopy prompts the inviting conclusion that both the nature and dynamics of the lowest lying excited state are essentially equivalent to those of the isolated molecule. In the previous chapter however evidence of the effect of the solid state environment on the excited states was presented, in particular in the absorption spectra where a solid state specific feature at 450nm was observed. Another strong indication of the effect of the solid state environment on the excited state photodynamics can be seen from the temperature dependence of the luminescence efficiency [77]. At room temperature the emission is weak, however it dramatically increases upon cooling to 100K [77]. The onset of the increase occurs at ~250K, leading to an association of the temperature dependence with the structural phase transition of solid state C_{60}.

The effect of the solid state environment on the optical properties of C_{60} greatly complicates the photophysics and as a result a simple extrapolation of the properties of the molecule to that of the solid is inadequate. This is further highlighted by the observation that the luminescence spectra can vary significantly from powder, film and crystal indicating a dependence on morphology, which is not consistent with a simple molecular origin. Feldmann et al. [66] showed that, on a single crystal, the emission profile can vary significantly from point to point. Analysis of the different

spectra led to the observation that the spectrum at any one point could be constructed from a weighted sum of several sub-spectra. The sub-spectra were attributed to fullerene molecules which resided in different chemical environments, specifically molecules adjacent to chemical impurities, vacancies or to crystal surfaces.

The suggestion that surface states or impurities have a strong influence in the optical and excited state properties of solid state fullerenes is nothing new. It does however lead to speculation that the observed similarities between the luminescence spectra for the solid state and solution are the direct result of surface states whereas the photoinduced absorption is the result of the bulk solid state. In the following sections the idea that solid state C_{60} may have a contribution from both surface and bulk species is explored in greater detail using Raman spectroscopy verifying that this is indeed the case.

5.3.2: Raman Spectroscopy of Molecular Triplet in Solution

The conflicting results of the photoinduced absorption in solution and solid measurements can lead to much speculation about the nature and homogeneity of the optical properties of the solid state of fullerenes. Certainly, a simple extrapolation from the molecule seems inadequate. It is apparent that surface states and impurities play an important role, illustrating again the sensitivity of the optical properties to any perturbation of the symmetry of the local environment. Although there is much evidence that the lowest energy transitions are similar to those of the isolated molecule, there is a strong suggestion that the bulk excited state species differs significantly between the solid and solution. This suggests a severe departure from the molecular properties. In this study the isolation and characterisation of the molecular triplet by Raman spectroscopy is reported for the first time. Similar analysis in the solid state will be discussed in section 5.3.3.

Attempts to isolate the molecular triplet were performed in two solutions; the first in chlorobenzene (5.2g/l) and the second in toluene (3.4g/l). The solutions were filtered

through a 0.5μm filter to remove any particles, which could potentially contribute to non-linear scattering [41]. The two C_{60} solutions displayed qualitatively the same behaviour, hence no differentiation between the solutions has been made in the discussion of the observed behaviour. Although the Raman spectra (at 514.5nm) of both solutions were dominated by the solvent modes, a number of the characteristic ground state C_{60} modes [50] were clearly discernible. For the purpose of comparison with previous studies [78,79,80], this study will concentrate on the A_{2g} pentagonal pinch mode at 1469cm^{-1}. Initially the laser was focussed into the cuvette, in a region where there was no direct interface between the solution and the wall of the cuvette (section 3.2 chapter 3). The incident power was varied using a range of neutral density filters and the sample transmission monitored. As shown in figure 5.4, the sample exhibits a strong inverse saturable absorption over the range studied.

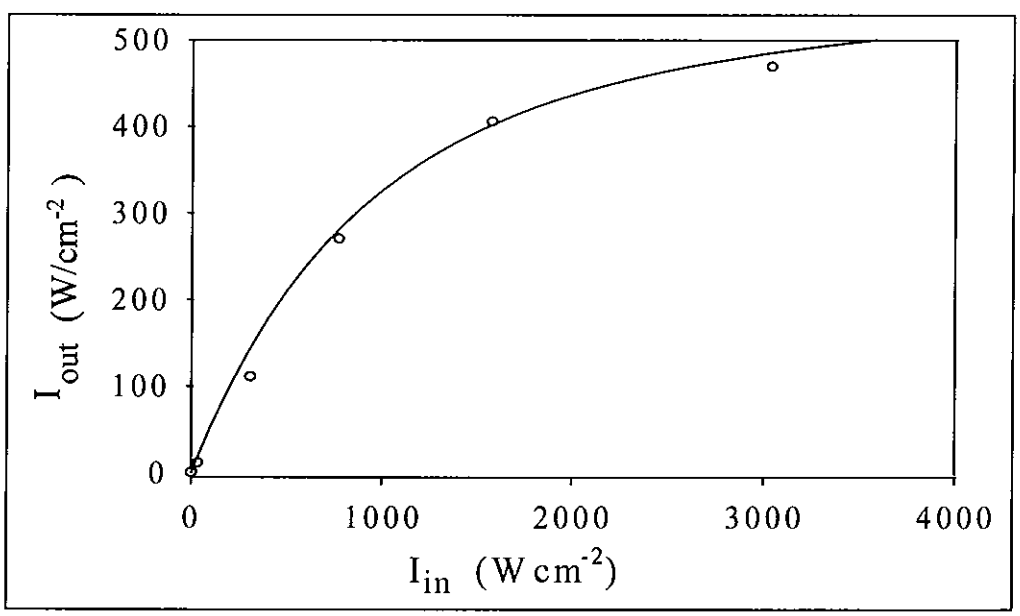

Figure5.4: Intensity dependent transmission curve for C_{60} in chlorobenzene (5.2g/l). The solid line is a fit of equation 5.9 to the curve

This behaviour has been much documented for C_{60} solutions and is ascribable to the strong absorption of the populated excited state triplet of the molecule [68,15]. It can be modelled according to a rate equation approach as discussed in section 5.2. In C_{60} the intersystem crossing time (τ_{IC}) is much less than the singlet state life time (τ_S). On time scales greater than τ_S, the singlet population (N_S) is approximately equal to zero

therefore it can be ignored and the system reduces to a three level system consisting of the ground state, triplet state and a higher excited triplet state. The intensity dependent transmission is then given by,

$$T = \exp[-(N_{gr}\sigma+N_{ex}\sigma_{ex})d] \qquad \text{(Eq 5.9)}$$

such that

$$N_{ex} = N_{gr}\frac{\tau\sigma I}{h\nu} \qquad \text{(Eq 5.10)}$$

$$N_{gr} + N_{ex} = N_{tot} = (-\ln T_o)/\sigma d \qquad \text{(Eq. 5.11)}$$

where N_{tot}, N_{gr} and N_{ex} are the total, ground and excited state populations respectively, σ and σ_{ex} are the ground and triplet state absorption co-efficients, τ is the triplet state lifetime, d is the sample thickness and I is the laser intensity. T_o is determined from the low level transmission. The solid line of figure 5.4 is a fit of equation 5.9 to the data with a value of $\sigma \sim 2.5 \times 10^{-18} cm^2$ and σ_{ex} as $\sim 1 \times 10^{-17} cm^2$ [81]. The fit yields a triplet state lifetime of 30μsec. This is within the range reported for partially degassed C_{60} solutions [73,74].

As shown in figure 5.5, the A_{2g} pentagonal pinch mode is positioned at $1469cm^{-1}$ at low intensities. At high intensities, where a strong inverse saturable absorption is observed, the mode is seen to be shifted to $1466cm^{-1}$. The evolution of the shift is not easily discernible within the resolution of the instrument, but the positioning at $1466cm^{-1}$ is stable from, 2 to 4 $x10^3$ Wcm^{-2}. At an intensity of 4 $x10^3$ Wcm^{-2} a significant triplet state population exists in the solution. It should be concluded that this feature at $1466cm^{-1}$ is a signature of the triplet state of molecular C_{60}.

Van Loosdrecht et al. [82] have reported an intensity dependent shifting of the A_{2g} pentagonal pinch mode from $1469cm^{-1}$ to $1459cm^{-1}$ in C_{60} crystals at low temperatures (~40K), and an assignment of this shifting to the triplet state appeared to be accepted [19]. It should be noted, however, that a population redistribution from ground to triplet state should be characterised by a decrease in the ground state mode and the

emergence of a single triplet mode, rather than the quasi-continuous shifting reported by van Loosdrecht et al. Close consideration of the data in question, however shows an initial discontinuous emergence of a mode at 1466cm^{-1} which, in comparison to the data presented here should be assigned to the molecular triplet [31].

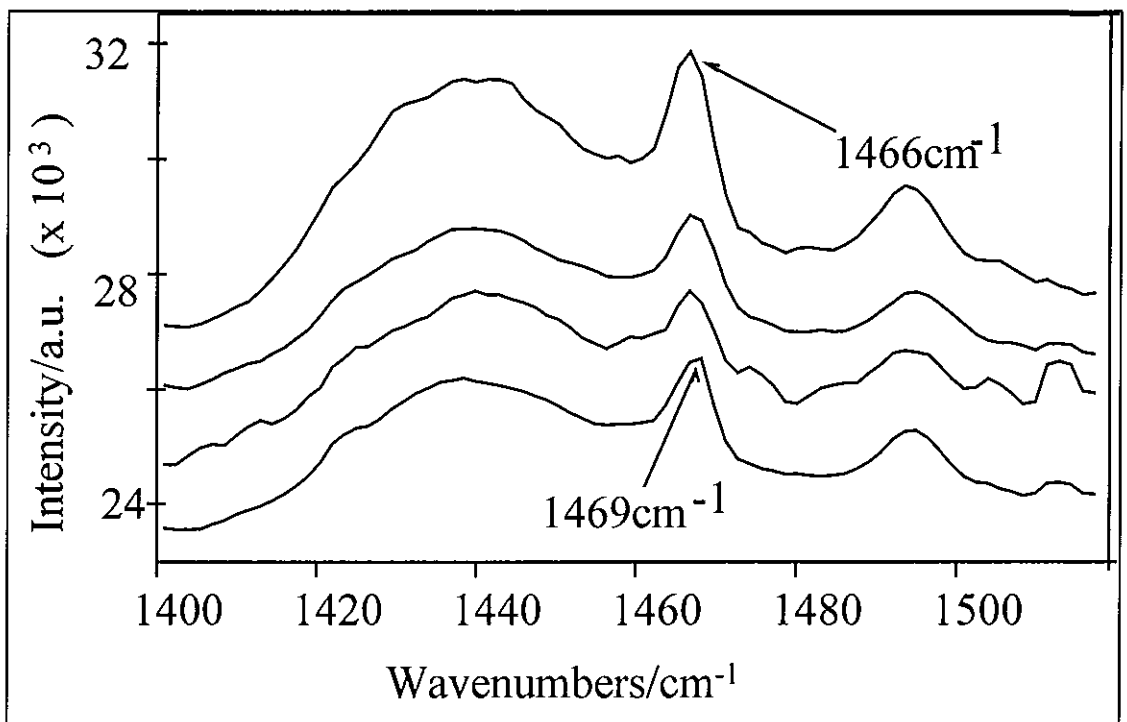

Figure 5.5: The evolution of the molecular triplet of C_{60} from 1469cm^{-1} to 1466cm^{-1} in the Raman spectrum

Further evolution of the state observed in solution will be discussed in terms of the photochemical process active within C_{60} in chapter 6. Nevertheless this data confirms the existence of the molecular triplet of C_{60} with a Raman signature of 1466cm^{-1}.

5.3.3: Raman of Excited state species in solid C_{60} including the Molecular Triplet

In the previous section the Raman spectroscopic signature of the molecular triplet in solution was associated with a positioning of the pentagonal pinch mode A_{2g} at 1466cm^{-1} at room temperature [31]. Similar measurements at room temperature in the solid however, are hampered by the much documented photopolymerisation of C_{60}

[19] which occurs via a 2+2 cycloaddition (discussed in chapter 6). At room temperature, the C_{60} molecules are packed in a face centred cubic (fcc) type geometry and are rapidly spinning about the lattice position. In this particular configuration, solid state C_{60} satisfies the general topochemical and photophysical requirements necessary for the formation of the C_{60} photopolymer via a number of intermediate excited states in accordance with the 2+2 cycloaddition reaction mechanism [83]. However below 249K, solid state C_{60} undergoes an orientational phase transition from a fcc to a simple cubic (sc) type geometry in which the rotation of the molecules is frozen out, inhibiting the formation of the photopolymer as discussed in chapter 2 [19]. Below this phase transition temperature, it should be thus possible to isolate the intermediate excited state species associated with the photopolymerisation and thus identify the Raman signature of the molecular triplet of C_{60} in the solid

The Raman spectrum of C_{60} at 77K was monitored at laser powers of ~300Wcm^{-2}. The spectrum was seen to be considerably richer then the room temperature spectrum due to crystal field and isotopic effects introducing a splitting of the H_g modes and overtones respectively [30]. Nevertheless the observed spectra were consistent with the low temperature spectra described in chapter 4 and previous studies where the A_{2g} mode is seen to be independent of temperature and is positioned at 1469cm^{-1} [19][50][84]. The frequency positions of each mode were found to be stable under prolonged low level illumination indicating that at the low temperature and low intensity no photochemistry was taking place. For the purpose of comparisons with the solution measurements above, this study will concentrate solely on the A_{2g} pentagonal pinch mode at 1469cm^{-1} [31][50][83].

Initially the laser was focused on to a single spot on the film. The incident power was then increased and the positioning of the A_{2g} mode was seen to shift reversibly. In order to correlate the observed intensity dependent shifts in the Raman with the known photodynamics of C_{60} and the previous measurements in solution the intensity dependent transmission of the C_{60} film was monitored. In general, molecular C_{60} exhibits an inverse saturable absorption due to the strong absorption of the excited state triplet in the wavelength range 650 –790nm as seen in figure 5.4. Figure 5.6

shows the curve obtained for the intensity dependent transmission of the C_{60} film obtained under similar conditions as the solution measurements. It can be seen that the film does not exhibit an inverse saturable absorption but rather a linear curve in the range studied. The absence of a nonlinearity does not however indicate that no population redistribution is occurring in situations where the ground state absorption co-efficient (σ_{gr}) and the excited state absorption co-efficient (σ_{ex}) are approximately equal at the wavelength employed. This may indeed be the case for C_{60} films as it can be seen from the photoinduced absorption spectrum that 514.5nm is situated close to the 'cross-over' or null point of the spectrum, shown in Figure 5.3 [69].

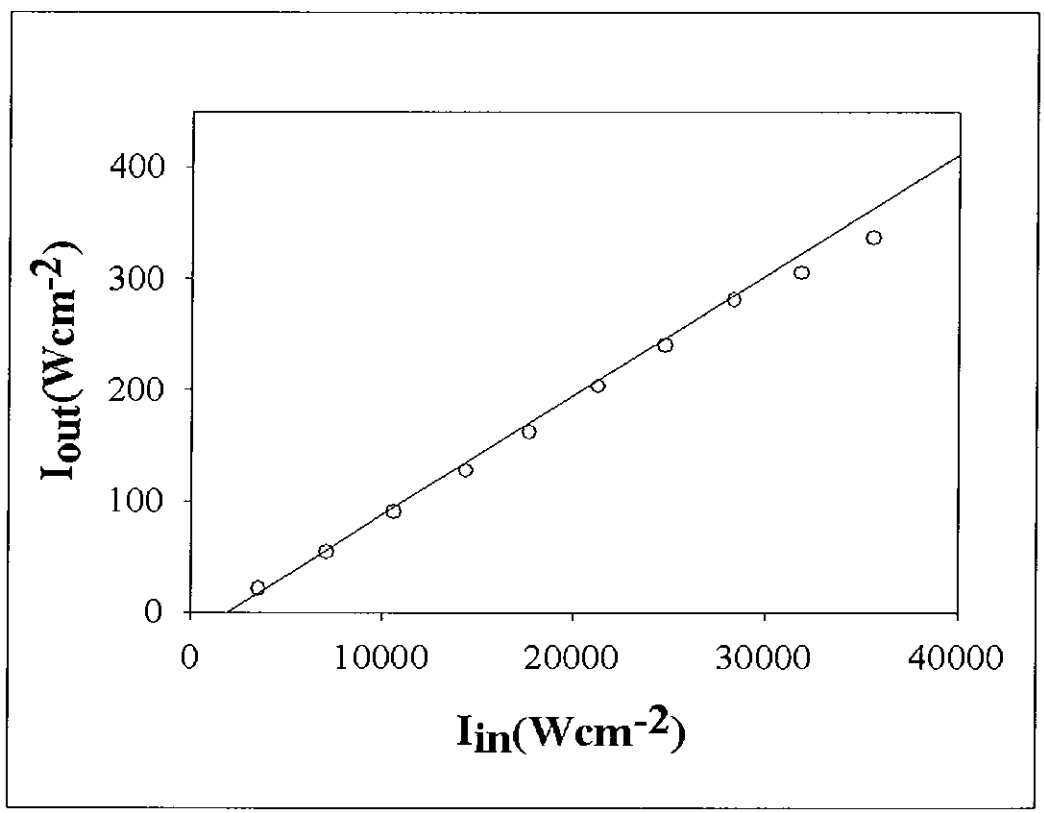

Figure 5.6: Intensity dependent transmission curve for C_{60} thin film (~0.8μm) at 514.5nm. The solid line is a fit of equation 5.9 to the curve.

The solid line of figure 5.6 is a fit of the intensity dependent transmission given by equation 5.9 (which was also applied to the solution measurements) with a value of ~ 2.5x 10^{-18}cm^2 for the ground state absorption cross-section (σ) and 2.6 x 10^{-18} cm^2 for the excited state absorption cross-section (σ_{ex}) [19, 91]. As before T_o was determined from the low level transmission. The fit yields an excited state lifetime of 7μsec for solid state C_{60} which is comparable to previously reported life times of C_{60} [19].

According to the fit, although the intensity dependent transmission is linear, a considerable excited state population can still be readily produced at the intensities used as seen from figure 5.7 which is a plot of the populations of the various levels (states) against the intensity. At an intensity of ~20000Wcm^{-2} the excited state population is ~55% of the total population N_{total}.

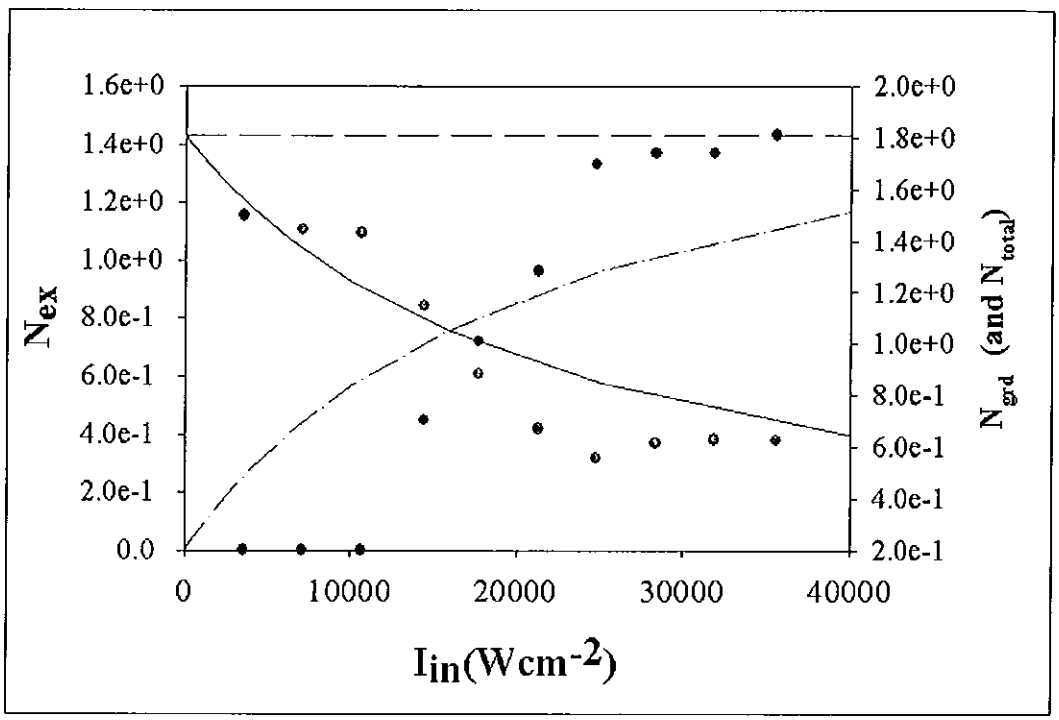

Figure 5.7: Plot of the relative populations of C_{60} for a simple two level system against the incident intensity at 514.5nm. N_{ex} is the excited state population and is represented by the short dashed line and is plotted with respect to the left y-axis, whereas N_{gr} (solid line) and N_{tot} (long dashed line) are the ground state population and the total population respectively and are plotted on the right hand y-axis. The black dots are the relative Raman intensities for the sum of the excited states and the red dots are ground state Raman intensities.

Figure 5.8 shows the in situ Raman spectra taken at various points along the intensity–dependent transmission curve of figure 5.6. The dashed lines in the spectra are Lorentzian/ Gaussian fits to the various components. Figure 5.8(A) shows the low intensity spectrum (>10^4Wcm^{-2}) of the pentagonal pinch mode where it is seen to be positioned at 1469cm^{-1}. However at laser powers approaching ~15000Wcm^{-2} two new components appear in the spectrum (figure 5.8(B)). The first component positioned at 1466cm^{-1} has a Raman signature analogous to that reported for the

molecular triplet of C_{60} in solution in the previous section [31][85]. This is the first Raman identification of the molecular triplet in the solid, which has a corresponding signature in solution.

The second feature at 1463cm^{-1}, is specific to the solid and is reminiscent of a feature observed in the depolymerisation of C_{60} and in nonlinear phenomenon observed in single crystals. The nature of the species responsible for this feature and the molecular triplet will be discussed below. Meanwhile the pentagonal pinch mode remains ever present but experiences a loss in intensity. The evolution of the three features is evident in figure 5.8(C) and figure 5.8(D) with the feature at 1463cm^{-1} becoming the dominant species at high laser intensities (35000Wcm^{-2}). Upon return to low laser intensities the pentagonal pinch mode once again becomes the dominant species suggesting that the photoinduced processes are fully reversible within the resolution of the instrument.

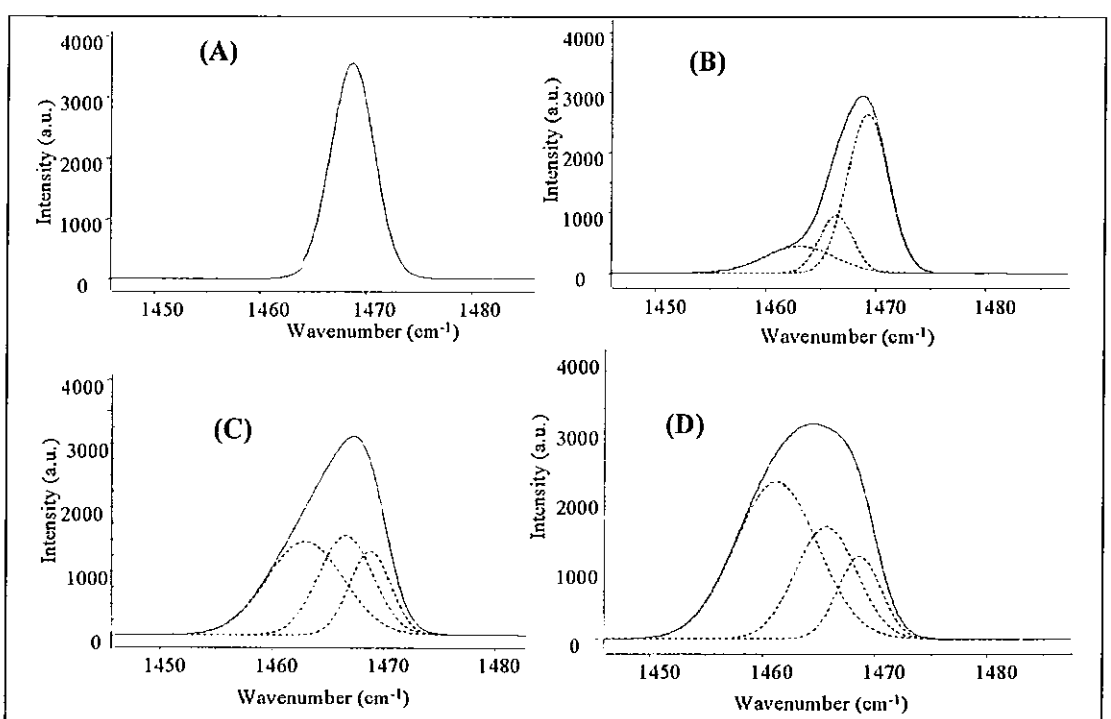

Figure 5.8: Raman spectra of the pentagonal pinch mode at 1469cm^{-1} as the incident intensity at 514.5nm is increased. (A) The low irradance spectrum (>10^4Wcm^{-2}) of the pentagonal pinch mode is seen to be stable (B) At ~15000Wcm^{-2} two new components appear in the spectrum at 1466cm^{-1} and 1463cm^{-1}. (C) and (D) the evolution of the three features is clearly evident with the feature at 1463cm^{-1} becoming the dominant species at high laser intensities (35000Wcm^{-2}) in (D).

The instantaneous reversibility coupled with the intensity dependence is a strong indication that the new peaks are vibrational modes of excited state C_{60} in the solid. Indeed one would expect excited state species of C_{60} to have a lower frequency of vibration as they should be in an antibonding state and hence have a weaker contribution to the intramolecular force constant in comparison to the ground state [80][85]. Furthermore a bond polarisability model of the Raman spectrum of C_{60}, illustrated that the polarisability constants, and therefore the Raman intensities, are dominated by those of the π-conjugated double bonds [86]. A non-linear increase in the Raman intensity of the pentagonal pinch mode is therefore consistent with a non-linear increase in the radial delocalisation of the π-electrons. Such an increase in the delocalisation results in a reduced force-constant, and therefore a mode softening, but since the force-constant is largely determined by the σ-bonds, the mode retains its molecular character and is only moderately perturbed.

Van Loosdrecht et al, as discussed in section 5.2.2 [82] have reported similar intensity dependent shifting of the A_{2g} pentagonal pinch mode from 1469cm^{-1} to 1459cm^{-1} in C_{60} crystals at low temperatures (~40K). They assigned the quasi-continuous shifting to electronically excited C_{60} and in particular the triplet state [82]. However as stated earlier, a population redistribution from ground to triplet state should be characterised by the emergence of a single triplet mode and a decrease in the ground state mode. The emergence of a feature at 1466cm^{-1} in the solid state spectrum presented here should thus be assigned to the molecular triplet appearing in the solid state spectrum. In particular if one considers van Loosdrecht's data and the previous measurements performed in solution. The identification of this feature in the solid indicates that solid state C_{60} does exhibit a molecular triplet and hence partially retains its molecular character.

In addition, however to the feature at 1466cm^{-1}, a further shift to 1463cm^{-1} at higher intensities can be identified both in the data presented here for a thin film and van Loosdrecht's data for single crystals. This feature at 1463cm^{-1} is an excited state species that appears to be specific to the solid state, as similar measurements in solution show no Raman evolution beyond 1466cm^{-1}. This feature has previously

been observed in the depolymerisation of solid C_{60} (chapter 6) [80], as well as in reversible processes in C_{60} crystals [87]. This high intensity state has been associated with that which is characterised by a nonlinear photoluminescence and photoconductivity [88] and has been speculated to be a co-operative interaction between excited sates in the solid, at high excitation densities. That such a non-linear species is present, in the solid state may be understood by drawing comparisons to excited state processes in indirect band gap semiconductors at low temperatures i.e. Si, and Ge [89,90]. In these materials the effect of many body processes has been extensively studied and it is known that they can form electron hole plasmas or liquids [90]. At high excitation intensities the dominating recombination process for excitons as well as free carriers in indirect band gap semiconductors is non-radiative Auger processes [70]. These processes coupled with the materials relatively long lived excited states leads to a high excitation density. In the model proposed by Mott [90], as the excitation density is increased the electron hole interaction is screened by the plasma environment until a critical density (or Mott density) [90]. Above which the exciton binding energy is overcome by exchange and correlation phenomena, resulting in an exciton condensation and thus a delocalisation [89,90]. This condensation also known as a Mott transition has been characterised for indirect band gap semiconductors by a non-linear (cubic) dependence of the photoluminescence output and the photocurrent. The potential contribution of such many particle interactions in fullerenes has been assessed and found to be consistent with such a model [89]. The existence of such a non-linear delocalised excited state in fullerenes may suggest that this excited state species is an alternative to the photopolymer at temperatures below the phase transition at 249K where polymer formation is inhibited as discussed in chapter 2.

The evolution of the Raman peak intensities of the various excited species and the ground state species with respect to the incident intensity is shown in figure 5.9. It can be seen at low laser powers ($>10^4 Wcm^{-2}$) that the ground state species remains relatively constant with no resolvable contributions from the excited states species. However at laser powers greater than $\sim 10^4 Wcm^{-2}$ the peak intensity for the ground state pentagonal pinch mode begins to decrease with the simultaneous growth of both

the triplet excited state species and the excited state co-operate species at ~14000Wcm^{-2}. Initially the triplet species at 1466cm^{-1} is seen to be dominant over the co-operative species at 1463cm^{-1}. However, as the intensity is increased it is seen that the co-operative state becomes the dominant species with both the triplet and ground state species levelling off in their respective evolutions. To attempt to fully understand the evolution of these excited state species the previous model (from figure 5.6) was applied to give a plot of the excited state populations against the intensity shown in figure 5.7. The fit, which is of a simple two level system, shows the relative change of the populations. Although the fit itself is flawed, as the experimental data clearly shows two excited state species in the solid, the addition of both excited state features (the black dots in figure 5.7) does indicate a trend similar to data predicted by the fit for the excited states. The apparent simultaneous growth of the solid state feature (1463cm^{-1}) and the molecular triplet (1466cm^{-1}) greatly complicates the photophysics of the system, raising questions about the possibility of competing or dual processes active in the solid which can produce the second excited state species positioned at 1463cm^{-1}. A potential explanation for the simultaneous appearance of these species may be the variation between surface species and bulk species in the solid. The molecular triplet at 1466cm^{-1} was seen to be dominant in solution suggesting that the corresponding feature in the solid may be the result of a surface species. The second species positioned at 1463cm^{-1}, which is specific to the solid and speculated to be the result of intermolecular interactions would thus correspond to excited state species in the bulk solid. Such an argument is in agreement with the observation made by Feldmann et al [66] in the fluorescence spectrum in which it was proposed that surface states play an important role.

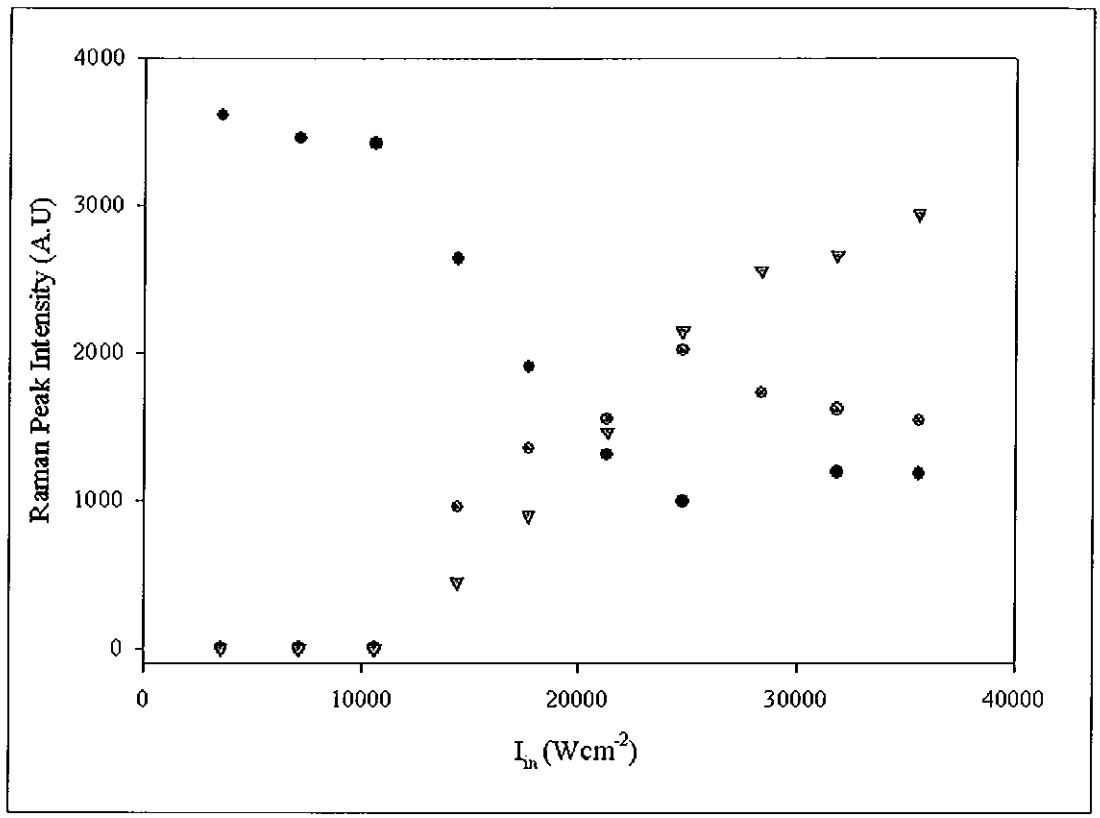

Figure 5.9: The evolution of the peak intensities of the various excited species and the ground state species with respect to the incident intensity at 77K. Black dots represent ground state mode (1469cm^{-1}). Red dots represent mode attributed to the molecular triplet (1466cm^{-1}) while the green triangles represent the high intensity state, 1463cm^{-1}.

5.3.4: Temperature dependence of excited state

As already seen in the previous chapters the properties of C_{60} are extremely sensitive to the local environment. The effect of temperature on the properties of solid C_{60} are clearly evident by the orientational phase transition from a face centred cubic arrangement to a simple cubic arrangement at 249K as discussed in chapter 2. The vibrational character of C_{60} as measured by Raman spectroscopy is also affected by changes in temperature. This is due to the relaxation of the selection rules and significant symmetry reduction as a result of crystal field effects at low temperature. A number of studies on the temperature dependence of the photophysics and the photochemistry of C_{60} have been reported [19, 91] confirming the importance of temperature in assessing the nature of the excited states observed in solid state C_{60}. In this study, the temperature dependence of the excited states reported in the previous section are examined. Similar reversible trends to those seen at 77K (in previous section) for the evolution of the 1469cm^{-1} pentagonal pinch mode and the respective excited states with respect to intensity are observed at temperatures up to ~200K. Above this temperature however the reversibility of the evolution is greatly reduced.

Figure 5.10 clearly shows the affect of temperature on the intensity-dependent transmission curves obtained for the C_{60} thin film in the temperature range of 77-273K. Initially the intensity dependent curve at 77K displayed a linear response (figure 5.6). However as the temperature is increased a more non-linear or cubic behaviour emerges and becomes dominant (figure 5.10 inset). The linear and non-linear components of the intensity dependent transmission curve at higher temperatures are highlighted in figure 5.11 for 198K. This non-linear increase in the transmission is indicative of bleaching in which the excited state absorption cross section is less than the ground state absorption cross section. In general at temperatures above the phase transition (249K), the bleaching process can be attributed to the onset of irreversible photochemical reactions (chapter 6). In this case for temperature below ~200K, no evidence of any photochemical reactions occurring is visible, as the in situ Raman spectra as well as the intensity dependent transmission curves are fully reversible. This suggests that the observed changes are purely

photophysical. While the intensity dependent transmission curve for 198K is significantly different to the corresponding curve at 77K, the in situ Raman spectra and the evolution of the respective excited states at 1466cm^{-1} and 1463cm^{-1} are comparable to those at 77K. A similar the temperature dependence for all temperatures below 198K is also seen.

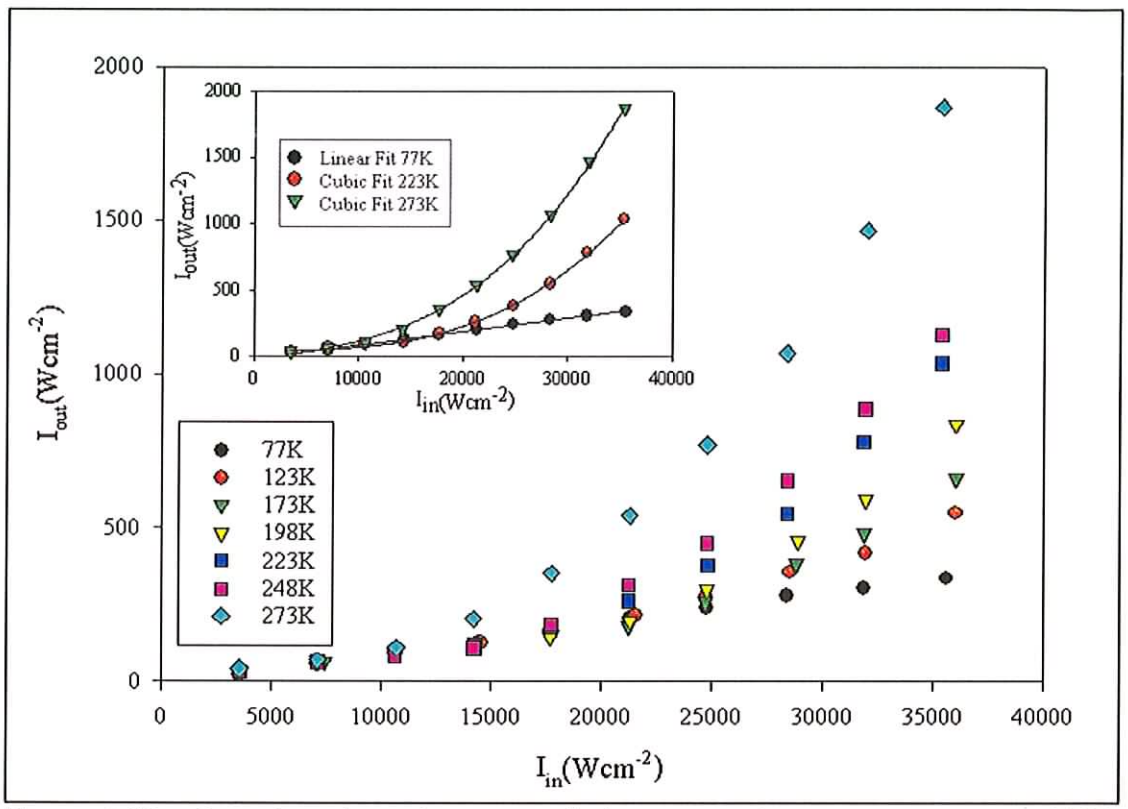

Figure 5.10: Intensity -dependent transmission curves in temperature range 77K-273K. Inset shows cubic fits at higher temperature.

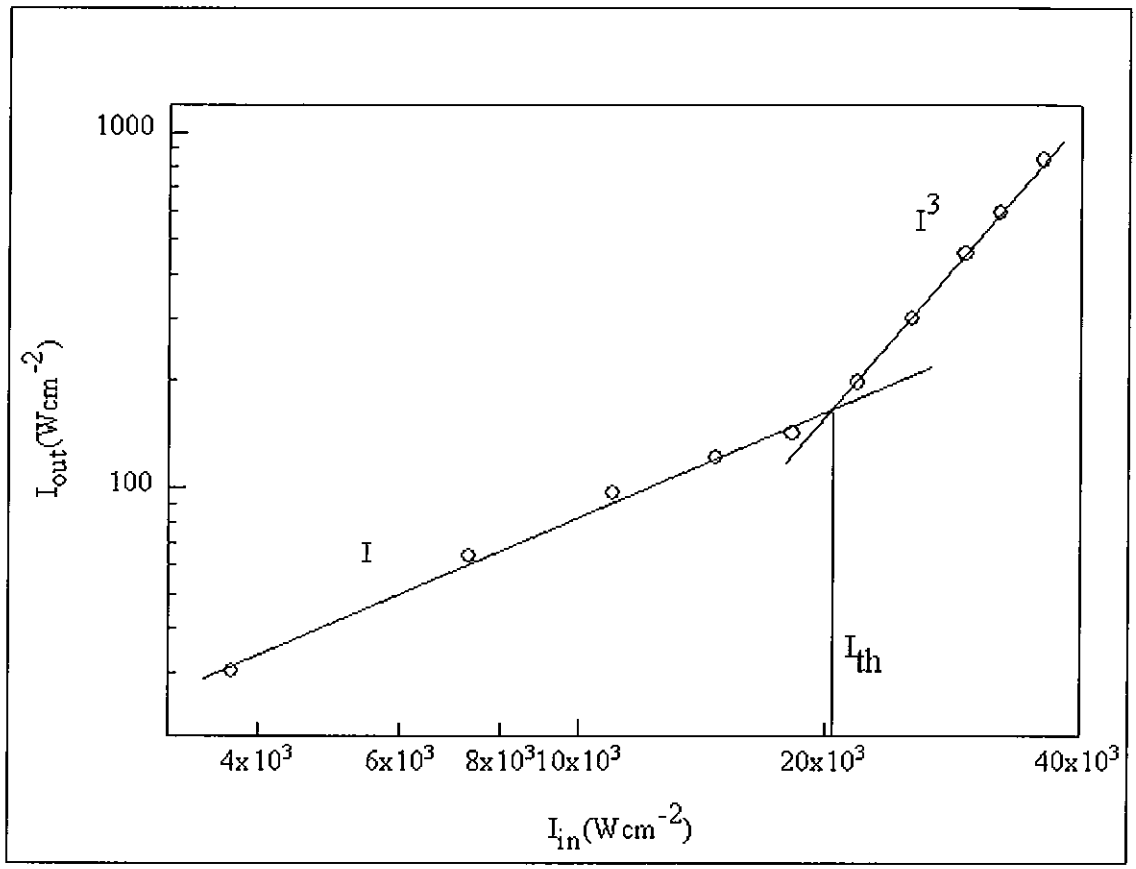

Figure 5.11: Intensity dependent transmission for C_{60} Thin Film at 198K showing cubic and linear components

The change with temperature of the non-linearity can be assessed from the point at which the system deviates from a linear response to a non-linear response in the intensity dependent transmission curves, I_{th} in figure 5.11. The excited state population at this point obtained for each temperature below 198K from figure 5.7 is on average ~50% of the total population N_{total}. Above this temperature the effect of the polymerisation has sever effects on the excited state population and hence the model breaks down. The in situ Raman spectrum of the onset of the non-linearity (i.e. at I_{th}) shows that the co-operative species is the dominant species at this point. A plot of the intensities of the onset of non-linearity (I_{th}) against the inverse of the temperature resulted in figure 5.12. It can be seen that the non-linearity is relatively independent of temperature up to ~220K. This suggests that the electronic delocalisation of the π-electron system, between the molecules in the solid state is intrinsic to the material at temperatures below 220K. It should be noted that this

temperature is remarkably close to the orientational phase transition temperature of 249K particularly when one considers the effect of localised laser heating at the point of measurement. The induced Raman shifts observed with intensity are also fully reversible up until 220K. Above 220K however the temperature independence of the non-linearity rapidly falls to lower intensities suggesting the non-linear delocalised species is formed at much lower intensities. This may be attributable to the increased rotation of the C_{60} molecules above the phase transition allowing the initiation of irreversible photochemical processes such as the photopolymerisation which has a similar effect on the π-electron system but involves the covalent bonding of neighbouring molecules.

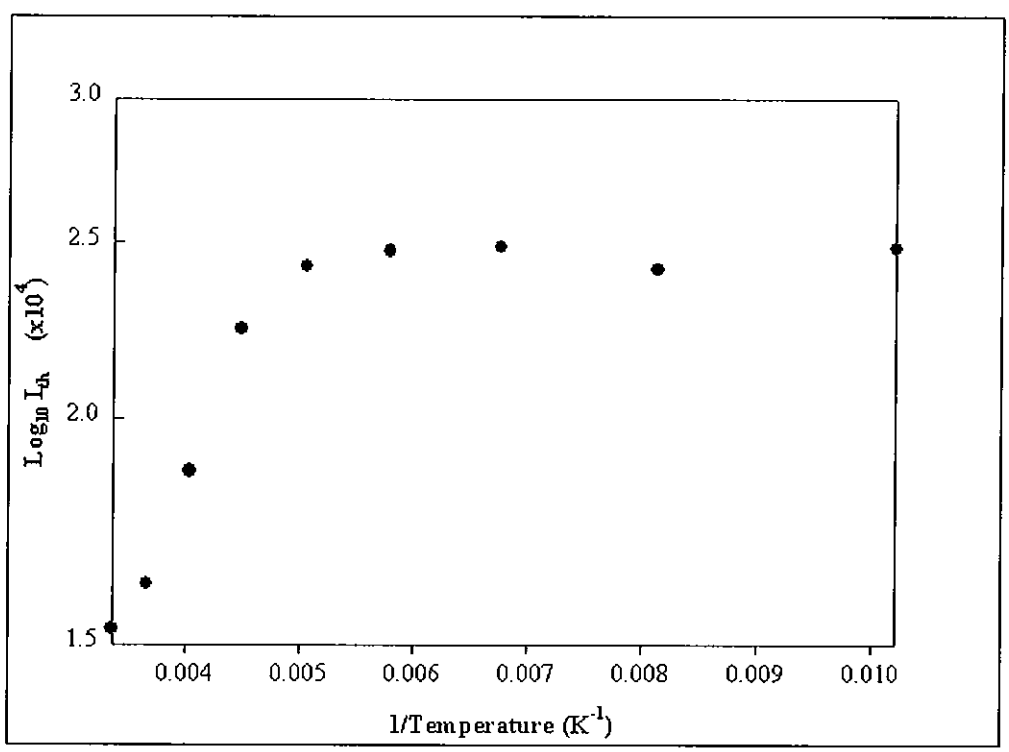

Figure 5.12: A plot of the intensity at which the system deviates from a linear response to a non-linear response in the intensity dependent transmission curves, (I_{th}) against the inverse of the temperature.

A similar temperature dependence of the luminescence and absorption spectra for solid state C_{60} was observed by Minami et.al. [77]. In C_{60} thin films (20nm thick) a relatively temperature independent luminescence intensity was observed at low temperatures in the range 77K-150K. Further temperature increases caused a dramatic

drop in the luminescence intensity with a significant change in the dependence at 260K. The data was fitted using a model characterised by thermally activated quenching of excited states with an activation energy E_a, of 0.12eV for temperatures below ~270K and 0.06eV for temperatures above ~270K. The authors attributed the change in the dependence and the resulting activation energies to the phase transition at 249K and suggested a connection between the thermally activated quenching processes and changes in the luminescence efficiency (emission monitored at 1.66eV). The changes in the luminescence efficiency [77][91] are centred around 2.3eV below which the spectral dependence of the efficiency reflects that of the luminescence excitation spectrum characterised by sharp peaks. Above 2.3eV however the efficiency is featureless and decreases with increasing excitation energy. This suggests that a new decay route opens up that does not contribute to the luminescence. In solution the luminescence efficiency was shown to be constant irrespective of the excitation energy [92]. Indicting that the decay route in C_{60} films should be regarded as the result of an intermolecular effect such as an intermolecular charge transfer excited state or indeed the high intensity excited state species proposed for the observed changes in our data.

In addition to the luminescence the absorption spectrum is also found to change with decreasing temperature [77]. In particular the solid state feature at 450nm is seen to increase more then the allowed transition at 350nm with decreasing temperature. The absorption of the allowed transition increases monotonously with the decreasing temperature while the feature at 450nm has a significant change in intensity below ~249K. In chapter 4 the feature at 450nm was attributed to a charge transfer type excited state in the solid which was strongly influenced by symmetry and hence by the phase change at 450nm. The fact that this feature has a greater increase in absorption then the allowed transition at low temperatures suggest a greater electronic interaction between the individual molecules in the solid. Hence supporting the notion that a highly delocalised excited state similar to that proposed for the Raman mode at ~1463cm^{-1} at low temperatures and for the non-linear response observed at high intensity in the intensity dependent transmission curves, is possible.

At temperatures above 220K the onset of the non-linearity (i.e. I_{th}) is seen to rapidly decrease. The linear and cubic components of the intensity-dependent transmission at 223K are highlighted in figure 5.13. This cubic response is indicative of bleaching whereby the excited state absorption cross section is greater then that of the ground state i.e. $\sigma_{ex} < \sigma$. The bleaching of the system may be attributable in part to the formation of the C_{60} photopolymer. The C_{60} polymer is known to shift the ground state absorption of C_{60} towards the blue hence inducing an apparent reduction in the ground state absorption cross section (chapter 6). The appearance of polymeric phases at 223K maybe the result of localised laser heating increasing the temperature at the point of measurement above the phase transition temperature of 249K.

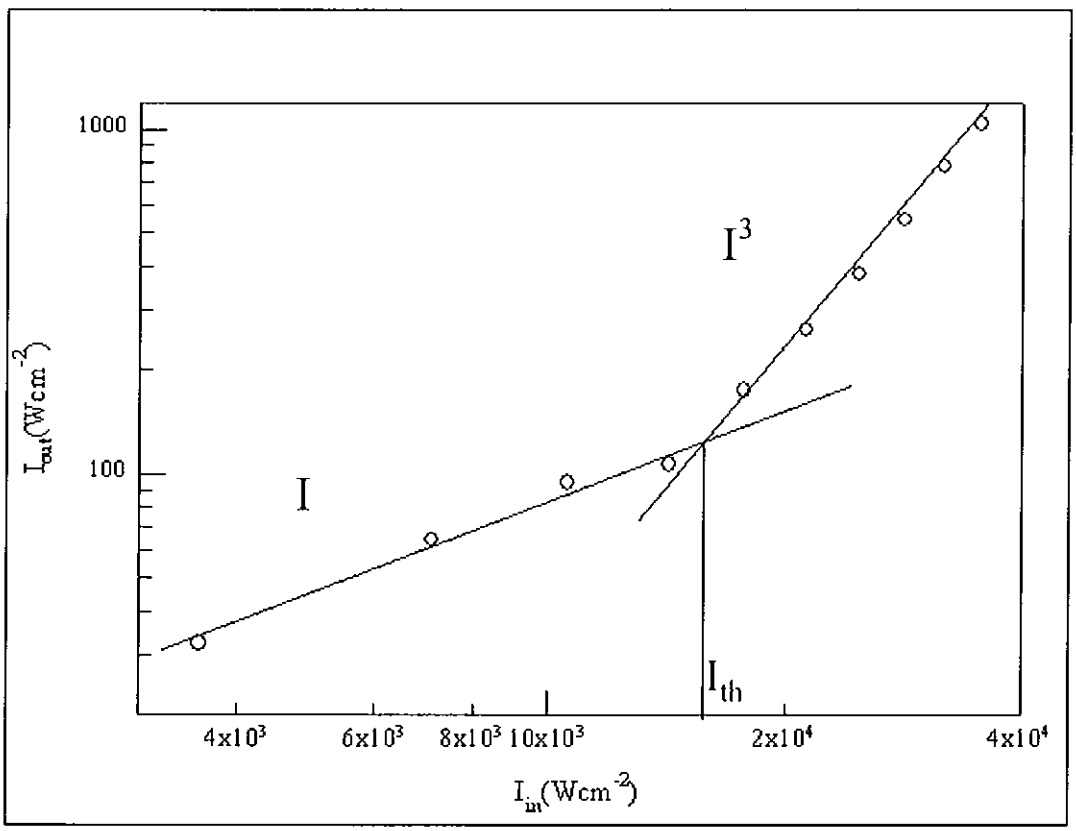

Figure 5.13: Intensity dependent transmission for C_{60} Thin Film at 223K showing cubic and linear components

The in situ Raman spectra of the intensity dependent transmission curve at 223K figure 5.14, confirms that some photochemistry is taking place. As upon the reduction of the incident intensity the original ground state pentagonal pinch mode is not fully regained. As with the previous in situ Raman measurements at 77K, figure 5.14

displays the low intensity (>10^4Wcm^{-2}) Raman spectrum (figure 5.14(A)) with a ground state peak position of 1469cm^{-1}. However as the intensity is increased the molecular triplet and the excited state co-operative species positioned initially at 1466cm^{-1} and 1463cm^{-1} respectively evolve until at high intensities (>40000Wcm^{-1}) the latter species becomes dominant (figure 5.14 (B)-(D)). In contrast to the Raman measurement at 77K the spectral features at 223K are much broader and are more consistent with van Loosdrecht's [82] data for a single crystal. Van Loosdrecht's attributed the reversible intensity dependent shifting of the A_{2g} pentagonal pinch mode from 1469cm^{-1} to 1459cm^{-1} at 40K to electronically excited state C_{60}.

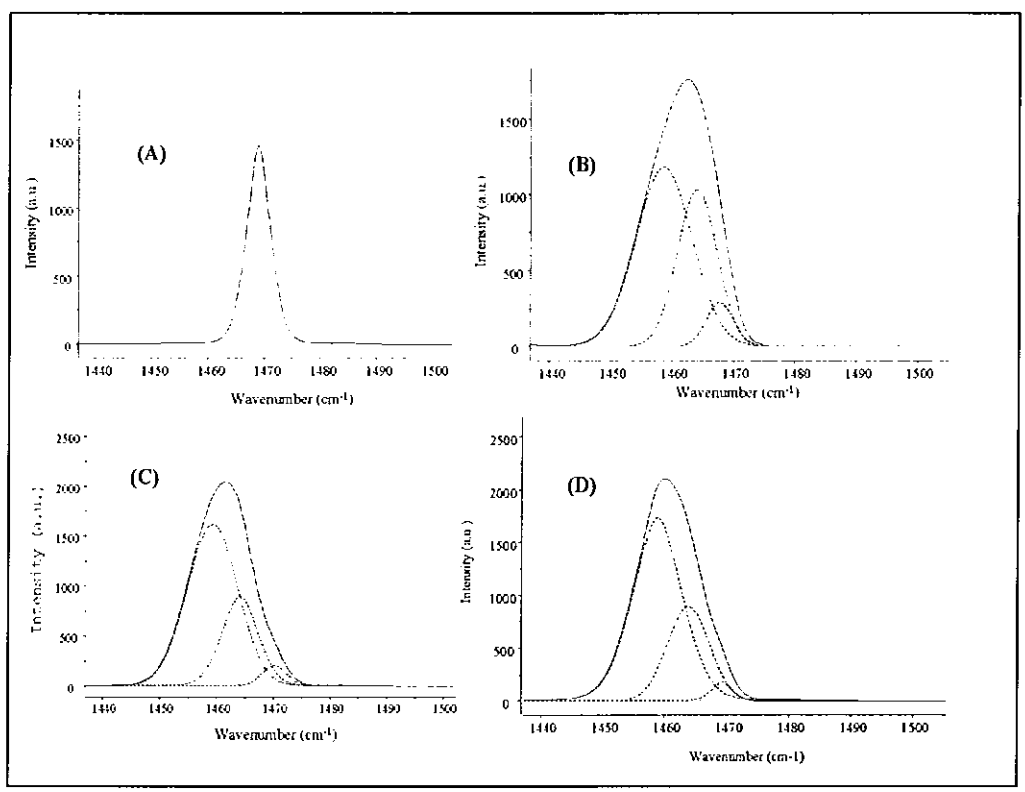

Figure 5.14: Raman spectra of the pentagonal pinch mode as the incident intensity at 514.5nm is increased at 223K. (A) At low intensities the pentagonal pinch mode is stable (10^4Wcm^{-2}) at higher intensities (B), (C) and (D) two additional features appear.

Figure 5.15 shows the partially reversible evolution of the pentagonal pinch mode at 223K. In comparison to the low temperature study at 77K this higher temperature regime begins to form both the excited state species at a lower intensity of

~7000Wcm^{-2}. At ~20000Wcm^{-2} the intensity of the peak at 1466cm^{-1}, which has been assigned to the molecular triplet is ~60% of the original intensity of the ground state feature at 1469cm^{-1} and hence is still in good agreement with the temperature independent model shown in figure 5.7. In addition to the two excited states forming at lower intensities the ground state mode decreases to almost background levels of ~200a.u. While both the molecular triplet and the excited state co-operative species reach a more defined plateaux than observed for the measurements below ~200K. The more defined plateaux at 223K may be the result of increased photochemistry.

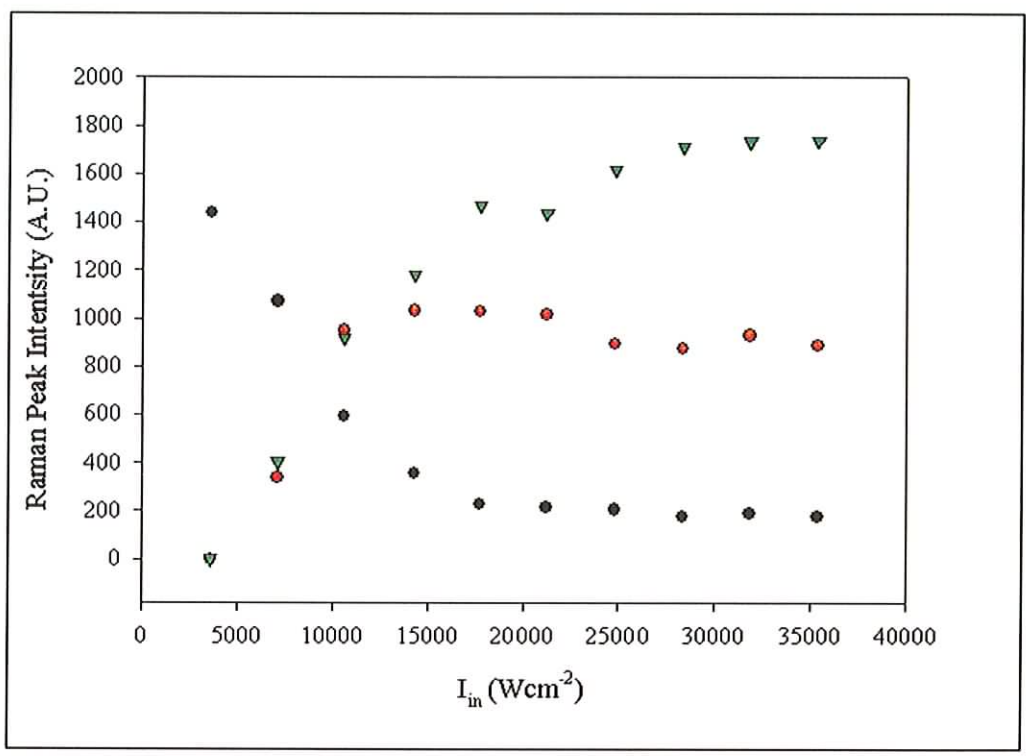

Figure 5.15: The evolution of the peak intensities of the various excited species and the ground state species with respect to the incident intensity at 223K. Black dots represent ground state mode (1469cm^{-1}). Red dots represent mode attributed to the molecular triplet (1466cm^{-1}) while the green triangles represent the high intensity state at 1463cm^{-1}

Although differences between temperatures below and above 220K exist the evolution of the pentagonal pinch mode in the Raman spectrum is exactly that observed by van Loosrecht in single crystals. A notable feature of Van Loosdrecht's data [82] is the step like behaviour of the luminescence measured at 540nm. The step like behaviour is suggestive of a non-linear phenomenon and thus the observed intensity dependence

of the Raman spectrum in both Van Loosdrecht's data and the data present here may be associated with the emergence of a non-linear species at all temperatures. The intensity-dependent transmission of the molecular triplet ($1466cm^{-1}$) in solution demonstrated the well documented inverse saturable absorption curve for C_{60} and it was only after moving into the solid state did the non-linearities become evident suggesting that the excited state species identified at $1463cm^{-1}$ is non-linear in nature. The spectral positioning and the degree of non-linearity of this feature strongly associates it with a highly luminescent, highly conductive phase previously reported to occur in the depolymerisation of C_{60} and single crystals [79, 80, 87]. Consideration of the results present here sheds further light on the nature of this phase. In particular the non-linearities of the observed behaviour again have remarkable parallels to those observed in indirect band gap semiconductors. In such systems a critical excited state density exists above which the exciton binding energy is over come resulting in a Mott like transition [90], suggesting the presence of an extremely delocalised species. The similarities of the behaviour of C_{60} and indirect band gap semiconductors in the high excitation density regime strongly indicates that they are of the same origin. Thermodynamically, however the systems are very different and the application of such models as electron-hole fluids is not straight forward. Nevertheless the non-linear delocalised co-operative species produced is intrinsic to C_{60} at low temperatures and may be an alternative species at low temperatures to the C_{60} photopolymer in which the molecular π-electron system also becomes delocalised between molecules in the highly excited state but rapidly forms a covalent bond.

5.4: Summary

The excited state properties of C_{60} have attracted considerable interest over the years nevertheless a true understanding of the photophysics of C_{60} is still after a decade not fully described. In this chapter it was hoped that a number of unresolved questions regarding the nature of the excited states in C_{60} could be resolved and new questions raised. Indeed the Raman signature of the molecular triplet of C_{60} was identified for the first time in both the solution and solid state at $1466cm^{-1}$, resolving the question as

to whether or not the molecular triplet existed in the solid state. The very presence of the molecular triplet in the solid also indicated that solid state C_{60} does partially retain it molecular character in the excited state. However a second excited state species which is specific to the solid was also identified with a Raman signature of 1463cm^{-1}. This species whose spectral positioning and non-linear evolution was associated with an excited state intermediate which is known to occur during the photo-depolymerisation of C_{60}. It was proposed that this species is a highly non-linear delocalised excited state co-operative involving two or more molecules. It was found that below the phase transition this species dominated at high intensities and was possibly an alternative at these low temperatures to the C_{60} photopolymer. Further investigations into the nature of this excited state co-operative are now need to fully elucidate its true nature and its influence on the potential applications such as optical limiting.

Chapter 6

Polymerisation of C_{60}

6.1: Introduction to Photo-induced processes in C_{60}

In the previous chapter, the reversible photophysics of C_{60} was discussed and two excited state species were identified [93]. The first was the molecular triplet, which was identified for the first time in both solution and solid state using Raman spectroscopy with a mode positioning of ~1466cm^{-1}. While the second species positioned at ~1463cm^{-1} was specific to the solid state and was speculated to be a high intensity excited state co-operative involving two or more molecules in the solid. A temperature dependent study also indicated that, at low temperatures (<249K), the high intensity excited state species was intrinsic to the material and may be an alternative to the photopolymer which is known not to form at temperatures below 249K [19]. In the discussion the role of these excited state species in the irreversible photochemistry of C_{60} was not discussed. However their importance in such processes was implied on several occasions and a good understanding of their nature is an extremely useful tool when assessing the photochemistry of C_{60}.

As with the excited state species, Raman spectroscopy was seen to be an excellent probe in the elucidation of the induced photochemical processes in C_{60} [52]. In chapter 2 it was highlighted that an underlining theme of this thesis would be the relative importance of the inter- and intramolecular processes in terms of their contribution to the electronic transport within the solid C_{60}. A strong indication of an intermolecular interaction is the photochemical transformation of C_{60} in the solid [83]. This phototransformation has been characterised by a shift in the ground state A_{2g} Raman mode at 1469cm^{-1} to a new mode at 1458cm^{-1} with time and low level illumination. The resultant photoproduct has been shown to be insoluble and has been attributed to the formation of a C_{60} polymer [71, 83].

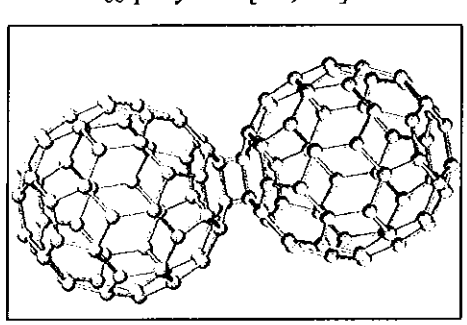

Figure 6.1: Photopolymer of C_{60} (dimer).

The polymer has been suggested to form via a 2+2 cycloaddition reaction, whereby the π bonds of adjacent molecules open to form a covalent coupling between the molecules, [83] as shown in figure 6.1. Although not irrefutably proven, such a picture is widely accepted. It has been proposed that the process occurs through a molecular excited state intermediate and the role of oxygen is as an excited state quencher, which inhibits the photodegradation process [44]. Curiously absent for many years was any report of such a photopolymerisation from solution.

In this chapter the photopolymerisation of C_{60} from solution is described, which strongly supports the 2+2 cycloaddition photopolymerisation model proposed by Eklund [71, 83] to explain the spectral changes in C_{60}. Further to this, based upon literature and IR spectroscopy a structure for the photopolymer produced from solution will be proposed. The final section of the chapter will attempt to look towards the future potential of polymeric phases of C_{60} and discuss the many open questions regarding this new class of material.

6.2: Polymerisation of C_{60}

In general, C_{60} is stable under ambient conditions and the degree of interaction between neighbouring molecules in the solid is minimal [94]. C_{60} however is known to undergo chemical reactions to a number of dense polymeric phases [91]. These phases can be crystalline or amorphous, they can be insulating or metallic and the geometry of the polymeric phases can be one, two or even three-dimensional. The type of polymer which is ultimately formed, is highly dependent upon the method used to produce it, such as intense light, or varying combinations of high temperature and pressure. Regardless of the method used to initiate the polymerisation, the proposed reaction mechanism is a 2+2 cycloaddition reaction [19, 83]. Such reactions are commonly known in organic chemistry and commonly involve the photoinduced coupling between the π-electrons of an excited triplet and those of a neighbouring ground state molecule. Figure 6.2 shows the general mechanism for a 2+2 cycloaddition in C_{60}. The 2+2 cycloaddition reaction is thermally forbidden but is one

photon allowed when adjacent π bonds are separated by less than ~4.2Å. Additionally the reaction may proceed via injection of a charge into the lowest unoccupied triply degenerate molecular orbital (thus creating a state comparable to the optically excited triplet) or by the forcing together of the molecules under pressure [91].

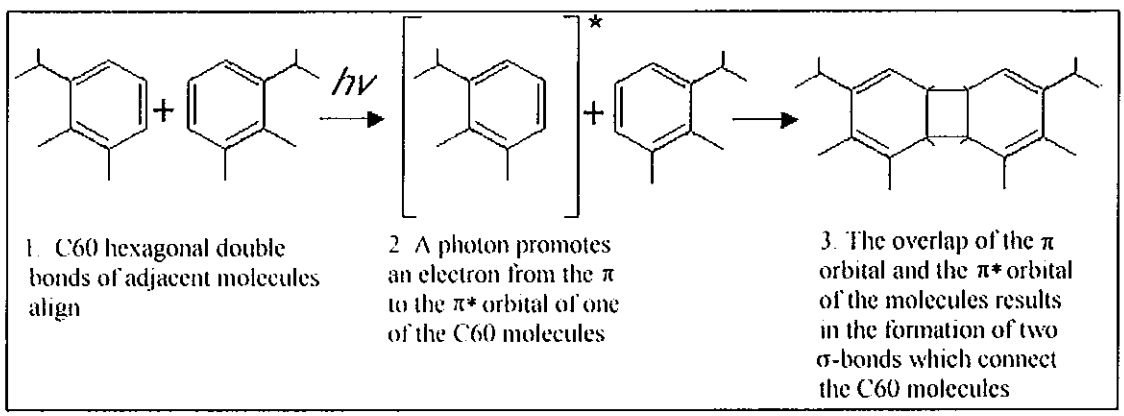

Figure 6.2: General reaction scheme of a 2+2 cycloaddition

The first polymeric phases of C_{60} were obtained by photopolymerisation at ambient temperature using intense visible or ultraviolet light [83]. The degree of polymerisation however is extremely localised, making structural analysis difficult. This has led many to speculate about the structure of the photopolymer and until sufficient X-ray diffraction analysis is obtained it will remain a point of debate. In contrast, a number of pressure and temperature induced polymeric phases of C_{60} have been identified [95]. In general pressure and temperature induced polymerisation tends to be a bulk process making structural analysis relatively easy. A number of high pressure and high temperature polymeric phases of C_{60} have been proposed. At a temperature of 300-400K and 5GPa pressure, Iwasa et al. [96] proposed a contracted fcc phase (termed fcc(pC_{60}) or 'soft fcc'). In this particular type of C_{60} polymer there is a small volume contraction of the lattice (3.7%) and it is not entirely clear if chemical bonds are involved [94]. As the temperature is increased to ~600K and a pressure of 8GPa an orthorhombic phase consisting of parallel running polymeric chains is formed [94] (figure 6.3). At higher temperatures and lower pressure (e.g.3GPa and ~800K), a mixture of tetragonal (figure 6.3) and rhombohedral (figure 6.3) polymeric phases

appear with 2D sheets of covalently bonded C_{60} cages [94, 95]. At pressures of 4GPa and ~900K a pure rhombohedral phase can be obtained and finally, at very high temperatures, the cage structure collapses and an amorphous phase is formed [94].

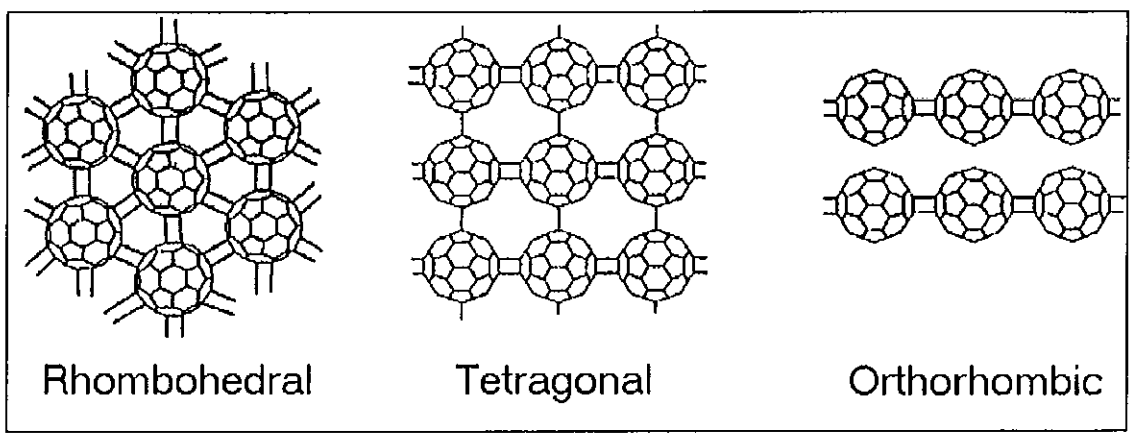

Figure 6.3: Pressure and temperature induced phase of polymeric C_{60}

6.3: Induced Photochemical Processes in solid C_{60}

The effect of the polymerisation of C_{60} on the optical properties of the material is still relatively unknown. The absorption spectrum is known to be blue shifted with respect to the pristine (unpolymerised) material and many of the transitions are broadened considerably [83]. The broadening of the bands in the absorption spectrum has been attributed to a random photochemical cross-linking of the C_{60} molecules, which reduces the symmetry and removes the degeneracies of the electronic energy levels thus contributing to line broadening [19, 78, 83]. Eklund [19] has explained the blue shift of the spectrum in terms of a simple energy level diagram in which the energy levels of the polymerised material are upshifted with respect to those of the pristine material. Similar changes in the photoluminescence spectrum of the photopolymer are also reported although the peaks are red shifted with respect to those of the pristine material [19]. This red shifting in the photoluminescence spectra is consistent the luminescence red shifts observed for oligomerisation (i.e. monomer to dimer; dimer to trimer, etc.) in the helicene series and in polyacences [97]. The broadening effect in both the absorption and the photoluminescence may also be

related to the lifting of the degeneracies in the vibrational modes of the C_{60} photopolymer [83]. Indeed vibrational spectroscopy has been used to great effect in the study of the properties of the photopolymerised material, although initial controversy over the position of the Raman modes did create some confusion [19].

Figure 6.4 shows the Raman spectrum of a single spot on a thin film illuminated at low intensities (~1mW) for ~1hour. In comparison to the initial spectrum taken for the first 30sec, several of the fundamental modes can be clearly seen to have shifted in position and new modes below 150cm^{-1} have appeared. In particular the A_{1g} mode (normally positioned at ~496cm^{-1}) and the A_{2g} mode (normally positioned at ~1468cm^{-1}) can be seen to have shifted to ~492cm^{-1} and ~1459cm^{-1} respectively.

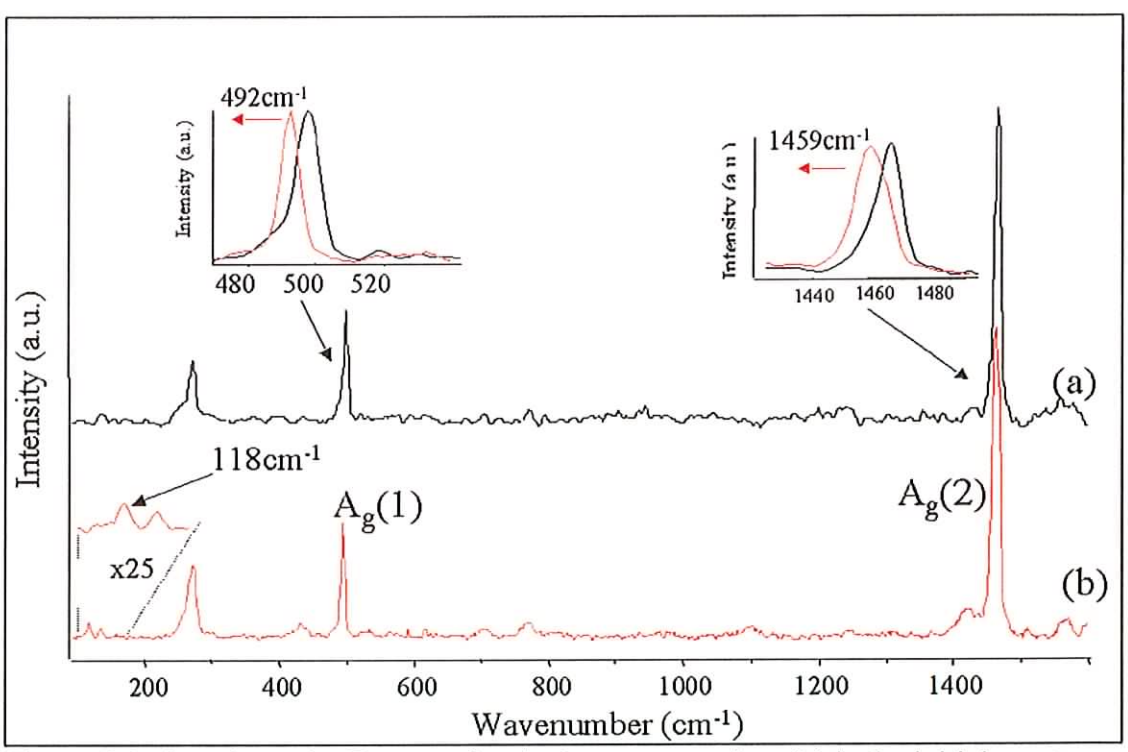

Figure 6.4 : Low intensity Raman of a single spot over time (a) is the initial spectrum (b) is after 3 hours illumination at 514.5nm.

These spectra highlight the initial controversy generated over the spectral positioning of the modes of the Raman spectrum. The essence of the debate can be illustrated by considering the positioning of the strongest mode, the A_{2g} pentagonal pinch mode. Measurements, which were conducted in air, yielded a mode positioning of 1469cm^{-1}

[98], whereas in the absence of air the mode was found to lie at 1459cm^{-1} [99, 100]. This, naturally, begged the conclusion that the latter was the true mode positioning, prompting consideration of photo-oxidation processes in the solid state. The debate, however, was further fired by the appearance of the mode at 1469cm^{-1} when measured in a vacuum at low temperatures [82]. Detailed studies revealed that, in a vacuum, the mode was stably positioned at 1469cm^{-1} at temperatures up to 249K, corresponding to that of the orientational phase transition, above which a time dependent decay of the oscillator strength at 1469cm^{-1} and concomitant appearance of a new, weaker and broader feature at 1459cm^{-1}, occurred [78]. After prolonged illumination, the irradiated material was observed to be no longer soluble in solvents known to dissolve C_{60} [78]. Furthermore, at temperatures of ~450K and higher, the mode is seen to revert to its original positioning of 1469cm^{-1}. Similar changes to the positioning of the other fundamental modes are also reported in literature [87].

This wandering of the A_g mode is clearly visible in the set of spectra in figure 6.5 taken for a thin film at room temperature. A single spot (~1μm) on the film was exposed to prolonged low level illumination (~1mW) for ten minutes. Spectra (a) to (e) show the evolution with time of the 1469cm^{-1} mode to the 1459cm^{-1} mode. It should be noted that in light of the previous chapter a weak contribution from the molecular triplet at 1466cm^{-1} may be visible in spectrum (c). However as the temperature dependence study showed, this feature becomes progressively weaker at temperatures approaching room temperature in the solid. Although the 1469cm^{-1} mode is still present in spectrum (e) it is considerably weaker and indicates a photochemical degradation of C_{60} to a species with a Raman signature at 1459cm^{-1}, which is stable at the low intensity. However, upon increasing the intensity above ~8mW this new mode (1459cm^{-1}) was seen to shift abruptly to a higher Raman frequency of 1463cm^{-1}, spectrum (f). This behaviour has been well documented in literature [79, 80, 87] and this new feature at 1463cm^{-1} has been assigned to a high energy excited state. This feature is identical to the excited state co-operative observed at low temperatures in chapter 5, which also has a Raman signature of

1463cm^{-1}. Finally, returning to low intensities (~1mW), the 1469cm^{-1} mode position is seen to partially reappear (g) suggesting a quasi-reversible process.

Similarly, with intensity dependent studies, the same reversible trend is observed. Figure 6.6 shows a collection of spectra taken for a spot on a thin film as the intensity was gradually increased at room temperature. Initially at low intensities (~1mW) the 1468cm^{-1} mode is present, shown in spectrum (a), and as the intensity is increased this mode diminishes in intensity and the appearance of a mode at 1459cm^{-1} begins to become evident, spectrum (c). This new mode at 1459cm^{-1} is stable below a threshold intensity of ~2 x 10^3 Wcm^{-2}. Once the intensity is increased beyond this threshold a peak at 1463cm^{-1} emerges and in accordance with the aforementioned time dependent studies and literature [87] can be ascribed to a high intensity excited state again similar to the species discussed in chapter 5 which is also positioned at 1463cm^{-1}. Finally a return to low intensities partially reproduces the original 1468cm^{-1} mode again indicating a partially revisable photochemical process.

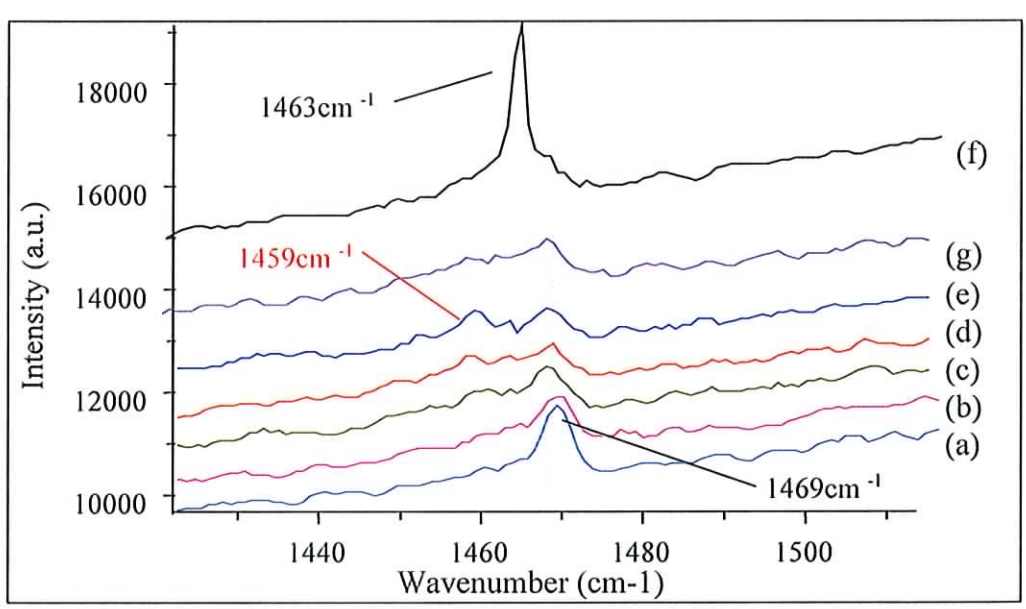

Figure 6.5: The evolution of the mode at 1469cm^{-1} to 1459cm^{-1} with respect to time. Prolonged illumination at low laser powers was seen to produce a peak at 1459cm^{-1} (a) to (e). Then upon an abrupt increase of the laser power a peak at 1463cm^{-1} appeared (f) and returning to the low laser powers regained the 1469cm^{-1} (g) pentagonal pinch mode. Indicating the cyclic nature of the processes.

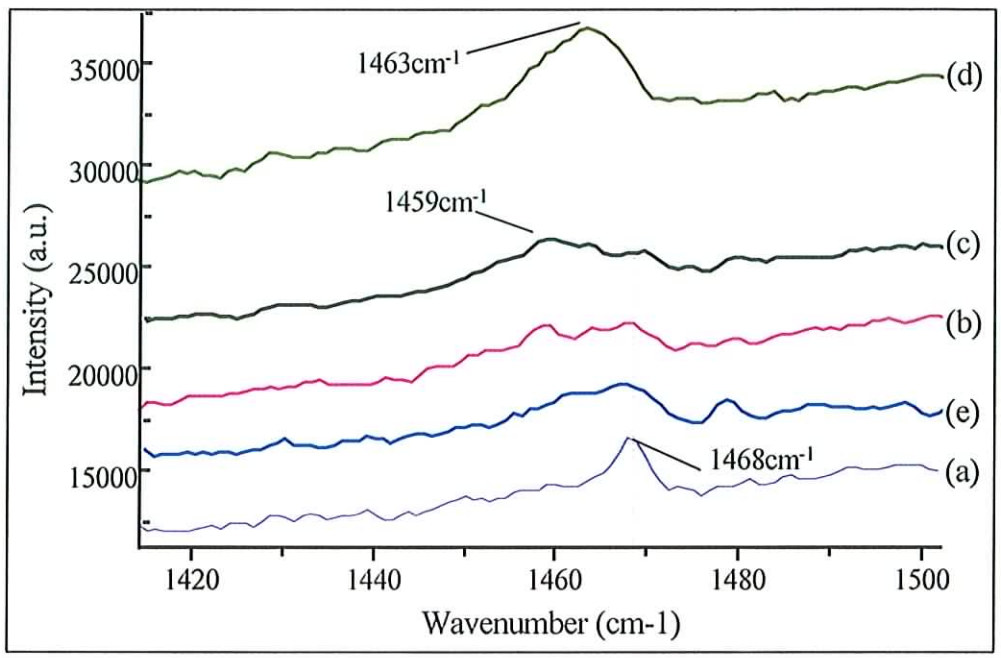

Figure 6.6: The evolution of the mode at 1469cm^{-1} to 1459cm^{-1} with respect to intensity. As the laser intensity was increased a shift to (c) 1458cm^{-1} was observed. By increasing the laser power again a peak at (d) 1463cm^{-1} appeared and was attributed to a high energy excited state specific to the solid. Returning abruptly to low laser powers reproduced the pentagonal pinch mode again at 1469cm^{-1} (e).

A proposal to solve the mystery of the wandering modes at low intensities, was put forward by Eklund et al [83], who attributed the process to the photochemical coupling between the molecules as the result of a 2 + 2 cycloaddition via an excited state intermediate (as discussed in section 6.2) [101]. Such a ground state- excited state coupling is consistent with the fact that the rate of the observed spectroscopic changes is linearly dependent on intensity [34]. It was proposed that such a coupling results in a randomly linked "photopolymer" which was insoluble in common solvents associated with C_{60}. Evidence for the existence of coupled molecules in irradiated material was subsequently obtained by mass spectroscopy [102]. In this proposed photochemical coupling, spectroscopically the mode retains most of its molecular character, which is governed by the strong σ-bonds. The loss of the π-contribution results in a decrease in the force constant, accounting for the 10cm^{-1} shift, whereas the reduced oscillator strength [78] can be accounted for by the reduced polarisability of the no-longer delocalised π-electrons. The proposal of a covalent coupling between molecules in the solid can also account for the apparent temperature dependence [78]

of the shift, since below the phase transition temperature (225K) the electron rich hexagons are aligned with the non-reactive pentagons preventing the formation of the bridging σ-bonds (chapter two, section 2.2.2). The proposed polymerisation model appears to account well for the observed behaviour and as a result has become widely accepted although it was not irrefutably proven, as there are many measurements, which are not immediately explained by the model. For instance the apparent absence for many years of the process from solution caused many researchers to put forward alternative explanations [53, 54, 103]. In all cases however, the approach is to invoke co-operative intermolecular processes, whether they result in a full chemical bond or weaker interactions. Nevertheless the observed behaviour represents a strong indication of intermolecular interactions in photoexcited species in the solid state.

6.4: Induced Photochemical Processes in Solution

The absence of any reported photochemical processes from solution for many years led many to believe that the photochemical transformation of C_{60} into a photopolymer was specific to the solid state. As a result many questions arose regarding the validity of the photopolymerisation mechanism proposed by Eklund and indeed whether the degree of translational freedom within solution inhibited chemical bonding between C_{60} molecules. In this study the polymerisation of C_{60} from solution is reported for the first time thus supporting the proposed 2+2 cycloaddition model and confirming equilibrium bond formation in solvated C_{60} [31].

As with the determination of the Raman signature for the molecular triplet, (chapter 5 section 5.3.2) two solutions of C_{60} were examined: (1) chlorobenzene (5.2g/l) and (2) toluene (3.4g/l). As before the two C_{60} solutions displayed qualitatively the same behaviour, hence no differentiation between the solutions has been made in the discussion of the observed behaviour. The solutions were placed into quartz cuvettes ($10cm^3$) and degassed for ~40 minutes and the cuvettes were then sealed. The Raman

scattering signal of C_{60} in solution was then monitored as a function of the excitation intensity at 514.5nm.

When the sample was illuminated at high intensities and the argon ion laser focussed at the interface between the sample and cuvette, an insoluble deposit, shown in figure 6.7 was seen to accumulate at the interface. The Raman spectrum of the photo-deposited material (figure 6.8) is shifted with respect to pristine C_{60}, indicative of the much documented C_{60} photopolymer produced in the solid state [19, 83]. In particular the pentagonal pinch mode, normally positioned at 1459cm^{-1} and the pentagonal breathing mode, normally positioned at 496cm^{-1}, are positioned at 1459cm^{-1} and 492cm^{-1} respectively in the photo-deposited material. Also clearly evident is the emergence of new features below 150cm^{-1}, which can be attributed to the formation of a covalent coupling between molecules [5] and is thus consistent with the suggestion that the photo-deposit is polymeric in nature.

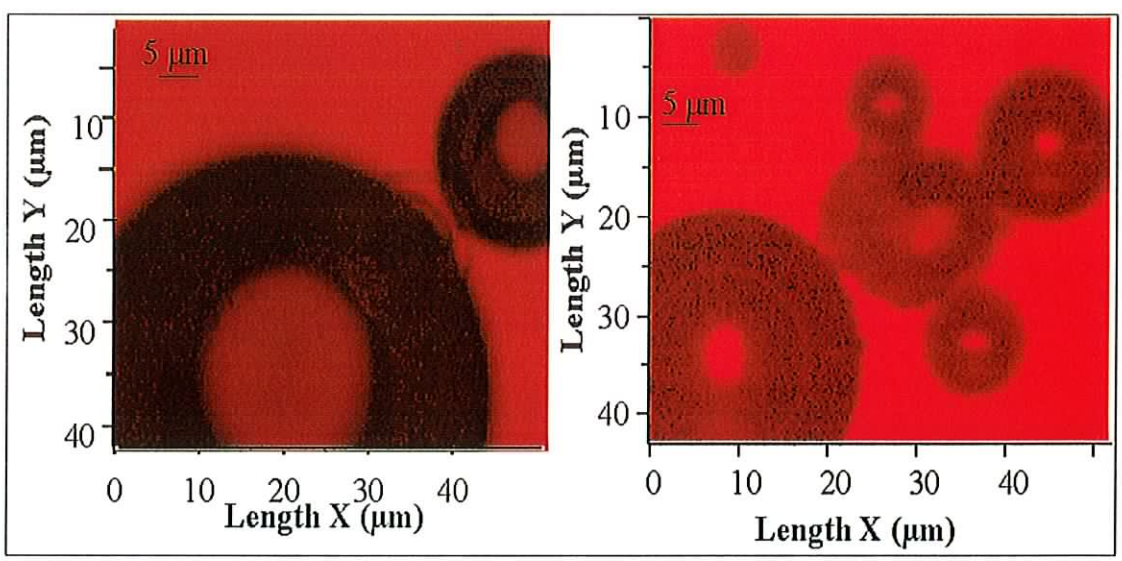

Figure 6.7: Optical microscope image of the insoluble deposits taken using the Instruments S.A. labram 1B microscope (x10 objective) and CCD camera. The hollow centre is thought to be due localised heating by the laser spot inhibiting the reaction mechanism.

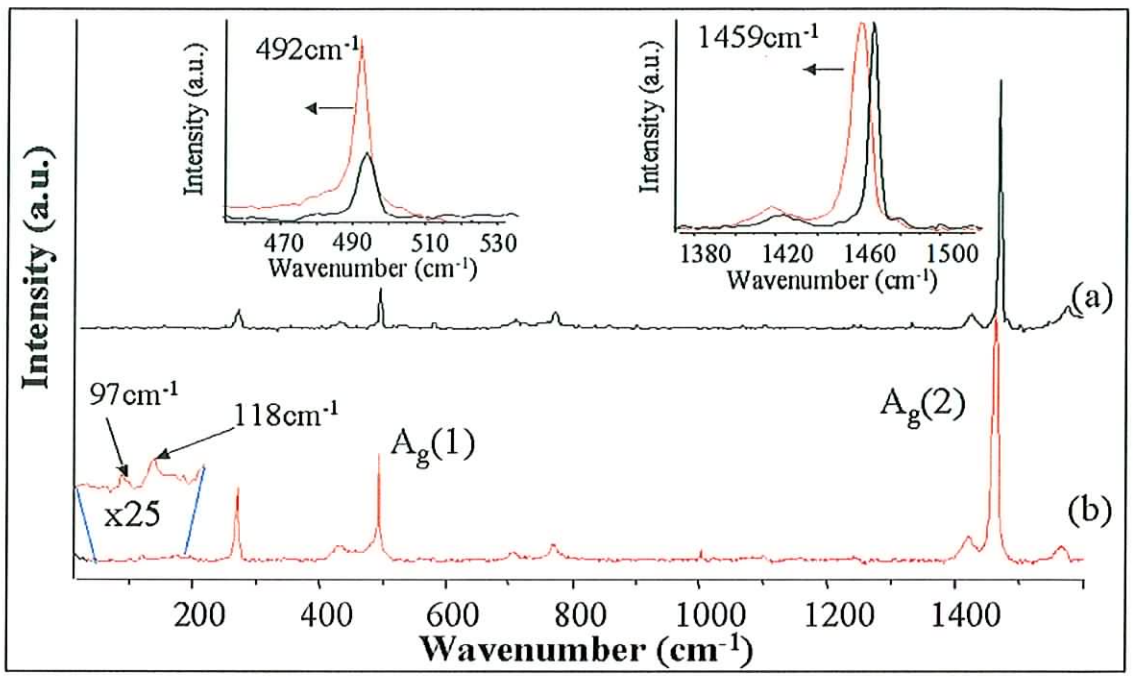

Figure 6.8: Raman spectrum of insoluble deposit, (a) is the pristine C_{60} spectrum (b) spectrum of deposit.

The formation of the insoluble photo-deposit is characterised by an evolution of the pentagonal pinch mode as shown in figure 6.9. Initially positioned, at $1469cm^{-1}$, as the laser power is increased an abrupt shift to $1466cm^{-1}$ followed by a further abrupt shift to $1459cm^{-1}$ was observed. The latter shift is not controllable by intensity and the $1466cm^{-1}$ positioning is not stable. The mode positioning of $1459cm^{-1}$ was stable at laser powers of ~2 $x10^{3}Wcm^{-2}$ and below. The shift to $1466cm^{-1}$ is consistent with the optical generation of a triplet population as seen in chapter 5. The scattering observed is strong compared to that of the triplet generation previously described (section 5.3.2), which may be indicative of an accumulation of these species at the interface as they are generated. As the triplet state population evolves, a deposit is formed on the interface which has a Raman signature of $1458cm^{-1}$, characteristic of the phototransformed solid state of C_{60}.

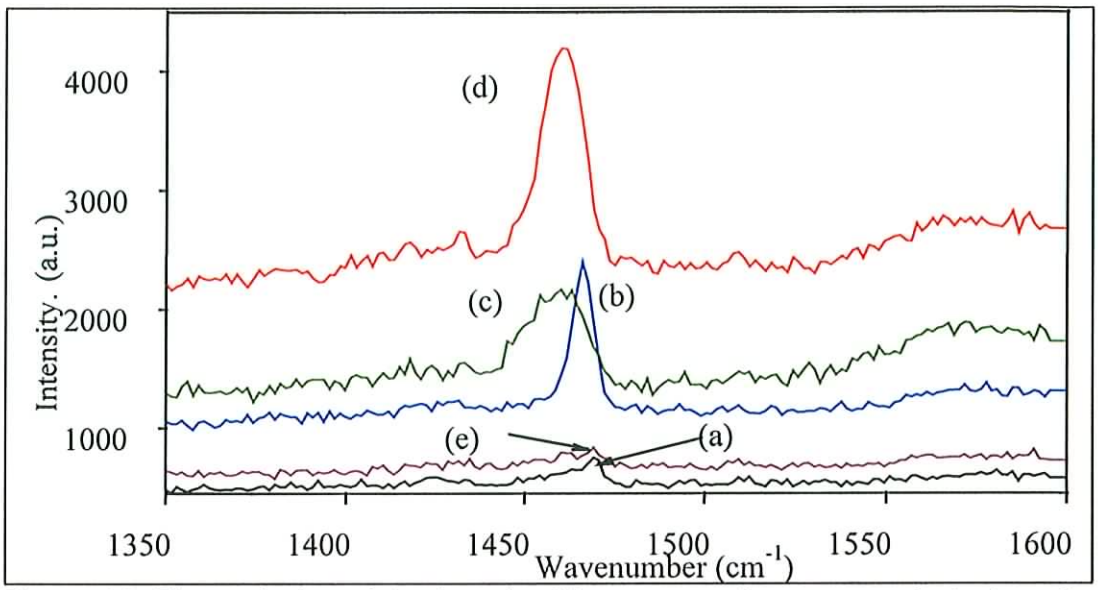

Figure 6.9: The evolution of the deposit with respect to the pentagonal pinch mode at 1469cm^{-1}(a). As the laser intensity was increased a shift to (b) 1466cm^{-1} and a further shift to (c) 1458cm^{-1} was observed. By increasing the laser power again a peak at (d) 1463cm^{-1} appeared and was attributed to a high energy excited state specific to the solid. Returning abruptly to low laser powers reproduced the pentagonal pinch mode again at 1469cm^{-1} (e).

The deposit mimics the behaviour of the phototransformed solid state with respect to intensity and time dependent illumination. As shown in figure 6.9, upon further increase in intensity, the mode position shifts to a value of 1463cm^{-1}, and, when the intensity is abruptly reduced the mode position reverts to that of the pristine C_{60}. Prolonged illumination at this low level results in an evolution of the peak to its position at 1458cm^{-1}, characteristic of the phototransformation of the solid as shown in figure 6.10. The process is cycleable, in that subsequent illumination at high intensities produces a strong feature at 1463cm^{-1}, which returns to 1469cm^{-1} upon abrupt reduction of the intensity. The reversible photochemical process is precisely that which has been previously observed in solid state C_{60} [79], supporting the proposal that the process is a photopolymerisation from solution.

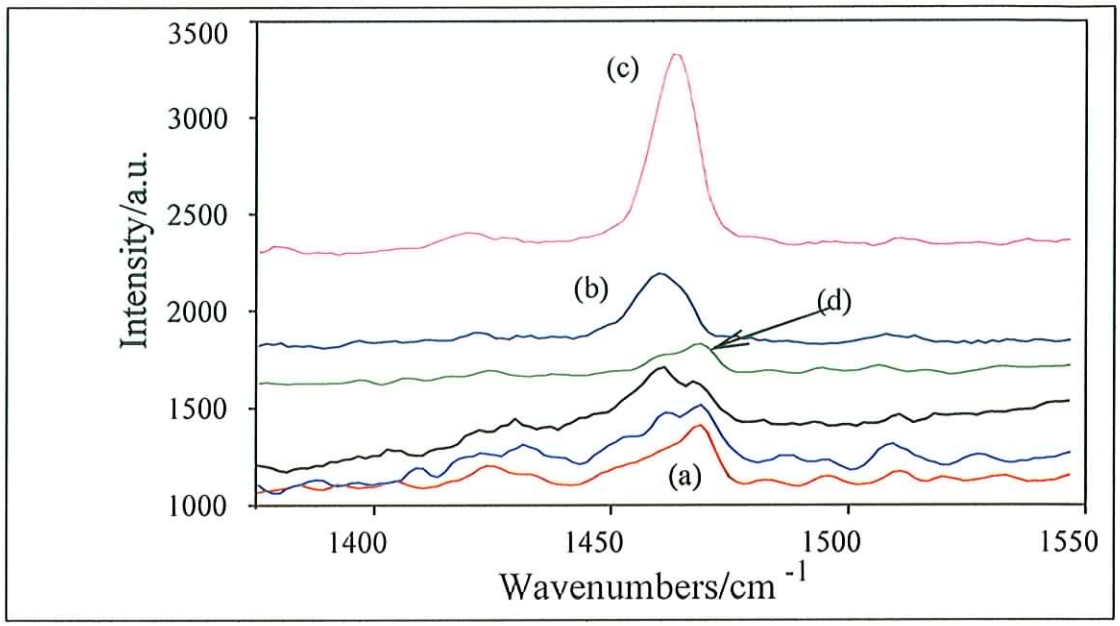

Figure 6.10: Prolonged illumination of the 1469cm-1 (a) at low laser powers was seen to produce the deposit and the resulting peak (b) at 1458cm^{-1}. Then upon an abrupt increase of the laser power the 1463cm^{-1} Raman peak (c) appeared and returning to the low laser powers regained the 1469cm^{-1} (d) pentagonal pinch mode. Indicating the cyclic nature of the processes.

Although it is difficult to speculate as to the mechanism for the deposition process, this is the first report of polymerisation of C_{60} from solution. The initial polymerisation occurs via the molecular triplet, characterised by a Raman signature of 1466cm^{-1}. It should be noted, however, that, once the deposit is formed this signature is no longer observable in the polymerisation - depolymerisation process. That it is observable in solid state measurements at low temperature [82] is due to the inhibition of the photopolymerisation process below the phase transition temperature of C_{60}. A high intensity intermediate with a signature at 1463cm^{-1} is observable in both these measurements and those of the solid state. This state is characterised by a very large Raman intensity accompanied by a very large background. These characteristics have previously been observed in the depolymerisation of solid C_{60}, as well as in reversible processes in C_{60} crystals. The high intensity state has been associated with that which evolves via a nonlinear photoluminescence and photoconductivity [88] and has been speculated to be a co-operative interaction between excited sates in the solid, at high excitation densities (chapter 5). That such a state is present as intermediate in the depolymerisation process may be understood by considering the symmetry conditions

for the proposed 2+2 cycloaddition polymerisation mechanism [19,78]. That the reaction is symmetry forbidden between two molecules in the ground state, but may be photoinduced, implies that it is similarly symmetry forbidden between two excited states. At high intensities, the weakly bound polymer is dissociated, leaving a high density of excited states in the solid.

In order to elucidate the type of C_{60} polymer produced from solution, an instantaneous Raman spectrum of the deposit as it evolved was obtained (i.e. the spectrum was taken just as the deposit began to form) figure 6.11. For comparison with earlier studies this spectrum concentrated upon the pentagonal pinch mode region [31,104]. Table 6.1 highlights the importance of this narrow region of the Raman spectrum in the elucidation of the photochemistry and photophysics of C_{60} with several species readily identifiable in within ten wavenumbers [104]. The table has been divided into species that are produced by photopolymerisation and those that are produced via high pressure and temperature. The two excited state species which were identified in chapter 5 have been included for completeness. It should be noted that the high intensity excited state co-operative has a Raman signature close to that of the dimeric species suggesting that the delocalisation of the excited state is concentrated over only a few molecules in the solid state.

Table 6.1: Raman signature of polymeric and excited state species which occur around the pentagonal pinch mode

Photo Induced	**Pressure Induced**	**Assignment**
1434.2cm^{-1}	1434.6 cm^{-1}	Polymeric planes
1446.3 cm^{-1}	1447.0 cm^{-1}	Polymeric planes
1454.0 cm^{-1}	1454.8 cm^{-1}	Branched chains
1460.5 cm^{-1}	1459.5 cm^{-1}	Linear chains
1464.6 cm^{-1}	1464.7 cm^{-1}	Dimers
1469.6 cm^{-1}	1468.8 cm^{-1}	Pristine C_{60}
1466.2 cm^{-1}	----	Molecular triplet
1463.2 cm^{-1}	----	High intensity excited state Co-operative

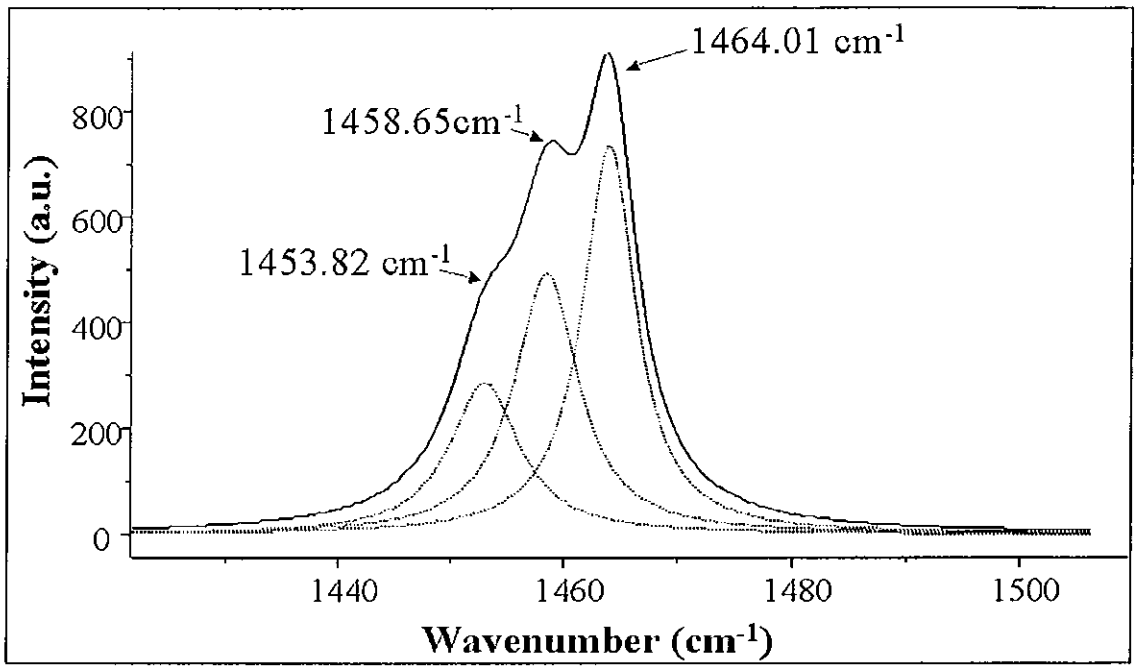

Figure 6.11: Instantaneous Raman spectrum of the pentagonal pinch mode region for the photo-deposit.

The instantaneous Raman spectrum of the deposit, figure 6.11 shows three main features in the region outlined in table 6.1. The feature at 1464cm^{-1} can be assigned to a number of species such as C_{60} clathrates [105], excited state species [93] and significantly C_{60} dimers [104]. Chlorobenzene and toluene are both known to form clathrate compounds with C_{60} which can cause the pentagonal pinch mode to shift to Raman frequencies comparable to 1464cm^{-1} as will be discussed in chapter 8. However as can be seen from table 6.1 the C_{60} dimer has a signature of 1464.6cm^{-1}. It is thus proposed that the photo-deposit is initially dimeric in nature. Indeed such a suggestion is consistent with the degree of transitional freedom one would expect a C_{60} molecule to have in solution. The strong feature at 1459cm^{-1} is clearly the signature of the C_{60} photopolymer while the weak feature at 1454cm^{-1} may be the result of chain branching as speculated by Sundqvist [104]. The absence of a feature at 1469cm^{-1} for the pristine C_{60} can be attributed to the formation of clathrates from solution as opposed to pristine C_{60} [105].

The evidence that the photo-deposited material is a polymeric species of C_{60} is further supported by the IR spectrum shown in figure 6.12. In comparison to the pristine

material the deposit exhibits a greatly enriched spectrum, with several new features evolving. While these features can be associated with the presence of C_{60} polymer [84] no direct comparison to the individual IR spectra of the photo- or pressure induced polymeric phase in the solid state can be made [19, 96, 106]. Instead the IR spectrum of the polymeric species produced from solution seems to consist of a complex mixture of phases namely that of the 'soft fcc' and the rhombohedral phase [96]. Nevertheless the presence of a new disordered phase produced form solution cannot be ruled out.

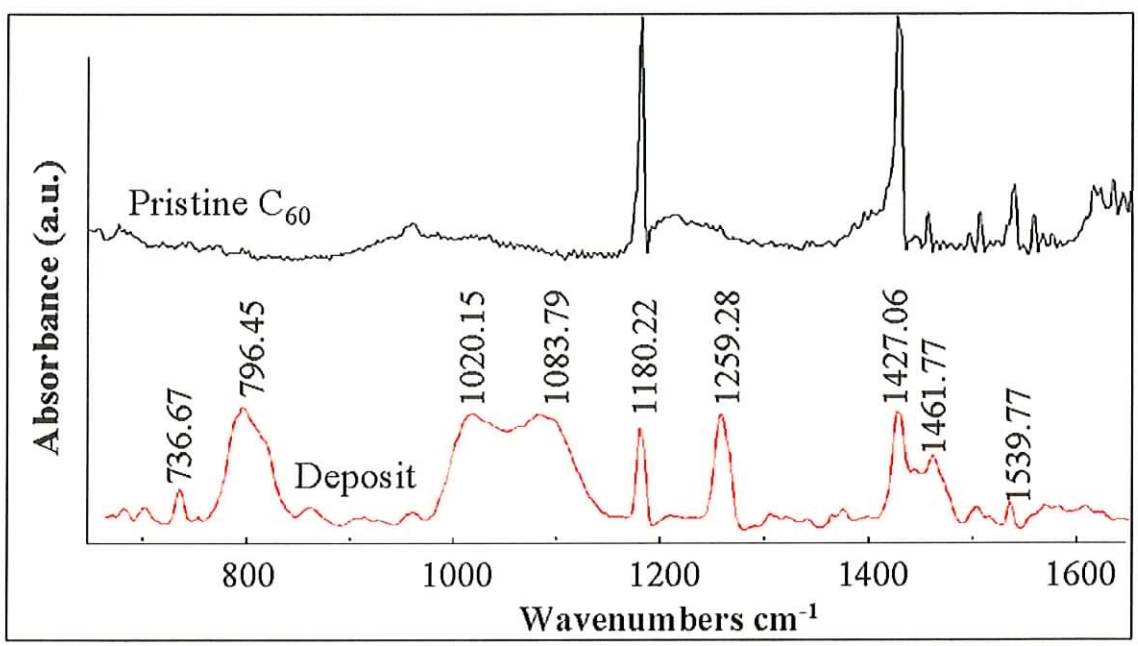

Figure 6.12: IR spectrum of the pristine C_{60} and the photodeposited material.

As can be seen from figure 6.12 the two F_{1u} modes present in the pristine material at 1183cm^{-1} and 1428cm^{-1} are considerably reduced in intensity and are slightly down shifted in the photo-deposited material. This is in part due to the formation of intermolecular bonds between C_{60} molecules which reduce the molecular symmetry and thus activate several new modes which can 'steal' oscillator strength from allowed modes of vibration [102]. The peaks at 1427.06cm^{-1} and 1461.77cm^{-1} can be associated with a splitting of the $F_{1u}(4)$ mode [106]. However it is interesting to note that the frequency position of these infrared bands matches rather well with those of

the Raman bands for the photopolymerised material in the solid. It is known from group theory, that the Raman and infrared active modes are no longer strictly complementary once the symmetry is broken: i.e. Raman active modes are also observed in the corresponding infrared spectrum and vice versa [44, 106]. The relatively large inhomogeneous broadened feature centred at 1106cm^{-1} is consistent with the polymeric material produced at high temperatures and pressures in the solid [106]. In particular the rhombohedral phase and the 'soft fcc' phase, [96] however in IR spectra reported in literature for the photopolymeric material produced in the solid no broad features are observed in this region [96, 102, 104, 106]. In addition to this the broad feature at 796.45cm^{-1}, while present in the solid state photopolymer is less resolved and resembles the feature observed in the same region for the 'soft fcc' polymeric phase [96]. It is suggested then that the polymeric phase produced from solution is a complex mixture of the phases consisting of mainly dimeric species. Additionally since the material is produced from solution it may even be a clathratic form of the photopolymer in which the solvent molecules force together the C_{60} molecules to produce a new polymeric phase which is a hybrid of the 'soft fcc' polymer and the photopolymer.

TEM pictures of the photodeposit shown in figure 6.13 (B and C) show it to be considerably different to pristine C_{60} (figure 6.13 (A)). At the edge of the deposit, string like fibres are seen in figure 6.13 (B) which is consistent with the formation of a polymeric type material. Closer to the centre of the ring of the deposit (i.e. see optical microscopy figure 6.7) the features are considerably larger with microscopic size granules clearly visible. These pictures coupled with the vibrational spectroscopy suggest the formation of a material which is considerably different to pristine C_{60} and which is polymeric in nature. However until sufficient X-ray structural analysis is performed no real assessment of the structure can be made other than that outlined from the spectroscopic data.

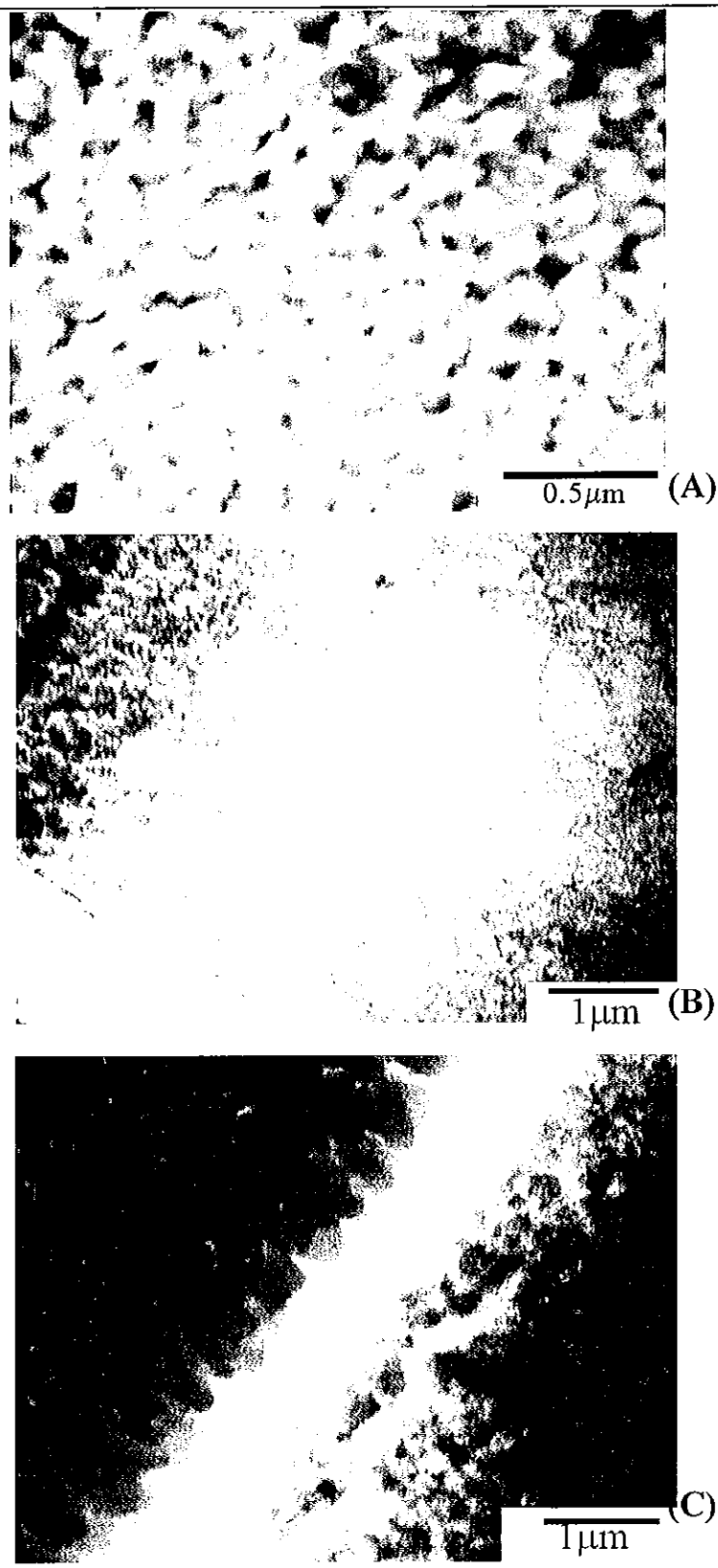

Figure 6.13: (A) TEM of pristine C_{60} (B) and (C) TEM pictures of deposit, Magnification: x 60,000

6.5: Summary and Future Directions for photopolymer

In this chapter the photochemistry of C_{60} was discussed in both the solid state and in solution. The C_{60} photopolymer produced form solution was reported for the first time and was seen to form via the molecular triplet whose Raman signature was obtained in the previous chapter. The formation of this species via an excited state intermediate supports the 2+2 cycloaddition reaction mechanism proposed [83] for the photopolymerisation of C_{60}. Vibrational spectroscopy indicates that the photopolymer produced from solution consists of a complex mixture of polymeric phases, which reduce the molecular symmetry and enrich the Raman and IR spectra. In particular, IR spectroscopy seems to indicate that the material is closely related to the pressure and temperature induced 'soft fcc' phase [96]. While Raman spectroscopy reveals features consisted with the formation of dimeric material [104] and clathrates [105], both of which are consistent with the notion of this polymeric material being produced from solution. However the quantities of the material, which can be produced from solution, are quite small (~0.5-1mg) and hence structural analysis using conventional methods is difficult, X-ray data of the photodeposit is needed to fully elucidate its structure.

It should be noted however that once the insoluble deposit forms, its behaviour mimics that seen for the solid state material with respect to intensity and can thus undergo a depolymerisation process via a high intensity excited state similar to the excited co-operative species discussed in chapter 5. The presence of such as species in the depolymerisation process coupled with the fact that the polymerisation occurs via the molecular triplet highlights the importance of the excited state properties of C_{60} when attempting understanding other aspects of fullerene science. Figure 6.14 summarises the species, which have been produced optically both in this chapter and in the previous chapter on excited states and attempts to show how each species is related. It also should be noted that this diagram is valid for both solid C_{60} and for solvated C_{60} in light of the work present here. It also shows the fine balance between photophysics and photochemistry in C_{60}.

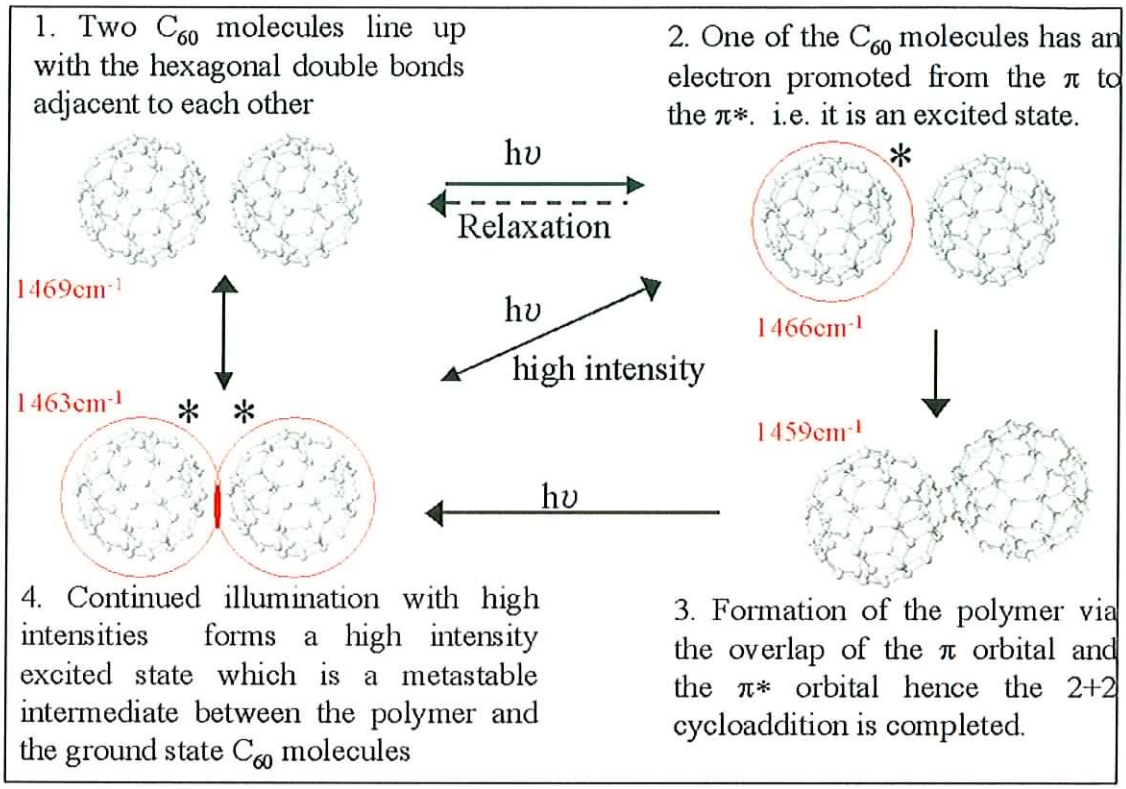

Figure 6.14: Summary of optical species which can be readily produced in C_{60}. The red numbers refer to the respective species Raman signature.

Polymeric phases of C_{60} represent a colourful new class of material with potentially interesting optical and electronic properties. Even though some of the basic properties of the polymerisation process and of the polymeric phases are reasonably well understood, several open questions remain and provide a wide field for future research work. The open questions are concerned for example with the structure of the photopolymer in the solid and of polymeric material produced from solution. Further spectroscopic and electronic analysis of the material produced from solution is essential to allow more comparisons between this material and the solid state polymer to be drawn. In addition the electronic properties of the material produced from solution will have to be investigated in order to assess its future potential. Doped polymeric phases such as AC_{60} (where A is K, Rb, Cs) which were not discussed in this study, have also exhibited great potential as metallic conductors [95] and are a vibrant research area in their own right [91].

Chapter 7

Electronic and Ionic species of C_{60}

7.1: Reasons for the Generation of Ionic Species of C_{60}

In previous chapters the optical properties of C_{60} and the characterisation, by Raman and excited state spectroscopy, of its optically generated excited states and related species were discussed. The discussion focused upon the difference between the solid and solution phase of C_{60}. It was noted that at low intensities, vibrational spectroscopy indicated that the solid state is predominantly molecular in character, with the solid state packing having only a weak influence on the spectra. Electronic spectroscopy however revealed features, which are specific only to the solid. These features have been attributed to an intermolecular charge transfer exciton, which contributes to the generation of photocarriers in the solid. At high intensities the Raman signatures of two excited state species, one assigned to an excited state co-operative which is specific to the solid and the other to the molecular triplet, were identified. The Raman signature for the phototransformed C_{60} polymer was also presented in chapter 6. As a result the spectroscopic "fingerprints" of all the optically generated species which could potentially contribute to the generation, or indeed inhibit the generation of charge carriers within a solid state C_{60} device have been catalogued.

In this chapter our attention turns to the electrical generation of ionically charged species with the ultimate aim of obtaining their Raman spectroscopic signature, hence building up a library of all the conducting species in C_{60}. It is widely known that when solid state C_{60} is doped 1:1 with an alkali metal (e.g. K) (figure 7.1a) the complex behaves as a metallic conductor [16]. Similarly when doped 3:1 with an alkali metal (figure 7.1 b) it has been shown to be superconducting e.g. K_3C_{60} salts [17,18]. Raman spectroscopy of these charge transfer salts has shown that the pentagonal pinch mode (positioned at 1469cm^{-1}) down shifts by approximately 6cm^{-1} per dopant molecule [29].

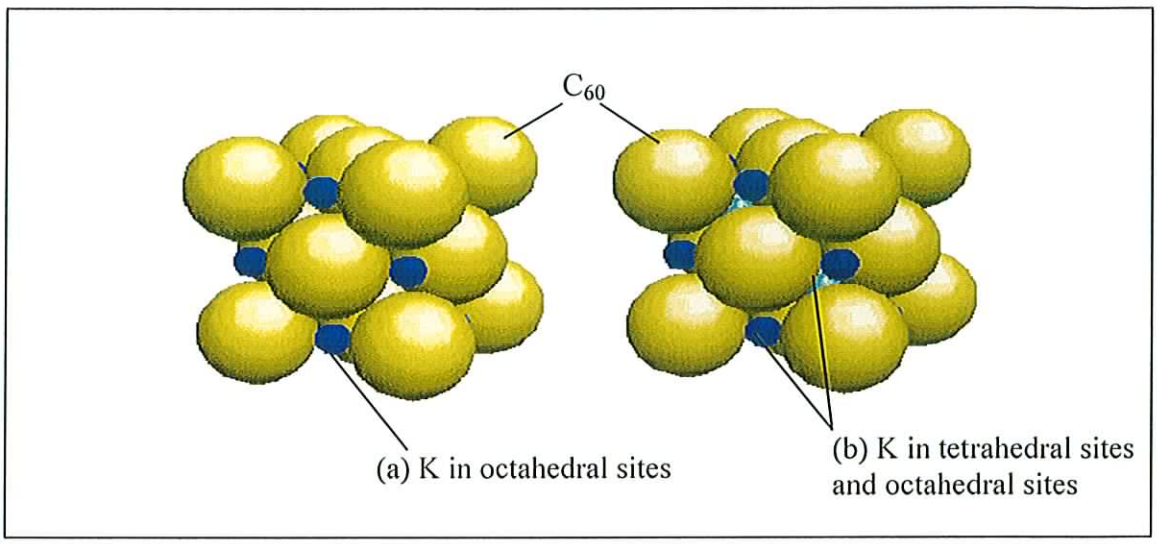

Figure 7.1: (a) KC_{60} metallic salt with the octahedral site filled by K. (b) When the tetrahedral sites are also filled (light blue colour), the K_3C_{60} metallic salt forms [19].

The charge transfer nature of these salts suggests that these doped systems (i.e. KC_{60} and K_3C_{60}) are analogous to the ionic states C_{60}^{-1} and C_{60}^{-3} respectively. Therefore it may be speculated that Raman signature of these ionic species would experience a similar down shift to those reported for the doped species. Indeed the mono-anionc species has been report to have a Raman signature that is down shifted by $6cm^{-1}$ [121] leading to speculation that the ionic species C_{60}^{-1} is similar to the optically excited co-operative state reported in the chapter 5 which is also shifted by $6cm^{-1}$ from the pristine material. As a result of the similarities to the doped systems the ionic states of C_{60} have received a considerable amount of attention in recent years. The characterisation of these species and any others, which may influence the conductivity of C_{60}, is essential if a true understanding of the electronic processes in C_{60} films is to be achieved. The result of which would contribute greatly to the development of future electronic applications of C_{60}. Furthermore the comparison of these states to the optically induced states reported in chapter 5 may also contribute to the development of linear and non-linear optical applications of C_{60}.

7.2: Introduction to Electrochemical and Related techniques

Electrochemical techniques are concerned with the interplay between electrical quantities such as current, potential and charge and the chemical parameters of the system being analysed. Such analysis can yield information about the thermodynamic properties of a system or the presence of trace amounts of metals or organic species in a particular sample [46]. In these examples the electrochemical methods are employed as tools in the study of chemical systems, just as spectroscopic methods are frequently applied. In this thesis electrochemical techniques are employed to generate the ionic species of interest after which the properties of these species themselves are of primary interest. A number of electrochemical methods have been devised over the years for just such investigations [46]. The most widely used technique and the technique employed in this study is Cyclic Voltammetry.

Cyclic Voltammetry involves linearly scanning the potential of the working electrode, using a triangular potential waveform. During the potential sweep, the potentiostat measures the current resulting from the applied potential. The result can then be plotted using an X-Y chart recorder, giving a plot of current versus potential. Such a plot is referred to as a cyclic voltammogram. The characteristic peaks in the cyclic voltammogram are caused by the formation and the recombination of ionic species at specific voltages near the electrode surface i.e. the reduction and re-oxidation of the starting species (or vice versa). The current peaks thus reflect the continuous change in the concentration of the ionic species with potential. The peak current (i_p) in a cyclic voltammogram, for a reversible system under ambient conditions, can be characterised by several important parameters given by the Randles-Sevcik equation (equation 7.1) [107]

$$i_p = (2.69 \times 10^5) n^{3/2} A C D^{1/2} \nu^{1/2}. \qquad \text{(Eq 7.1.)}$$

Where ν is the scan rate, set on the potentiostat, D is the diffusion coefficient, C the concentration of the analyte, A the electrode area and n the number of electrons

involved. It can thus be seen that the current is directly proportional to the concentration and increases with the square root of the scan rate.

The position of the current peaks on the potential axis E_p can be related to the formal potential of the redox process E^o as follows [107].

$$E^o = \frac{E_{pa}-E_{pc}}{2} \qquad \text{(Eq. 7.2)}$$

Where E_{pa} is the peak position of the reduced species (anodic) and E_{pc} the position of the re-oxidised species (cathodic). Information about the ionisation potential and the electron affinity of a system may also be derived through electrochemical techniques. A system with a low electron affinity can be readily reduced at low negative voltages and similarly a system with a low ionisation potential can be easily oxidised at low positive voltages. Hence the ionisation potential and electron affinity of a system will ultimately dictate the formal potential of that system. The separation of the reduced and re-oxidised peak potentials (for a reversible couple) is given by [46]:

$$\Delta E_p = E_{pa} - E_{pc} = \frac{0.059}{n} \text{ Volts} \qquad \text{(Eq. 7.3)}$$

Thus the peak separation can be used to determine the number of electrons transferred, and it can be seen that a one electron process should exhibit a ΔE_p value of about 59mV.

For irreversible or quasi reversible processes the above treatment becomes more complex and is beyond the scope of this study. A detailed analysis of general electrochemistry and cyclic voltammetry is given by Bard and Faulkner [46]. However in this study the concern is with the generation via cyclic voltammetry of ionic species associated with C_{60}, and their subsequent optical analysis using Raman spectroscopy. The electrochemistry of C_{60} is extremely rich with six successive reversible one electron reduction reported for solvated C_{60} [108].

The coupling of optical and electrochemical methods, spectro-electrochemistry, has been employed for over two decades to investigate a wide variety of inorganic, organic and biological systems [107]. The combination of electrochemical perturbations with the molecular specificity of optical monitoring successfully addresses the limited structural information available from the current response, hence yielding more information about the nature of a particular ionic species. A variety of informative optical methods can be coupled with electrochemical techniques, however, this study will focus on Raman spectroscopy.

7.3: Cyclic Voltammetry of C_{60}

Calculations performed on the electronic energy levels (figure 2.6, chapter 2) of C_{60} by Haddon et al. [4], under the assumption that C_{60} has a perfect truncated icosahedral symmetry with no static Jahn-Teller distortions, suggest that the LUMO ($4t_{1u}$) is triply degenerate. Thus C_{60} is expected to be highly electronegative with the potential of accepting up to six electrons forming a hexa-anionic molecule (i.e. C_{60}^{-6}). This possibility was also demonstrated by the formation of solids like K_6C_{60} [109]. Hence it was predicted through a combination of the highly symmetrical structure and the high molecular orbital degeneracy that C_{60} would have an extremely rich electrochemistry [40]. Indeed extensive work has been reported for the reduction and the oxidation of C_{60}. In general, the electrochemical oxidation of C_{60} is expected to be difficult because the ionisation potential of C_{60} is quite high at 7.50 – 7.72 eV [110]. Nevertheless a number of reports on the oxidation of C_{60} have been presented [111][112]. In this chapter the focus will be on the electrochemical reduction which should be more favourable than the oxidation.

7.3.1: Cyclic Voltammetry of C_{60} in Solution

The original study of the electrochemical properties of C_{60} was conducted in a methylene chloride electrolyte and showed only two reversible reduction peaks [113], which were ascribed to single electron transfers by controlled potential coulometry

measurements [46]. Shortly thereafter a third reversible reduction peak was reported in the same electrolyte [114], after which a succession of reports on the electrochemical reduction of C_{60} were published [115, 116, 117]. Six reversible reductions of C_{60} were first observed by Xie et al. [108]. This was accomplished by the use of a mixed electrolyte system and low temperature (~-10°C). The optimal electrolyte composition was between 15% and 20% by volume of acetonitrile in toulene. Tetrabutylammonium phosphorushexafluoride ($TBAPF_6$) was used as supporting electrolyte. The electrolyte mixture allowed an extremely wide potential window to be examined in comparison to previous studies, extending the region of study down to –3.3V vs Fc/Fc^+. The six reversible reduction peaks observed were seen to have half-wave potentials ($E_{½}$) of –0.98V, -1.37V, -1.87V, -2.35V, -2.85V, and -3.26V.vs Fc/Fc^+.

Figure 7.2 shows a cyclic voltammogram obtained for C_{60} (0.5mM) in dichloromethane electrolyte, at a platinum disc electrode. In this study $TBABF_4$ (0.1mM) was used as the support electrolyte. Ferrocene (0.1mM) was also added to the solution as an internal standard. The ferrocene couple (Fc/Fc^+) was observed as a sharp well-defined reversible peak at +0.4V for the electrochemical system used. The system used has been discussed in detail in chapter 3. The cyclic voltammogram in figure 7.2, clearly shows three irreversible reduction peaks. These peaks have been ascribed to the formation of C_{60}^{-1}, C_{60}^{-2} and C_{60}^{-3} anions with $E_{½}$ potentials of –0.73V, -1.28V and –1.89V vs. Fc/Fc^+ respectively (variations in position in comparison to literature may be due to the electrolyte). The integrated areas of the first two reduction peaks are approximately equal (~2cm^2) which suggests that similar process is occurring for both these peaks [112] i.e. a single electron reduction. The absence of the re-oxidation peaks and the extremely weak third peak, however, makes it difficult to draw any real conclusion about the electrochemistry of C_{60} from this cyclic voltammogram.

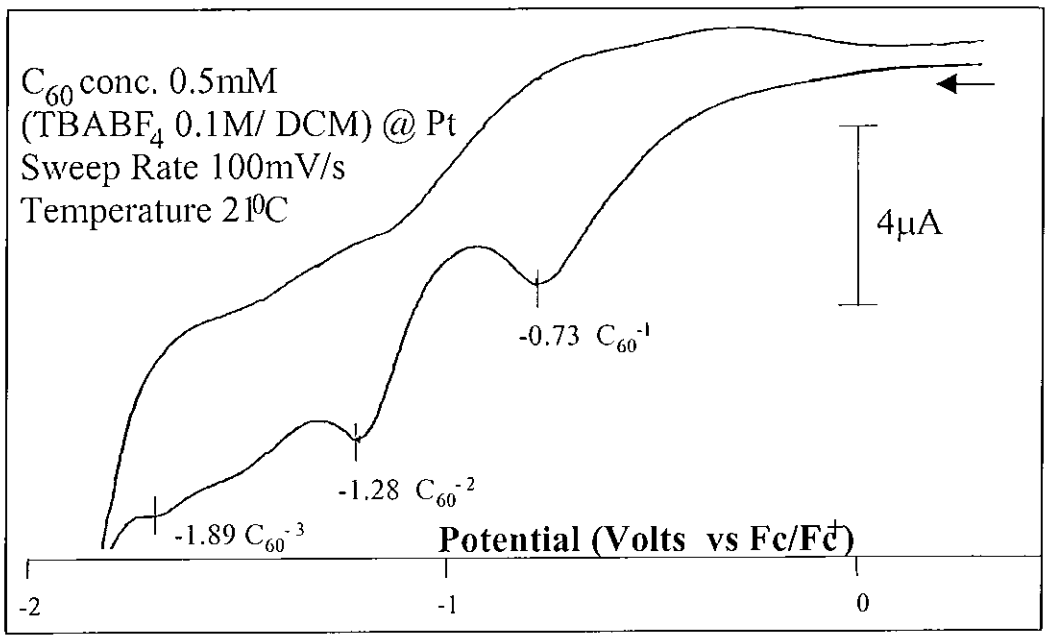

Figure 7.2: Cyclic voltammogram of C_{60} in solution

The absence of the re-oxidation peaks can be attributed to a number of factors such as the temperature, the scan rate and the electrolyte. In order to increase the resolution in an attempt to resolve the re-oxidation peaks a move to lower temperatures ~5°C and lower scan rate (~50-25mV/s) would be required. Similarly a move to a mixed solvent system would also greatly improve the cyclic voltammogram. Early studies using DCM have reported irreversible and quasi-reversible peaks [14,118] dependent upon the support electrolyte. Such a move would also increase the potential window allowing the search for further reduction peaks. Nevertheless the electrical generation of the anionic forms of C_{60} is clearly evident in figure 7.2, in particular C_{60}^{-1} and C_{60}^{-3} which are of primary interest to this study, since they are analogous to the highly conducting metallic and superconducting salts KC_{60} and K_3C_{60} respectively. The isolation and identification of these molecular ionic species is also vitally important in order to differentiate between conducting species in the solid which are molecular in origin and those (if any?) which are specific to the solid state. The concentration of C_{60} in the electrolyte is extremely weak (~0.5mM), as a result obtaining a spectral signature of the ionic species in solution is extremely difficult. Attempts to do so in this study were not successful (see section 7.4).

7.3.2. Cyclic voltammetry of C_{60} films

The electrochemical behaviour of C_{60} thin films is very different to that observed for the dissolved species. Early voltammetric studies of C_{60} films on platinum electrodes in acetonitrile (MeCN) solution containing quaternary ammonium salts such as tetra-n-butylammonium [112] reported four reduction peaks with $E_{½}$ potentials of -1.17V, -1.39V, -1.88V and –2.24V vs Fc/ Fc^+. The first three peaks closely resemble the first three reduction peaks seen for the dissolved species in figure 7.2. However, reported with these $E_{½}$ potentials was a large potential splitting between the reduction and the re-oxidation peaks. In the solution the reduction and re-oxidation peaks are reported to occur at approximately the same potential with a peak separation ΔE_p of ~59mV [19,111]. This is characteristic of a single electron transfer as can be deduced from equation 7.3. The films were also seen to be unstable beyond the third and fourth reduction peaks due to the solubility of reduced forms of C_{60} in Acetonitrile [112], hence scanning beyond the second reduction peak can cause irreversible damage to the film.

Figure 7.3 shows a typical cyclic voltammogram obtained for a C_{60} drop cast film showing the first two reduction peaks. The film was prepared by evaporating a few microlitres of a C_{60}/toulene solution, on the surface of a platinum electrode. The electrolyte used was Acetonitrile and the support electrode was $TBABF_4$. The cyclic voltammogram shows the first two reduction peaks for C_{60} at -1.17V and -1.39V vs Fc/Fc^+ and the corresponding re-oxidation peaks at –0.65V and –0.89V vs. Fc/Fc^+ respectively.

It can also be seen that the peak separation ΔE_p for the both the reduction and re-oxidation couples are quite large i.e. approximately 500mV. This considerable peak separation has been attributed to large structural rearrangements of the film following the first electron transfer [112,119,120]. Initially the drop cast film should consist of C_{60} crystallites, each with a fcc packing geometry and a small percentage of toluene, which was trapped in the crystallites during film preparation. Upon reduction, most of the C_{60} in the film reduces to C_{60}^{-1}. The TBA^+ counter ion must then diffuse into the

lattice in order to balance the negative charges [46]. This counter ion however is comparable in size to the C_{60} molecule and physically cannot intercalate into the spaces of the fcc structure. Therefore the system rearranges into a new more stable structural configuration which allows the TBA^+ ion to balance the charges.

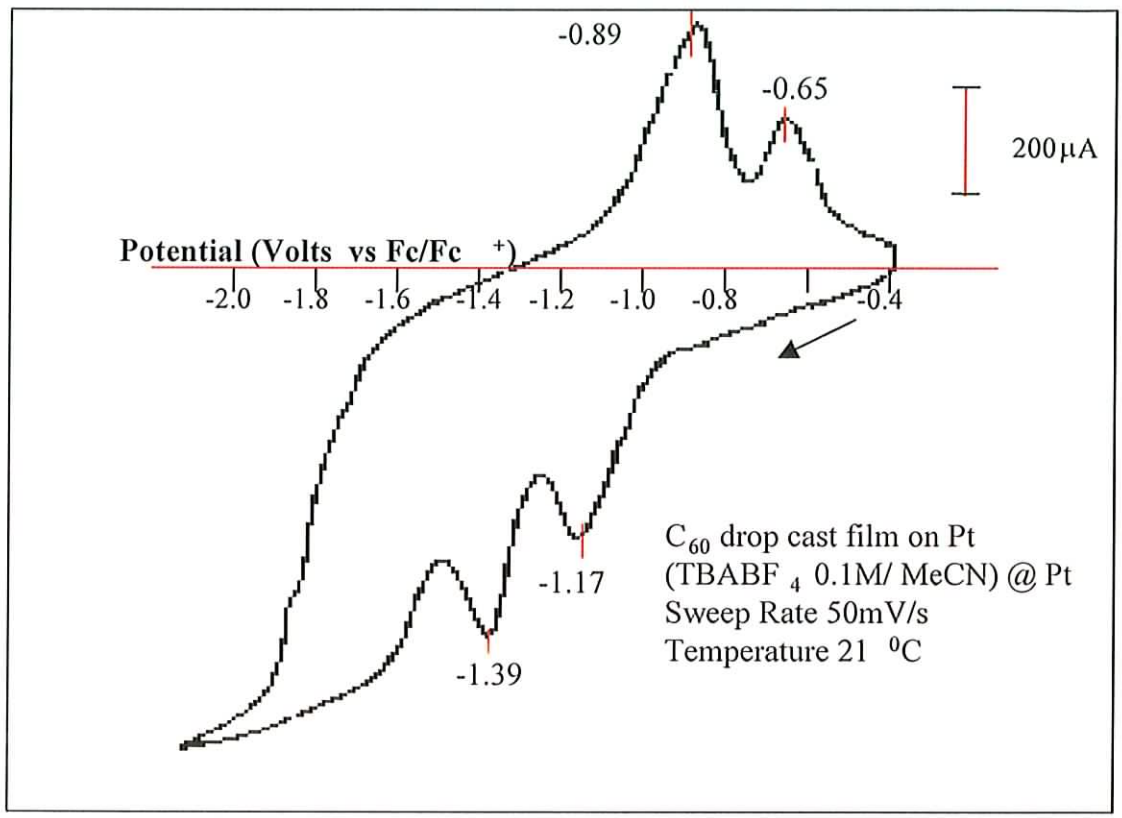

Figure 7.3: Cyclic voltammogram for C_{60} drop cast film.

The effect of this proposed rearrangement can be readily observed in the in situ Raman spectro-electrochemistry spectra shown in figure 7.4. Initially at 0V the A_{2g} pentagonal pinch mode is positioned at ~1469cm^{-1}. As a negative potential is applied the pentagonal pinch mode is seen to broaden considerably, and at potentials approaching the first reduction peak (-1.17V) a new feature emerges between ~1463-1464cm^{-1}. The mode positing of this new feature (initially at 1464cm^{-1}), is reminiscent of a mode known to occur in the Raman spectrum of annealed C_{60} films which, has also been attributed to a structural rearrangement of the C_{60} lattice from an fcc arrangement to a hexagonal closed packed (hcp) phase [106]. The structural rearrangement of annealed films will be discussed in greater detail in chapter 8.

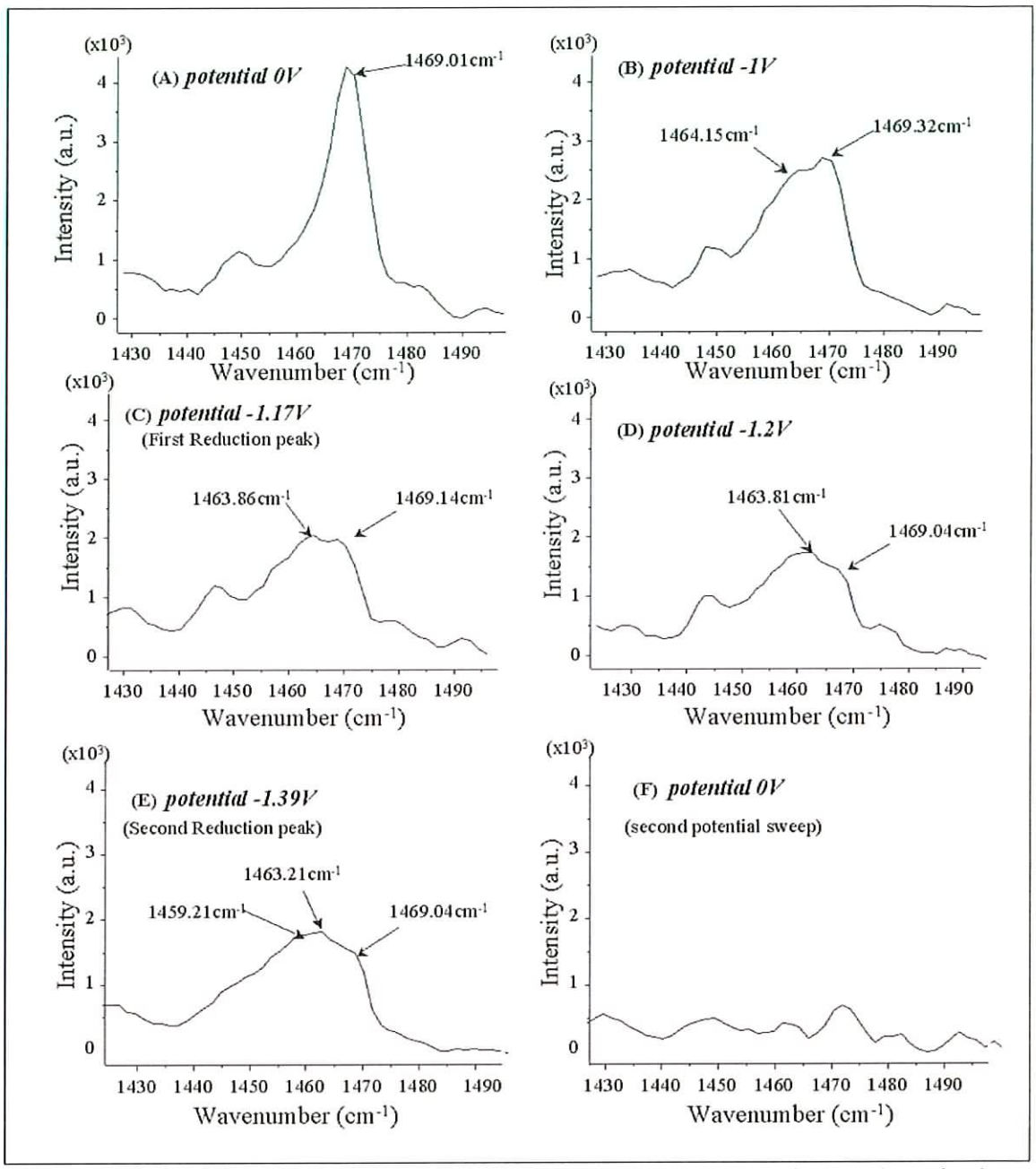

Figure 7.4 : In situ Raman spectra of Cyclic voltammetry, A-E first cycle F is the second cycle.

The proposed structural changes in the cyclic voltammogram of solid C_{60} have also been supported by scanning tunnelling microscopy (STM) [119]. Initially the STM image of the drop cast film showed individual spherical C_{60} molecules on the top layer of the film. When the film was reduced in $TBABF_4$/ MeCN the STM image no longer displayed individual C_{60} molecules. Instead the film appeared to consist of large clumps of material. After re-oxidation, the TBA^+ leaves the film and the C_{60} film

rearranges to its original fcc structure freeing the trapped toluene in the process. Figure 7.5 shows the proposed reaction scheme for the first reduction and re-oxidation of C_{60} thin films in $TBABF_4$/ MeCN [119].

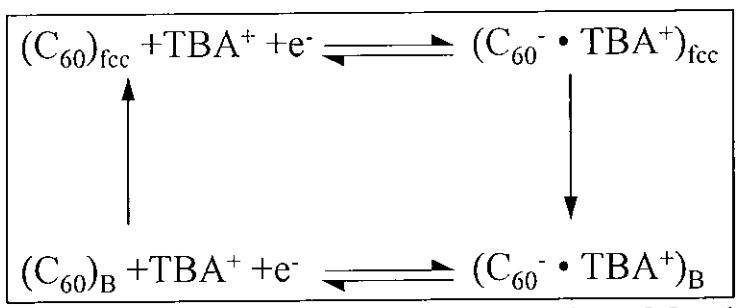

Figure 7.5: Proposed reaction scheme for the first reduction of C_{60} thin films. The molecules are originally in an fcc arrangment and after reduction rearrange in to a new film structure B.

The mode positioning at 1463.86cm^{-1} for the first reduction peak at 1.17eV is also in good agreement with previously reported resonant Raman measurements of anionic C_{60} which characterised the mono-anionic signature as a shift of ~6cm^{-1} from the pentagonal pinch mode at 1469cm^{-1} [122]. The shifts observed are also similar to those observed by Kuzmany [29] for doped C_{60} films i.e. KC_{60}, in which a 6cm^{-1} shift was also observed. Hence the in situ Raman spectra indicate as excepted that the formation of the mono-anionic species and any proposed structural rearrangements occur simultaneously. Furthermore the mode positioning at ~1463cm^{-1} of C_{60}^{-1} also allows comparisons to be drawn not only to the charge transfer salts but to the high intensity excited state species produced in chapter 5. The high intensity excited state species reported in chapter 5 also had a mode positioning of ~1463cm^{-1} and was proposed to be an excited state co-operative between two or more molecules in the solid. Therefore suggesting that the ionic species responsible for the first reduction peak in figure 7.3 displays some degree of an intermolecular electronic interaction.

Intuitively, the mechanism for the second reduction peak in figure 7.3 should be similar to that of the first reduction, however the reduction occurs at a film whose electronic configuration is significantly different to the pristine fcc structure. For this reason it has been suggested that further processes can take place in addition to the electron transfer and incorporation of counter ions. It has been proposed [120] by

analogy to similar findings with electron-attracting aromatics and conjugated chain like oligimers, that after the generation of C_{60}^{-1}, dimeric dianions are immediately formed i.e. $(C_{60}^{-1})_2$ the formation of which is independent of cationic inlusion. The Raman spectrum for the second reduction peak, figure 7.4 shows a further softening of the pentagonal pinch mode towards the lower Raman frequency of ~1460cm^{-1}. The softening of this mode is indicative of increased intermolecular interactions between the π-electron, which, is consistent with the suggestion that this reduction peak is due to the production of dimeric dianions $(C_{60}^{-1})_2$. In situ ESR and conductivity measurements reported by Smie and Heinze [120] seem to further support this concept. Moreover the conductivity measurements revealed that neither electrochemically doped films (which are essentially doped with the counter-ion e.g. C_{60}^{-}•TBA^{+}) nor the 'dimeric' films are conductive. Instead the evidence suggests that the 'undoped' C_{60}^{-1} anions which are in abundance prior to intercalation by the counter-ion into the lattice are conductive i.e. before the peak maximum for the first reduction peak in figure 7.3. Indeed the in situ Raman does indicate the presence of a delocalised species at this point with a Raman signature similar to the excited state co-operative reported in chapter5. Furthermore the excited state reported in chapter 5 was associated with that which is characterised by a nonlinear photoluminescence and photoconductivity [87]. Nevertheless it is difficult to assign any spectroscopic feature shown in figure 7.4 to that of the reduced conducting species proposed by Sime [120]. As confirmation of spectroscopic signatures for a single film is hampered by the apparent loss of C_{60} from the electrode surface as shown in figure 7.4 for 0V of second potential sweep.

In recent years a number of studies on the spectro-electrochemistry of C_{60} have been reported [118,121,122]. Dubois et al. [118] reported one of the first in situ spectro-electrochemical absorption spectra for C_{60} anions in solution. In the study the allowed transitions at 257nm and 330nm in the UV were seen to decrease in intensity as the anionic species were produced. No mention however of the solid state feature at 450nm (chapter 4) was made. A more recent study on thin films [121] reported the in situ FTIR spectra for C_{60} anions obtained using an attenuated total reflection

technique. The spectra were characterised by shifts in the dominant IR mode at 1428cm^{-1}, which correlated well to the number of electrons transferred.

To date however no definitive Raman signature of all the C_{60} ionic species generated via electron injection techniques in the solid state have been reported. Although resonant Raman and Surface Enhanced Raman Spectroscopy (SERS) studies have reported spectra for C_{60}^{-1} [122,123]. SERS refers to the phenomenon by which certain molecules, absorbed on specially prepared metal surfaces, exhibit a Raman spectrum whose intensity is increased by a factor of 10^5-10^6 compared to the normal Raman spectrum [123]. A SERS spectrum interpreted to be that of C_{60}^{-1}, produced by electrochemically reducing the neutral molecule has been reported by Weaver and co-workers [124]. They characterised the spectrum in terms of a shift of 18cm^{-1}, from the characteristic C_{60} pentagonal pinch mode at 1469cm^{-1}. Resonant Raman measurements of anionic C_{60} as previously reported [122] and shown here have characterised the mono-anionic signature as a shift of ~6cm^{-1} from the pentagonal pinch mode. however complications due to cationic intercalation resulted in poor agreement between the results both of the SERS and Resonant Raman measurements.

The proposed mechanism for the first reduction and re-oxidation of C_{60} films (figure 7.5) and its influence on subsequent reductions, suggest that the nature and size of the counter-ion or cation should have an effect on the cyclic voltammogram and the corresponding Raman spectra. Indeed smaller cations should be intercalated more easily into the spaces of the fcc lattice, thereby preventing the need for any structural rearrangements, thus eliminating any subsequent shifts in the Raman spectra. A number of studies in literature [119,120,124] have used cations which are significantly smaller than the C_{60} molecule such as K^+, Cs^+ and Na^+ and the obtained cyclic voltammograms were seen to be quite different than that observed for large cations such as TBA^+. In each case however the first reduction peak is seen to be constant irrespective of the cation. Reducing the potential beyond the first reduction peak results in what appears to be unstable reduced forms of C_{60} hence processes beyond the first reduction peak are less clear. Although it is still believed that the dimeric species are involved [119, 120]. Nevertheless conductivity measurement on

the films indicated, as with the large cations, that the conducting species is a reduced form of C_{60} which is in abundance prior to any charge balancing intercalations and or dimerisation processes.

7.4 Current-Voltage characteristics of C_{60} Sandwich type Structures

The cyclic voltammetric studies, which have been performed on C_{60} both in solution and in film form, suggest that the cationic inclusion and diamerisation as discussed above can inhibit the conductivity of the reduced films. Conductivity measurements on films have shown that the presence of an undoped reduced C_{60} species can enhance the electronic conductivity of the film. The exact nature of this highly conducting reduced species despite several studies has remained somewhat a mystery, because of the rapid inclusion of the counter ion into the lattice and the collapse of the lattice to dimeric phases [119, 118, 124]. It is proposed that in the absence of any charge balancing cation sufficiently high quantities of this reduced species can be generated, revealing more about its nature while simultaneously yielding a film with good electronic properties. To do this thin films of C_{60} were prepared on Indium Tin Oxide (ITO) ($1cm^2$) by vacuum evaporation. ITO is a transparent conducting substrate which was used as the bottom electrode in a sandwich type geometry (figure 3.5 chapter 3) which will eventually allow in situ spectroscopic measurements to be obtained. Aluminium was selected as the top electrode in the structure and was vacuum deposited subsequent to the C_{60} deposition. The electrical properties of the structure were monitored using a Keithley electrometer and power source.

Initially, a sample of thickness 2μm was examined at room temperature. At low voltages (<1V), the sample was seen to be weakly conducting (10^{-12}A). However as the voltage was increased in the positive direction with respect to the aluminium electrode the behaviour dramatically changed. Figure 7.6 shows the current-voltage characteristics observed for the structure. Note that the current axis is plotted logarithmically. It can be seen that at what appears to be a threshold value of the applied voltage, a sharp increase in the current, by over six orders of magnitude,

occurs. Further increases in the voltage result in only a small change in the current. However at approximately 2.5V for this sample a sharp reduction in the current is observed followed by a second maximum. As the voltage was increased to 4V the characteristics were seen not to be reversible, indicating that a change in the material has occurred. Reversal of the polarity however results in similar sharp features, after which the positive bias characteristic of figure 7.6 can be reproduced.

The observed behaviour in figure 7.6 correlates well with the results of the experiments reported by Smie and Heinze [120] in which solid state cyclic voltammetery measurements were combined with both in situ conductivity and ESR measurements. In their study they found that the onset of the first reduction peak coincided with a strong increase in the conductivity although at the point of maximum reduction, the conductivity values were substantially reduced. This reduction in conductivity was attributed to charge balancing cations entering the lattice and the formation of dimeric dianions. The reduction in conductivity due to these processes was also strongly supported by the peak ESR signal, which corresponded to the peak in the conductivity rather than in the voltammogram.

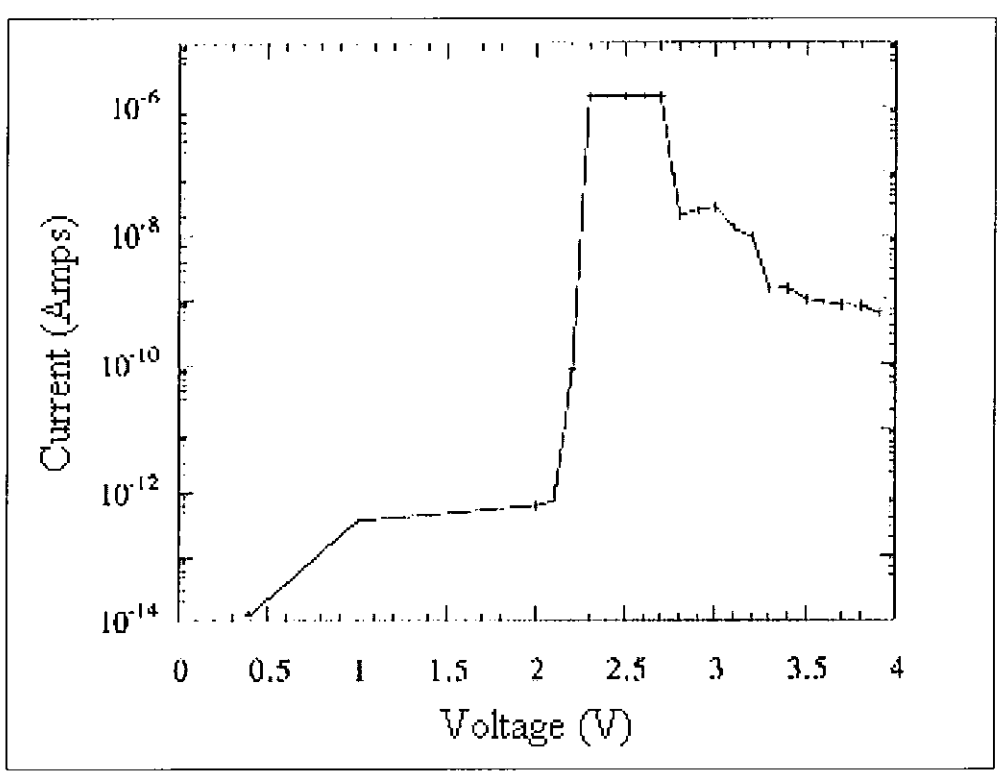

Figure 7.6: The current -voltage characteristics observed for ITO/C_{60} /Al sandwich structure at room temperature.

In figure 7.6 a similar process can be seen in which at a well defined voltage a sharp increase in the conductance is observed. However upon increasing the voltage further only a small change in the conductance resulted. The relative stability observed for this highly conducting species may be due to the absence of any charge balancing cation in the sandwich type structure. However further increasing the voltage results in a sharp reduction with a second maximum. The cyclic voltammagram in figure 7.3 also displays a second reduction maximum which in accordance with Smie and Heinze [120] has been attributed to the formation of dimeric dianions. The presence of a second maximum in figure 7.6 may thus suggest that the C_{60} lattice is unstable to the addition of electrons and readily can collapse to a polymeric species once a substantial number of C_{60}^{-1} species is produced hence allowing the π-electrons of neighbouring molecules to interact.

The dimerisation or polymerisation of C_{60} has been extensively discussed in chapter 6, where the molecular dynamics and photochemical properties of C_{60} were seen to be strongly temperature dependent, due primarily to an orientational phase transition at 249K. Below this temperature the lattice is frozen and structural modification is inhibited [125]. In light of this temperature dependence the experiment was repeated at low temperature (20K) in order to prevent the lattice collapsing and hence the conductance dropping. Figure 7.7 shows the I-V characteristics, at positive voltages with respect to the aluminium electrode, at a temperature of 20K. The cycle begins at point number 1, where a negative current is observed at zero volts. The negative current at this point (with no voltage) is most probably attributable to the variation in the Fermi levels of each of the electrodes. (Note that both the current and voltage axis are plotted logarithmically, and that zero voltage is plotted at an arbitrarily low value. Also the voltage plotted is actually the measured voltage divided by the threshold voltage since the latter tended to change due to contact resistance and thermal expansion).

As is the case at room temperature, increasing the voltage results in an initial decrease in the negative current, followed by a slow increase in the positive current. Again, at a threshold voltage (~1V), a dramatic increase in the current of over six orders of

magnitude is observed, resembling the build up of space charge in a Schottky barrier [126]. However, while at room temperature further increases result in a substantial drop in the conductance (due to the lattice collapsing), at low temperatures the current continues to increase approximately linearly with increasing voltage, at least until point two on the plot, suggesting that the dimerisation process is inhibited.

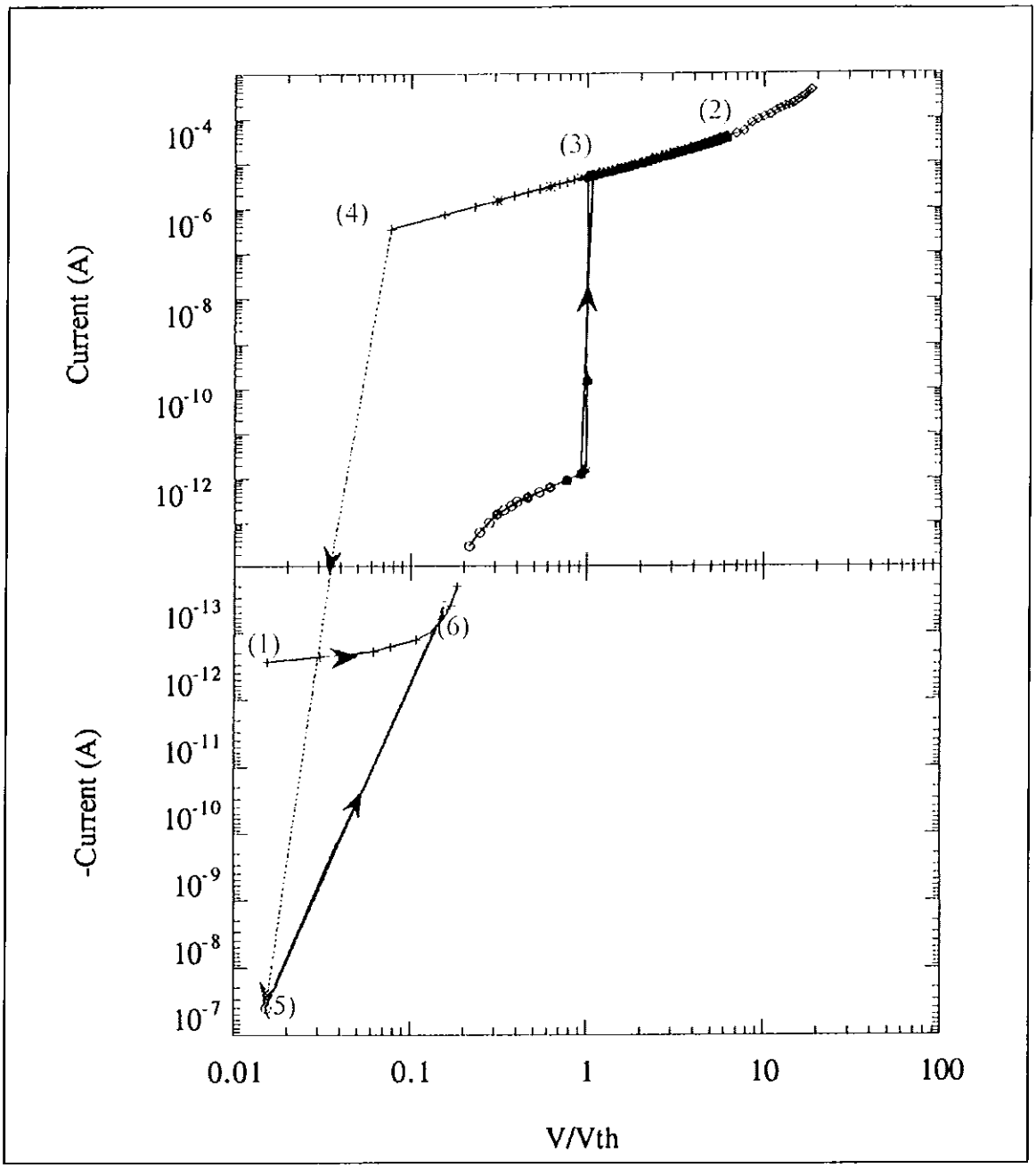

Figure 7.7: The current -voltage characteristics observed for ITO/C_{60} /Al sandwich structure at 20K temperature.

Having increased the voltage to this point (point 2), reduction of the voltage reproduces the initial curve until point three after which the structure does not revert to its low conductance state, but continues to decrease linearly until point four on the plot. Between points two and four, the current is stable for periods of at least days and the curve can be reproduced apparently *ad infinitum*. Further reduction in the applied voltage from point four to zero volts results in an abrupt switch to a negative current of some tenths of μA at point five. This zero voltage current is again stable for at least days. Increasing the voltage again, the I-V curve rapidly rejoins the initial curve, at point six, whereupon the process is completely cycleable and reproducible. Furthermore reduction of the voltage to zero from point six reproduces the current at point one. If however, voltages above point two are applied the characteristics become non-linear and the reproducibility begins to reduce. It is proposed that beyond this point further reductions to C_{60}^{-3} may be plausible, however more work is required to determine if this species could indeed be produced in this way.

Essentially the behaviour which is displayed in figure 7.7 is a reversible switch, at a well defined voltage from a material which is weakly conducting at low voltages to a material which is highly conducting, comparable to a metallic-like conductor, at higher voltages (~1V). This large increase in conductance is indicative of a percolation type effect [126]. However in order to attempt to understand the behaviour of the electronic properties of the sandwich structure, the energetics of the system would have to be mathematically modelled. In general the current voltage behaviour of organic conductors can be modelled by bulk limited processes such as space charge limited current (SCLC) [127, 128]. However models involving injection mechanisms such as Fowler-Nordheim tunnelling [126] and Schottky theory [126] may also be useful. In addition, it is proposed that to further examine the observed phenomenon, a temperature dependence of the conductance would have to be obtained. A temperature independent conductivity would confirm that the behaviour is in fact characteristic of a metallic-like conductor, which is intrinsic to C_{60} and combined with in situ spectroscopic measurements some light may be shed on the exact nature of the conducting species.

7.5 Summary

The work presented in this chapter raises some very intriguing questions regarding the Buckminsterfullerene's capability as an electronic conductor and the nature of the conducting species. Initially the voltammetric studies showed that C_{60} both in solution and in the solid can be readily reduced. In solution it was seen that the ionic species C_{60}^{-1} and C_{60}^{-3}, which are analogous to the highly conducting metallic salts KC_{60} and K_3C_{60} respectively, could be readily produced. In the solid state, reduced C_{60} films were reported to be non-conducting due to the intercalation of cations into the lattice and dimerisation processes as indicated by Raman spectroscopy. However conductivity measurements in literature revealed that undoped or partially reduced films were highly conducting, suggesting that some metastable intermediate state was the conducting species. It was speculated that this species may not be too dissimilar from the optically excited species discussed in chapter 5. It was proposed that in the absence of a charge balancing cation and dimer formation that this conducting species would dominate and a highly conductive film would result. Initial experiments using a sandwich type geometry of ITO/C_{60}/Al have indeed shown that at low temperatures a highly conductive metallic-like film can be produced and can be subsequently cycled between this highly conducting state and the weakly conducting states i.e. it is fully reversible.

In conclusion, the studies described are further testimony to the wealth of physics which has yet to be clarified in fullerenes. The concept of being able to generate a highly conducting species through the application of moderate voltages would be extremely attractive to electronics based technologies. However further work on both the nature and optical characterisation of those species which can potentially enhance the conductivity of C_{60} needs to be performed.

Chapter 8

Enhancing Lattice Stability

8.1: Introduction

In chapters 6 and 7 it was shown that the C_{60} lattice is unstable to the addition of electrons and is prone to polymerisation above ~249K. The measurements reported in chapter 7, on the induced insulator to metal transition at 20K suggests that, at low temperatures, (below the phase transition temperature of 249K) the lattice is stable against collapse and that the highly conducting state can be preserved at low temperatures. Similarly the photo induced polymerisation is inhibited at temperatures below 249K and it has been suggested that the conducting species mentioned in chapter 7 may be analogous to the optically produced high intensity excited state species formed at low temperatures in the solid state, as reported in chapter 5.

While the prospect of being able to induce an insulator to metal transition in C_{60} at a moderate voltage and possibly optically is exciting, its use in potential electronics based applications is extremely limited due to the extremely low temperature required to achieve and maintain the 'metallic–like' conducting state. If the lattice can thus be stabilised at ambient temperatures it will greatly increases the potential for device applications. In this chapter two techniques proposed to enhance the stability of the C_{60} lattice at ambient temperature are examined. The first is the formation of clathrate compounds of C_{60}, that is the inclusion of solvent molecules into the fcc lattice which essentially behave as 'molecular spacers' [83, 105]. The second method is thermal annealing, which involves the structural reordering of the lattice [129, 130]. The degree of stability achieved has been assessed using a number of techniques. In particular Raman spectroscopy, which was used to assess the photochemical stability of the material and Differential Scanning Calorimetry (DSC) which was used to assess the thermal stability, by monitoring the position of the phase changes at 249K. The two techniques used to enhance the lattice stability are discussed in more detail in the following sections

8.2: Enhancing Lattice Stability

8.2.1: Solvent Inclusion

The electronic properties of solid state fullerenes can be modified by the control of the relative contributions of intra- and inter- molecular interactions via the incorporation of solvent molecules into the lattice [19]. When thin films are exposed to solvent vapour, the solvent molecules can be included into the lattice and providing the molecules are neutral i.e. no electronic interaction, they should inhibit any lattice collapse, by behaving like 'molecular spacers'. Additionally the molecular rotation of the C_{60} is also influenced shifting the phase transition temperature. Figure 8.1 shows a schematic of a fcc C_{60} lattice with n-pentane molecules intercalated between the C_{60} molecules. The physical presence of these secondary molecules inhibits the formation of polymeric phases of C_{60} thus preventing the lattice collapsing upon the injection of charge.

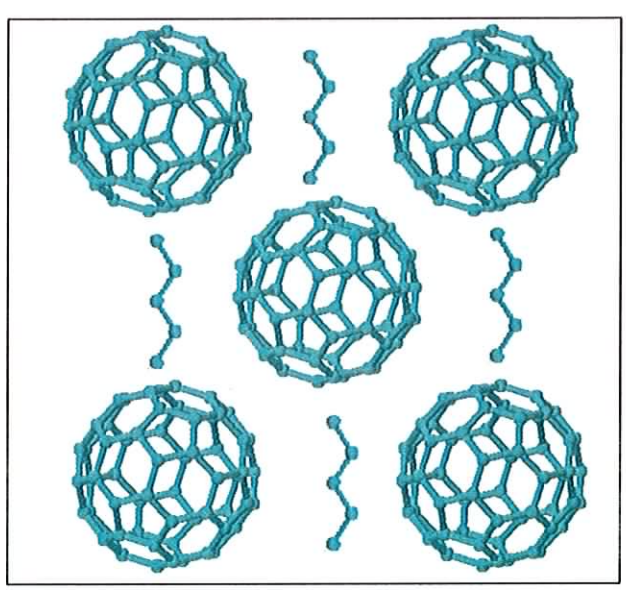

Figure 8.1: Schematic of how a n-pentane C_{60} clathrate might look.

This type of doping where no electronic interaction occurs is referred to as the formation of a clathrate compound. Clathrate C_{60} solids can be produced using a range of molecular species, such as O_2, S_8 and n-pentane [19]. If the molecular species used as the dopant is small enough then it can fit comfortably into the pristine

C_{60} fcc lattice without significant changes. However where large dopant molecules are used substantial rearrangement of the fullerene lattice can occur. The incorporation of such molecules reduces the symmetry of the crystals to an orthorhombic phase [131]. The effect of this reduction in symmetry is to shift the absorption edge to higher energies and the orientational phase transition at 249K to higher temperatures [131]. The incorporation of such non-electronically interacting species into the lattice may thus preserve the 'metallic–like' conducting species, at more ambient temperatures then previously described in chapter 7. Additionally the incorporation of such molecules may enhance the photostability of C_{60} [105, 132]. In this study three solvents were used to make C_{60} clathrate compounds, N,N-diethylamine ($(CH_3)_2$ NH), (DEA), hexane (C_6H_{14}) and chlorobenzene (C_6H_5Cl).

N,N-diethylamine (DEA)

The initial spectrum in figure 8.2 shows the UV/visible spectrum of a pristine C_{60} film (200nm thick). In such relatively thin films, the HOMO-LUMO peak at ~630nm is somewhat obscured by scattering effects. However the intermolecular charge transfer feature between 400 and 500nm and the molecular HOMO-LUMO+1 peak at ~340nm are clearly visible. Upon exposure to the DEA vapour as described in chapter 3 section 3.9.2, the features are seen to smear out and reduce in intensity, as shown in figure 8.2. This occurs in a similar fashion to that observed upon heat treatment of fullerene films and will be discussed in section 8.3 [129]. It can be clearly seen that there is a reduction in the HOMO-LUMO+1 peak at 350nm and a resultant rise of the feature at 400nm. Between 450nm and 550nm the spectral features appear to be slightly red shifted with respect to the pristine sample. This spectral shifting is remarkably similar to that observed in electroabsorption [62], being centered around 475nm and 525nm, corresponding to the positioning of two intermolecular charge transfer states in the solid state C_{60}. The drop wise addition of DEA to a C_{60}/toluene solution, as reported by Henderson [133], shows the emergence of a new feature at ~720nm. This feature has been attributed to a DEA/C_{60} molecular charge transfer [133]. Such an interaction between the DEA and C_{60} molecules can strongly influence the formation of any C_{60} species which could potentially contribute

to electrical conduction in the solid. As a result the inclusion of DEA molecules into the lattice may not supply the stabilising effect originally desired.

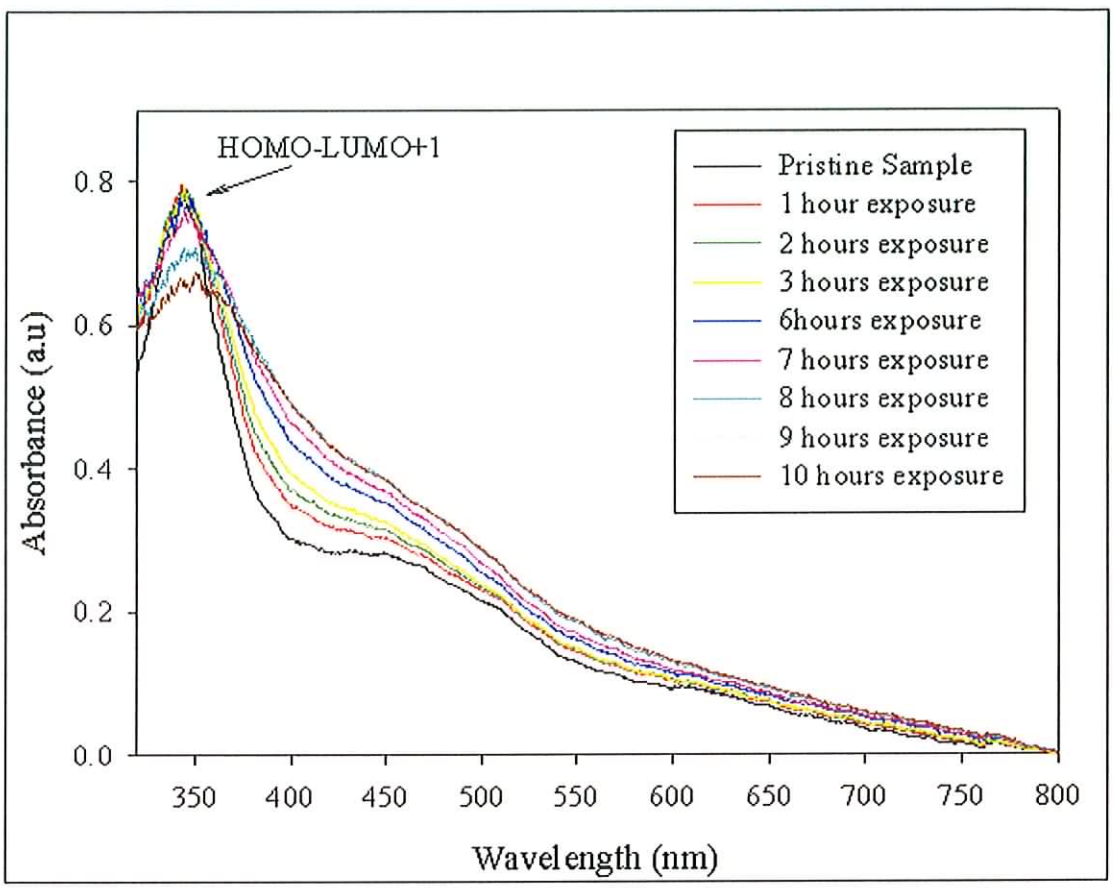

Figure 8.2: Absorption spectra for C_{60} as a function of exposure to DEAvapour.

An assessment of any enhanced stability of the lattice can be readily obtained by attempting to photopolymerise the C_{60} whilst measuring the Raman spectra. Raman spectroscopy of the pristine films reveals the expected results in accordance with chapter 6. In particular, the strong 1469cm^{-1} pentagonal pinch mode is seen to be unstable to prolonged exposure and is seen to shift to the photopolymer mode at 1459cm^{-1} [129]. In the exposed films however, two additional modes at ~1464cm^{-1} and ~1456cm^{-1} can be seen in figure 8.3. The feature at 1464cm^{-1} appears to be stable to prolonged low level illumination (~10mW), while the feature at 1469cm^{-1} is seen to undergo the polymerisation process as seen in the pristine sample discussed in

chapter 6. The spectral positioning of the feature at 1464cm^{-1} is particularly interesting as such a photostable spectral positioning has been previously reported for thermally annealed C_{60} films [129] and has been attributed to a structural arrangement of the C_{60} lattice. In addition spectroelectrochemical measurements in chapter 7 for C_{60} drop cast films also indicate that at the point at which the counter-ion enters the film a structural rearrangement occurs leaving a newly orientated film which has a spectroscopic signature of ~1464cm^{-1}. The feature at ~1456cm^{-1} can be attributed to the detection of DEA as the Raman spectroscopy of the solvent does show the presence of a mode of vibration in this region.

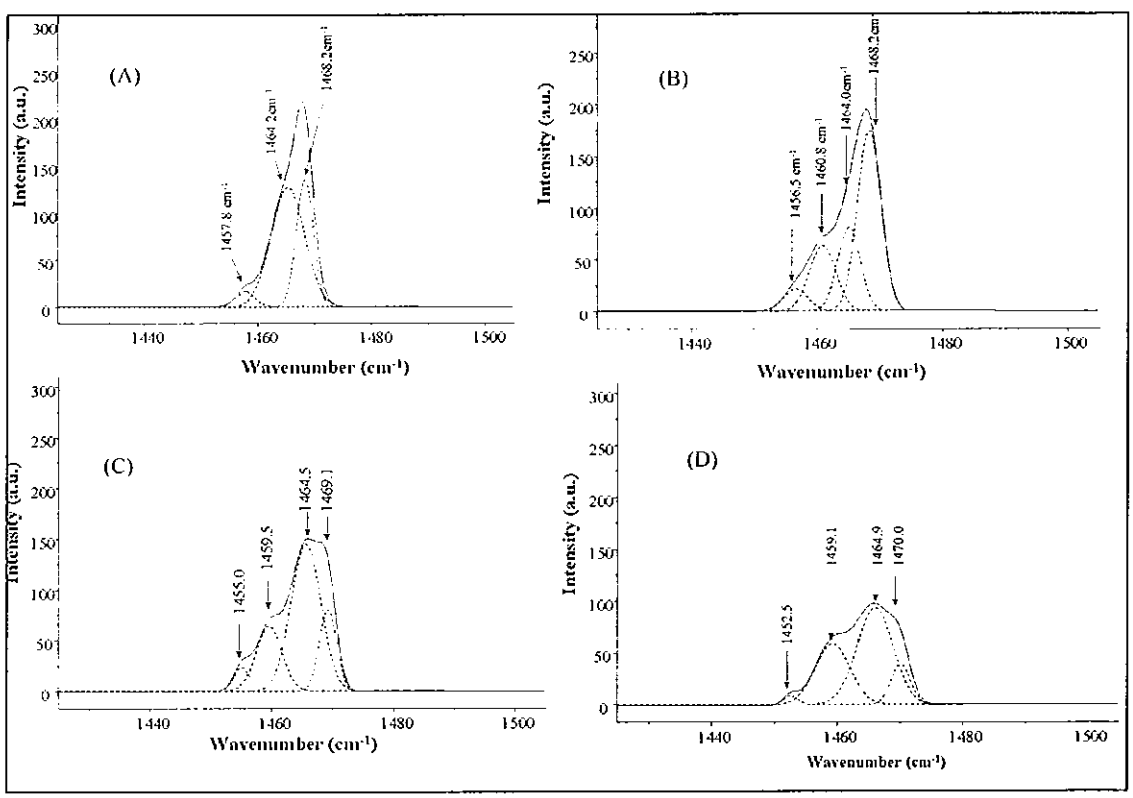

Figure 8.3: Raman spectroscopy of the pentagonal pinch mode with prolonged low level illumination, (A) is the initial spectrum taken after 30s while (D) is 30mins later (D) and (C) are intermediates.

Nevertheless the partially enhanced photochemical stability of the films indicates that a change in the crystal packing has occurred and has increased the rotational phase transition temperature. The similarities between the shifts described above and those

observed in the spectro-electrochemistry of C_{60} films suggests that they are structural in origin. This proposal is supported by optical microscopy of the films, showing them to be smooth when pristine and shattered into domains of tens of microns dimensions after exposure to DEA [132]. As shown in figure 8.4.

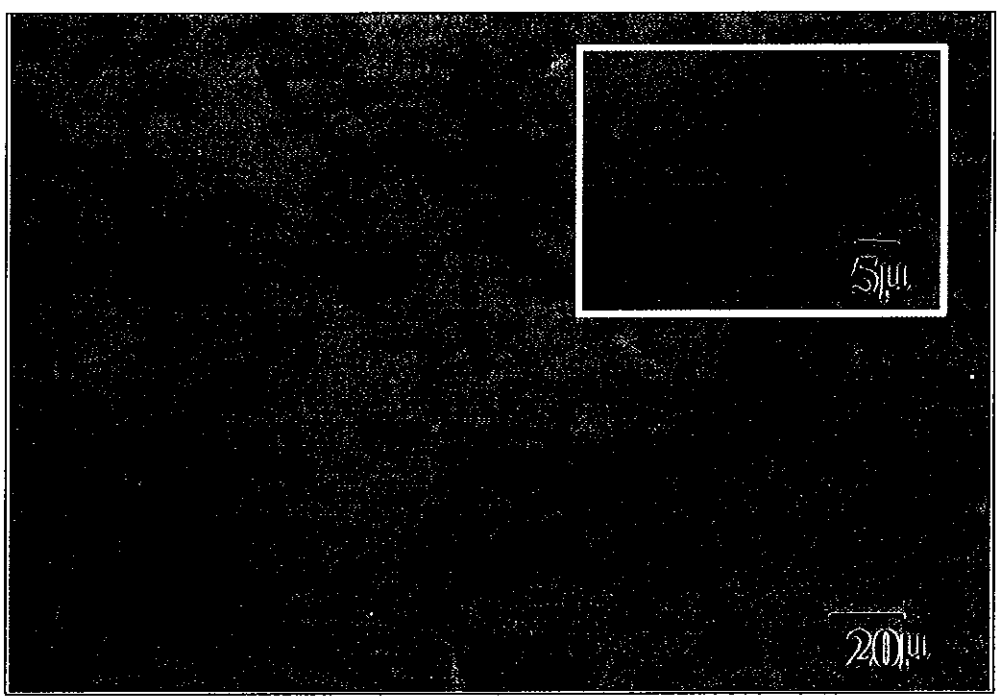

Figure 8.4: Optical microscopy of DEA exposed C_{60} film

The proposal that the observed changes are structural in nature is further supported by the results of x-ray powder diffraction measurements (figure 8.5). Whereas the pattern for a pristine film is characteristic of an fcc unit cell, that of material exposed to DEA is best fitted to a hcp unit cell [129]. This assignment strongly associates the behavior with that reported upon thermal annealing of C_{60} films [129] which will be discussed later. A clear sharpening of the features for the exposed film in comparison to the pristine sample is indicative of an increase in the crystallinity associated with a more ordered cubic phase [132]. In addition a number of new lines have appeared in the x-ray powder diffraction pattern which cannot be associated with the fcc packing of pristine C_{60} but are more in line with a hexagonal close packed (hcp) phase particularly at $2\theta=20°$ [19]. However it should be noted that the x-ray diffraction also

shows a difference to the expected hcp, at 2θ=10° which one would expect to be split for a true hcp phase.

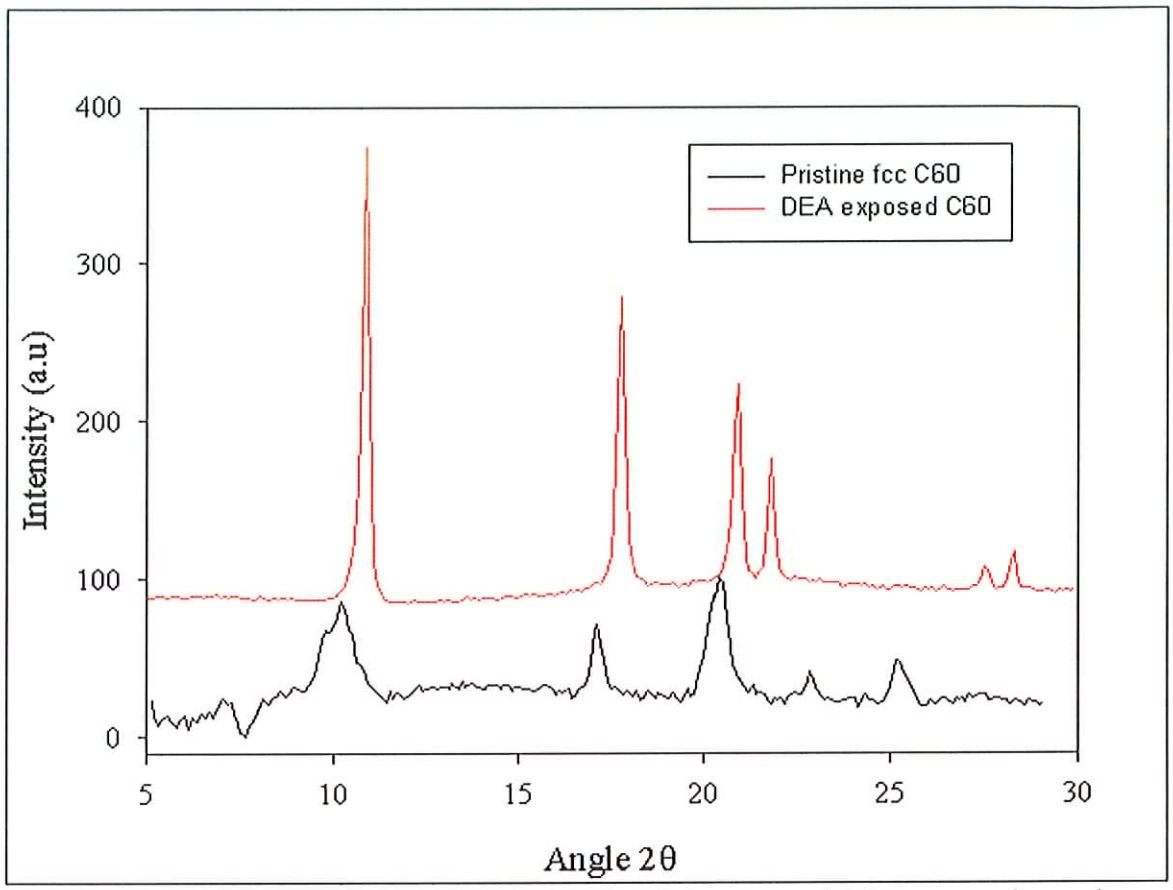

Figure 8.5: X-ray powder diffraction pattern for pristine C_{60} and DEA exposed sample

It has been demonstrated that the observed changes are the result of a electronic and structural rearrangement of the C_{60} lattice due to the intercalation of DEA solvent molecules. The interaction however of C_{60} with the DEA molecules via a charge transfer state is not surprising since DEA has a NH–group i.e. $((CH_3)_2NH)$, making it a strong electron donor [101]. As a result when the DEA molecules diffuse into the lattice they can readily donate electrons to C_{60} creating an anionic form of C_{60} which is similar to those seen in the electrochemistry. The dopant DEA cations reside in the interstitial sites of the C_{60} lattice, in order to balance the charge. This in turn forces a structural rearrangement of the lattice. This type of compound where the dopant species interacts electronically with the C_{60} is referred to as a charge transfer

compound [19]. Such a compound however has no significant value to this study, in helping to stabilise the C_{60} lattice and thus preserve the conducting species observed in chapter 7. The enhanced photostability observed in the Raman spectra however does suggest that the charge transfer compound has an increased rotational phase transition temperature, which is confirmed by the DSC measurement shown in figure 8.6. It can be seen that in comparison to pristine C_{60}, the endotherm, which represents the C_{60}, phase transition at 249K (-24°C in DSC shown) is shifted slightly to 252K. However a second endotherm at 259K (-14°C in DSC shown) is present, even after a second cycle, suggesting this feature is the result of the DEA electronically binding to some of the C_{60} molecules in the solid. The binding energy for the DEA to the C_{60} for this system was calculated using equation 8.1 and was found to be ~0.022eV.

$$E \alpha \frac{1}{kT} \qquad \text{(Eq. 8.1)}$$

In conclusion it has been shown that the intercalation of DEA solvent molecules into the C_{60} lattice does result in an enhanced lattice stability. However the evidence suggest that the DEA forms a charge transfer complex with C_{60} which in turn would inhibit the preservation of the conducting species observed in chapter 7.

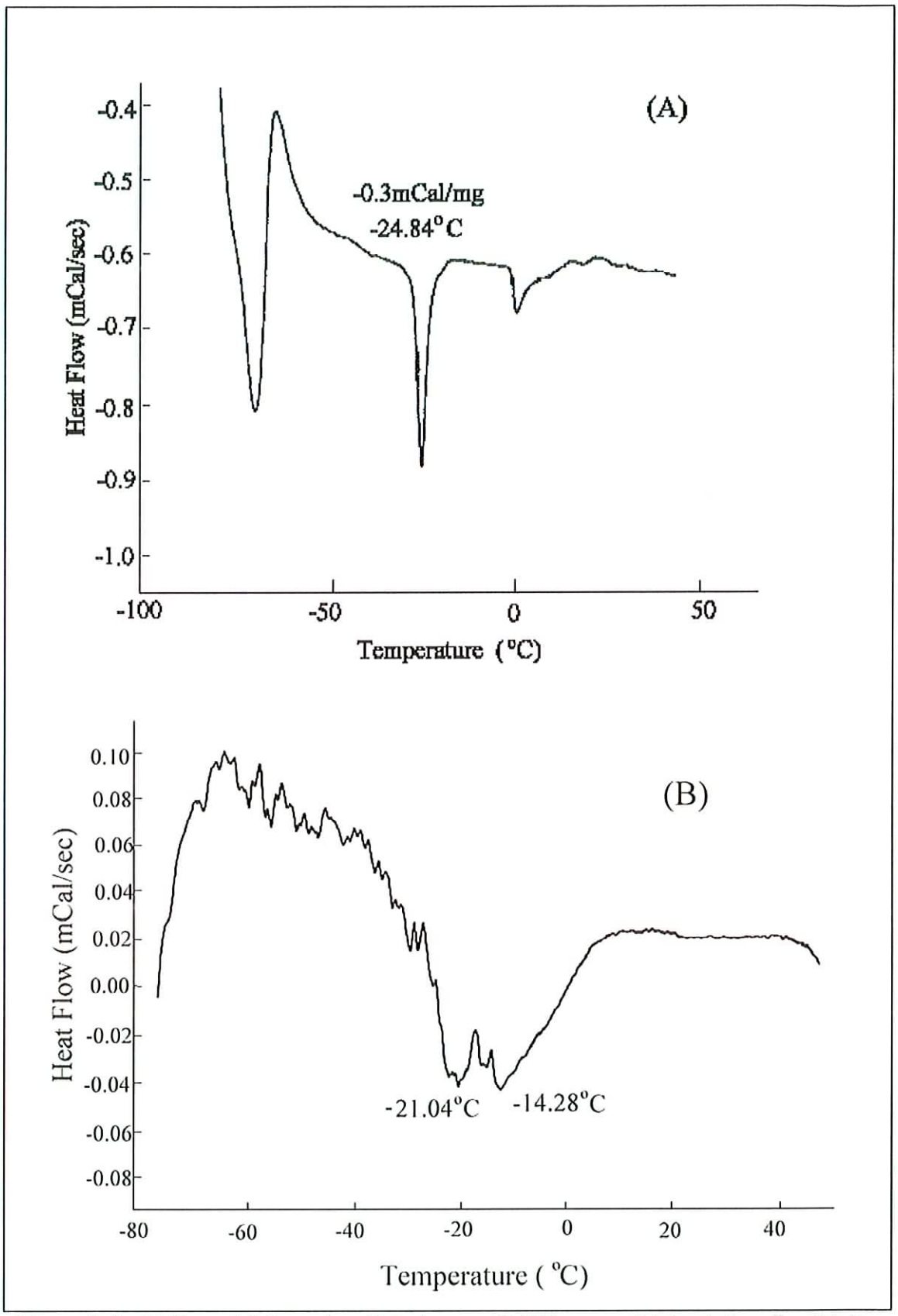

Figure 8.6: Differential Scanning Calorimetry (DSC) trace of (a) pristine C_{60} (b) C_{60} exposed to DEA.

Non-interacting Chlorobenzene and Hexane

The two other solvents examined chlorobenzene and hexane, are known not to interact electronically with C_{60}, as solvated C_{60} in the respective solvents shows no solvato-chromic effects in the absorption spectra. Indeed solvated C_{60} in both solvents has been used as a good approximation of the isolated molecule [48, 105]. The results described in this section for the stabilisation of the C_{60} lattice using clathrates produced from chlorobenzene and hexane will concentrate solely upon the chlorobenzene/ C_{60} clathrate. In general clathrates produced from both these solvents exhibited the same behaviour. However appropriate discussion will be given where necessary regarding any significant differences observed between the solvents.

Figure 8.7 shows the changes in the absorption spectrum of pristine C_{60} as a function of exposure to chlorobenzene solvent vapour. Initially the unexposed film shows the well accepted solid-state C_{60} spectrum as described in chapter 4. Upon exposure to the chlorobenzene vapour, the HOMO-LUMO peak at ~630nm appears to remain unchanged while the solid state features between 400 and 500nm display significant losses of oscillator strength accompanied by a continuous red shift of up to 20nm. These changes are similar to those observed for the DEA and likewise are remarkably similar to the changes observed in the electroabsorption of C_{60} thin films in comparison to C_{60} in a PMMA matrix [62]. The electroabsorption measurements show significant changes in features associated with the charge transfer states at 475nm and 525nm as the C_{60} molecules become more isolated in the PMMA matrix. The changes in the spectra shown in figure 8.7 may thus be related to a change in the crystal packing of the C_{60} due to the diffusion of the chlorobenzene molecules into the lattice thus reducing the C_{60} charge transfer.

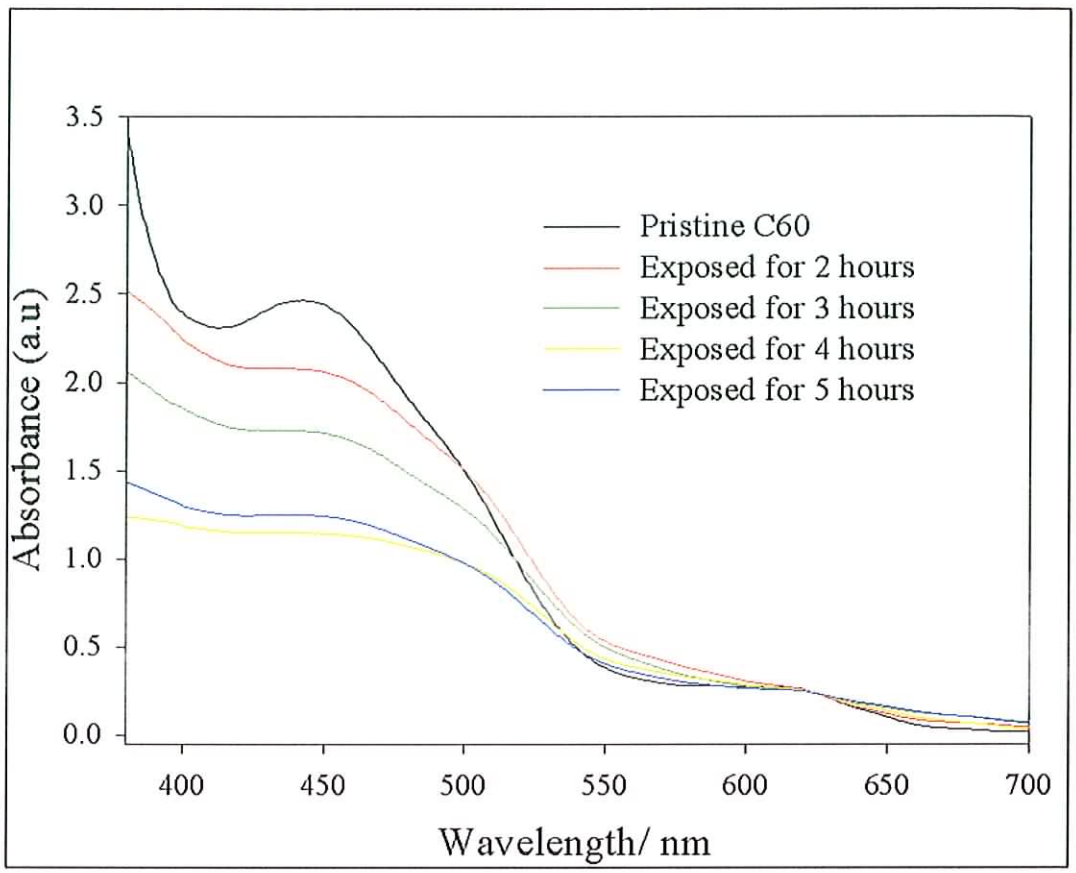

Figure 8.7: Absorption spectra for C_{60} as a function of exposure to chlorobenzene

As previously suggested for the DEA/C_{60} complex the changes observed in the absorption spectra shown in figure 8.7 are due to structural rather then chemical changes. Microscopic analysis of the film surface after exposure also seems to support this notion. Optical microscopy reveals a number of distinct regions consisting of microscopic crystal like deposits as shown in figure 8.8, whereas the pristine film surface is smooth. Similarly Scanning Electron Microscopy (SEM) figure 8.9 shows the pristine sample to be a polycrystalline material with few distinct features at a resolution of 2μm. However a SEM image of the chlorobenzene exposed sample shows a considerable loss of integrity of the film surface with defects ≤ 0.5μm in size.

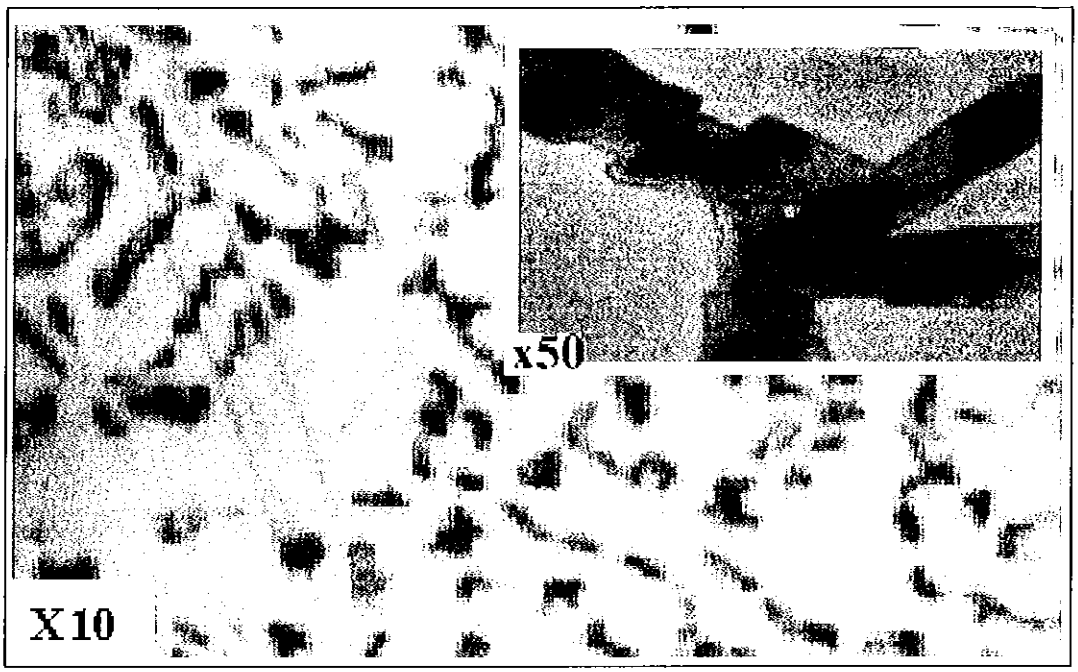

Figure 8.7: Optical microscopy of chlorobenzene exposed film surface.

The change in the film integrity may suggest a change in the crystal packing and thus an enhanced photostability as seen previously for the DEA/C_{60} charge transfer compound. As before in situ Raman spectroscopy can reveal if there has been any enhanced photostability of the C_{60} lattice due to the intercalation of the chlorobenzene molecules. Raman spectroscopy of the pristine films revealed the expected results with the strong 1469cm^{-1} pentagonal pinch mode shifting to the photopolymer mode at 1459cm^{-1} under prolonged illumination [129]. However in the Raman spectrum of the crystal like deposits of the exposed films, the mode has been shifted to 1464cm^{-1}, and, as is the case for the DEA/C_{60} complex, is stable to prolonged illumination as seen in figure 8.8. It should be noted that no detectable mode at 1469cm^{-1} for the pentagonal pinch mode was observed in the chlorobenzene/C_{60} clathrates. The hexane/C_{60} clathrates however did display a mode at 1469cm^{-1}, which under went polymerisation, whilst the mode at 1464cm^{-1} remained constant. The appearance of a feature at 1469cm^{-1} in the hexane/C_{60} clathrates and the apparent absence of this feature in the chlorobenzene clathrates may be attributed to the relative size of the molecules [101].

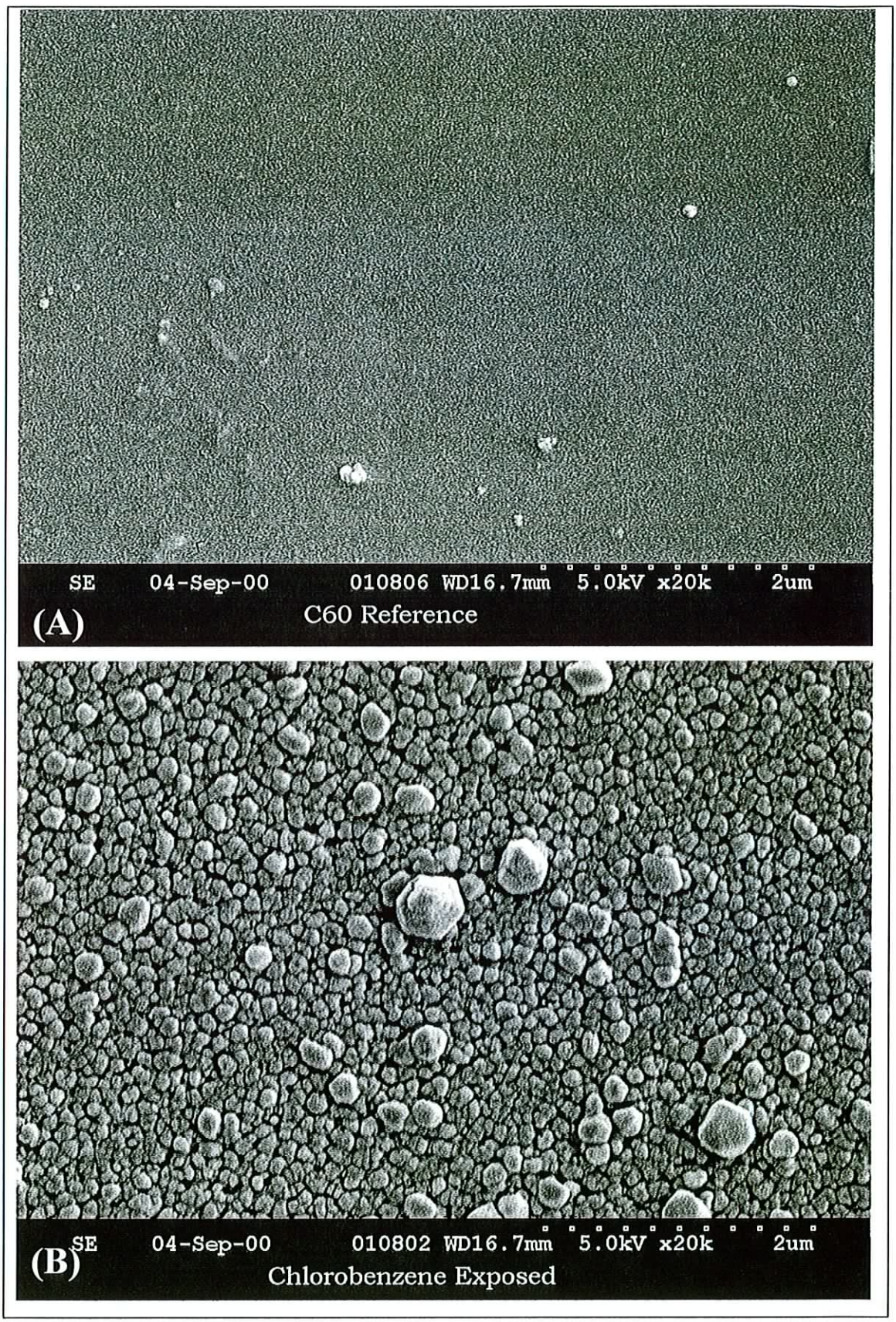

Figure 8.8: SEM images of (a) pristine C_{60} film (b) of chlorobenzene exposed C_{60} film.

The chlorobenzene being the bigger molecule should cause the biggest change in the crystal packing. The single Raman mode at 1464cm^{-1} in the chlorobenzene/C_{60} clathrate spectra indicates a complete transformation of the original fcc C_{60} structure to a new structure at room temperature, which like the low temperature simple cubic phase is photochemically stable.

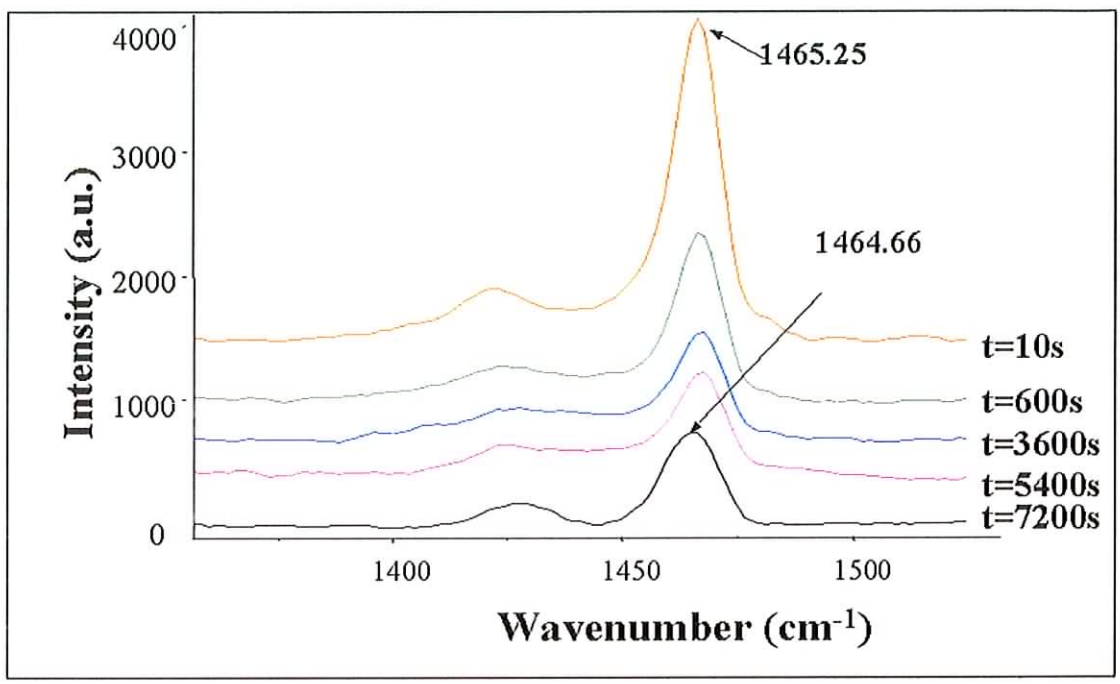

Figure 8.8: Raman spectra of chlorobenzene/C_{60} clathrate species

This change in crystal packing as in the DEA/C_{60} complex may indicate an increase in the rotational phase transition temperature. Indeed DSC analysis has shown that the pristine fcc C_{60} undergoes a phase transition to a sc structure at 249K. The films exposed to the solvent vapour however have a phase transition shifted closer to room temperature at 261K as shown in figure 8.9. It can be also clearly seen that the chlorobenzene does not interact electronically with C_{60} as no secondary peaks (as in the DEA/C_{60} charge transfer compound) were observed.

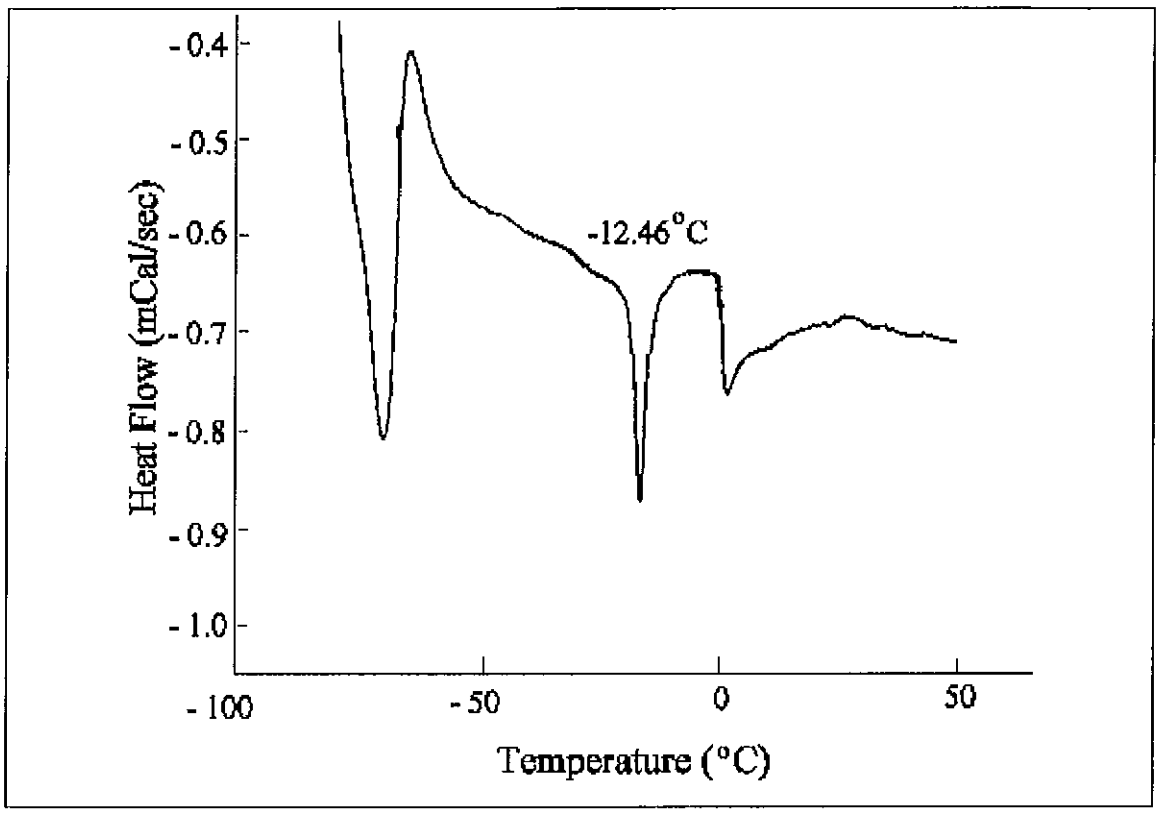

Figure 8.9: Differential Scanning Calorimetry (DSC) trace of chlorobenzene/C_{60} clathrate.

The enhanced thermal and photo- stability of the chlorobenzene/C_{60} clathrates can be attributed solely to the change in the crystal packing. The proposal that the observed changes are structural in origin is further supported by the results of x-ray powder diffraction measurements. The observed pattern for a pristine film is characteristic of a fcc unit cell as seen in figure 8.10. In contrast, x-ray diffraction patterns of chlorobenzene exposed films show a sharpening consistent with increased crystallinity and a splitting of peaks, indicative of mixed phases, namely that of the cubic phase. Also present are new features consistent with hexagonal packing [87] at 2θ = ~10° and 22°. Hexagonal packing is associated with a more closely packed lattice, which is in agreement with the earlier observation of the changes in the absorption spectra with exposure to the solvent vapours. This assignment strongly associates the behaviour with that reported upon thermal annealing of C_{60} films, which will be discussed in section 8.2.2 [87].

The results reported here indicate that the incorporation of neutral solvent molecules into the C_{60} lattice can enhance the photochemical and thermal stability of C_{60}. The photostable forms of solid C_{60} produced via the formation of C_{60} clathrates have electronic properties, which differ significantly from those of fcc films and are present in small crystal-like deposits on the film surfaces. The degree of stability achieved appears to be strongly dependent upon the size of the solvent molecule used. The photochemically and thermally stable species produced from the inclusion of chlorobenzene molecules into the lattice is particularly promising to this study to inhibit the lattice collapse upon the injection of charge at room temperature. However the film losses its integrity due to the crystal like deposit which create a number of defect sites as seen in the SEM images. These defects would thus inhibit any bulk conduction in the solid state such as that observed in figure 7.7 chapter 7.

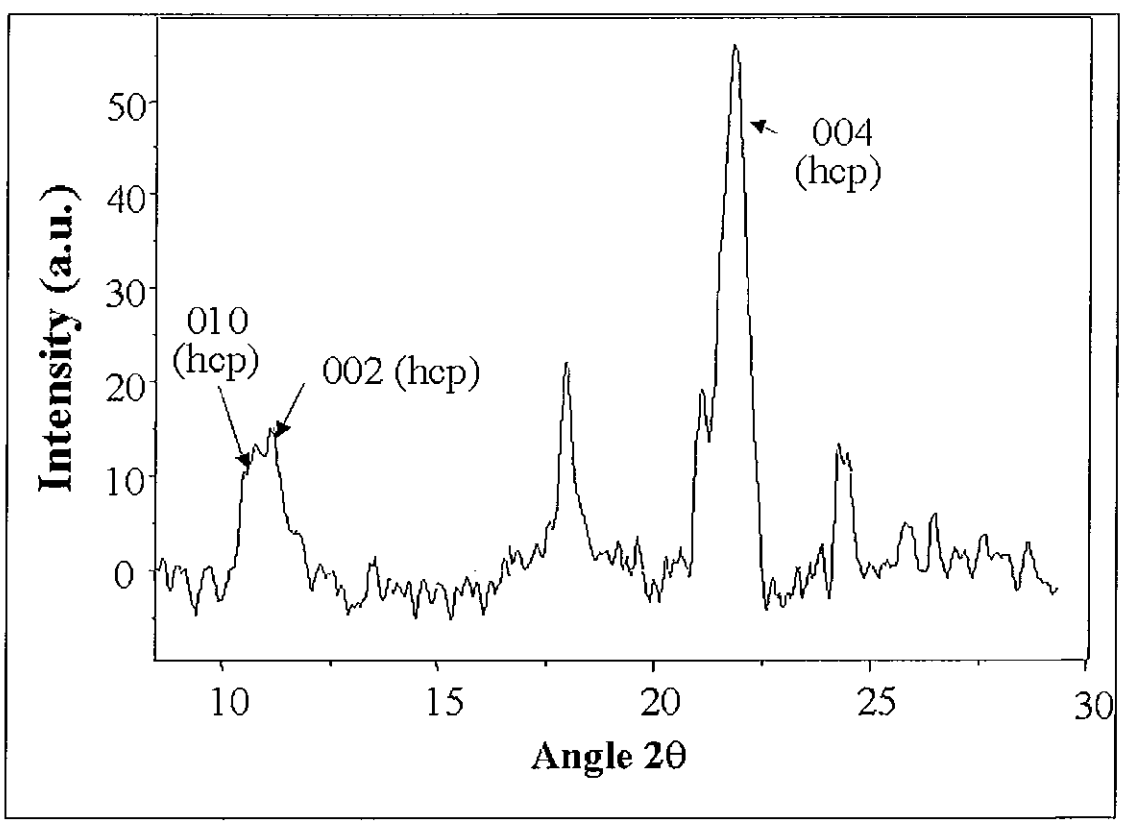

Figure 8.10: X-ray powder diffraction pattern of pristine C_{60} and the chlorobenzene/C_{60} clathrate

8.2.2. Thermal Annealing

Thermal annealing is an alternative approach to stabilising the C_{60} lattice, which in principal should maintain the film integrity. Thermal annealing is essentially where thin films are heated at a temperature sufficiently below the sublimation temperature of the vacuum deposited sample. C_{60} thin films can be annealed by heating under vacuum (~10^{-5}mbar) for a fixed time at a temperature of ~200°C. A number of studies on annealed films have been reported [129, 130] where it was seen that UV/Vis and IR spectra show no indication of any chemical alteration of the sample but rather an apparent structural change is observed [129].

Figure 8.11 shows a comparison of the absorption spectra taken for a C_{60} thin film (~0.8μm thick) annealed as a function of time. The unheated film shows the well accepted pristine solid state C_{60} spectrum. After measurement of this spectrum the film was transferred into a vacuum oven and heated for 9 hours after which the spectrum was retaken. This procedure was repeated for further heating times of 20 hours and 54 hours. With increasing annealing time, significant changes in the optical absorption spectrum are clearly observable (figure 8.11). Firstly there is a dramatic selective loss of intensity in the features at 470nm and 520nm. Secondly there is a continuous red shift of these solid state features while the HOMO-LUMO absorption at 620nm appears to remain constant. This apparent shifting accompanied by the loss in intensity can be attributed to a closer packing of the molecules in the solid state phase similar to effects seen in luminescence spectra of organic molecular crystals and significantly in the aforementioned clathrate compounds. As with the aforementioned solvent inclusion the absorption spectra of annealed films indicate a structural change as opposed to a chemical or thermal change. Unlike the solvent included films however the annealed films appear to retain their structural integrity, as evidenced by the optical microscopy which shows the film surface to be relatively free of defects figure 8.12. However, occasionally films did display a cracking of the film surface as shown in the inset of figure 8.12. This cracking appeared to be ordered with almost pentagonal and hexagonal features suggesting maybe, that they are the result of dislocations in the polycrystalline structure of the film [135]. In general dislocations

occur parallel to the directions of close packed crystal structures suggesting that the C_{60} film has undergone a change in the crystal packing [135]. However further investigation into the occasional appearance of these features would have to be done to confirm that these cracks are the result of such dislocations.

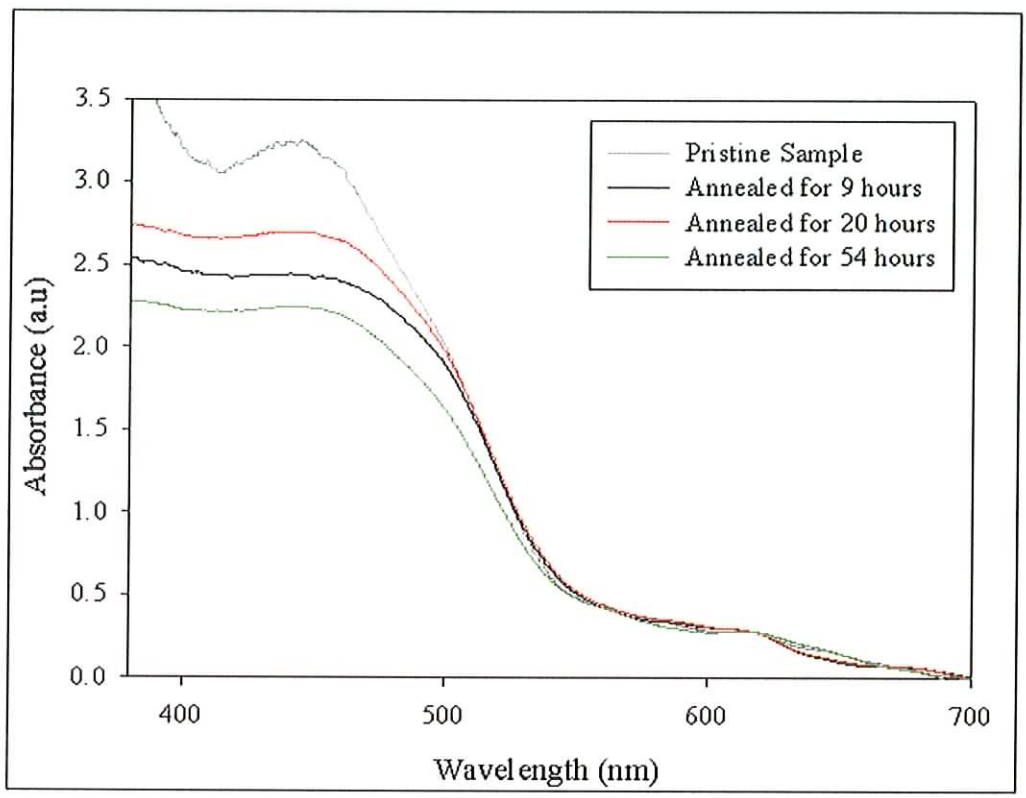

Figure 8.11 : Absorption spectra as function of time for annealed film

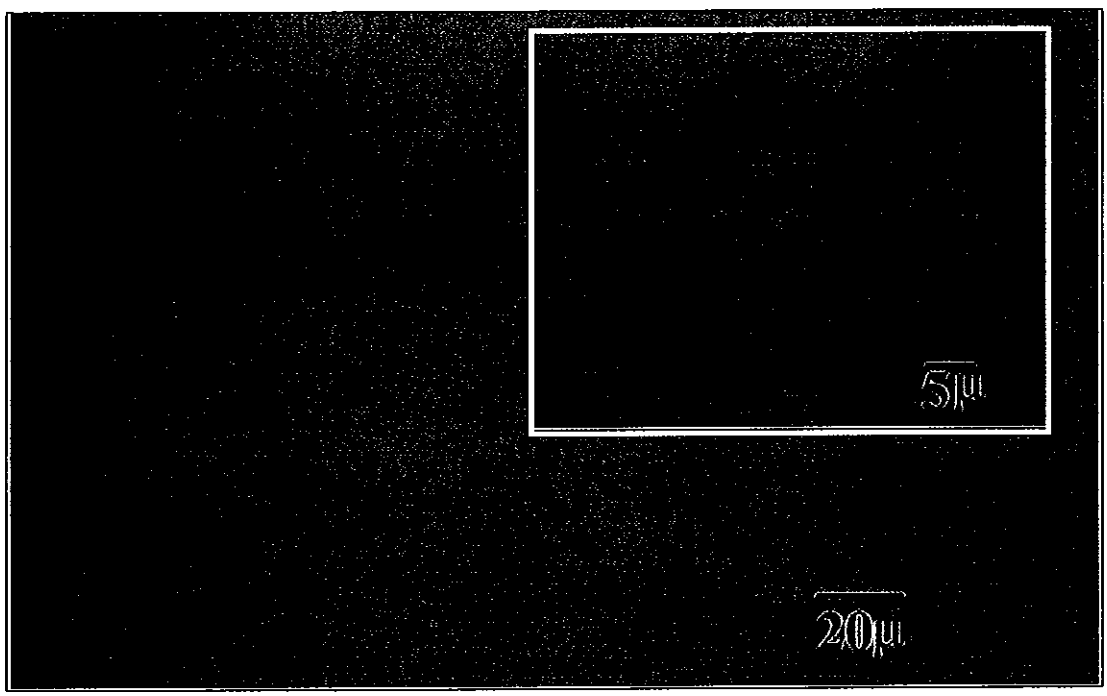

Figure 8.12: Optical microscopy of Annealed film surface. Inset shows a cracking which was occasionally seen in on film surfaces.

In addition to optical microscopy, a SEM image (figure 8.13), also confirms that the changes observed are structural in origin rather then chemical. The image shows particles of similar size to each and in comparison the SEM image for the chlorobenzene/ C_{60} clathrate the annealed film is considerably more uniform while showing significant differences from the pristine sample.

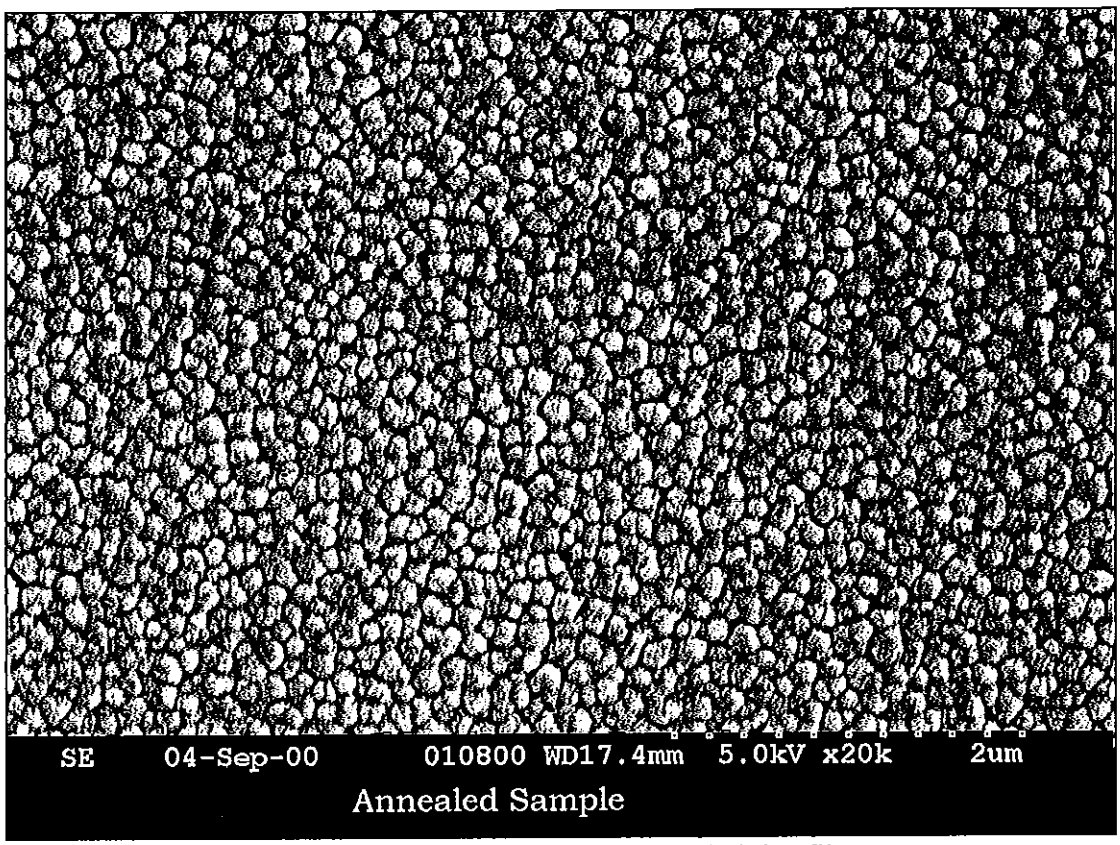

Figure 8.13: SEM images of annealed C_{60} film.

Further evidence for a structural change is supplied from the x-ray powder diffraction data shown in figure 8.14 [129]. Upon annealing several significant changes from the x-ray diffraction pattern of pristine C_{60} (figure 8.5) were observed in the diffraction pattern of annealed C_{60} (figure 8.14). First, an increase in the sharpness of the peaks was observed which indicates an increase in the overall crystallinity of the film. A similar sharpening of the x-ray diffraction peaks was also seen for the clathrate species. Secondly, a number of new lines are clearly visible in the spectrum, which also appear in the chlorobenzene/C_{60} clathrate compound. These new features highlighted in figure 8.14 can be attributed to a hexagonal close packed (hcp) arrangement as opposed to a fcc arrangement. However there is still evidence of the original fcc phase being present particularly at 2θ=~18°, suggesting a mixture of the hcp and fcc phase.

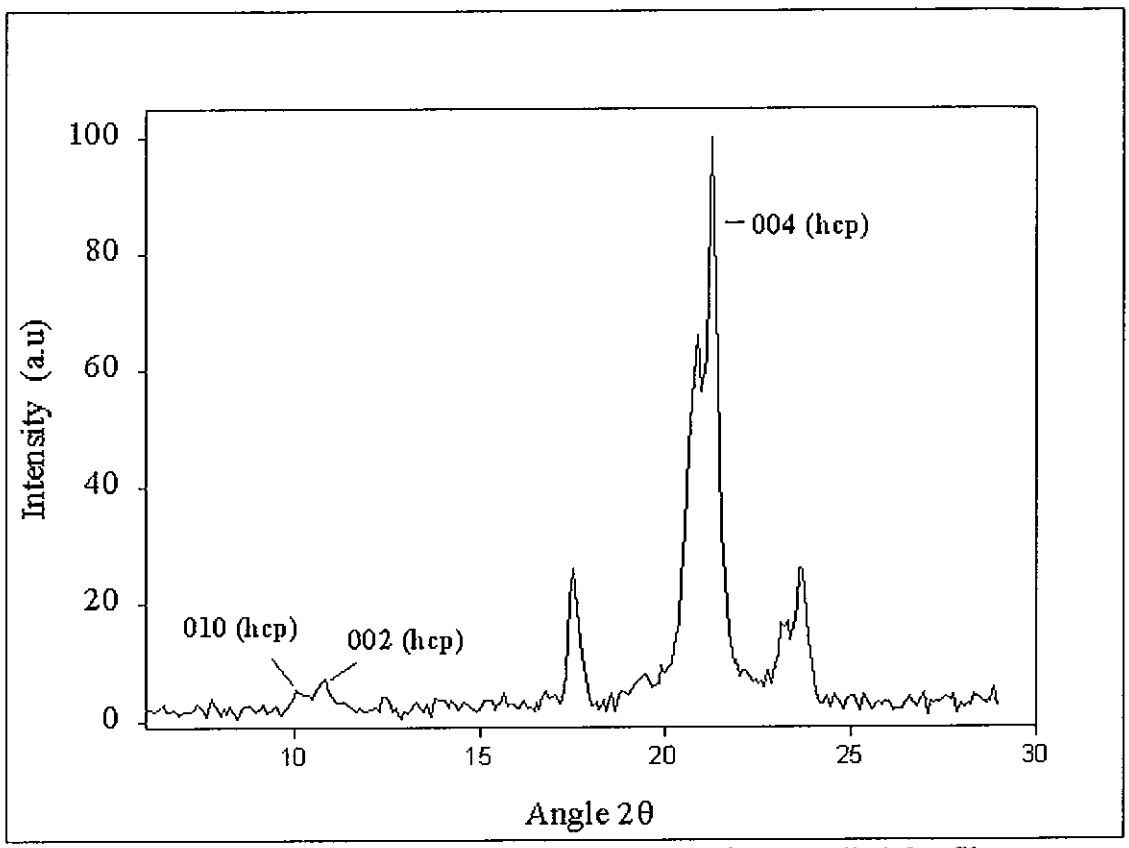

Figure 8.14: X-ray powder diffraction pattern for annealled C_{60} film

As aforementioned, solid state C_{60} subject to resonant excitation is extremely photochemically unstable. This is identifiable by the softening in the Raman spectrum of the pentagonal pinch mode at ~1469cm^{-1} under prolonged low level illumination at room temperature, to the lower Raman frequency of ~1459cm^{-1} associated with the polymer. Thermally annealed films have been reported to be photochemically stable by Akselrod et al [129]. Indeed the changes observed in the absorption spectra, x-ray powder diffraction and microscopy do mimic the behaviour observed for C_{60} clathrates, which are seen to have an enhanced photochemical and thermal stabilty. The Raman spectrum of C_{60} for a thermally annealed film, figure 8.15 also displays changes, which are consistent with those observed upon clathrate formation. Initially the characteristic pentagonal pinch mode is positioned at 1469cm^{-1}. However a new feature at ~1464cm^{-1} is also seen. This feature is also present in the clathrate species and has been ascribed to the emerging hcp phase observed in the x-ray diffraction pattern by Akselrod for annealled films.

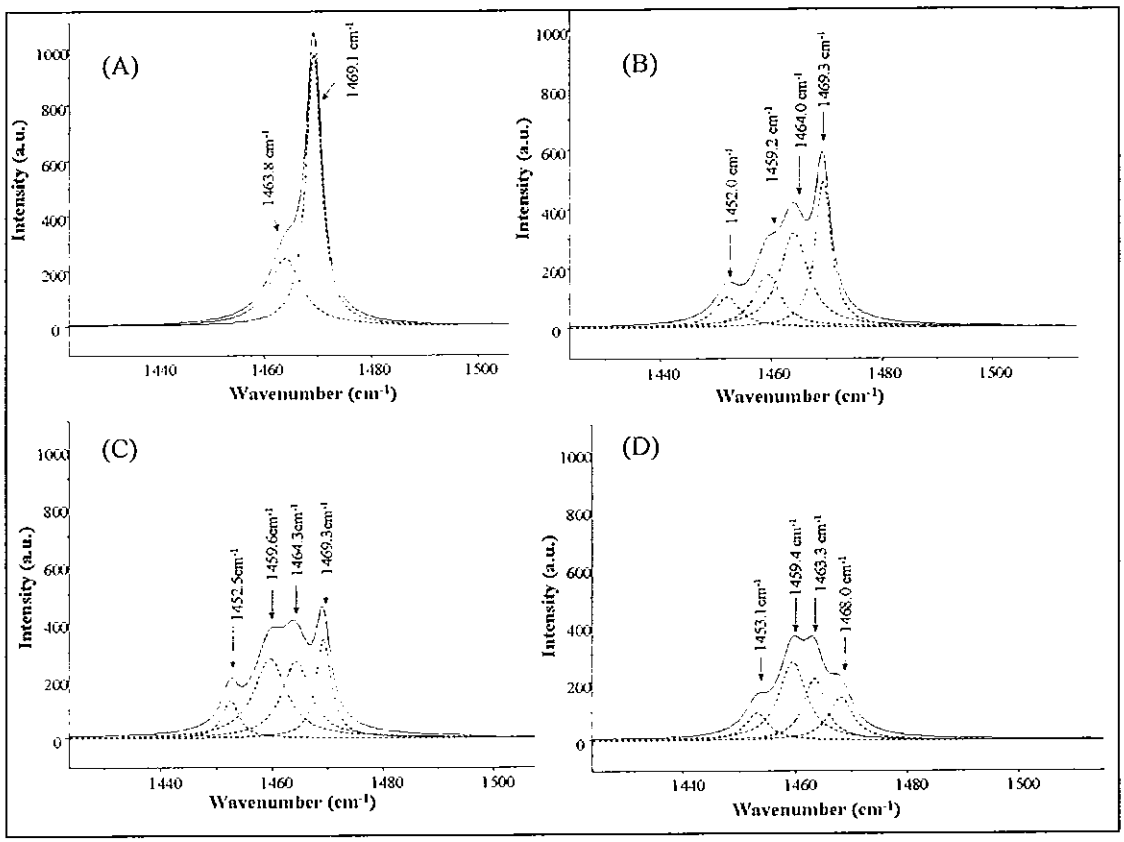

Figure 8.15 : Raman spectra of annealled films

Upon illumination no change in the peak positioning or the relative intensity of the 1464cm^{-1} feature is observed, whilst all the other characteristic Raman modes shift accordingly, similar again to that observed for the clathrates. It has been suggested that the hcp phase at 1464cm^{-1} is stable against prolonged low level illumination due to a hindrance of the free rotation of the C_{60} molecules similar to the low temperature simple cubic phase in which the polymerisation is also inhibited [19]. In other words this new hcp phase mimics the behaviour one would expect for an increased phase transition temperature.

Indeed an assessment of the thermal stability obtained from DSC (figure 8.16) does show that the phase transition temperature has been shifted closer to room temperature by ~7K (i.e. to 256K).

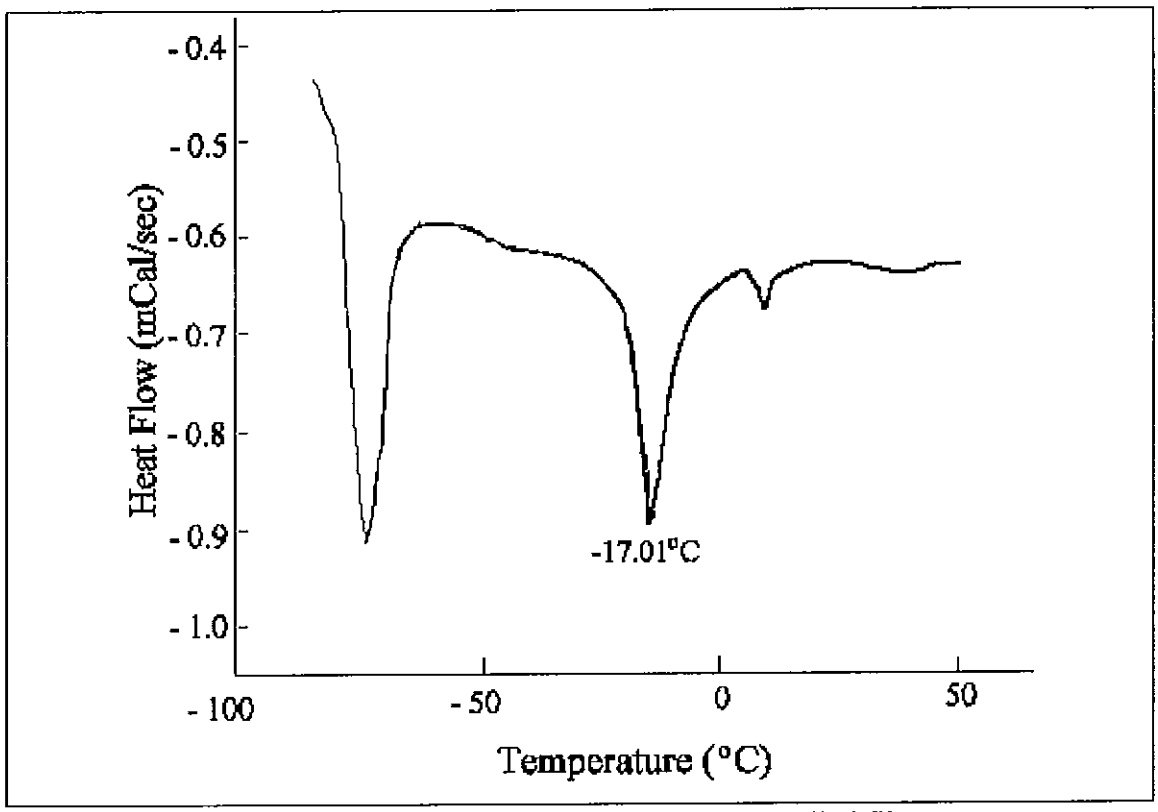

Figure 8.16: DSC trace of a thermally annealled film

The shift of the phase transition endotherm in the DSC again associates the changes observed in the thermal annealing with those reported upon the formation of C_{60} clathrates. Thermally annealed films however have the additional advantage of retaining the film integrity making such films genuine candidates for preserving the 'metallic-like' conducting species reported in chapter 7 at low temperatures. It should be noted however that while annealed films are reasonably ordered (defect free) they exhibit only a partial photochemical stability. It may thus be proposed that in order to obtain a C_{60} film which can both maintain its integrity and display a fully enhanced photochemical and thermal stability, a combination of annealing and solvent inclusion may be necessary.

8.3: Summary

In summary, structural and spectroscopic analyses of annealed and solvent included C_{60} films leads to the conclusion that a structural reordering of the lattice has occurred. The resultant films appear to consist of a mixture of the original fcc phase and an emergent hcp phase. The emergent hcp phase appears to have an enhanced chemical and thermal stability, which is indicative of a hindrance of the free rotation of the molecules similar to the low temperature simple cubic phase. The changes inflicted upon the lattice structure of the films also result in an increased phase transition temperature as seen by DSC measurements. Such an increase in the phase transition temperature may also be produced by applying external pressure to the cubic phase [136]. The difference in the lattice parameters of the mixed phases may therefore be sufficent to raise the transition temperature, accounting for the improved lattice stability.

The spectral shifting observed in the absorption spectra for both the annealing process and the inclusion processes correlates well with similar changes seen in pressure dependent absorption and luminescence spectra of C_{60} crystals [62, 91]. Indeed the effect of a closer packing on the spectral positioning of the optical resonances may be seen as a continuation of the small shifts which occur on going from solution to solid state [42]. A theoretical analysis of the effects of crystal packing on both the spectral positioning and oscillator strengths of the π-π^* transitions of C_{60} in the solid state has been performed by Wu and Ulloa [137]. The analysis indicated that the oscillator strength and spectral positioning of transitions can have considerable anisotropy due to different Coulomb interactions between molecules in different packing arrangements. This predicted sensitivity of the optical absorption spectrum to crystal packing is consistent with the variations observed in this study. Indeed such packing effects can be likened to effects observed in other systems. The loss of oscillator strength in both techniques in this study can be compared to hypochromic effects seen in for example highly stacked DNA. In highly stacked DNA the alignment of individual dipole moments leads to a screening effect which decreases the π-π^*

transition and thus the absorption of the system as a whole is less than the sum of the individual absorptions of the nucleotides [129].

The fact that the changes observed in this chapter are attributable to structural rather then chemical changes is extremely interesting as these materials process significantly different optical and electrical properties to those of the pristine material. The importance of such structural differences to the preservation at ambient temperature of the highly conducting species reported in chapter 7 is immense if realistic electronic applications of C_{60} are to be successful. Nevertheless both the annealed and clathrate C_{60} films constitute new forms of C_{60} whose properties need further investigation. Again highlighting that after nearly 15 years the properties C_{60} and its derivatives have still not been fully elucidated.

Chapter 9

General Discussion

9.1: Prelude: Summary of key Raman spectra

Throughout this study, Raman spectroscopy was seen to be an extremely useful probe of the optical and electronic properties of C_{60}. In particular the A_{2g} pentagonal pinch mode of C_{60} (positioned at 1469cm^{-1}) is extremely sensitive to changes in the local environment. A number of interesting results have thus emerged in the course of this work characterised by shifts in this mode reflecting, photo-physical, photo-chemical, electrical and structural changes to the C_{60} lattice. It is useful therefore at this point, prior to the general discussion, to summarise the key Raman results. Table 9.1 displays these results in conjunction with their assignment.

Table 9.1: Summary of key Raman results.

Photo-Physical (Chapter 5)		**Photo-Chemical (Chapter 6)**		**Electrical (Chapter7)**		**Structural (Chapter 8)**	
Mode (cm^{-1})	*Assign.*	*Mode (cm^{-1})*	**Assign.**	*Mode (cm^{-1})*	*Assign.*	*Mode (cm^{-1})*	*Assign.*
1469	Pristine C_{60}	1469	Pristine C_{60}	1469	Pristine C_{60}	1469	Pristine C_{60} (fcc)
1466	Molecular triplet	1464*	Dimeric species	1463	Mono anionic species C_{60}^{-1}	1464*	hcp phase
1463	co-operative excited state	1459*	Photo-polymer	1460	Polymeric species		
**** irreversible species***							

This table may be a useful aid when reading the following general discussion of the thesis as it clearly outlines the various modes and their significance. It can be seen from the table that a number of species can be identified within ten wavenumbers of each other. The photochemical and the structural modes are irreversible whereas the photophysical and the electrical modes are fully and partially reversible. As indicated from the table, a direct comparison between the electrical and the photophysical (optical) species can be made, particularly the mono anionic species and the co-operative species. While not highlighted in this table several changes in the peak intensity and the luminescence background have also been documented in literature [19, 34, 65] for each species. Significantly the feature at 1463cm^{-1} has been previously associated with a large increase in the luminescence background in crystals. The results reported in this thesis do indicate that this species is accompanied by such a luminescence increase when produced via the photopolymer i.e. in the depolymerisation process. However when produced directly from a C_{60} film the change in the background luminescence is minimal.

9.2: General Discussion

The discovery of the Buckminsterfullerene at the closing stages of the last century is testimony to the importance of interdisciplinary research in this the 21st century. The discovery ranked with some of the greatest moments in modern science, generating interest from both the scientific community and laymen alike. As a result the area of material science received a considerable boost with commercial giants such as NEC, Du Pont and IBM backing a highly competitive search to unlock the potential of this remarkable molecule [9,10]. In 1996 the award of the Nobel Prize in chemistry for the discovery of C_{60} further emphasised the importance of this molecule and its derivatives to material science. In recent years however the Buckminsterfullerene has taken a back seat, to its close relations, carbon nanotubes [138]. Indeed carbon nanotube research has been considerably more productive in the development of commercial products and has shown huge potential for future applications [19, 91, 94]. As the emphasis in main stream

fullerene research shifted from C_{60} to carbon nanotubes many open ended questions about the nature of C_{60} remained. In particular questions regarding the exact nature of the electronic processes in the solid, the structure of the C_{60} photopolymer and the apparent absence of any photopolymerisation from solution, have resulted in a number of heated debates and discussions over the last ten years. This thesis has attempted to address these questions and others to help develop a true understanding of C_{60} in solid.

The emphasis throughout the work has been upon the generation and spectroscopic identification of any species, which could potentially contribute to electronic conduction in thin films of C_{60}. As a result an underlying theme of the thesis has been the comparison of the isolated molecule (solvated) with the solid state. This argument was set up initially in chapter two in which the structure and symmetry of the molecule and the solid was discussed. It was highlighted in chapter two that as one moves from solution to the solid the potential for an intermolecular interaction between the 60 delocalised π-electrons of each molecule increases. The first indication of such an intermolecular interaction was presented in chapter four, where absorption spectroscopy of the solid state revealed two features one at 450nm and the other at 575nm both of which are absent from solution measurements. A comprehensive study of these features via electroabsorption was carried out by Kazaoui et al. [62]. It was shown that these solid state features were the direct result of intermolecular charge transfer excited states which can potentially contribute to the generation of photocarriers in the solid state of C_{60}. Vibrational spectroscopy, however revealed that solid state C_{60} is predominantly molecular in character, with the solid state packing having only a weak influence on the spectra.

Further evidence for an intermolecular interaction in the solid state was obtained by probing the excited state properties of C_{60}. In chapter five and six a considerable understanding of the photophysical and photochemical properties of C_{60} both in solution and solid evolved. In solution, optical excitation was seen to lead to the rapid population (1.2ns) of the long lived triplet state, via the singlet state [65]. This process has been well

characterised by transient absorption measurement performed by Ebbesen [68] and is characterised by a strong triplet-triplet absorption at 750nm. However this strong feature was not observed in the photo-induced absorption of the solid state C_{60} [69]. The absence of an equivalent behaviour in the solid state strongly suggests that the triplet state species are not the majority species in the solid and that the bulk excited state species have a character which is significantly different to that of the isolated molecule. Indicating a substantial departure from the molecular character in the solid. The crucial question then is what is the nature of the excited state species in the solid. Raman spectroscopy was used to probe the excited state species in both solution and in the solid and two species were clearly identified. The first species was the molecular triplet, which was identified for the first time in both solution and solid state using Raman spectroscopy with a mode positioning of ~1466cm^{-1}. The identification of this species in both the solution and the solid has thus resolved many questions about the existence of the molecular triplet in the solid, verifying that solid state C_{60} does partially retain its molecular character. The second species positioned at ~1463cm^{-1} in the Raman spectrum was seen to be specific to the solid state and was speculated to be a high intensity excited state co-operative, involving two or more molecules in the solid. Intensity-dependent transmission curves of the solid state suggest that this co-operative species is non-linear in nature. A temperature dependent study between 77K and 300K indicated that at low temperatures (<249K) this excited state species is intrinsic to solid state C_{60}. Parallels between this species and many-particle interactions in indirect band gap semiconductors i.e. Si and Ge at low temperatures were also drawn and it was suggested that solid state C_{60} can undergo a 'Mott-like' transition at high intensities [89, 90].

The most comprehensive evidence for intermolecular interactions in the solid state is the photopolymerisation of C_{60} [83]. In general C_{60} is stable under ambient conditions, however when it is exposed to intense visible or ultraviolet light (above 249K) it can form a number of dense polymeric phases [83, 95]. These polymeric phases have been suggested to form via a 2+2 cycloaddition reaction [83]. In such a reaction the π bonds of adjacent molecules open to form a covalent coupling between the molecules. The 2+2

cycloaddition reaction is thermally forbidden but is one photon allowed when adjacent π bonds are separated by less then ~4.2Å. Solid C_{60} has been seen to satisfy the general topochemical and photophysical requirements for a 2+2 cycloaddition reaction at room temperature. Although not irrefutably proven, such a picture is widely accepted. It has been shown that the process occurs through a molecular excited state intermediate and the role of oxygen is as an excited state quencher, which inhibits the photodegradation process. Curiously absent for many years was any report of such a photopolymerisation from solution. This led many to believe that the photochemical transformation of C_{60} into a photopolymer was specific to the solid state. As a result many questions arose regarding the validity of the photopolymerisation mechanism proposed by Eklund [83] and indeed if the degree of translational freedom within solution allowed chemical bonding between C_{60} molecules. In this study the photopolymerisation of C_{60} from solution is reported for the first time thus supporting the proposed 2+2 cycloaddition model and confirming equilibrium bond formation in solvated C_{60} [31]. In addition vibrational spectroscopy indicated that the photopolymer produced from solution consisted of a complex mixture of polymeric phases, which reduce the molecular symmetry and enrich the Raman and IR spectra. In particular, IR spectroscopy seems to indicate that the material is closely related to the pressure and temperature induced 'soft fcc' phase [96]. While Raman spectroscopy displays features consistent with the formation of dimeric material [104] and clathrates [105], both of which are consistent with the notion of this polymeric material being produced from solution. However the quantities of the material, which can be produced from solution, are quite small ~0.5-1mg hence structural analysis using conventional methods such as x-ray diffraction is difficult. Nevertheless the formation of polymeric bonds in the solid is the first indication of a truly intermolecular molecular interaction. In addition to photopolymerisation, polymeric forms of C_{60} can be produced via the injection of charge [91].

As seen in chapter 7 solvated C_{60} has an extremely rich electrochemistry and can accept up to six electrons forming a hexa-anionic molecule (i.e. C_{60}^{-6}). This is also demonstrated by C_{60}'s ability to form solids like K_6C_{60} [109]. However the

electrochemistry of C_{60} drop cast films is considerably different to that of the isolated molecule, highlighting again a deviation from the molecular properties in the solid state of C_{60}. The cyclic voltammogram for a drop cast C_{60} film shows two main reduction peaks. The first peak can be attributed to a C_{60}^{-1} film which has undergone a significant structural rearrangement in order to accommodate charge balancing counter ions. The second reduction peak however has been attributed to the formation of dimeric dianions. Indeed in situ Raman spectroscopy does support this suggestion with a considerable softening of the pentagonal pinch mode at $1469cm^{-1}$ to the lower Raman frequency of $1460cm^{-1}$. Conductivity measurements of reduced films by Smie and Heinze [120] revealed that the 'undoped' C_{60}^{-1} anions, which are in abundance prior to intercalation by the counter-ion into the lattice, are conductive i.e. before the peak maximum for the first reduction peak in figure 7.3, chapter 7. The Raman signature of the species at this point is $\sim 1464cm^{-1}$ which may allow comparisons to the aforementioned optically excited states to be drawn, in particular to the excited state co-operative positioned at $1463cm^{-1}$.

It was proposed that in the absence of any charge balancing cation, sufficiently high quantities of this conducting species could be generated yielding a film that should have good electronic properties. To do this thin films of C_{60} were prepared in a sandwich type geometry with Indium Tin Oxide (ITO) as the bottom electrode and aluminium as the top electrode. Initially at room temperature the I-V curves for the film correlated well with the electrochemistry of the drop cast films, showing two apparent maxima. However at 20K the I-V curves showed the presence of a stable highly conducting 'metallic–like' species upon the application of a moderate voltage. That such a species is present at temperatures where the polymerisation of C_{60} is inhibited, indicates that the conducting species is analogous to the excited state co-operative species (with a Raman signature of $1463cm^{-1}$), which was also seen to exist within this low temperature regime. The commercial potential of a material which can switch reversibly, from a weakly conducting material to a material which is highly conducting, comparable to a 'metallic-like' conductor at a well defined voltages or optically is unlimited. However the highly conducting species reported in this work has only been produced at 20K. In order

therefore to unlock its potential, it is necessary to preserve this conducting species at more ambient temperatures.

The enhancement of the C_{60} lattice against electronic and photochemical polymerisation, was attempted by forcing the room temperature C_{60} lattice into a new structural arrangement thus creating a pseudo low temperature phase at higher temperatures. This was done initially by including neutral solvent molecules into the lattice [105. 132], which essentially force the lattice into a new structural arrangement similar to the electrochemical rearrangement reported in chapter 7. A photochemically stable form of C_{60} was produced at room temperature via the incorporation of chlorobenzene molecules into the lattice creating a clathrate type compound [105]. This new material was proposed to have a mixture of a hexagonal close packed and a face centred cubic type structure. In addition to exhibiting an enhanced photochemical stability this clathrate compound also showed an enhanced thermal stability. However the integrity of the film during the inclusion of the solvent molecules was lost creating a number of defect sites, hence rendering it a poor conducting material. The film integrity can be preserved by thermal annealing [129, 130] although the results indicate that annealed films produce only a partially stable material. Nevertheless these materials represent a new class of C_{60} whose electronic properties differ significantly form the pristine material. As a result these materials warrant a full investigation of their properties and potential applications.

In attempting to answer many of the remaining questions about C_{60} this work has raised a number of new and intriguing questions, for example what is the nature of the excited states species that was identified in the solid and what is its relationship to the electronically produced anionic species? Additionally one must ask, can the electronic properties of C_{60} be tuned sufficiently in order to maintain a stable conducting C_{60} film at room temperature. If the answer to the latter question is yes then the future of C_{60} looks extremely promising with many exciting applications.

9.3: Potential of the results of this Thesis.

The stabilisation of the highly conducting state of C_{60} at room temperature coupled with a thorough knowledge of the electronic processes in C_{60} would lead to the realisation of numerous applications. However despite the huge potential for commercial applications to date no specific application of C_{60} has been reported although there are unconfirmed reports of C_{60} being used in shampoo by a leading cosmetics company have arisen in recent years [139]. The proposed areas of application to which it is envisaged that this thesis will contribute to are, non linear optical applications and the electronics based applications.

9.3.1: Non Linear Optics

Since the early seventies the areas of photonics and non-linear optics have seen revolutionary developments in the search for new materials for optical signal processing, optical switching and optical limiter technologies. Organic conjugated polymers, due to their structural flexibility both at the molecular and bulk levels emerged as a new novel class of non linear optical material. Their delocalised π-electron backbones exhibited large non-linear susceptibilities [140] with ultrafast response and recovery times [141]. In addition their electronic properties and tailorability coupled with their easier processability, as compared with earlier inorganic materials, made them ideal candidates for use in integrated optical technologies. Although the drive to develop these materials grew rapidly, it became apparent that their off-resonant non linearities remained too low for realistic applications and the C-H bonds of the polymer backbone resulted in overtones which interfered with the telecommunications window, around 1.3μm, limiting them severely in the development of optoelectronic devices [140]. A number of polymers were reported with off-resonant non linearities (approximately) between 10^{-10} - 10^{-12} esu [142] which is significantly less then that required for realistic application to optical switching technologies, and thus the emphasis shifted to more novel approaches. Push -

pull polymers or charge transfer techniques where utilised to enhance the non linear susceptibilities of organic polymers [143] other approaches include the doping of organometallic [144] compounds into the polymer matrix and the probing of the non linear optical properties of excited state species [145]. The result has as led to a thriving research area in the continuous search for novel materials which can be utilised in optical technologies.

It was not surprising then in the aftermath of the discovery of C_{60} that a number optical applications were suggested. The general belief that C_{60} would be a good non linear optical material was wide spread. This belief was born of the fact that C_{60} had a large delocalised cloud of π electrons situated in and around the carbon cage, which resulted in a relatively high non linear susceptibility [146]. Also the absence of hydrogen meant that it would not display overtones in the region of the telecommunications window. The excitement grew as Kost and Tutt [15] reported that C_{60} was a more efficient optical limiter than chloroaluminum-phthalocyanine (CAP), which at the time was one of the most promising materials for limiting applications. However C_{60} has yet to live up to its potential in the area of optical technology. It is therefore proposed in light of the work reported here that further analysis into this potential be carried out with particular reference to the excited state species discussed in chapter 5. Excited state species in general have non-linear susceptibilities (χ^3) approximately 100 times that of the ground state molecules. In C_{60} it has been shown that the optical generation of not only a molecular excited state but also an excited solid state species is possible, in which the electrons become delocalised across a number of molecules. It may be speculated that such a solid state delocalisation would have an extremely high non-linearity. However in order to generate and maintain such an excited species it is necessary to have high laser powers. It is thus proposed that through electron injection techniques states similar to those optically produced, excited states may be produced at moderate voltages which would have comparable non-linearities. It is thus envisaged through the generation of such species that a novel opto-electronic switching device may be designed and fabricated.

9.3.2: Electronics

Electronic based applications of pure C_{60} have for over a decade remained an elusive target for many researchers. To date a variety of rectifying diodes, field effect transistors as well as photovoltaic and photorefractive devices have been proposed [19] and measurements on prototype devices have been carried out [13,14]. However most of the C_{60} devices which have been reported, tend to be unstable in air and/ or at room temperature. One of the most interesting devices proposed is a field effect transistor based on C_{60} [19]. A conventional silicon based metal-oxide-semiconductor field effect transistor (MOSFET) consists of two p-n junctions placed immediately adjacent to the region of the semiconductor controlled by the MOS gate. The current carriers enter the structure through the source (S), leave through the drain (D), and are subject to control by the bias voltage on the gate (G). Increasing the bias voltage at the gate creates a source-to-drain channel in which current can flow. The current -voltage characteristics of the drain can then be monitored for various gate voltages giving the characteristics of the transistor. The basic structure of an n-type MOSFET and the corresponding current - voltage characteristics of the drain are shown in figure 9.1.

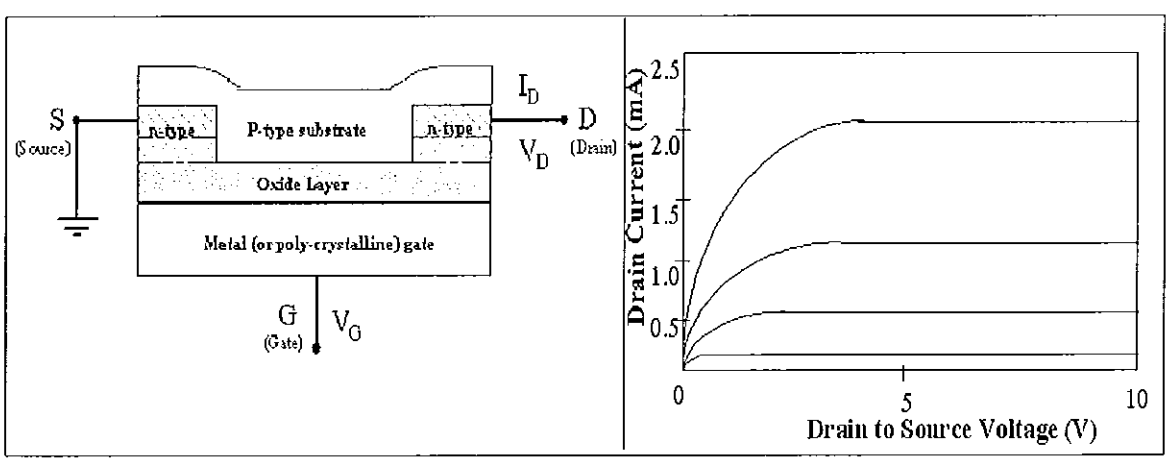

Figure 9.1: The basic structure of an n-type MOSFET and the corresponding I-V characteristics of the drain. [19]

Fullerene-based n-channel FETs have been constructed [19]. Figure 9.2 displays a schematic of such a device. In this device a highly doped n-type silicon wafer takes the place of the gate metal, SiO_2 serves as the oxide, and the fullerene film as the semiconductor. When an appropriate positive gate voltage (V_G) is applied, the drain current I_D increases, which indicates that a conduction channel is formed near the fullerene-insulator interface. The sign of the current response indicates that the fullerene transistors are n-channel devices, consistent with C_{60} anion formation.

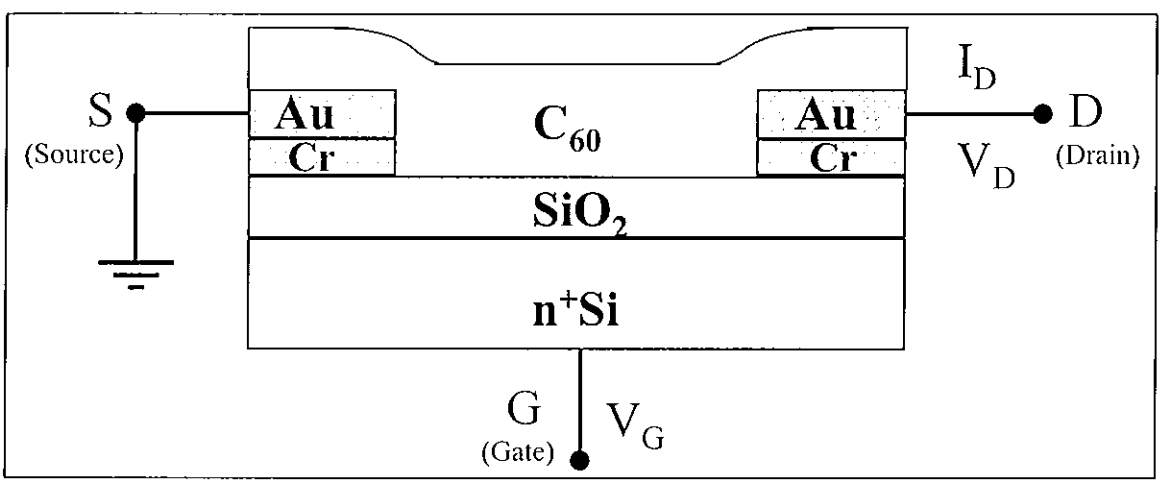

Figure 9.2: Fullerene -based n-channel FETs [19]

Field effect mobilities obtained from the current -voltage characteristics of the drain for the device in figure 9.2 compare well with mobilities obtained for other organic FETs [19,14]. However because C_{60}- based FETs operate as n-channel devices, they are subject to problems that are not experienced by the majority of organic materials investigated to date, which tend to be p-type materials. The main problem is that field effect mobilities degrade rapidly upon exposure to oxygen. This is presumably because charge transfer in C_{60}-FETs depends on electron transport rather than hole transport common to most other organic FETs. The C_{60} device however is stable under nitrogen suggesting that oxygen molecules act as electron traps in the lattice of C_{60}.

Overall, the electronic properties of C_{60} as a FET channel material show a strong resemblance to amorphous semiconductors. The mobility of fullerene FETs may perhaps be improved by using a better fabrication procedure to reduce the concentration of defect traps. It is proposed that the highly conducting state reported in this thesis and the work done on stabilising the C_{60} lattice against degradation could help similar devices to be developed in the not to distant future. Further to this however it is envisaged that a new proto-type device could be designed and fabricated by analogy to the FET discussed above. The device is expected to behave as a "current effect transistor (CET)". In which the flow of charge from the source to the drain will be current controlled from the gate. Such a device would be extremely useful in the electronics industry in particular in integrated circuit technology.

It is foreseen that such a device would work on the principle that as electrons are injected into a thin layer of C_{60} through the 'gate' the film would rapidly (in an avalanche type effect) become conducting through the rapid generation of C_{60}^{-1}. In turn this would produce a conduction channel for electrons to pass from the 'source' to the 'drain' under the influence of a weak potential (analogous to the decrease in the depletion layer of a FET, due to the application of a gate voltage). Figure 9.3 shows a schematic of the proposed device.

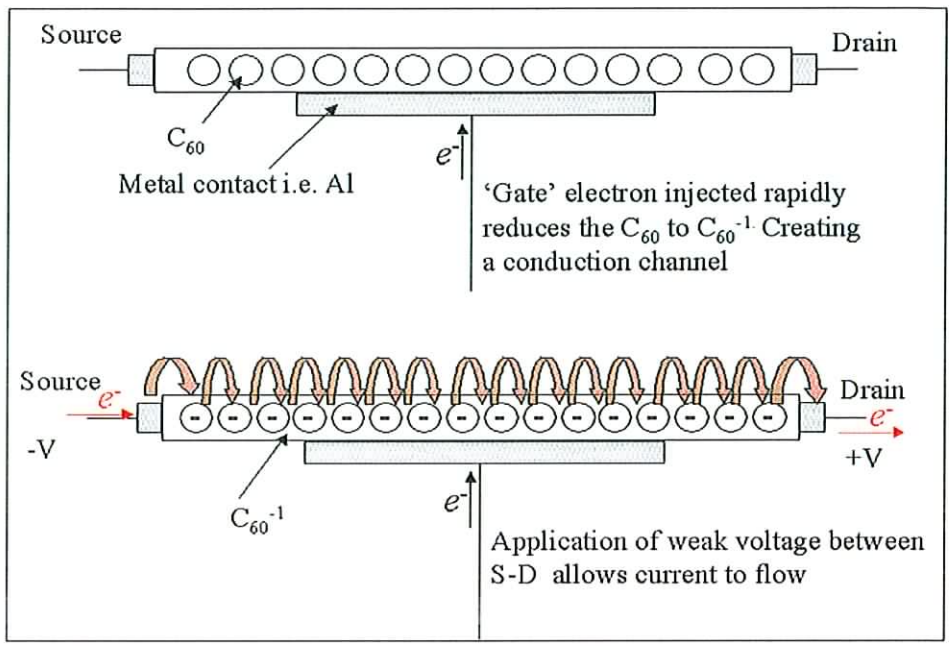

Figure 9.3: Schematic of the proposed CET device.

Similarities between this device and a bi-polar transistor may also be seen, as both devices produce a current output, which is controlled at the 'gate' (or base for a bi-polar transistor). Furthermore by the use of positive feedback through the 'gate' the current can be considerably amplified. While no figure can be put on the current amplification for this device a typical transistor can amplify a signal current by nearly 100 times. Hence for this C_{60} device to be actually used to amplify current it would have to be comparable to this figure. Nevertheless the prospect of fabricating such a device through the optimisation of the structural enhancements to the C_{60} lattice would be an exciting development and extremely attractive to industry as a switching mechanism and current amplifier.

9.2.3: Potential as a model of other Materials

In addition to contributing to a greater understanding of the electronic processes in C_{60}, which in turn can help the development of commercial applications of C_{60} this work may have academic potential in areas other then C_{60}. It has been suggested that the chemical and physical properties C_{60} are unique to this a model molecular system. However, it is proposed here that the photophysical properties of C_{60} reported in chapter 5 are not specific solely to C_{60}. It was seen in chapter 5 that the Raman signature of the molecular triplet of C_{60} was identified both in the solution and solid state with a spectra positioning of 1466cm^{-1}, resolving the question as to whether or not the molecular triplet existed in the solid state. However a second excited state species which is specific to the solid was also identified with a Raman signature of 1463cm^{-1}. It was indicated that this species is a highly non-linear delocalised excited state co-operative involving two or more molecules in the solid state. It is proposed that this type of excited state species may not be unique to C_{60} but instead is common to all large cluster type compounds, which exhibit signs of being molecular solids.

Obvious candidates for materials which have a similar photophysics to C_{60} are higher fullerenes such as C_{70}, C_{76}, and C_{84} etc. Due to the small quantities of higher fullerenes available only a very limited amount of work has been done on their photophysics [19]. The optical properties of C_{70} however have been studied extensively [19, 34, 62, 91]. A comparison of the UV/visible absorption spectrum of molecular C_{70} to that of C_{60} shows signs of the reduced symmetry of the larger molecule. Similar to C_{60}, the spectrum of C_{70} contains strong features in the region of 200-300nm and weaker features in the region 300-400nm [147]. The onset of the absorption, corresponding to the HOMO-LUMO transition, also occurs in the region of 670nm and the primary difference between the spectrum of C_{70} and C_{60} is that this absorption reaches a relatively strong maximum at 468nm. The absorption is also strongly vibrationally structured. The strength of the transition in comparison to C_{60} has been ascribed to the reduced symmetry of the molecule. In the solid state the absorption spectrum retains its molecular character as in

C_{60} and a new solid state feature is observed at ~550nm for C_{70}. Detailed electroabsorption measurements have ascribed this feature to a charge transfer excited state and have identified a further solid state feature at 344nm, again similar to C_{60}. The known excited state properties of C_{70} are also similar to those of C_{60}, differences arising again as a result of the reduced symmetry of the molecule. As in C_{60} the singlet state depopulation is dominated by intersystem crossing [148], giving a triplet state yield close to unity. The depopulation of the singlet state to the triplet has been shown by photoinduced absorption spectroscopy and although the kinetics are similar to those observed in C_{60} solution, spectrally there are some differences. Notably, the triplet-triplet absorption, which is exceptionally strong and lies at ~740nm in C_{60} solutions, is positioned at ~950nm as well as being very much weaker in C_{70} solutions [149]. The triplet in C_{70} is proposed to be similar in character to that of C_{60}, being molecularly delocalised and axially symmetric [34]. In the solid state however, like C_{60} the photodynamics of C_{70} differ considerably from that of the isolated molecule, with no apparent evidence of a molecular triplet [150]. It is thus proposed that a similar Raman study to the one performed in this thesis, on the photodynamics of C_{70} may reveal similar excited state species to C_{60}. Indeed it can be suggested that such excited state species may be common to even higher fullerenes such as C_{76} and C_{84}.

Furthermore the investigation of other fullerene type compounds such as $C_{59}N$, non carbon based inorganic fullerenes of tungsten sulphide [151], and indium-based fullerenes [152] may also reveal similar excited state phenomena to those reported for C_{60} in this study. Moving away from fullerene based materials one could envisage C_{60} being used as a model for other large cluster compounds such as polymetallate compounds in particular, phosphomolybdic acid ($H_3Mo_{12}PO_{40}$) and tungstosilicic acid, ($H_4W_{12}SiO_{40}$). Like C_{60} these compounds are highly electronegative and can readily accept electrons creating anionic species similar to C_{60} [153]. Like C_{60} the absorption spectra of phosphomolybdic acid ($H_3Mo_{12}PO_{40}$) and tungstosilicic acid, show the emergence of new features in the solid state which are absent in solution suggesting the presence of similar excited state processes to those active in C_{60} [153]. Hence it may be envisaged that the

photophysics reported in this thesis for C_{60} may eventually be used as a model for other materials.

9.4: Future of fullerene Science

The work presented in this thesis raises some intriguing questions about the properties and potential applications of C_{60} and may eventually contribute to the realisation of one of the many proposed applications. However researchers are increasingly coming under pressure to produce commercial applications for industry and in many cases basic fundamental research is being overlooked. In some ways C_{60} has fallen victim to this 'gold rush' type of research and has taken a back seat, to its close relations, carbon nanotubes [138]. Carbon nanotubes have attracted a considerable amount of attention due to their potential for the development of viable commercial products.

Carbon nanotubes are fullerene-related structures, which consist of graphene cylinders closed at either end by hemispherical fullerenes [19,138]. They were first observed in 1991 by Sumio Iijima [138]. By analogy to a C_{60} molecule, one can specify an idealised single wall carbon nanotube by bisecting a C_{60} molecule along its equator and joining the two hemispheres with a cylindrical graphitic tube one monolayer thick with the same diameter as C_{60}. If the C_{60} molecule is bisected normal to a five fold axes, then the tube is referred to as an 'armchair' tube [19]. If however the C_{60} is bisected normal to a three fold axes the tube is referred to as a 'zigzag' tube [19]. In addition to these structures a large number of chiral tubes can be formed which have a screw axis along the axis of the tube. Figure 9.4 show the various types of single walled carbon nanotubes, which can be formed. As well as single walled carbon nanotubes, multi-wall carbon nanotubes are possible, which are essentially capped concentric co-axial assembles [19,91].

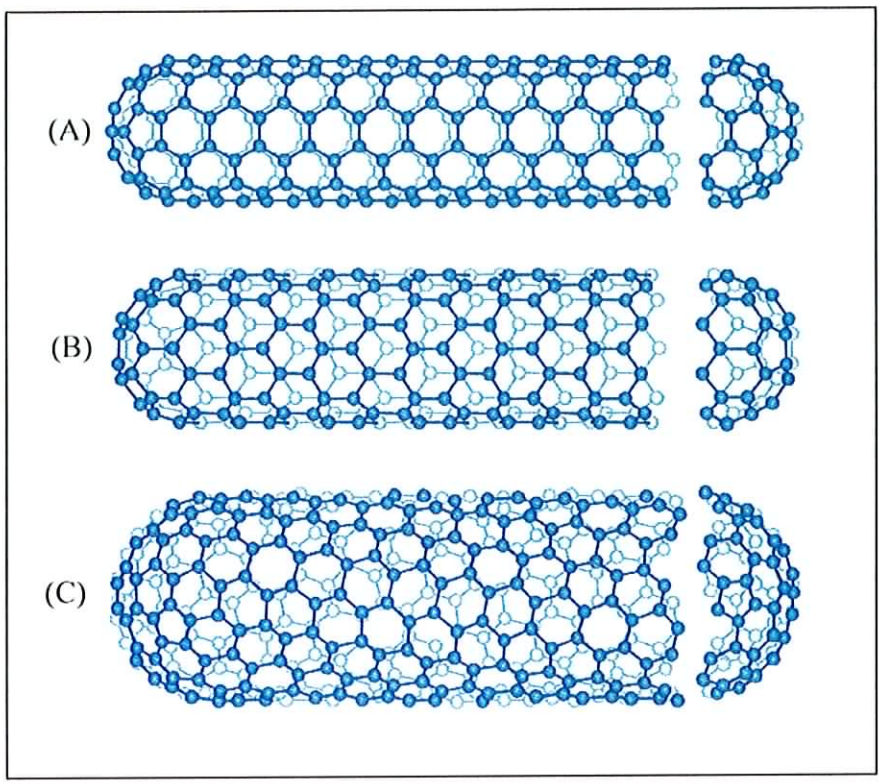

Figure 9.4: Various types of single walled carbon nanotubes (A) armchair tubes, (B) zigzag tubes and (C) chiral tube [154]

Much of the potential of carbon nanotube like C_{60} originates from their unique structure and properties. Nanotubes are known to be exceptionally strong, low in weight, stable, extremely flexibile, good thermal conductors, and have intriguing electronic properties. In particular the electrical properties of nanotubes have attracted a considerable amount of attention with reports that a single carbon nanotube can act as a nano- transistor [155]. In addition carbon nanotubes have been shown to emit electrons at a relatively low voltage, making them ideal candidates for field emitters in flat panel display [156, 157]. Pioneer have recently started to use nanotubes as the field emitters in their new car radio displays. Other areas where carbon nanaotubes are currently being investigated for use is as reinforcement agents in space suits [158], the storage of hydrogen in the development of super fuels [9] and as drug delivery systems in medicine [128, 9].

While mainstream fullerene science appears to have its future firmly based in the exploration and exploitation of carbon nanotudes and related materials many researchers still believe that C_{60} has a lot to offer. In particular, the investigation of the pressure induced polymeric and doped polymeric phases of C_{60} has developed into a vibrant research area, with many exciting discoveries predicted for the future, such as ultra hard conductors and superconductors [95]. In addition the biological applications of C_{60} have also begun to show real potential in chemotherapy [14]. The development of a viable commercial application of C_{60} would be a fitting tribute to this remarkable molecule, which in just over ten years has inspired a generation of scientists and layman alike. However for the moment C_{60}'s greatest contribution to mankind has been the development of a true interdisciplinary branch of science, which will feature strongly in the coming years.

Conclusions

Conclusions

The discovery of the Buckminsterfullerene (C_{60}) [3] triggered an explosion of research in the early 1990's, which essentially gave birth to fullerene science. The aspects of fullerene science that have been explored in this study are the electronic and optical properties of C_{60}. These properties have been the subject of much research over the past decade [25,35]. The emphasis throughout the work has been upon the generation and spectroscopic identification of any species, which could potentially contribute to electronic conduction in thin films of C_{60} with the aim of establishing an understanding of the electronic processes in fullerenes. Electronic conduction in general is a bulk process and indicates a departure from molecular properties and behaviour. As a result the underlying theme of the thesis is the comparison of the properties of the isolated molecule and the solid state.

Initially the low intensity optical properties of C_{60} were examined [34] where it was seen that vibrational spectroscopy indicated that the solid state is predominantly molecular in character. An assessment of the low intensity optical response of C_{60} does leads to the conclusion that, although the lowest energy transitions are optically forbidden due to the high degree of symmetry of the molecule, any small perturbation to that symmetry is sufficient to relax the restrictions imposed by the selection rules. Such a perturbation to a weak response can be dominant and an awareness of this sensitivity to changes in symmetry, either of the molecule or of the local environment, is of vital importance in addressing the nature and properties of the solid state.

Electronic spectroscopy revealed features that are specific only to the solid. In particular the presence of a new feature in the solid state absorption spectrum at ~450nm which has been attributed to an intermolecular charge transfer exciton thus contributing to the generation of photocarriers in the solid. The evidence from the absorption spectrum is the first indication of an intermolecular interaction in the solid [37,48].

At high intensities the excited state properties of molecular C_{60} were seen to be dominated by an extremely fast intersystem crossing rate (~1.2ns) [65] to the first triplet state manifold. As a result a strong triplet –triplet absorption is seen in transient absorption measurements at ~750nm for the isolated molecule [68]. However no corresponding absorption was observed in the solid state leading to questions about the nature of the excited state properties of solid state C_{60}.

Raman spectroscopy was seen to be an extremely useful probe of the excited states of C_{60} and revealed for the first time the Raman signature of molecular triplet of C_{60} in both the solution and solid state. A second species was also identified in the solid and is thought be an excited state co-operative specific to the solid state [31,77]. A temperature dependence study of the excited states in the solid indicated that the excited state co-operative is non-linear in nature and is intrinsic to the solid below 249K suggesting that this state is related to the solid state phase transition. It has been proposed that this solid state feature is the result of a bulk interaction in the solid whereas the molecular triplet in the solid is a surface species.

The identification of the Raman signature of the molecular triplet was also instrumental in the elucidation of a proposed mechanism for the first reported photopolymerisation of C_{60} from solution. IR spectroscopy indicated that the resultant photopolymer is similar to the 'soft' fcc polymer [96] produced at low temperature and pressure in the solid (300K, 5GPa). The subsequent Raman signature of the photopolymer thus completed the spectroscopic characterisation of all the optically generated species, which could potentially contribute to the generation or indeed inhibit the generation of charge carriers within a solid state C_{60} device.

Ionic species, which could potentially contribute to the electronic transport processes in solid state C_{60}, were also examined using cyclic voltammetric techniques and in situ Raman spectroscopy. In solution it was seen that the C_{60}^{-1} and C_{60}^{-3} ionic species which are analogues to the highly conducting metallic salts KC_{60} and K_3C_{60}, could be readily

produced by the application of specific voltages [110, 111]. However in the solid state, structural rearrangements and subsequent electronic interactions forming a polymeric species, complicated the generation of anionic species and inhibited the conductivity of the solid state. The effect of this was evident from conductivity measurements on C_{60} drop cast films [119], and the current-voltage characteristics of vacuum evaporated C_{60} films incorporated into a sandwich type structures. The effect of the structural rearrangements and electronic interactions however, was overcome for the sandwich type structure by cooling the arrangement down to 20K. At this low temperature a relatively stable, highly conducting film was produced upon the application of a moderate voltage, which could then be cycled between the conducting and non-conducting states. The species responsible for the enhanced conductivity was speculated to be a reduced state of C_{60} and Raman spectroscopy indicated that it may have some similarities to the excited state co-operative species observed in the solid.

In order to preserve this conducting species at room temperature two methods were examined. The first method solvent inclusion resulted in a photochemical and thermally stable clathratic form of C_{60}. However the incorporation of the solvent molecules results in a loss in the film integrity. The second method thermal annealing did help retain the film integrity. However only a partially stable form of C_{60} resulted. Nevertheless the results do point the way towards a method of tuning the electronic properties of C_{60} for potential use in electronic and optical applications.

Appendix I

Appendix 1

Hyper-Chem Model

Hyper-Chem is a versatile and powerful molecular modelling and computational package. It offers several types of molecular and quantum mechanical calculation methods. The semi-emperical AM1 method has been used in this study to model C_{60}. This method is generally accepted as the most accurate semi-emperical method in Hyper-Chem and is the method of choice for most Hyper-Chem models.

Initially the C_{60} molecule was optimised for geometry by using a single point calculation with the following parameters:

Convergence limit = 0.01	Iteration limit = 50
Accelerate convergence = Yes	Singlet state calculation

Results: Energies and Gradient

Total Energy	-176296.3828979 (kcal/mol)
Total Energy	-280.940559851 (a.u.)
Binding Energy	-9128.1163379 (kcal/mol)
Isolated Atomic Energy	-167168.2665600 (kcal/mol)
Electronic Energy	-2382427.5112596 (kcal/mol)
Core-Core Interaction	2206131.1283617 (kcal/mol)
Heat of Formation	1125.2836621 (kcal/mol)
Gradient	61.8769732 (kcal/mol/Ang)

The script below was then written to allow the geometry optimisation using a number of calculations i.e. steepest descent, Flecther-Reeves and Polak-Ribiere.

```
calculation-method semiempirical
semi-empirical-method am1
scf-convergence 0.01
```

screen-refresh-period 10000

start-logging X_am1.log no

file-format hin

open-file X_.hin

select none

do-optimization

write-file X_am1.hin

append-omsgs-to-file Xam1.log

query-value total-energy

stop-logging

It was found that the optimization algorithm Polak-Ribiere gave the best optimised geometry under the following conditions:

Convergence limit = 0.01	Iteration limit = 50
Accelerate convergence = Yes	RMS gradient = 0.001 kcal/(A mol)
Maximum cycles = 900	Singlet state calculation

Results:

Average Bond lenght of pentagon = 1.44·Å

Average Bond lenght of hexagon = 1.38·Å

Bond Angle of pentagon = 108.00^0

Bond Angle of hexagon = 120.01^0

Energies and Gradient:

Total Energy	-176449.1687220 (kcal/mol)
Total Energy	-281.184034699 (a.u.)
Binding Energy	-9280.9021620 (kcal/mol)
Isolated Atomic Energy	-167168.2665600 (kcal/mol)
Electronic Energy	-2342770.7611128 (kcal/mol)
Core-Core Interaction	2166321.5923908 (kcal/mol)

First ionisation potential	9.634eV
Heat of Formation	972.4978380 (kcal/mol)
Gradient	0.0008140 (kcal/mol/Ang)

Vibrational spectrum:

This structure was then used to calculate the vibrational modes:
174 modes of vibration were calculated, 3 translation modes and 3 rotational modes.
The resultant spectrum is displayed in figure A.1

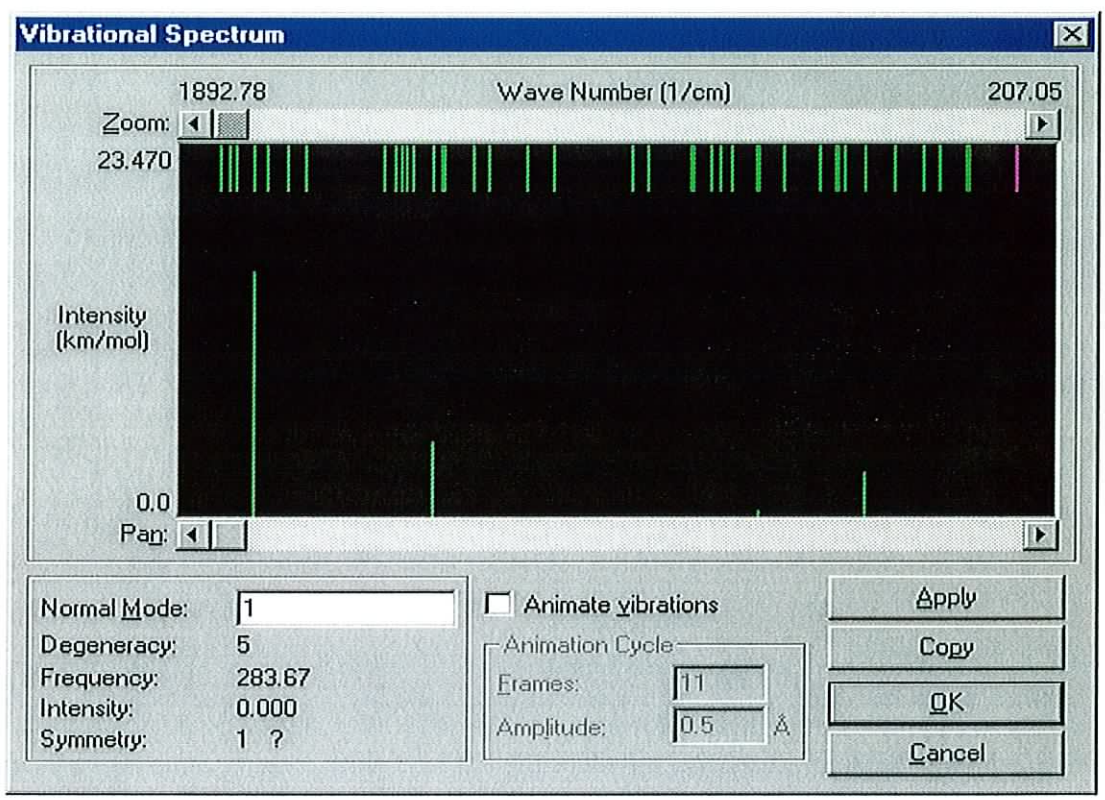

Figure A.1: Vibrational spectrum

The four modes displayed at the bottom of the of the dialogue box above represent the IR modes. The values which Hyper-Chem gave for these were:

573.10 cm,$^{-1}$ 775.52 cm^{-1}

1405.04 cm^{-1} 1752.61 cm^{-1}

Electronic spectroscopy:

The same parameters as above where then used to calculate the electronic spectrum of C_{60} except the CI parameter was changed to excited state and the following were set;

Number of Occupied Orbitals Used in CI = 8

Number of Unoccupied Orbitals Used in CI = 8

Starting molecule had the following energy and gradient:

Energy: -9128.116338 Gradient: 61.876973

Results:

Energies and Gradient	
Total Energy	-176296.3828979 (kcal/mol)
Total Energy	-280.940559851 (a.u.)
Binding Energy	-9128.1163379 (kcal/mol)
Isolated Atomic Energy	-167168.2665600 (kcal/mol)
Electronic Energy	-2382427.5112596 (kcal/mol)
Core-Core Interaction	2206131.1283617 (kcal/mol)
CI Energy	-0.0000000 (kcal/mol)
Number of Configurations Used	129
Heat of Formation	1125.2836621 (kcal/mol)
Gradient of Reference Configuration	61.8769732 (kcal/mol/Ang)

The electronic spectrum calculated showed 128 transitions which are shown below in figure A.2.

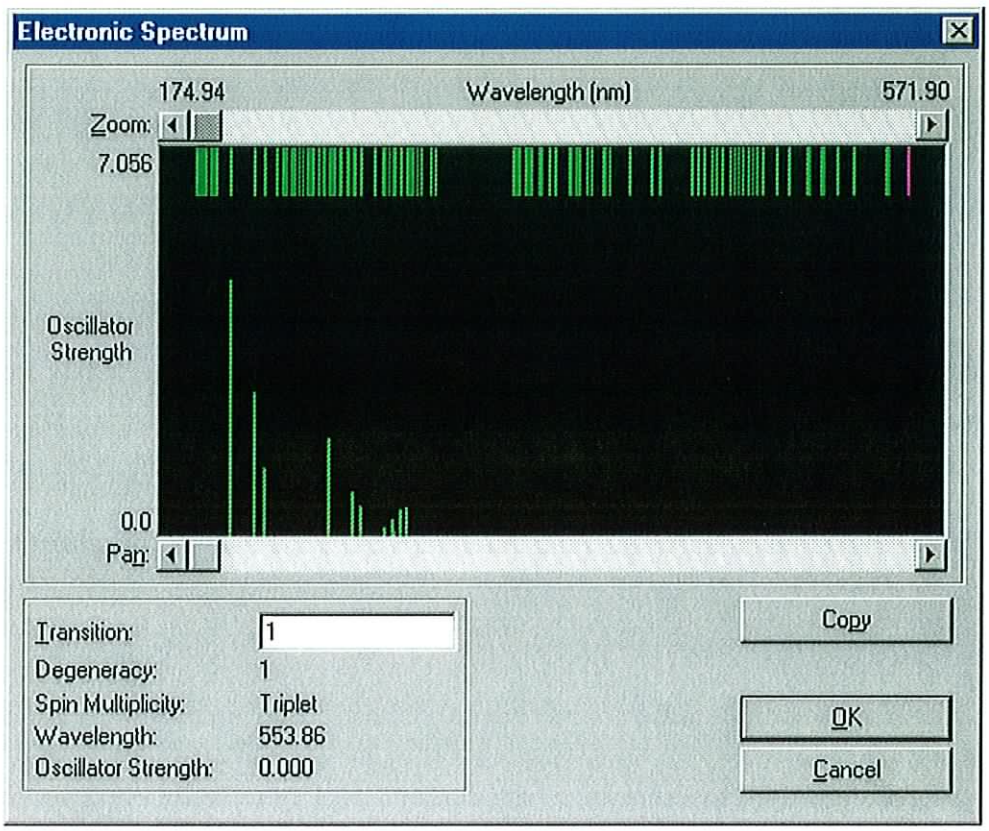

Figure A.2: Electronic spectrum of C_{60} calculated by Hyper-Chem

Several other parameters have to be analysed using Hyper-Chem as well as exploring other calculation methods such as the extend Hückel, ZINDO, or MNDO etc. Hence this model needs to be extended.

Appendix II

Appendix 2

Publication and Presentation List

Oral Presentations

1. "In search of the Molecular Triplet in C_{60} thin films" G. Chambers, A.B. Dalton, H.J. Byrne, presented at The Materials Research Society (MRS) spring seminars (San Francisco, USA. 15th-20th April 2001)

2. "Structure and characterisation of photo-polymerised C_{60} from solution" G. Chambers, K. Henderson, A.B. Dalton, B. Mc Carthy, H.J. Byrne, presented at the International Conference on Science and Technology of Synthetic Metals, (ICSM 2000) (Gastein, Austria. 15th-21st July, 2000)

3. "Electronic Transport processes in Fullerene Thin Films". G. Chambers, H.J. Byrne, presented at the 4th Biennial International Workshop on Fullerenes and Atomic Clusters (IWFAC'99) (St. Petersburg, Russia. 4th-8th October, 1999)

4. "Insitu Spectroscopic monitoring of Electronic Transport processes in Fullerene Thin Films". G. Chambers, H.J. Byrne, presented at the International Poastgraduate Research Conference (DIT Aungier Street. Nov. 19th-21th 1998)

Poster Presentations

1. "Spectroscopic and structure analysis of precursors to hexagonal closed packed phases in C_{60} thin films" G. Chambers, D. Fenton, J.R. Lawrence, K. Henderson, A.B. Dalton and H.J. Byrne, presented at the International Conference on Science and Technology of Synthetic Metals, (ICSM 2000) (Gastein, Austria. 15th-21st July, 2000)

2. "A functional conjugated polymer to process purify and selectively interact with single wall carbon nanotubes" A.B. Dalton, K. Henderson, G. Chambers, J.N. Coleman. W.J. Blau. C. Stephan. S. Lafrant, P. Bernier, and H.J. Byrne, presented at the International Conference on Science and Technology of Synthetic Metals, (ICSM 2000) (Gastein, Austria. 15^{th}-21^{st} July, 2000)

3. "Solvent effects on the optical properties of conjugated polymers" K. Henderson, A.B. Dalton, , G. Chambers, A. Dury, W.J. Blau, H.J. Byrne, presented at the International Conference on Science and Technology of Synthetic Metals, (ICSM 2000) (Gastein, Austria. 15^{th}-21^{st} July, 2000)

4. "Isomeration and interchain effects in conjugated materials" A.B. Dalton, K. Henderson, L. Reeves, G. Chambers, D. Bradley, A. Dury, J.N. Coleman, W.J. Blau, H.J. Byrne, presented at the International Conference on Science and Technology of Synthetic Metals, (ICSM 2000) (Gastein, Austria. 15^{th}-21^{st} July, 2000)

5. "Photochemical Reactions and Excited States of Fullerenes" ". G. Chambers, H.J. Byrne , 51^{ST} Irish Universities Chemistry Research Colloquim DIT, 23^{rd}-25^{th} June 1999.

6. "Spectroscopic study of the Photo-polymerisation of C_{60} and it related Photophysics". G. Chambers, H.J. Byrne, presented at International Poastgraduate Research Conference DIT Aungier Street. Nov. 19^{th}-21^{th} 1998

7. Insitu Spectroscopic monitoring of Transport Processes in C_{60} Thin Films". G. Chambers, H.J. Byrne, presented at Europhysics Conference on Marcomolecular Physics. Varenna (Italy) Sept. 13^{th}-17^{th} 1998

8. "Electronic Properties of Structurally Modified C_{60} Films", G. Chambers, K. Henderson, and H.J. Byrne, presented at ICSM98, Montpellier July 12-18th (1998)

Journal Publications

1. "Raman spectroscopic study of excited states and photo-polymerisation of C_{60} from solution" G. Chambers, H.J. Byrne *Chem Phys Lett.* 302 (1999) 307-311

2. "Electronic properties of structurally modified C_{60} films" K. Henderson, G. Chambers, H.J.Byrne, *Synthetic Metals* 103 2360-2361 (1999)

3. "Photoexcited states and electronic processes in C_{60} thin films" G. Chambers, H.J. Byrne *Molecular Materials* 13 193-200 (2000)

4. "Structure and characterisation of photo-polymerised C_{60} produced from solution" G. Chambers, K. Henderson, A.B. Dalton, B. Mc Carthy, H.J. Byrne. *Synthetic Metals*, In press

5. "Spectroscopic and structural analysis of precursors to hexagonal close packed phases in C_{60} thin films" G. Chambers, D. Fenton, J.R. Lawrence, K. Henderson, A.B. Dalton and H.J. Byrne *Synthetic Metals*, In press

6. " A functional conjugated polymer to process, purify and selectively interact with single wall carbon nanotubes" A.B. Dalton, K. Henderson, G. Chambers, J.N. Coleman. W.J. Blau. C. Stephan. S. Lafrant, P. Bernier, and H.J. Byrne, *Synthetic Metals*, In press

7. "Solvent effects on the optical properties of conjugated polymers" K. Henderson, A.B. Dalton, , G. Chambers, A. Dury, W.J. Blau, H.J. Byrne, *Synthetic Metals*, In press

8. "Isomerisation and interchain effects in conjugated materials" A.B. Dalton, K. Henderson, L. Reeves, G. Chambers, D. Bradley, A. Dury, J.N. Coleman, W.J. Blau, H.J. Byrne, *Synthetic Metals*, In press

9. "Observation and identification of the Molecular triplet in C_{60} thin films" G. Chambers, A.B. Dalton, L.M. Evans, and H.J. Byrne, *Chem Phys Lett*. Submitted April 2001.

References

1. D.E.H. Jones New Sci., 32, 245, (1966).
2. E. Osawa, Chem Abstr. 75698, 74, (1971).
3. H.W Kroto, J.R Heath, S.C O'Brien., R.F. Curl, and R.E. Smalley, *Nature* 318, 162, (1985).
4. R.C. Haddon, L.E. Brus and K. Raghavachari, Chem. Phys. Lett. 125, 459, (1986).
5. D.E. Manolopoulos, J.C May and S.E. Down, Chem. Phys. Lett. 181, 105, (1991).
6. W. Krätschmer, K, Fostiropoulos and D.R. Huffman Chem. Phys. Lett. 170, 167, (1990).
7. H. Ajie, M. A. Marcos, J.A. Samir, B.D. Rainer, and W. Krätschmer *etal.* J. Phys. Chem. 94, 8630, (1990).
8. W. Krätschmer, L. D. Lamb, K, Fostiropoulos and D.R. Huffman Nature, 347, 354, (1990).
9. H. Aldersey-Williams 'The most Beautiful Molecule' John Wiley and sons Inc (1995).
10. J Baggott, 'Perfect Symmetry' Oxford Press (1996).
11. T. Pradeep, Current Science, 72, 124, (1997).
12. S.H. Freidman, D.L. DeCamp, R.P. Sijbesma, G.Srdanov. F. Wudl, and G. L. Kenyon, J. Am. Chem. Soc. 115, 6506, (1993).
13. J.C.Withers, R. O. Loufty, T.P.Lowe. Fullerene Science and Technology 5(1), 1, (1997).
14. D.Koruga, S. Hammeroff, J.C.Withers, R. O. Loufty, M Sundareshan. 'Fullerene C_{60}' North-Holland (1993).
15. L.W. Tutt and A. Kost, Nature 356, 225, (1992).
16. R.C. Haddon, A.F. Hebard, M.J. Rosseinsky, D.W. Murphy, S.J. Duclos, *etal.* Nature, 350, 320, (1991).
17. A.F. Hebard, M.J. Rosseinsky, R.C. Haddon, D.W. Murphy, S.H. Glarum, T.T.M. Palstra, A.P. Ramirez and A.R.Kortan. Nature, 350, 600, (1991).
18. M.J. Rosseinsky, A.P. Ramirez S.H. Glarum,. D.W. Murphy, R.C. Haddon, A.F Hebard, T.T.M. Palstra, A.R.Kortan, Am. Phys. Soc. 66, 2830, (1991).
19. M.S. Dresselhaus, G Dresselhaus, P.C. Eklund, 'Science of fullerenes and carbon nanotubes' Academic press inc. (1995).
20. H. Weber App.Phys Lett. 81, 3749, (1998).
21. R.M. Fleming, A.P.Ramirez, M.J. Rosseinsky, D.W. Murphy R.C. Haddon Nature, 352, 787, (1991).
22. H.J. Byrne, W.K. Maser, M. Kaiser, W.W. Rühle, L. Akselrod, A.T. Werner, J. Anders, X.-Q. Zhou, G. Mahler, T. Kuhn, A. Mittelbach and S. Roth, Appl. Phys. A, 57, 303, (1993).
23. A.T. Werner, H.J. Byrne, D. O'Brien and S. Roth, J. Mol. Crys. Liq. Crys., 256, 795, (1994).
24. H. Kuzmany, M. Matus, T. Pichler and J. Winter, in "Physics and Chemistry of Fullerenes", K. Prassides ed., Klewer Academic, Dordrecht (1994).
25. G. Dresselhaus, M.S. Dresselhaus and P.C. Eklund, Phys. Rev. B, 45, 6923, (1992).
26. http://www.hyper.com/
27. K.L. Akers Ph.D disesertation Unversity of Toronto (1994).

28. K. Hedberg, L. Hedberg, D.S. Bethune, C.A. Brown, H.C. Dorn, R.D. Johnson, M. de Vries, Science 254, 410, (1991).
29. H. Kuzmany , m. Matus, B. Burger, J. Winter Adv Mater 10, 731, (1994).
30. J.E. Fisher, P.A. Heiney, D.E. Luzzzi, E. Cox, Fullerenes: Synthesis, Properties and Chemistry of large carbon clusters, from American Chemical Society Symposium 481, 55, (1992).
31. G. Chambers, H.J. Byrne Chem Phys Lett. 302, 307, (1999).
32. P.C. Eklund, A.M. Rao, Y. Wang, P. Zhou, M.J. Holden and K.A. Wang, in "Progress in Fullerene Research", H. Kuzmany, J. Fink, M. Mehring and S. Roth eds., World Scientific Singapore, p336, (1994).
33. C.C. Chancey, M.C.M. O'brien 'The Jahn-TellerEffectin C_{60} and other icosahedral complexes' Princeton University Press New Jersey (1997).
34. H.J. Byrne, in "Physics and Chemistry of Fullerenes and Derivatives", H. Kuzmany, J. Fink, M. Mehring and S. Roth eds., World Scientific Singapore, p183 (1995).
35. "Electronic Structure Calculations on Fullerenes and their Derivatives" Jerzy Cioslowski. Oxford Universsity Press (1995).
36. M. Braga. S. Larsson, A. Rosén, A. Volosov. Atron. Astrophys. 245, 232 (1991).
37. S. Leach, M. Vervloet, A. Desprès, E. Bréheret, J.P. Hare, T. J. Dennis, H.W. Kroto, R. Taylor, and D.R.M. Walton, Chem. Phys., 160, 451, (1992).
38. J.R Heath, Am. Chem. Soc. Symposium Series 481, 1,(1992).
39. D.S. Bethane, G. Meijer, W.C. Treacy, and H.J. Rosen, Chem Phys Lett 174, 219, (1990).
40. R. Taylor, J.P. Hare. A.K. Abdul-Sada and H. Kroto. J. Chem. Soc. Chem. Commun. 201, 1423, (1990).
41. A. Kost, J.E. Jensen, M.B. Klein, J.C. Withers, R.O. Loufty, M.B. Haeri and M.E. Ehritz, in "Fullerenes and Photonics", Z.H. Kafafi ed, Proc. SPIE 2284, 208, (1994).
42. L. Akselrod PhD disesertation Unversity of Dublin, Trinity College. (1993).
43. L. Akselrod, H.J. Byrne, J. Callaghan, A. Mittelbach and S. Roth, in "Electronic Properties Fullerenes", H. Kuzmany, J. Fink, M. Mehring and S. Roth eds., Springer Series in Solid state Sciences, Springer Verlag Heidelberg, 117, 219, (1993).
44. P.W. Atkins, Physical Chemistry, Oxford University Press (1990).
45. http://www.isainc.com/raman/showroom/labram/lramroot.htm
46. A.J. Bard, L.R. Faulkner. 'Electrochemical methods, fundamentals and applications' John Wiley and son inc. (1980).
47. D.R. Huffman, Adv. Phys., 26, 129, (1977).
48. S, Leach in "Physics and Chemistry of Fullerenes",K.Prassides (ed.) NATO ASI Series, Kuluwer Academic Publishers 443, 117, (1994).
49. C.V. Raman and K.S. Krishan, Nature 121, 501, (1928).
50. L. Akselrod, H.J. Bryne, S. Donovan., S. Roth, *Chemical Physics* 192, 307, (1995).
51. Z-H. Dong, P. Zhou, J.M. Holden, and P.C. Eklund, M.S. Dresselhaus, G. Dresselhaus, Phys. Rev. B, 48, 2862, (1993).

52. H.Kuzmany, M. Matus, T. Pichler and J. Winter, in "Physics and Cemistry of Fullerenes", K. Prassides ed., Klewer Academic, Dordrecht (1994).
53. J.E. Fisher, P.A. Heiney, D.E. Luzzi, and D.E. Cox, Fullerenes: Synthesis, Properties, and Chemistry of Large Carbon Clusters, from the American Chemical Society Symposium Series, 481, 55, (1992).
54. P.H.M. van Loosdrecht, P.J.M. van Bentum, M. Verheijen and G. Meijer, Chem. Phys. Lett., 198, 587, (1992).
55. S.P. Love, D. McBranch, M. Salkolka, N.V. Coppa, J.M. Robinson, B.I. Swanson, and A.R. Bishop, Chem. Phys. Lett., 225, 170, (1994).
56. B. Burger and H. Kuzmany, in "Progress in Fullerene Research", H. Kuzmany, J. Fink, M. Mehring and S. Roth eds., World Scientific Singapore (1994).
57. K.-A. Wang, A.M. Rao, and P.C. Eklund, M.S. Dresselhaus, G. Dresselhaus, Phys. Rev. B, 48, 11375, (1993).
58. J. Cioslowski 'Electronic Structure Calculations on fullerenes and their deivatives' Oxford University press (1995).
59. M. Braga, S. Larsson, A. Rosén and A. Volosov, Astron. Astrophys., 245, 232, (1991).
60. S. Leach, M. Vervloet, A. Desprès, E. Bréheret, J.P. Hare, T. J. Dennis, H.W. Kroto, R. Taylor, and D.R.M. Walton, Chem. Phys., 160, 451, (1992).
61. C. Bulliard, M. Allan and S. Leach, Chem. Phys. Lett., 209, 434, (1993).
62. S. Kazaoui, N. Minami, Y. Tanabe, H.J. Byrne A. Elimes, P. Petelenz, Phys Rev B. 58, 7689, (1998).
63. M. Kaiser, J. Reichenbach, H.J. Byrne, J. Anders, W. Maser, S. Roth, A. Zahab and P. Bernier, Solid State Commun., 81, 261, (1992).
64. Y. Wang, J. Phys. Chem., 96, 764, (1992).
65. H.J. Byrne, W.K. Maser, W.W. Rühle, A. Mittelbach, W. Hönle, H.G. von Schnering, B. Movaghar and S. Roth, Chem. Phys. Lett., 204, 461,(1993).
66. W. Guß, J. Feldmann, E.O. Göbel, C. Taliani,, H. Mohn, P. Haeusslerand and H.-U. ter Meer, Phys. Rev. Lett., 72, 2648, (1994).
67. P.A. Lane, L.S. Swanson, Q.-X. Ni, J. Shinar, L.P. Engel, T.J. Barton and L. Jones, Phys. Rev. Lett. 68, 887, (1991).
68. T.W. Ebbesen, T. Tanigaki and S. Kuroshima, Chem. Phys. Lett., 181, 501, (1991).
69. T.W. Ebbesen, Y. Mochizuki, K. Tanigaki and H. Hiura, Europhys. Lett., 25, 503, (1994).
70. J.B.Birks, "Organic Molecular Photophysics" John Wiley and Sons, London (1975).
71. P.C. Eklund, A.M. Rao, Y. Wang, P. Zhou, M.J. Holden and K.A. Wang, in "Progress in Fullerene Research", H. Kuzmany, J. Fink, M. Mehring and S. Roth eds, World Scientific Singapore 336, (1994).
72. G. Porter, Science 160, 1299, (1968).
73. J.W. Arbogast, C.S. Foote and Michelle Kao, J. Am. Chem. Soc., 114, 2277, (1992).
74. J.W. Arbogast, A.P. Darmanyan, C.S. Foote, Y. Rubin, F.N. Diederich, M.M. Alvarez, S.J. Anz and R.L. Whetten, J. Phys. Chem., 95, 11, (1991).

75. E.J.J Groenen, J. Schmidt in "Progress in Fullerene Research", H. Kuzmany, J. Fink, M. Mehring and S. Roth eds., World Scientific Singapore, 397, (1994).
76. T.N. Thomas, R.A. Taylor, J.F. Ryan, D. Mihailovic and R. Zamboni, in "Electronic Properties of Fullerenes", H. Kuzmany, J. Fink, M. Mehring and S. Roth eds., Springer Series in Solid State Sciences, Springer Verlag, Berlin Heidelberg 117, (1993).
77. N. Minami, S. Kazaoui, and R. Ross. Synthetic Metals, 70, 1397, (1995).
78. P.C. Eklund, Z.-H. Dong, Y. Wang, M.J. Holden, K.A. Wang, P. Zhou, A.M. Rao, G. Dresselhaus and M.S. Dresselhaus, in "Electronic Properties of Fullerenes", H. Kuzmany, J. Fink, M. Mehring and S. Roth eds., Springer Series in Solid State Sciences, Springer Verlag, Berlin Heidelberg, 117, (1993).
79. L. Akselrod, H.J. Byrne, C. Thomsen and S. Roth, Chem. Phys. Lett., 215, 131, (1993).
80. H.J. Byrne, L. Akselrod, C. Thomsen, A. Mittelbach and S. Roth, Appl. Phys. A, 57, 299, (1993).
81. S.R. Mirsha, H.S. Rawat, M.P. Joshi, S.C. Mehendale and K.C. Rustagi, in "Fullerenes and Photonics", Z.H. Kafafi ed, Proc. SPIE 2284, 220, (1994).
82. P.H.M. van Loosdrecht, P.J.M. van Bentum and G. Meijer, Chem. Phys. Lett., 205, 191, (1993).
83. A.M. Rao, P. Zhou, K.A. Wang and P.C. Eklund, Science, 259, 955, (1993).
84. P.M. Rafailov, V.G. Hadjiev, C. Thomsen, K. Kamarás, S. Pekker, Chem. Phys. Lett. 326, 58, (2000).
85. G. Chambers, K. Henderson, A.B. Dalton, B. Mc Carthy, H.J. Byrne. Synthetic Metals, In print.
86. D.W. Snoke, K. Syassen and A, Mittelbach, Phys. Rev. B, 47,4146 (1993)
87. L. Akselrod, H.J. Byrne, C. Thompsen, A. Mittelbach and S. Roth, Chem. Phys. Lett., 212, 384, (1993).
88. H.J. Byrne, A.T. Werner and S. Roth, in "Organic Electroluminescent Materials and Devices", S. Miyata and H. Nalwa eds., Gordon and Breach Science, Amsterdam, 263, (1997).
89. H.J. Byrne, W.K. Maser, M. Kaiser, W.W. Rühle, L. Akselrod, A.T. Werner, J. Anders, X.-Q. Zhou, G. Mahler, T. Kuhn, A. Mittelbach and S. Roth, Appl. Phys. A, 57, 303, (1993)
90. J.T. Dortmund, "Advances in solid state physics", Germany Physical Society Vieweg, (1979).
91. J, Shinar, Z.V. Vardeny, Z.H. Kafafi "Optical and electronic properties of fullerenes and and fullerene-based materilas" Marcel Dekker Inc. New York (2000).
92. R.M. Williams, and J.W. Verhoeven. Spectrochim. Acta 50A, 251, (1994).
93. G. Chambers. L.M. Evans, A.B. Dalton, H.J. Byrne. Chem. Phys. Lett. In print (2001).
94. L. Forro, A. Janossy, D. Ugarte and Walt A de Heer in "Advances in Synthetic Metals: Twenty years of Progress in Science and Technology" ed., P. Bernier, S. Lefrant and G. Bidan, Elsevier Science S.A. (1999)
95. B. Sundqvist, Advances in Physics 48, 1, (1999).

96. Y. Iwasa, T. Arima, R.M. Fleming, T. Siegrist, O. Zhou, R.C. Haddon, L.J. Rothberg, K.B. Lyons, H.L. Carter Jr, A.F. Hebard, R. Tycko, G. Dabbagh, J.J. Krajewski, G.A. Thomas, T. Yagi, Science 264, 1570, (1994).
97. J. B. Birks. 'Photophysics of Aromatic Molecules. John Wiley and Sons, London. A general review of the molecular spectroscopy of Aromatic molecules.' (1970).
98. D. Bethune, G. Meijer, W.C. Tang, H.J. Rosen, W.G. Golden, H. Seki, C.A. Brown and M.S. de Vries, Chem. Phys. Lett., 179, 181, (1991).
99. S.J. Duclos, R.C. Haddon, S.H. Hebard and K.B. Lyons, Solid State Commun, 80, 481, (1992).
100. M. Matus, H. Kuzmany and E. Sohmen, Phys. Rev. Lett., 68, 2822, (1992).
101. T.W.G. Solomons 'Organic Chemistry' John Wiley and Sons (1980).
102. P.C. Eklund, A.M. Rao, P. Zhou, Y. Mang, K.-A. Wang, G.T. Hager and J.M. Holden, Mat. Science and Engin., B19, 154, (1993).
103. K. Akers, K. Fu, P. Zhang and M. Moskovits, Science, 259, 1152, (1993).
104. T. Wågberg P. Jacobsson, B. Sundqvist. Phy. Rev. B. 60, 4535, (1999).
105. J. R. Lawrence, G. Chambers, D. Fenton, K. Henderson, A.B. Dalton, H.J. Byrne Synthetic metals in print (2001).
106. A.M. Rao, P.C. Eklund, J-L. Hodeau, L. Marques, M. Nunez-Regueiro, Phys. Rev. B 55, 4766, (1997).
107. J. Wang "Analytical Electrochemistry", VCH publishers Inc. (1994).
108. Q, Xie. E, Pérez-Cordero, L, Echegoyen. *J.Am. Chem. Soc.* 114, 3978, (1992).
109. R. Tycko, G. Dabbagh. M.J. Rosseinsky, D.W. Murphy, R.M. Flemming, A.P. Ramirez and J.C. Tully, Science 253, 884, (1991).
110. J.A. Zimmerman, J.R.Eyler, S.B.H.Bach, S.W. Mc Elvany, J. Chem. Phys. 94, 3556, (1991).
111. Q, Xie. F. Arais, L, Echegoyen. J.Am. Chem. Soc. 115, 9818, (1993).
112. C, Jehoulet. A. J. Brad, F. Wudl Am. Chem. Soc 113, 5456, (1991).
113. RE Haufler, J Conceicao, LPF Chibante, Y Chai, NE Byrne, S Flanagan, MM Haley, SC O'Brien, C Pan, Z Xiao, WE Billups, MA Ciufolini, RH Hauge, JL Margrave, LJ Wilson, RF Curl, RE Smalley .J. Phys. Chem. 94, 8634, (1990).
114. D.M. Cox, S. Behal. M. Disko, S.M. Gorun, M. Greaney. C.S.Hsu. E.B. Kollin et al. J. Am. Chem. Soc. 113, 2940, (1991).
115. D. Doubois, K.M. Kadish. S Flanagan, RE Haufler, L.P.F. Chibante. L.J Wilson J. Am. Chem. Soc. 113, 4363, (1991).
116. D. Doubois, K.M. Kadish. S Flanagan, L.J Wilson J. Am. Chem. Soc. 113, 7773, (1991).
117. P-M Allemand, A Koch F. Wudl. Y Rubin F. Diederich M.M Alverez, S.J. Anz R.L. Whetten J. Am. Chem. Soc. 113,1050, (1991).
118. D. Doubois, G. Moninot, W. Kunter, T.M. Jones K.M. Kadish. J. Phys. Chem. 96, 7137, (1992).
119. C, Jehoulet.Y.S. ObengY-Tkim, F.Zhou A. J. Brad, J Am. Chem. Soc 114, 4237, (1992).

120. A,Smie J. Heinze in "Physics and Chemistry of Fullerenes and Derivatives", H. Kuzmany, J. Fink, M. Mehring and S. Roth eds., World Scientific Singapore, 254, (1995).
121. C. Kvarnstrom, H. Neugebauer, G. Matt, H. Sitter, N.S. Sariciftci Synthetic Metals 103, 2430, (1999).
122. M.L. McGlasnen, M.E. Blackwood T.G.Spiro J. Am. Chem. Soc. 115, 2074, (1993).
123. Y. Zhang, W. Edens, M.J. Weaver, J. Am. Chem. Soc. 113, 9395, (1991).
124. F.M. Zhou, S.L. Yau, C. Jehoulet, D.A. Laude, Z.Q. Guan, A.J. Bard J. Phys. Chem. 96, 4160, (1992).
125. P.A. Heiney, G.B.M. Vaughan, J.E. Fischer, N. Coustel, D.E. Cox, J.R.D. Copley, D.A. Neumann, W.A. Kamitakahara, K.M. Creegan, D.M Cox, J.P. Mccauley, A.B. Smith Phys. Rev B 45, 4544, (1992).
126. S.M. Sze 'Semiconductor devices- physics and technology' John Wiley and sons inc. (1985).
127. J.N. Coleman, S. Curran, A.B. Dalton, A.P. Davey, B. Mc Carthy, W.J. Blau, and R.C. Barklie. Phys. Rev. B 58, 7492, (1998).
128. B.K. Ridely "Quantum processes in semiconductors" Clarendon Oxford University Press (1999).
129. L. Akselrod, H.J. Byrne. T.E. Sutto, S. Roth. Chem. Phys. Lett. 233, 436, (1995).
130. M. Kaiser, W.K. Maser, H.J. Byrne, A. Mittelbach and S. Roth. Solid State Commun., 87, 281, (1993).
131. K, Kamarás, A. Breitschwerdt, S. Pekker, K. Fodor-Csorba, G. Faigel, M. Tegze. App. Phys. A 56, 231, (1993).
132. K. Henderson, G. Chambers, H.J. Byrne, Synthetic Metals 103, 2360, (1999).
133. K. Henderson, Final year BSc Project (FT222 Physics Option), DIT Kevin Street (1998).
134. R.J. Sension, A.Z. Szarka, G.R. Smith amd R.M. Hochstrasser, Chem. Phys. Lett. 185, 179, (1991).
135. A.R. West. "Basic solid state Chemistry" John Wiley and Sons Ltd. (1988).
136. G.A. Samara, J.E. Schirber, B. Morosin, L.V. Hansen, D. Loy and A.P. Sylwester, Phys. Rev. Lett. 67, 3136, (1991).
137. X. Wu and S.E. Ulloa, Phys. Rev. B 49, 7825, (1994).
138. S Iijima Nature, 354, 56, (1991).
139. P. Bernier, Speaking at COST meeting in Maynooth March (1999).
140. W,M, Dennis, W. Blau, D.J. Bradley. App. Phys. Lett. 47, 200, (1985).
141. G.M. Carter, J.V. Hryniewicz, M.K. Thakur, Y.J. Chen, S.E. Meyler, App Phys. Lett 49, 998, (1986).
142. C. Sauteret, J-P. Hermann, R. Frey. F. Pradére, J. Ducing, R.H. Baughman, R.R. Chance. Phys. Rev. lett. 36, 956, (1976).
143. F. Meyer J.L. Brédas in "Organic Molecules for Nonlinear Optics and Photonics", J. Messier, F. Kajzar and P. Prasad eds., NATO ASI Series E: Applied Sciences., Klewer Academic Dordrecht, 194, 391, (1991).
144. A.P. Davey , H.J. Byrne, H. Page, D.J. Cardin and W.J. Blau, Synthetic. Metals, 58, 161, (1993).
145. H.J. Byrne, R. MacRuairí and W. Blau, Synthetic Metals", 41, 3217, (1991).
146. J. Callan PhD disesertation Unversity of Dublin, Trinity College. (1996).

147. J. P. Hare, H.W. Kroto and R. Taylor, Chem. Phys. Lett., 177, 394, (1991).
148. T.J. Dennis, J.P. Hare, H.W. Kroto, R. Taylor, D.R.M. Walton and P.J. Hendra, Spectrochimica Acta, 47A, 1289, (1991).
149. M. Lee, O. K. Song, J. –C, D. Kim, Y. D. Suh, S.M. Jin anf S.K. Kim, Chem. Phys. Lett. 196, 325, (1992).
150. X. Wei, S Jeglinski, O. Paredes, Z.V. Vardeny, D.Moses, V.I. Srdanov, G. D. Stucky, K.C. Khemani and F. Wudl. Solid State Comm. 85, 455, (1993).
151. A. York. Chemistry in Britain, 1 40 (2000).
152. S. Sevov, J. Corbett, Science, 5, 45, (1993).
153. F. Pedreschi, Final year BSc Project (WSAD4 Physics Option), DIT Kevin Street (1997).
154. http://cnst.rice.edu/pics.html
155. S. J. Tams, A.R.M Verschuereen, C. Dekker, Nature, 49, 339, (1998).
156. W.A. de Heer, A. Châtelain, and D. Ugarte, Science 270, 1179, (1995).
157. http://www.foresight.org/Conferences/MNT6/Papers/Chatelain/#17468
158. Private communication A.B. Dalton (2001).